Spatiotemporal tracking of heme-bound and heme-free yeast cytochrome c peroxidase in live cells and probing its regulation of the H_2O_2 stimulon at the proteome level

Samaneh Dastpeyman

A Thesis

in The Department of

Chemistry and Biochemistry

Presented in Partial Fulfillment of the Requirements

For the Degree of

Doctor of Philosophy (Chemistry) at

Concordia University

Montreal, Quebec, Canada

September 2020

CONCORDIA UNIVERSITY SCHOOL OF GRADUATE STUDIES

This is to certify that the thesis prepared

By: Samaneh Dastpeyman

Entitled: Spatiotemporal tracking of heme-bound and heme-free yeast cytochrome c peroxidase in live cells and probing its regulation of the H_2O_2 stimulon at the proteome level

and submitted in partial fulfillment of the requirements for the degree of

Doctor Of Philosophy (Chemistry)

complies with the regulations of the University and meets the accepted standards with respect to originality and quality.

Signed by the final examining committee:

_____ Chair
Dr. Malcolm Whiteway

_____ External Examiner
Dr. Lars Konermann

_____ External to Program
Dr. William Zerges

_____ Examiner
Dr. Dajana Vuckovic

_____ Examiner
Dr. Alisa Piekny

_____ Thesis Supervisor
Dr. Ann English

Approved by _____
Dr. Yves Gelinas, Graduate Program Director

September 3, 2020 _____
Dr. André Roy, Dean Faculty of Arts and Science

Abstract

Spatiotemporal tracking of heme-bound and heme-free yeast cytochrome c peroxidase in live cells and probing its regulation of the H_2O_2 stimulon at the proteome level

Samaneh Dastpeyman, Ph.D.
Concordia University, 2020

Independently of its peroxidase activity, yeast cytochrome c peroxidase (Ccp1) functions in H_2O_2 sensing and signaling, including regulation of heme catalase A, Cta1. Since the maturation of Cta1, a highly efficient H_2O_2 detoxifying enzyme, involves the recruitment of Ccp1's heme in respiring yeast mitochondria, I aimed to track the heme status of Ccp1 in live cells spatiotemporally. To do this, I had to develop a tool to investigate when and where an endogenous heme-binding protein such as Ccp1 is heme-loaded or heme-free in live cells. As described in Chapter 2, analysis of GFP fluorescence lifetimes by time-correlated single photon counting (TCSPC) indicates that heme efficiently quenches green fluorescent protein (GFP) in a recombinant Ccp1-GFP fusion protein *in vitro* and the amplitude of the quenched lifetime increases linearly with heme binding to Ccp1. Thus, in Chapter 3, I used fluorescence lifetime imaging microscopy (FLIM) of cells chromosomally expressing the same Ccp1-GFP fusion under the control of Ccp1's native promotor to show that Ccp1-GFP is fully heme-loaded and resides in the mitochondria of two-day respiring cells but more than half of Ccp1-GFP is heme-free and extra-mitochondrial in seven-day respiring cells. Since Ccp1 is the first heme-based H_2O_2-sensing protein to be identified and its W191F variant behaves as an amplified H_2O_2 sensor, the second goal of my research was to compare the H_2O_2-responsive proteins regulated by Ccp1 and Ccp1W191F in cells. Using mass spectrometry-based label-free proteomics, a switch of cellular activity from biosynthesis to defense and a redirection of carbohydrate metabolism to NADPH and trehalose production were found in both yeast strains on H_2O_2 challenge as reported in Chapter 4. However, cells expressing Ccp1W191F mounted a significantly more sustained response to H_2O_2 and the *in vitro* experiments described in Chapter 5 suggest that Ccp1W191F is a dedicated H_2O_2 sensing/signaling protein in cells. Overall, my research findings confirm that Ccp1 functions as a heme-donor protein in cells and that it acts as a regulator of the H_2O_2 stimulon.

Acknowledgement

As an incredible adventure in my life, completing a Ph.D. made me a stronger and more confident individual. Doing a Ph.D. in science equipped me with a power of scientific thinking which has led to a significant personal and professional growth. I would like to gratefully acknowledge the support I have received from several amazing people.

First and foremost, I would like to thank my supervisor, Dr. Ann English, for opening the door to doctoral studies for me and for her invaluable support and expert guidance throughout my Ph.D. journey. I have greatly benefited from her critical thinking, motivation, patience and novel research ideas.

I would also like to thank my committee members, Dr. Dajana Vuckovic and Dr. Alisa Piekny, for their expert advice and constructive critique. I would like to express my sincere gratitude to Dr. Joanne Turnbull for her generosity, continued support, and valuable advice over the past few years.

My sincere appreciation goes to Dr. Heng Jiang and Alain Tessier for their tremendous support and expertise in my training of mass spectrometry at the Centre for Biological Applications of Mass Spectrometry (CBAMS) at Concordia University.

I am grateful to Dr. Gonzalo Cosa for providing me the opportunity of working on time resolved fluorescence spectroscopy, and to Dr. Robert Godin for his technical advice at McGill University. I also wish to thank Dr. Claire Brown and Dr. Erika Wee at Advanced BioImaging Facility (ABIF) at McGill University for providing training in fluorescence lifetime imaging microscopy (FLIM). I would also like to thank Dr. Jackie Vogel for kindly offering me a lab bench to express fresh yeast cultures at McGill University. I am deeply grateful to Dr. Chris Law and Dr. Chloe van Oostende for their support and advice on my microscopy experiments at the Centre for Microscopy and Cell Imaging (CMCI). I would like to express my great gratitude to Dr. Andreas Bergdahl for allowing me to use Oxygrapgh-2k in his lab at Concordia University, as well as Dr. Pamaela-Hanic Joyce for constructing the CCP1W191F strain and for her valuable guidance and advice in the biological experiments of my study.

Thank you to all my lab colleagues over the past seven years. Thank you, Marc Ouellet, Dr. Dorival Martins, Dr. Meena Kathiresan, Dr. Vinod Parmar, Dr. Maria Shadrina, Zornitsa Stoyanova, Alan De Aguiar Lopes, Dr. Esam Orabi and Dr. Ritu Arora for their massive support, kindness and companionship. I also want to thank my friends, Dr. Paknoosh Pakarian and Khalil Rahman, for their generosity and support.

A huge thank you goes out to my husband, Dr. Mehdi Babaei, for his countless support, true love, thoughtfulness, kind-heartedness, and his words of inspiration. We were both determined

to pursue a doctoral degree at the same time. I am blessed to have my 4-year old little princess, Lillian, who gave me the joy of motherhood. Thank you, Lillian, for cheering me up during the hardships of my doctoral studies. I wish to thank my dear mother for her generous support and dedication in the early months of my daughter's arrival.

Lastly, I am grateful to the NSERC CREATE Training Program in Bionanomachines (Bionano) and PROTEO for offering me doctoral scholarships, and to Concordia University for the Concordia Special Entrance Award, which helped me go along the way with peace of mind.

Table of Contents

List of Tables

List of Figures

List of abbreviations

AAH1	Gene encoding adenine deaminase
ABTS	2,2'-azino-bis(3-ethylbenzothiazoline-6-sulfonic acid)
ACN	Acetonitrile
Ccp1	Cytochrome c peroxidase protein
CCP1	Gene encoding cytochrome c peroxidase
Ccp1W191F	Ccp1 variant with the W191F mutation
Ccp1Δ	*Ccp1-null* cells
CpdI	Compound I, the two-electron oxidized form of Ccp1
CpdII	Compound II, the one-electron oxidized form of Ccp1
Cta1	Catalase A protein
Ctt1	Catalase T protein
CTT1	Gene encoding catalase T
CYC1	Gene encoding cytochrome c iso-1
Cytb562	Cytochrome b562 protein
Cytc	Cytochrome c protein
DBNBS	3,5-dibromo-4-nitrosobenzenesulphonate
DEAE	Diethylaminoethyl cellulose
DTT	DL-dithiothreitol
E	FRET efficiency
ECM4	Gene encoding glutathione S-transferase omega-like 2
EDTA	Ethylenediaminetetraacetic acid
ESI	Electrospray ionization
FA	Formic acid
FLIM	Fluorescence lifetime imaging microscopy
FP	Fluorescence protein
FRET	Förster resonance energy transfer
GFP	Green fluorescence protein
GO	Gene Ontology
GPD1	Gene encoding glycerol-3-phosphate dehydrogenase [NAD(+)] 1
GPT2	Gene encoding glycerol-3-phosphate O-acyltransferase 2
GPX2	Gene encoding glutathione peroxidase-like peroxiredoxin 2
GRE2	Gene encoding NADPH-dependent methylglyoxal reductase GRE
GRX2	Gene encoding glutaredoxin-2
HAM1	Gene encoding inosine triphosphate pyrophosphatase
HBD	Heme binding domain
HEPES	4-(2-hydroxyethyl)-1-piperazineethanesulfonic acid
HRP	Enzyme horseradish peroxidase
HSP104	Gene encoding heat shock protein 104
HSP26	Gene encoding heat shock protein 26
HSP42	Gene encoding heat shock protein 42

HSP78	Gene encoding heat shock protein 78, mitochondrial
HSP82	Gene encoding ATP-dependent molecular chaperone HSP82
IMAC	Immobilized metal-ion affinity chromatography
IMS	Inter-membrane space
IPTG	Isopropyl β-D-1-thiogalactopyranoside
IRF	Instrumental response function
KPi	Potassium phosphate
LC-MS	Liquid chromatography–mass spectrometry
LoaOOH	Linoleic acid hydroperoxide
MES	2-(N-morpholino)ethanesulfonic acid
MNP	2-Methyl-2-nitrosopropane
Ni-NTA	Ni^{II} complex of nitrilotriacetic acid
OYE2	Gene encoding NADPH dehydrogenase 2
OYE3	Gene encoding NADPH dehydrogenase 3
P10	mitochondria-enriched subcellular fraction
PBS	Phosphate buffered saline
PC	Principal component
PDB	Protein data bank
PES	Polyethersulfone
PMSF	Phenylmethylsulfonyl fluoride
PRX1	Gene encoding peroxiredoxin PRX1
PTM	Post-translational modification
Q-ToF MS	Quadrupole time-of-flight mass spectrometry
RFU	Relative fluorescence units
ROI	Regions of interest
ROS	Reactive oxygen species
S10	Extramitochondrial subcellular fraction
SCD	Synthetic complete medium with dextrose
SDS-PAGE	Sodium dodecyl sulphate-polyacrylamide gel
Sod1	Cu/Zn superoxide dismutase protein
SOD1	Gene encoding superoxide dismutase [Cu-Zn]
SOD2	Gene encoding superoxide dismutase [Mn]
TCA	Tricarboxylic acid cycle
TCSPC	Time-correlated single photon counting
TDH1	Gene encoding glyceraldehyde-3-phosphate dehydrogenase 1
TDH2	Gene encoding glyceraldehyde-3-phosphate dehydrogenase 2
TDH3	Gene encoding glyceraldehyde-3-phosphate dehydrogenase 3
TIC	Total ion chromatogram
TRR1	Gene encoding thioredoxin reductase 1
TRR2	Gene encoding thioredoxin reductase 2
TRX1	Gene encoding thioredoxin-1
TRX2	Gene encoding thioredoxin-2

TSA1	Gene encoding thiol-specific antioxidant TSA1 enzyme
TSA2	Gene encoding thiol-specific antioxidant TSA2 enzyme
TSL1	Gene encoding trehalose synthase complex regulatory subunit TSL1
WT	Wild type
YAP1	Gene encoding yeast AP-1 transcription factor
ZWF1	Gene encoding Glucose-6-phosphate-1-dehydrogenase

Chapter 1: General introduction

1.1) Cytochrome c peroxidase (Ccp1)

Abrams, Altschul, and Hogness discovered cytochrome c peroxidase (Ccp1), a heme-containing enzyme, in *S. cerevisiae* in 1939.[1,2] Ccp1 has a negative charge (pI 5.5), medium size (34 kDa) with 294 amino-acids, and noncovalently binds heme b. Ccp1 can be purified from *S. cerevisiae* [1,3] and overexpressed in *E. coli*.[4–6] The crystal structure of Ccp1, which represented the first heme enzyme structure, was published 40 years ago.[7] Since then, the progress on Ccp1 structure and function has been intense. Ccp1 has been considered as a paradigm for interprotein electron transfer.[8] *In vitro*, Ccp1 is an efficient H_2O_2 scavenger in the presence of its putative biological partner, cytochrome c (Cyt c),[9] an essential component of the eukaryotic respiratory chain.[2] Residue W191 of Ccp1 plays a critical role in catalytic H_2O_2 turnover forming a radical cation center.[9] H_2O_2 oxidizes Ccp1(Fe^{III}) to Compound I (Fe^{IV}, $W191^{+\cdot}$). The first electron from Cyt c (Fe^{II}) to Compound I generates Compound II (Fe^{IV}, W191). An electron from a second Cyt c (Fe^{II}) molecule to Compound II generates Ccp1(Fe^{III}).[9] The Ccp1W191F variant forms Compound I (Fe^{IV}, porphyrin π-cation radical) but displays negligible Cyt c-oxidizing activity.[10]

Peroxidases, catalases, cyclooxygenases, hemoglobin, and myoglobin all bind heme b noncovalently, with a single coordination bond between the heme iron and the polypeptide.[11] Iron (Fe^{III}) in the center of heme b coordinates to four nitrogen atoms in the porphyrin, which acts as a tetradentate ligand (Figure 1.1A). In contrast, Cyt c has a heme c, with the two vinyl (-$CH{=}CH_2$) side chains bound covalently to cysteine sulfhydryl residues of the polypeptide.[11]

The noncovalently bound heme b of Ccp1 is buried in a hydrophobic pocket (Figure 1.1B),[2] which can be divided into proximal and distal cavities. In the proximal cavity, three key residues, H175, W191, and D235, modulate axial ligation, the fifth heme ligand being Nε of H175, which coordinates to Fe^{III}.[12] W191 is in van der Waals contact with both the imidazole ring of H175 and the porphyrin ring.[12] Both W191 and H175 hydrogen bond to the carboxylate group of D235.[12] The highly hydrogen-bonded distal cavity is defined by residues, R48, W51, and H52.[12] The 5-coordinated heme in Ccp1 has a vacant coordination site to bind H_2O_2. Both R48 and H52 expedite heterolytic cleavage of the peroxide oxygen-oxygen bond, which forms an oxyferryl (Fe^{IV}) and porphyrin π-cation radical.[12] Rapid radical transfer to W191 gives the stable form of Compound I.[12]

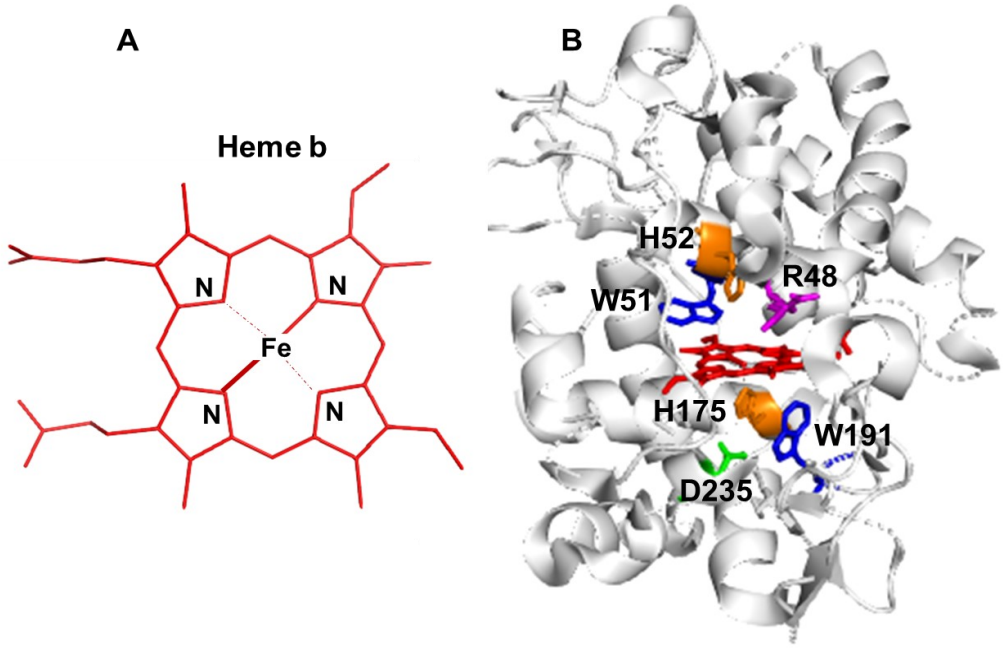

Figure 1.1 Chemical structure of heme b and its buried location in the hydrophobic pocket of Ccp1. A) Protoporphyrin IX heme with its two vinyl, four methyl, and two propionic acid side chains. The two vinyl side chains in heme c, synthesized from heme b, are covalently bonded to cysteine sulfhydryl residues of the apoprotein in Cyt c. B) PyMOL was used to generate a cartoon of Ccp1's residues (PDB 1ZBY) in the proximal and distal cavities. Key catalytic residues are H52, H175 (orange), W51, W191 (blue), R48 (magenta) and D235 (green).

The structure of Ccp1 is very similar to that of ascorbate peroxidase (APX).[13] Notably, W179 in APX occupies the same proximal location as W191 in Ccp1. However, W179 in APX does not transfer an electron to the porphyrin π-cation radical. Instead, this radical is reduced by W41, analogous to W51 in Ccp1, which results in covalent heme-W41 crosslinking in oxidized APX in the absence of a reducing substrate.[14] Heme crosslinking to W51 in Ccp1 is avoided by rapid electron transfer from W191 to the porphyrin π-cation radical. M230, M231, and M172 in the proximal cavity of Ccp1 stabilize the W191 cation radical site.[13] Mutating the analogous residues S160, L203, and Q204[15] to Met stabilized a Trp179 radical in APX Compound I.[16]

The function of peroxidases as H_2O_2 scavengers is well studied. However, catalases are more efficient H_2O_2-metabolizing heme enzymes that rapidly disproportionate H_2O_2 to water and oxygen. This raises the question as to why cells need heme peroxidase to scavenge H_2O_2 in the presence of catalase. Many heme peroxidases play other roles in cells. For example, human cells have multiple heme peroxidases such as myeloperoxidase, lactoperoxidase, and salivary peroxidase that play an antimicrobial role by catalyzing the H_2O_2 oxidation of acceptor molecules

to generate reactive oxidants that kill invading microbes.[17] However, other peroxidases such as Ccp1 seemed to have primarily a H_2O_2 scavenging function but its *in vivo* role has received little attention.

1.2) *In vivo* role of Ccp1

Yeast Ccp1 is a nuclear-encoded protein that is directed to mitochondria by a 68-residue N-terminal targeting sequence.[18] This presequence is cleaved in the inner membrane [19,20] and mature heme-loaded Ccp1, modified post-translationally by insertion of a single noncovalently bound heme b, is released into the inter-membrane space (IMS) of mitochondria.[21,22] Immature Ccp1 is present in cells under anaerobic conditions, which do not support heme biosynthesis.[21,22] When cells are exposed to oxygen, heme is synthesized by eight different enzymes,[23] the final steps occurring in mitochondria, and apoCcp1 matures to holoCcp1.[21,22] Unstressed *ccp1-null* cells (*ccp1Δ*) show similar viability as wild-type (WT) cells.[24] However, *ccp1Δ* cells show poor survival on challenge with exogenous H_2O_2, which suggests that Ccp1 is used for cellular defense in response to exogenous H_2O_2.[24] On H_2O_2 challenge, both Ccp1 and catalytically inactive Ccp1W191F transmit an oxidative stress signal to Skn7, a nuclear regulator of the oxidative-stress response in yeast.[25] This reveals that activation of Skn7 is independent of Ccp1's peroxidase function.

Recent research in our group indicates that basal H_2O_2 levels in respiring yeast cells expressing catalytically inactive Ccp1W191F are lower than those in WT cells and *ccp1Δ* cells.[24] Furthermore, Ccp1W191F-expressing cells (W191F cells) exhibit higher Cta1 (the peroxisomal/mitochondrial catalase isoform in yeast) catalase activity than WT and *ccp1Δ* cells.[24] This suggests that Ccp1, independently of its peroxidase activity, functions in H_2O_2 sensing and signaling to regulate Cta1 *in vivo*.[24] Also, Ccp1 exits mitochondria in the heme-free form while peroxisomal/mitochondrial Cta1 activity increases in respiring cells.[24] Thus, we proposed that Cta1 maturation in respiring yeast mitochondria involves the recruitment of Ccp1's heme, which was supported by biochemical data.[26]

Direct monitoring of heme transfer between Ccp1 and Cta1 would confirm our hypothesis and would reveal if other proteins are involved. However, as a first step, spatiotemporal tracking in live cells of the heme-bound vs heme-free forms of Ccp1 needed to be probed to address two key questions: (a) where is heme-loaded Ccp1 located in live cells, and (b) when is heme released from Ccp1 in live cells? My research has developed and optimized a reliable method to answer these questions.

Finally, it is relevant to note that there is no Ccp1 homolog in humans. However, understanding the *in vivo* functions of yeast Ccp1 will shed light on how eukaryotic cells

coordinate their responses to oxidative stress. Yeast serve as relatively simple model eukaryotic cells to investigate such biological complexity.

1.3) Green fluorescence protein (GFP) fusion as a promising *in vivo* heme sensor

Fluorescence proteins (FPs) have been utilized in live cells as localization probes,[27] and as sensors of pH,[28] chloride,[29–31] and Ca^{2+}.[32,33] Also, the fluorescence intensity of FPs has been shown to be quenched by free zinc, copper, cadmium, and nickel ions *in vitro.*[34,35] Heme is an extremely effective quencher of GFP fluorescence as exhibited for the cytochrome b562-enhanced GFP fusion protein (Cytb562-EGFP) *in vitro*.[36–39] This arises because GFP emission has significant overlap with heme absorption, which promotes quenching via Förster resonance energy transfer (FRET).[40–43] Thus, GFP with a high fluorescence quantum yield is a promising *in vivo* heme sensor. Furthermore, in the Yeast GFP Clone Collection, which is commercially available, most full-length ORFs are C-terminally fused to GFP via a nine-residue linker (GRRIPGLIN). The Ccp1-GFP clone from this collection has been examined in several studies and we are already aware that: (i) the Ccp1-GFP fusion protein matures in the cells by the same mechanism as native Ccp1 without GFP tag interference;[9] (ii) mature Ccp1-GFP locates to the IMS in fermenting cells without GFP tag interference;[26] and (iii) apoCcp1-GFP is found in respiring cells as is native apoCcp1.[25,44] Thus, we hypothesized that GRRIPGLIN-linked Ccp1-GFP is a suitable probe to monitor the heme status of mature Ccp1 in live cells. In this thesis, I have tested this hypothesis by characterizing heme-free and heme-loaded Ccp1-GFP fluorescence *in vitro* and *in vivo.*

1.4) Fluorescence intensity vs fluorescence lifetime measurements

Steady-state fluorescence measures the intensity of the fluorescence from excited molecules as they return to the ground level. Time-resolved fluorescence measures the average time (lifetime) that excited electrons occupy the S_1 excited state shown in the Jablonski diagram[31] (Figure 2.2). The fluorescence intensity is dependent on the concentration of fluorophore, whereas the fluorescence lifetime (τ) is independent of this concentration.[31,45] For example, excited electrons in 10 vs 1000 excited molecules spend the same average time in the S_1 state (τ) but the intensity of the fluorescence they emit will differ by a factor of 100. Both fluorescence lifetime and intensity are decreased in the presence of a quencher, which provides an additional nonradiative decay channel (Figure 2.2) and adds k_q, the quenching rate constant, to the overall rate constant for excited-state decay, k ($1/\tau$), which includes the rate constants for radiate (k_r) and nonradiative decay (k_{nr}):

Equation 1.1 $\tau = k^{-1} = (k_r + k_{nr} + k_q)^{-1}$

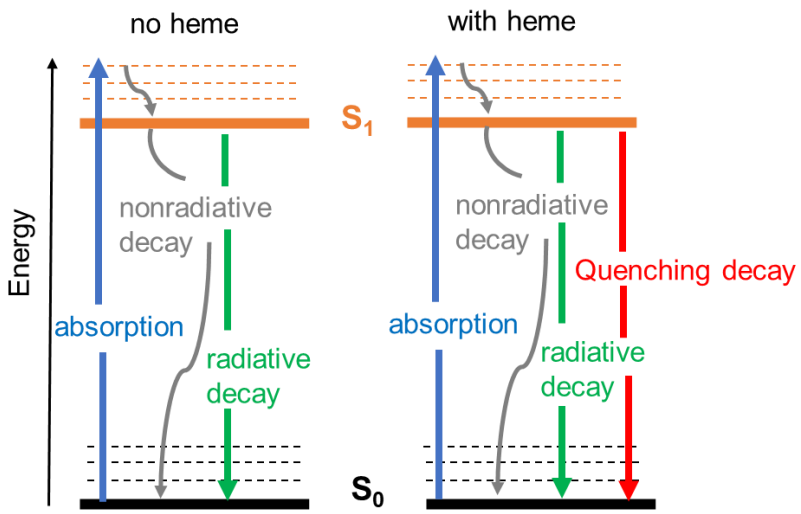

Figure 1.2. Jablonski diagram in the absence and presence of a quencher such as heme. Electrons are excited from S_0 (ground state) to S_1 (excited state). After a few nanoseconds, the energy of excited electron decreases by **nonradiative (k_{nr})** and **radiative (k_r)** processes, returning the electron to S_0. In the presence of a quencher such as heme, an extra nonradiative decay pathway decreases the fluorescence lifetime and the fluorescence intensity. This figure is adapted from Joachim Mueller (2006), Fluorescence Workshop UMN Physics.

Since time-resolved fluorescence measurements are concentration independent they will allow a more accurate determination of the apo- and holoCcp1-GFP population in cells. To gain information on Ccp1 localization and heme loading in live cells, fluorescence lifetime imaging microscopy (FLIM) was performed on cells expressing Ccp1-GFP.

1.5) Cooperation between antioxidant enzymes to buffer *endogenous* H_2O_2 in *respiring* cells

When a fermentable carbon source such as glucose is depleted, yeast cells shift from fermentation to respiration, which is known as the diauxic shift.[46] Mitochondrial reactive oxygen species (ROS) increase during the diauxic shift. An imbalance between the generation and elimination of ROS is called oxidative stress.[47] ROS, such as hydrogen peroxide (H_2O_2), the superoxide radical anion ($O_2^{\cdot-}$), and the highly reactive hydroxyl radical ($OH^{\cdot-}$), can damage lipids, proteins, and DNA, causing cell death.[47] In humans, elevated ROS levels are associated with cancer, diabetes, and neurodegenerative disorders.[47–55]

Biochemical data for yeast indicate that mitochondrial H_2O_2 levels increase as respiratory metabolism is established.[26] Thus, fermenting yeast cells must be ready for this impending spike in mitochondrial ROS. They express antioxidant enzymes such as superoxide dismutases to catalyze $O_2^{\cdot-}$ removal and peroxidases and catalases to metabolize H_2O_2. Cooperation between antioxidant enzymes is needed to control ROS levels in cells. Yeast enzymes known to decompose H_2O_2 include catalases (Cta1 and Ctt1),[56–58] glutathione peroxidases (Gpx1, Gpx2, and Gpx3),[59] Ccp1[2] and thioredoxin peroxidases or peroxiredoxins (Tsa1, Tsa2, Ahp1, Prx1, and Tpx).[60–63] Respiring *ccp1Δ* cells show the highest levels of H_2O_2 but accumulation of H_2O_2 is less in respiring W191F vs WT cells, while mitochondrial Cta1 activity varies in cells as: *ccp1Δ* < WT < W191F. Also, mitochondrial superoxide dismutase Sod2 activity and total peroxiredoxins (Prx) activity varies in cells as: *ccp1Δ* > WT > W191F, and *ccp1Δ* cells show the lowest levels of $O_2^{\cdot-}$.[24]

The high activity of Cta1 in W191F cells results in a weak mitohormesis[64] response, which shortens lifespan.[24,65] Thus, Ccp1 is needed to maintain an advantageous H_2O_2 stress signal and adjust mitohormesis, which controls $O_2^{\cdot-}$ levels and Sod2 activity.[24] In other words, Ccp1 modulates other antioxidant enzymes to achieve a H_2O_2 level that is beneficial for respiring cells.[24]

1.6) Cooperation between antioxidant enzymes to buffer *exogenous* H_2O_2 in *fermenting* cells

Godon et al.[66] showed that 115 proteins respond to the challenge of fermenting yeast cells (OD_{600} 0.3) with a sublethal dose (0.2 – 0.8 mM) of exogenous H_2O_2. They largely focused on thiol-based H_2O_2 sensing proteins such as cytosolic glutathione peroxidase 3 (Gpx3), which conveys the redox signal to the transcription factor Yap1 to regulate the transcription of several antioxidants in the nucleus.[66,67] The transcription factor Skn7 also is involved in the cellular defense mechanism that regulates the oxidative stress response.[68] The regulation of Ccp1, Ctt1, Sod1, Sod2, Trr1, Trr2, and Tsa1 in response to H_2O_2 requires both Yap1 and Skn7, [69] and Ccp1 transmits the oxidative stress signal to Skn7 in the nucleus.[25,44]

Previously, our group challenged fermenting WT, *ccp1Δ,* and W191F cells (0.5-day) with 0.4 mM exogenous H_2O_2.[24] Consistent with Ccp1's role in activating Skn7, *ccp1Δ* cells showed low viability. This is attributed to the lack of stimulation of total Prx activity and of Ctt1 activity, and also to significantly repressed Sod1 and Sod2 activity.[24] Fermenting W191F cells were more viable than WT cells after H_2O_2 challenge and exhibited stimulated cytosolic Ctt1 activity and total Prx activity.[24] Also, mitochondrial Sod2 activity was repressed in H_2O_2-challenged WT and

W191F cells but cytosolic Sod1 was repressed only in the latter.[24] Combined, these results reveal that nuclear Ccp1 regulates the activity of other antioxidant enzymes to protect fermenting cells against exogenous H_2O_2. In my research (Chapter 4), we have identified a large number of H_2O_2-responsive proteins after challenge of fermenting WT and W191F cells to better elucidate the cell's adaptation to exogenous H_2O_2.

1.7) The H_2O_2 stimulon in *fermenting S. cerevisiae*

In 1998, a total of 115 proteins responsive to exogenous H_2O_2 were identified in the YPH98 strain of *S. cerevisiae* using 2D-gel electrophoresis.[66] Antioxidant enzymes were stimulated to buffer the elevated ROS in fermenting cells in response to challenge with a sublethal dose of H_2O_2.[66] Moreover, stimulation of heat shock proteins, proteases and proteasome subunits and repression of proteins involved in the translation apparatus and ribosome biogenesis, and of enzymes involved in amino acid biosynthesis also protected fermenting cells against exogenous H_2O_2.[66] In sum, the identification of 44 repressed and 71 stimulated proteins revealed increased antioxidant defense, decreased biosynthesis, and redirection of carbohydrate fluxes to NADPH regeneration.

We re-examined the H_2O_2 stimulon regulated by Ccp1 in the BY4741 strain of *S. cerevisiae* in response to challenge with sublethal H_2O_2. Specifically, we compared the proteomes following H_2O_2 challenge of fermenting yeast producing WT Ccp1 and its W191 variant, an amplified H_2O_2 sensor, to better elucidate Ccp1's role in coordinating the cell's response to H_2O_2.

1.8) Use of label-free proteomics to quantify the H_2O_2 stimulon in *fermenting* cells following H_2O_2 challenge

In 1995, the term *proteomics* was defined for the first time.[70] Proteomics has been used for the global analysis of protein abundance.[71] Proteomics allows us to probe the abundance and biological functions of large numbers of proteins in cells. Labeled quantification using SILAC (stable isotope labeling by amino acids in cell culture) or TMT (tandem mass tags) is a robust approach to achieve high-quality quantitative measures of the proteome with only a small amount of total protein extract. However, label-free proteomics was selected in this research because (1) it requires less sample preparation, (2) is less time consuming, (3) allows more flexibility in study design, (4) is less expensive, and (5) samples from different runs can be straightforwardly compared with each other. In labeled-quantitation experiments only those samples that were physically mixed in the same run can be directly compared.

In my research, label-free proteomics was used to investigate the impact of the W191F mutation in Ccp1 on the H_2O_2 stimulon. Such functional proteomics requires the analysis of many samples so we minimized sample processing to increase reproducibility. For example, proteins were collected in a single band on a 6% stacking gel for all samples. Trypsin in-gel digestion was performed, and the tryptic peptides were analyzed by LC-MS/MS. MS/MS sequencing was done following data dependent acquisition (DDA) of the ten most abundant multiply charged ions in a narrow window (2 Da) per cycle time (2 - 4 s).[72] The opposite approach, data independent acquisition (DIA), continuously selects all charged ions for fragmentation to effect MS/MS sequencing. DIA provides more data but needs further deconvolution analysis due to loss of direct correlation between a precursor ion and its fragment ions.[72,73] In my research, ~1700 proteins were identified, and the fold change in their abundance calculated as outlined in Section 4.4.6.

1.9) Outline and scope of the thesis

ROS such as H_2O_2 trigger ROS-sensing and signaling functions in cells. The yeast heme peroxidase, Ccp1, is a suitable model for the study of the non-peroxidase functions of heme peroxidases *in vivo*. Although human cells do not express a protein with cytochrome c peroxidase activity, a better understanding of Ccp1's roles in coordinating the H_2O_2-stress response in yeast will shed more light on how this response is regulated in other eurkaryotic cells and possibly lead to the identification of functional homologues in human cells, which would inform the diagnosis and treatment of ROS-associated diseases.

In yeast mitochondria, Ccp1 functions as a heme-based H_2O_2 sensor that releases its heme in respiring cells. This suggests that the change in its heme status is a key determinant of its physiological role. Thus, in **Chapter 2**, ratiometric fluorescence lifetime measurements of a Ccp1-GFP fusion were investigated *in vitro* as a method for probing Ccp1-heme binding in live cells. The aim of this study was the photophysical characterization of heme-loaded and heme-free recombinant Ccp1-GFP to determine its suitability as a probe to track heme binding to Ccp1 in cells. Our Ccp1-GFP probe successfully estimated the percentage of holoCcp1 in mixtures of apo- and holoCcp1 *in vitro* so the next step was to examine the suitability of this probe *in vivo.*

In **Chapter 3**, the post-translation modification of Ccp1 by noncovalent insertion of heme was tracked spatiotemporally by FLIM in live cells chromosomally expressing Ccp1-GFP. The specific aims of this study were to: (1) monitor the location of heme-loaded and heme-free forms of Ccp1 in respiring live yeast cells from 2- and 7-day cultures, and (2) estimate the percentage of heme-loaded and heme-free Ccp1 in subcellular compartments in the same cells. The FLIM data confirm that Ccp1 acts as a heme donor in respiring cells and supports our hypothesis that

recruitment of Ccp1's heme by Cta1 defends cells against excess H_2O_2 produced as a by-product of respiration.

Ccp1 senses H_2O_2 by oxidation of its single heme[9,24,74] and we[24] and others[44] have shown that its W191F variant exhibits amplified H_2O_2 sensing and signaling. This led us to ask what proteomics would divulge about how fermenting cells with normal vs amplified sensing/signaling respond to challenge with exogenous H_2O_2. Thus, the study **Chapter 4** investigates at the proteome level the impact of the W191F mutation in Ccp1 on the H_2O_2 stimulon in yeast. Using mass spectrometry-based label-free, peptide-centric, proteomics we identified numerous H_2O_2-responsive proteins and found that amplified H_2O_2 sensing can be linked to a more persistent suppression in cells of proteins involved in biosynthesis.

Ccp1W191F has no CCP activity but it does react rapidly with H_2O_2 like native Ccp1. To understand at the molecular level why Ccp1W191F is a better H_2O_2 sensor than WT Ccp1, in **Chapter 5** we compare the oxidized forms of the recombinant proteins following their reaction with excess H_2O_2. The properties of the oxidized proteins differ considerably but the results do not provide clear insight into why Ccp1W191F is the better H_2O_2 sensor in cells.

1.10) Objectives of the thesis

Overall, the key objectives of the research presented in the thesis can be outlined as follows**:**

(a) Quantify heme-free and heme-loaded Ccp1 from ratiometric fluorescence lifetime measurements on its GFP fusion protein.

(b) Track in live cells where and when Ccp1 is post-translationally modified by insertion of noncovalent heme.

(c) Characterize the H_2O_2 stimulon in *S. cerevisiae* cells with normal (Ccp1) and amplified (Ccp1W191F) heme-based H_2O_2 sensing using label-free proteomics.

(d) Investigate at the molecular level why Ccp1W191F is a more efficient H_2O_2 sensor protein than WT Ccp1.

Chapter 2: Quantifying heme-protein maturation from ratiometric fluorescence lifetime measurements on the single fluorophore in its GFP fusion

2.1) Preface

The work presented in Chapter 2 was published in: Dastpeyman S, Godin R, Cosa G and English AM (2020). Quantifying Heme-Protein Maturation from Ratiometric Fluorescence Lifetime Measurements on the Single Fluorophore in Its GFP Fusion. J. Phys. Chem. A 124, 4, 746-754. RG taught SD the method of time resolved fluorescence spectroscopy and its TCSPC data analysis. The production and interpretation of other data, and revision of the manuscript was performed by SD. GC and AME contributed to discussion, data analysis, writing, editing and revisions of the paper.

2.2) Abstract

Protein maturation by heme insertion is a common post-translation modification of key biological importance. Nonetheless, where and when this maturation occurs in eukaryotic cells remain unknown for most heme proteins. Here we demonstrate for the first time that maturation of a chromosomally expressed, endogenous heme protein fused to green fluorescent protein (GFP) can be tracked in live cells. Selecting yeast cytochrome c peroxidase (Ccp1) as our model heme-binding protein, we first characterized the emission *in vitro* of recombinant Ccp1-GFP with GFP fused C-terminally to Ccp1 by the linker GRRIPGLIN. Time-correlated single-photon counting reveals a single fluorescence lifetime for heme-free apoCcp1-GFP, τ_0 = 2.84 ± 0.01 ns. Heme bound to Ccp1 only partially quenches GFP fluorescence since holoCcp1-GFP exhibits two lifetimes, τ_1 = 0.95 ± 0.02 and τ_2 = 2.46 ± 0.03 ns with fractional amplitudes a_1 = 38 ± 1.5% and a_2 = 62 ± 1.5%. Also, τ and a are *independent* of Ccp1-GFP concentration and solution pH between 5.5 and 8.0 plus a standard plot of a_1 vs % holoCcp1-GFP in mixtures with apoCcp1-GFP is linear, establishing that the fraction of Ccp1-GFP with heme bound can be determined from a_1. Fluorescence lifetime imaging microscopy (FLIM) of live yeast cells chromosomally expressing the same Ccp1-GFP fusion revealed 30% holoCcp1-GFP (*i.e.*, mature Ccp1) and 70% apoCcp1-GFP in agreement with biochemical measurements on cell lysates. Thus, ratiometric fluorescence lifetime measurements offer promise for probing heme-protein maturation in live cells and we can dispense with the reference fluorophore required for ratiometric intensity-based measurements.

2.3) Introduction

Fluorescence proteins (FPs) have been used in cells to probe protein expression,[75] protein localization,[27] protein-protein interaction,[76] pH[28] and chloride[29–31] and calcium levels.[32,33] Also, the fluorescence intensity of GFP-His_6,[35] GFP10C-S147H/Q204H, and GFP10C-E95H/Q184H[34] has been monitored to determine zinc, copper, cadmium and nickel ion concentrations *in vitro,* while a fusion of cytochrome b_{562}, a heme-binding protein, and enhanced GFP ($Cytb_{562}$-EGFP) can function as a heme sensor.[36–38]

We aim to monitor maturation of endogenous heme proteins expressed under the control of their natural promoters in live cells. This post-translational modification (PTM) involves noncovalent heme insertion into the apoprotein but where and when maturation occurs have not been established for most heme proteins as very little is known about heme trafficking in eukaryotic cells. A heme protein of current interest is cytochrome c peroxidase (Ccp1) since we have demonstrated using heme blotting of cell lysates that Ccp1 exists in the holoform in fermenting yeast but the apoform appears in respiring cells.[24,26] Fusing Ccp1 to a FP should report on its maturation since many studies have demonstrated the high quenching efficiently of bound heme in fusions. For example, adding heme to a circularly permutated apo$Cytb_{562}$-EGFP fusion quenches its fluorescence 100%.[36] On the other hand, $Cytb_{562}$-EGFP with a Gly-Ser linker[37,38] could not be fully heme loaded and its fluorescence could not be fully quenched because the short linker interferes with heme binding.[37] Clearly, the choice of linker between the FP and heme-binding protein is key to the fusion's reliability in reporting on its heme binding.

Most full-length ORFs in yeast have been C-terminally tagged with GFP (*Yeast GFP Clone Collection*) using a nine-residue linker (GRRIPGLIN). The Ccp1 clone from this collection has been examined in a number of studies and we already know that: (i) the Ccp1-GFP fusion protein is processed in the cell in the same manner as native Ccp1;[19] (ii) mature Ccp1-GFP correctly localizes to the mitochondrial intermembrane space (IMS) in fermenting cells;[26] and (iii) apoCcp1-GFP accumulates in respiring cells as does native apoCcp1.[26] Thus, we hypothesized that Ccp1-GFP with the GRRIPGLIN linker would be a suitable sensor of mature Ccp1 in live cells. In this study we test this hypothesis by examining Ccp1-GFP fluorescence *in vitro* and *in vivo*.

Specifically, recombinant Ccp1-GFP was purified from *E. coli* cells and the fluorescence properties, including fluorescence lifetimes, of apo- and holoCcp1-GFP were characterized in detail. Importantly, we note that the Ccp1-GFP fusion examined here is fluorescent in both its apo- and holoforms. We further note that the fluorescence lifetimes report on heme binding to Ccp1-GFP and are independent of its concentration and solution pH, unlike fluorescence

intensity. These key attributes of Ccp1-GFP guided our analysis using fluorescence lifetime imaging microscopy (FLIM) of heme binding to Ccp1 in live yeast cells chromosomally expressing Ccp1-GFP under the native Ccp1 promoter. Our results clearly demonstrate the potential of ratiometric fluorescence lifetime measurements in monitoring endogenous protein maturation by heme binding in live cells. In particular, monitoring lifetimes obviates the need for the second, heme-insensitive reference FP required in ratiometric fluorescence-intensity measurements to correct for any variation in concentration. Fusing a protein of interest to more than one FP is undesirable since this increases the likelihood that its localization and maturation in the cell will be altered compared to the native protein.

2.4) Materials and Methods

2.4.1) Materials

Suppliers of (bio)chemicals were as follows: hemin protoporphyrin IX chloride, LUDOX colloidal silica, horse heart myoglobin, ampicillin , IPTG, sequencing grade modified trypsin from porcine pancreas, DEAE-Sephacel (Sigma Aldrich), thrombin (Calbiochem), DTPA (ICN Biomedicals), HPLC grade acetonitrile (Fisher Scientific), Ni-NTA Agarose (QIAGEN GmbH) and CentriPure P10 gel filtration columns (emp Biotech). All other chemicals were the purest grades available. Ccp1-GFP expressing *Saccharomyces cerevisiae* BY4741 strain was purchased from Invitrogen Life Sciences (Yeast GFP clone collection; Clone: YKR066C, Plate No: GFP(+)21 and Well No: D12).

2.4.2) ApoCcp1-GFP-His_6 expression and purification

BL21(DE3) *E. coli* cells expressing GFP-His_6 and Ccp1 C-terminally fused to GFP-His_6 via the GRRIPGLIN linker were prepared by TopGene Technologies (Montreal, QC). The sequence encoding mature Ccp1-GFP in *S. cerevisiae* (GFP-tagged ORF YKR066C) was amplified by PCR using forward primer
5'-CAATTCCCCTCTAGAAATAATTTTGTTTAACTTTAAGAAGGAGATATACATATGACTACA
CCGCTCGTTCATGT-3' and reverse primer
5'-GTGATGGTGCTCGAGGCTGCCGCGCGGCACCAGGTATAGTTCATCCATGCCATG-3',
and cloned into the *NdeI* and *XhoI* sites of the pET21a vector (Figure A2.1). This vector expresses Ccp1-GFP-His_6 with a thrombin cleavage site to allow removal of the His_6 tag. The Ccp1-GFP-His_6 insert was sequenced (Table A2.1), and it corresponds to isoform 2 of mature Ccp1 (294 amino acid residues plus M at position -1) with a single point mutation E167D on the protein's surface linked by GRRIPGLIN[77] to 236 residues of *Aequorea victoria* GFP (S65T, Q80R minus M1 and K238).[78] Extensive mutation of GFP has been performed to optimize its properties

and the S65T mutation increases fluorescence, photostability and shifts the major excitation peak to 488 nm[79] whereas the trivial Q80R mutation is present in many constructs.

Ccp1-GFP-His_6 was overexpressed in BL21 (DE3) cells. LB medium (10 mL) supplemented with 100 µg/mL ampicillin was inoculated with a single clone, and after overnight growth at 37°C with shaking at 225 rpm, 5-mL cultures were diluted into 500 mL of fresh LB medium with 100 µg/mL ampicillin, and incubated at 37°C/225 rpm to OD_{600} ~0.8 (~ 2 h). The temperature was lowered to 18°C, 0.6 mM IPTG added, and maturation of the GFP fluorophore appeared complete after 20 h (Figure S2.1), which was confirmed by ESI-MS (Figure S2.2). Cells were harvested by centrifugation at 5000 g for 20 min at 4 °C, the pellet was resuspended in 25 mL of lysis buffer [20 mM HEPES pH 7.5, 500 mM NaCl, 10% glycerol, 10 mM imidazole, 100 µg/mL lysozyme] on ice, and after 15 min, cells were lysed by 3 freeze/thaw cycles in LN_2/37°C H_2O baths followed by 8 x 10-s cycles of sonication. The lysate was centrifuged at 12000 g for 20 min at 4 ºC, the supernatant was collected and 10 mL was added to a 15-mL Falcon tube containing 2 mL of Ni-NTA Agarose that had been washed with deionised water and twice with lysis buffer. Ccp1-GFP-His_6 was bound to the resin with gentle rotation at 4°C for 1 h, the sample was centrifuged at 1000 g for 5 min, and after removing the supernatant, the resin was washed twice with wash buffer (20 mM HEPES pH 7.5, 500 mM NaCl, 10% glycerol, 10-25 mM imidazole). Bound Ccp1-GFP-His_6 was eluted from the resin with the Ni-NTA elution buffer (20 mM HEPES pH 7.5, 500 mM NaCl, 10% glycerol, 500 mM imidazole). Elution was performed twice, the supernatants were combined, and dialyzed (6 kDa MW cut-off membrane; Spectra/Por) overnight with stirring against 2 x 4 L of dialysis buffer [20 mM potassium phosphate (KPi) pH 7.0, 10 % glycerol, 100 µM DTPA] at 4 °C. Heme-free apoCcp1-GFP-His_6 was isolated from *E. coli*, its concentration was determined spectrophotometrically using ε_{488} (mM^{-1} cm^{-1}) = 39.4 (39.2 for GFP[80] + 0.2 for apoCcp1), and it was stored at -80 °C. A typical yield of apoCcp1-GFP-His_6 was ~ 60 mg/L.

The sequence encoding GFP only also was amplified by PCR from clone YKR066C using forward primer 5'-CAAAGATGACGGGAACTAC-3' and reverse primer 5'-TAGACGTACCGTACAAACG-3', and cloned into the *NdeI* and *XhoI* sites of the pET21a vector to express GFP-His_6 (Figure A2.1). DNA sequencing (Table A2.2), confirmed expression of the GFP-His_6 construct described above, and GFP-His_6 was overexpressed, purified and stored at -80 °C as outlined for Ccp1-GFP-His_6. The typical GFP-His_6 yield was ~ 60 mg/L assuming ε_{488} = 39.2 mM^{-1} cm^{-1}.[80]

2.4.3) Reconstitution of apoCcp1-GFP-His_6 and apoCcp1-GFP with heme

The His_6 tag was cleaved from 1 mg of purified Ccp1-GFP-His_6 by incubation with 1 μg (500 U) of thrombin for 1 h at 4 °C with rotation in 20 mM KPi pH 7.0. The free His_6 tag and any remaining tagged protein were removed by adding Ni-NTA resin as confirmed by LC-ESI-MS (Figure S2.2B). A stock 720-μM hemin protoporphyrin IX chloride solution was prepared in 0.1 N NaOH, filtered through a 0.45-μm nylon filter (Millipore), and the heme concentration was determined using the pyridine hemochromogen assay (ε_{557} = 34.4 mM^{-1} cm^{-1}).[81] Purified apoCcp1-GFP-His_6 or apoCcp1-GFP (30 μM) was incubated with rotation in 20 mM KPi pH 7.0 with 1.1-fold molar excess of heme for 15 min at 4 °C. Excess heme was removed on a 20 x 100-mm DEAE-Sephacel column, protein was eluted with 20 mM MES pH 6.5 with 500 mM NaCl, and stored at -80 °C.

2.4.4) UV–Visible absorption and steady-state fluorescence spectroscopy

Spectra were recorded at room temperature in 1-cm quartz cuvettes in the buffers indicated in the figure captions. We added 100 mM NaCl to the buffers (where indicated) since Cl^- binds close to the GFP fluorophore and modulates its emission (Figure S2.3). Also, high NaCl mimics physiologic salt conditions. DTPA (100 μM) also was added to inhibit any redox processes induced by trace-metal impurities. Absorption and fluorescence measurements were recorded, respectively, on a Beckman Coulter DU800 UV-Visible spectrophotometer at 1-nm resolution and on a Cary Varian Eclipse spectrofluorometer (Model FL0812M000) with 5-nm excitation and emission slits and the photomultiplier tube set at 600 V. For the fluorescence measurements, buffers and sample solutions were filtered through a 0.2-μm polyethersulfone (PES) filter (VWR), and sample absorbance was ≤ 0.05 to avoid inner-filter effects and ensure linearity of the fluorescence intensity.

2.4.5) GFP lifetime determination by time-correlated single photon counting (TCSPC)

Time-resolved fluorescence decay was monitored on a Picoquant FluoTime 200 spectrometer with a time-correlated single photon counting (TCSPC) PicoHarp 300 module consisting of 65,536 histogram time bins of 4 ps minimum width. Ccp1-GFP was added to buffers containing 10 mM KPi, 10 mM MES, 100 mM NaCl, 100 μM DTPA in pH the range 5.5–8.0. Notably, Cl^- does not modulate the fluorescence lifetime of GFP[31] but NaCl was added to the buffers as before. The absorbance was ≤ 0.05 at 488 nm for GFP and apoCcp1-GFP, and ≤ 0.05 at 408 nm for holoCcp1-GFP to avoid PMT saturation. GFP fluorescence decay was measured at room temperature following excitation at 467 nm from a pulsed diode laser (360 μW per 0.47-ns pulse, 10-MHz repetition rate; Picoquant).[82] With the polarizer set at the magic angle (54.7°) to remove fluorescence anisotropy contributions, GFP emission was detected at

510 nm using a PMT. Although GFP was excited by the laser every 100 ns (10 MHz), the photon-count rate was limited to one per 5 μs (0.2 MHz) to exceed the detector dead time and prevent pulse pile-up. Photons were recorded until the peak channel contained ~10^4 counts. The instrumental response function (*IRF*) was measured using LUDOX colloidal silica, and fluorescence decay curves were best fit to mono- or biexponential decay functions by iterative reconvolution with the *IRF* using FluoFit data analysis software (PicoQuant). Only fits with χ^2 values close to 1 and residuals randomly distributed around 0 were deemed acceptable.

2.4.6) Confocal fluorescence lifetime imaging microscopy (FLIM)

FLIM was performed using a Zeiss LSM 710 microscope equipped with a fluorescence-lifetime module (PicoQuant FLIM Kit), which includes a 50-MHz pulsed laser diode emitting at 473 nm, GFP emission filter (520 ± 17 nm), a single-photon avalance diode (tau-SPAD) and a Picoharp 300 module. The laser power was < 2.5 μW to minimize GFP photobleaching, and the photon-count rate was 2.5 MHz. The components of the FLIM Kit were synchronized to the scanning of the confocal microscope to assign each photon to a pixel in the image.

2.5) Results

2.5.1) Absorption spectra of apo- and holoforms of recombinant Ccp1-GFP

Following confirmation by mass spectrometry that Ccp1-GFP-His_6 was isolated from *E. coli* with GFP in its mature form (Figure S2.2), the fusion protein was characterized spectroscopically. Its absorption spectrum (Figure 2.1A) shows protein (280 nm) and GFP peaks (488 nm) and trace heme absorption at 408 nm, revealing that Ccp1 is isolated mainly as the apoform (Figure 2.1A). Also, the spectrum of apoCcp1-GFP-His_6 (Figure 2.1A) corresponds to the sum of the spectra of apoCcp1-His_6 and GFP-His_6 so the fusion retains the absorption properties of the individual proteins.

Before adding heme to apoCcp1 in the fusion protein, the His_6 tag was removed as it also binds heme. This is evident from the Soret (412 nm) plus visible bands (533 and 560 nm) of GFP-His_6 (Figure S2.4A), which signal the presence of bis-His ligated low-spin heme[83] following addition of heme and removal of its excess. The weak shoulder around 350 nm may arise from some high-spin heme. Only a weak broad band appears at ~ 400 nm when heme is added to tag-free GFP (Figure S2.4A), confirming that the His_6 tag binds heme.

Heme titration of apoCcp1-GFP shows the expected 1:1 stoichiometry (Figure 2.1B). Following removal of excess heme, the Soret band of holoCcp1-GFP is at 408 nm (Figure 2.1C) as reported for holoCcp1.[1,84–87] An A_{408}/A_{280} ratio of 0.98 is predicted for holoCcp1-GFP from the sum of the extinction coefficients of holoCcp1 and GFP but the observed value is 1.15 (Figure 2.1C), which may arise from a little nonspecific heme binding to the GFP moiety (Figure S2.4).

Since the His_6 tag binds heme and interferes with Ccp1 heme absorption in holoCcp1-GFP-His_6 (Figure S2.4B), GFP fluorescence quenching was only examined in Ccp1-GFP after the His_6 tag was removed.

Finally, the catalytic activity of holoCcp1-GFP is similar to that of holoCcp1.[74] Average specific activities ± SD (μmol of ferrocytochrome c oxidized per mg Ccp1 per min) of 0.03 ± 0.01 (apoCcp1-GFP), 1.92 ± 0.02 (holoCcp1-GFP) and 1.70 ± 0.01 (holoCcp1) were calculated in three independent assays (n = 3) (Figure S2.5).

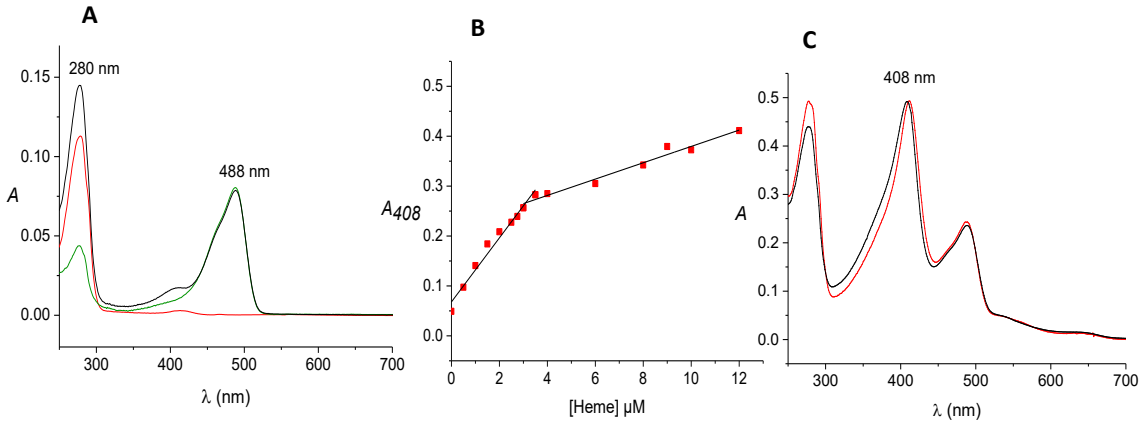

Figure 2.1. Absorption of Ccp1-GFP ± His_6 tag and titration of apoCcp1-GFP with heme. (A) UV-Vis spectra of 2 μM apoCcp1-His_6 (red trace), GFP-His_6 (green trace) and apoCcp1-GFP-His_6 (black trace). (B) Spectrophotometric titration at 408 nm of 3.0 μM His_6-tag-free apoCcp1-GFP with heme (added as hemin protoporphyrin IX chloride). The break point at 3.0 μM reveals the expected 1:1 stoichiometry for heme binding to apoCcp1. Note, the lines through the data points serve as a visual guide only. (C) UV-vis spectra of 5 μM holoCcp1-GFP (black line) overlayed on the sum of the spectra of 5 μM holoCcp1 and 5 μM GFP (red line) (see Figure S2.6). Proteins were dissolved in 10 mM KPi, 10 mM MES, 100 mM NaCl, 100 μM DTPA at pH 7.0 and absorption was measured in 1-cm cuvettes at room temperature.

2.5.2) Dependence of GFP fluorescence intensity on Ccp1-GFP concentration, added heme and solution pH

As expected, apoCcp1 does not emit when excited at 488 nm but essentially identical emission spectra with a maximum at 510 nm were recorded for apoCcp1-GFP-His_6 and GFP-His_6 (Figure 2.2A). Figure 2.2B reveals that apoCcp1-GFP fluorescence intensity decreases on dilution and on heme addition. Since heme significantly quenches GFP-His_6 fluorescence (Figure S2.7A), the affinity tag was removed from apoCcp1-GFP-His_6 to examine quenching by Ccp1-bound heme only, as was required in the absorption studies (Figure S2.4B). Quenching of

tag-free GFP fluorescence by free heme (Figure S2.7A), holoCcp1 or holomyoglobin (Figure S2.7B) is negligible, revealing that noncovalent complexation of heme or the hemoproteins with GFP also is negligible. The fluorescence intensity of Ccp1-GFP also varies with pH (Figure 2.2C and Figure S2.8). In fact, the emission and absorption of free GFP and Ccp1-GFP exhibit the same pH dependence (Figure S2.8) since this is an intrinsic property of the GFP fluorophore,[28]

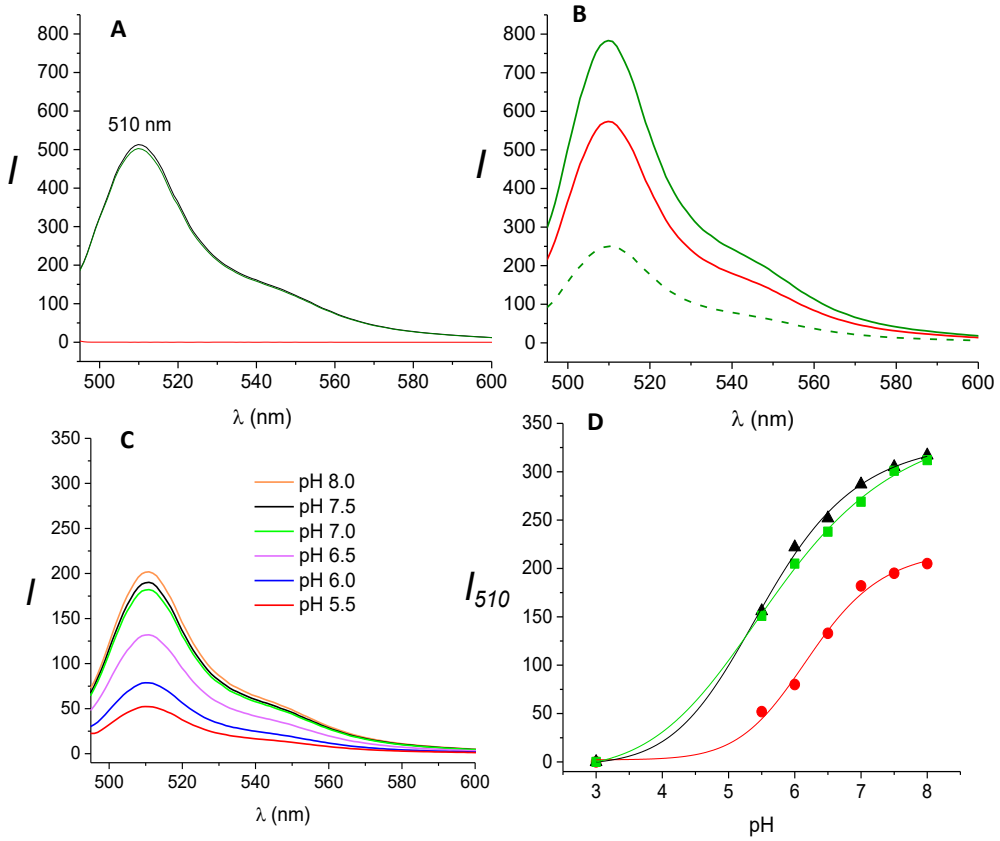

Figure 2.2. Steady-state fluorescence intensity (*I*) vs Ccp1-GFP concentration, heme loading and pH. Emission spectra upon excitation at 488 nm in 1-cm cuvettes at room temperature of: (A) 0.4 μM apoCcp1-His$_6$ (red line), GFP-His$_6$ (green line) and apoCcp1-GFP-His$_6$ (black line) recorded in 20 mM KPi pH 7.0; (B) 1 μM apoCcp1-GFP (solid green line), 0.4 μM apoCcp1-GFP (dotted green line) and 1 μM holoCcp1-GFP (red line) in 20 mM MES pH 6.5; and (C) 0.4 μM holoCcp1-GFP in 10 mM KPi, 10 mM MES, 100 mM NaCl and 100 μM DTPA. Either NaOH or HCl was added here to adjust the pH. Following subtraction of buffer emission, spectra were recorded at 600 nm/min with 5-nm slits and represent the average of 10 scans. (D) Plots of emission intensity at 510 nm (I_{510}) vs pH for holoCcp1-GFP ●, and for GFP-His$_6$ ■ and apoCcp1-GFP-His$_6$ ▲ based on the data in Figure S2.8A,B. The solid lines show fits of a logistic function to the data (OriginPro 2016) with a pK_a value of 6.0 ± 0.2 for the GFP fluorophore (see text).

which transitions from a nonfluorescent state with ~390-nm absorption to a fluorescent state that absorbs at 488 nm.[28] A pK_a of ~ 6 [28,88] has been reported for this transition and our plots of I_{510} vs pH (Figure 2.2D) are consistent with this value. In summary, the data in Figure 2.2 reveal that the observed fluorescence *intensity* depends on concentration and pH as well as heme binding. Since protein expression levels and local pH can vary in cells, a property of Ccp1-GFP that is sensitive to heme loading only is desirable. Thus, we next investigated the concentration and pH dependence of fluorescence lifetimes.

2.5.3) Time-resolved fluorescence of free GFP and Ccp1-GFP

TCSPC was used to measure the time dependence of GFP and Ccp1-GFP fluorescence decay, following pulsed-laser excitation at 467 nm. After counting ~10^4 photons at the peak time-bin per sample, histograms of fluorescence decay at 510 nm vs time were constructed (Figure S2.9). The decay models stated in the caption to Figure 2.3 were fitted to traces derived from the histograms using FluoFit software, and the goodness-of-fit is demonstrated by reduced chi-squared (χ^2) values of ~ 1 plus the random distribution of the weighted residuals around zero as shown for apoCcp1-GFP in panel A and for holoCcp1-GFP in panel C of Figure 2.3. The semi-log decay traces are plotted in panels B and D following reconstruction from the fitted parameters. Heme-free, apoCcp1-GFP exhibits monoexponential decay with a lifetime (τ_0) of 2.84 ± 0.01 ns (panel A, B). The same value was obtained for free GFP (data not shown), in excellent agreement with the reported value of 2.9 ns.[89] HoloCcp1-GFP, on the other hand, exhibits biexponential decay with long (τ_2 = 2.46 ± 0.03 ns) and short (τ_1 = 0.95 ± 0.02 ns) lifetimes of 62 ± 1.5% and 38 ± 1.5% fractional amplitude (a_2, a_1), respectively (panel C, D).

2.5.4) Ccp1-GFP fluorescence lifetimes and amplitudes vs concentration and pH

GFP and apoCcp1-GFP exhibit the same monoexponential decay (τ_0 = 2.84 ± 0.01 ns) that does not vary over the concentration range 0.2–0.8 μM at pH 6.5 (Figure 2.4A). The two decays of holoCcp1-GFP also possess τ and a values that are concentration independent (Figure 2.4A). Furthermore, the lifetimes vary little with pH (Figure 2.4B); for example, holoCcp1-GFP exhibits τ_1 values of 0.93 ± 0.02 and 1.09 ± 0.03 ns with a_1 values of 39 ± 1% and 34 ± 1% at pH 6.0 and 8.0, respectively (Table S2.1). In fact, overall averages of all the lifetime data summarized in Figure 2.4 for 30 samples are: τ_0 = 2.84 ± 0.01 ns, τ_1 = 0.96 ± 0.04 ns (a_1 = 39 ± 1%) and τ_2 = 2.49 ± 0.04 ns (a_2 = 61 ± 1%). Hence, the excited-state lifetimes and their fractional amplitudes should exhibit negligible dependence on changes in Ccp1-GFP expression in cells or on local fluctuations in intracellular pH. On the other hand, GFP fluorescence intensity drops with pH since its fluorophore becomes protonated and the protonated form is non-fluorescent.[28]

In sum, as the ground-state concentration of the *unprotonated* GFP fluorophore decreases, the fluorescence intensity decreases (Figure 2.2C and Figure S2.8) but its lifetime remains the same (Figure 2.4B).

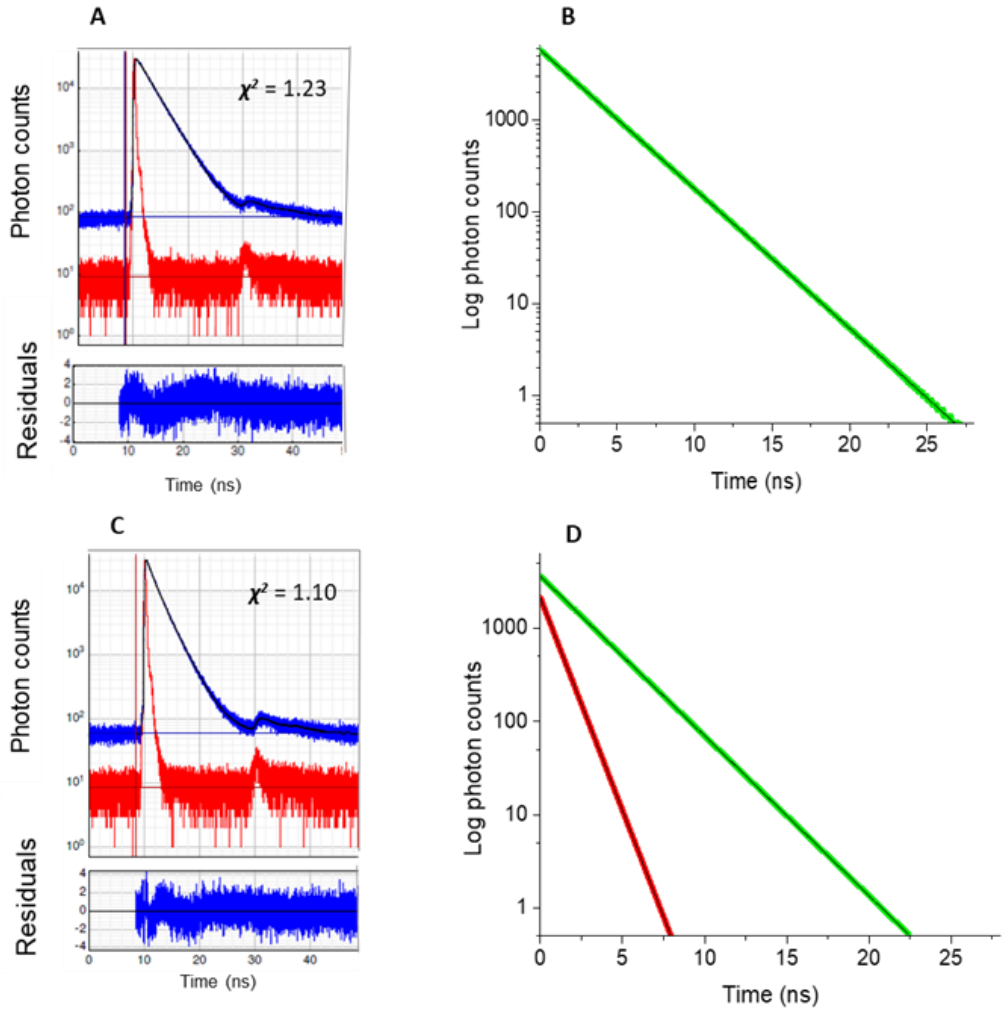

Figure 2.3. Analysis of apoCcp1-GFP and holoCcp1-GFP fluorescence by time-correlated single-photon counting. The large panels on the left show the TCSPC instrument response function (*IRF*, red trace), the fluorescence decay at 510 mn (blue trace) following excitation at 467 nm with a 0.47-ns laser pulse, and the fit (black trace) by: (A) monoexponential decay with χ^2 = 1.23 for apoCcp1-GFP, and (C) biexponential decay with χ^2 = 1.10 for holoCcp1-GFP. The small panels show weighted residuals (blue). Following *IRF* deconvolution, semi-log plots reveal (B) a single component extracted from the monoexponential fit (black line) with τ_0 = 2.84 ns (a_0 = 1.0) for apoCcp1-GFP and (D) two components extracted from the biexponential fit (black lines) with τ_1 = 0.95 ns (a_1 = 0.38) and τ_2 = 2.46 ns (a_2 = 0.62) for holoCcp1-GFP. Proteins (0.4 μM) were dissolved in 10 mM KPi, 10 mM MES, 100 mM NaCl, 100 μM DTPA at pH 6.5 in a 1-cm cuvette at room temperature. Data analysis was performed with FluoFit software (PicoQuant).

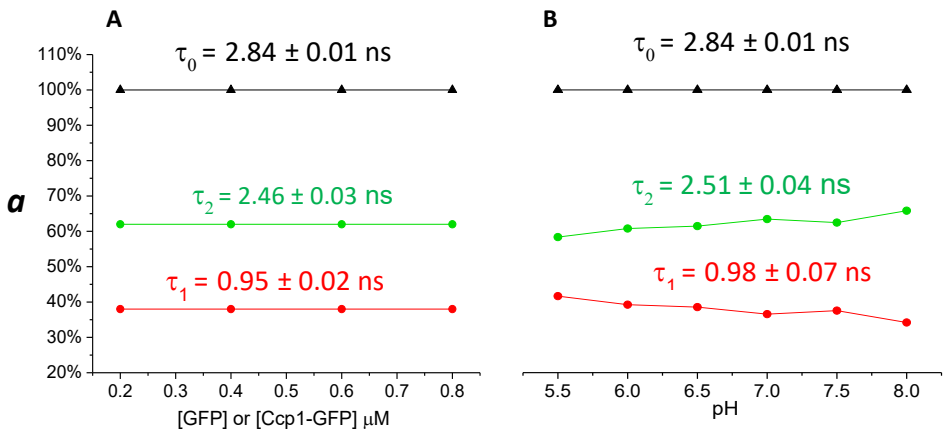

Figure 2.4. The fractional amplitudes (a) of the fluorescence lifetimes (τ) of GFP, apoCcp1-GFP and holoCcp1-GFP vs concentration and pH. The a_0 values for GFP •, a_0 for apoCcp1-GFP▲, a_1• for holoCcp1-GFP and a_2• for holoCcp1-GFP vs (A) concentration at pH 6.5 and (B) pH at 0.4 μM protein. Note that the black dots (•) are obscured by the triangles (▲) in both panels. The a values are averages of three independent samples at each concentration (data not shown) and each pH (Table S2.1) with SD values < 1.5%, which are within the symbols. The τ_0, τ_1, and τ_2 values listed in panel A and B each represent the overall averages ± SD of the same 12 and 18 samples (Table S2.1), respectively. Proteins were dissolved in 10 mM KPi, 10 mM MES, 100 mM NaCl, 100 μM DTPA and the pH was adjusted with NaOH or HCl. Fluorescence decay curves were analyzed as described in Figure 2.3.

2.5.5) Quantification of heme binding to Ccp1 from the fractional amplitude a_1 measured for mixtures of holo- and apoCcp1-GFP

Since holoCcp1-GFP exhibits a well-resolved short lifetime (τ_1), we predicted that its fractional amplitude a_1 would reliably indicate the percentage of holoCcp1-GFP in mixtures with apoCcp1-GFP.[90,91] Thus, mixtures containing known amounts of holo- and apoCcp1-GFP were prepared and their time-resolved fluorescence (Figure 2.5A) analyzed using a three-exponential decay model [Intensity = IRF(t)*a_0 exp(-t/τ_0) + a_1 exp(-t/τ_1) + a_2 exp(-t/τ_2), where t is time] with fixed lifetimes (τ_0 = 2.84, τ_1 = 0.95 and τ_2 =2.46 ns) to obtain the fractional amplitudes. As expected, a_1 expressed as a percentage increases linearly with the percentage of holoCcp1-GFP in a mixture (Figure 2.5B). Normalizing a_1 by its percentage in samples containing 100% holoCcp1-GFP, gives the fraction of holoCcp1-GFP recovered from a mixture. Thus, we plotted the recovered vs the known fraction of holoCcp1-GFP for each mixture and obtained a straight line with a slope of 0.97 and an intercept of 0.04 (Figure 2.5B, inset). The excellent recovery indicates that heme binding to Ccp1-GFP can be reliably quantified from the fractional amplitude a_1 of τ_1 of holoCcp1-GFP using a calibration curve retrieved from the data in Figure 2.5B.

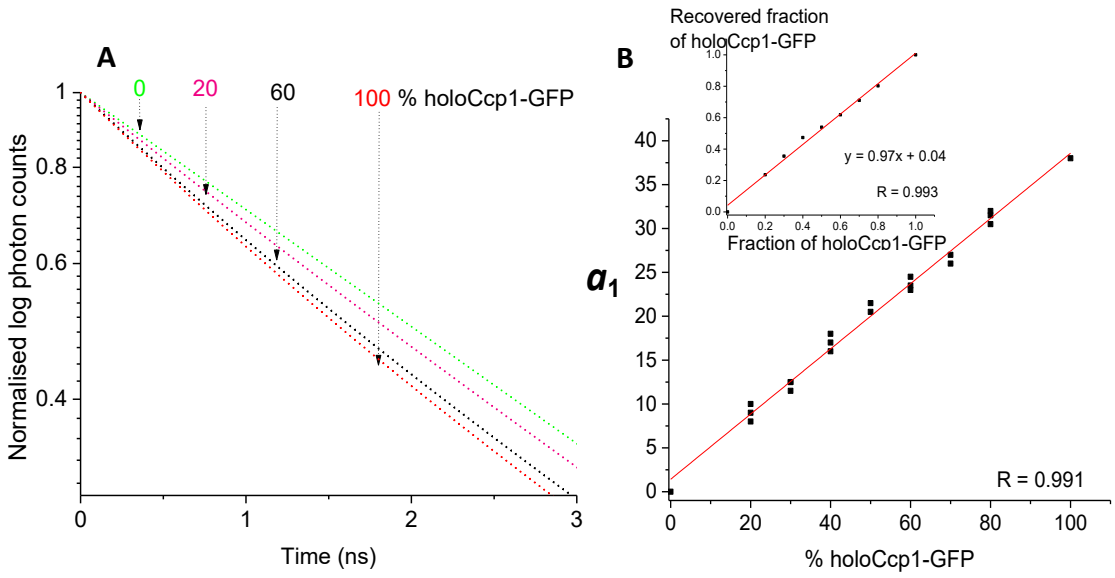

Figure 2.5. Variation in the fractional amplitude a_1 of the fluorescence lifetime τ_1 of holoCcp1-GFP in mixtures with apoCcp1-GFP. (A) Representative normalised fluorescence decay profiles of mixtures containing the indicted % holoCcp1-GFP recorded as outlined in Figure 2.3. (B) a_1 vs holoCcp1-GFP in percentages and (inset) the recovered fraction of holoCcp1-GFP (i.e., normalized a_1, see text) vs fraction of holoCcp1-GFP in the mixtures. The solid red lines show the linear fit (y = ax + b) to the data from 3 independent experiments (n = 3). Note slope of 0.97 for the plot in the inset. Proteins (0.8 μM total in each sample) were dissolved in 10 mM KPi, 10 mM MES, 100 mM NaCl, 100 μM DTPA at pH 6.5.

2.5.6) Levels of mature Ccp1 in live cells expressing Ccp1-GFP

Cells were grown in synthetic complete medium with dextrose (SCD) to reduce yeast autofluorescence.[92] Fast FLIM analysis of 7-day cultures (Figure 2.6A) showed an average lifetime of 2.30 ns or long (2.55 ns, 87%) and short components (0.65 ns, 13%). Based on our standard plot (Figure 2.5B), a short lifetime with an amplitude (a_1) of 13% indicates the presence of 30% mature holoCcp1-GFP in live cells. The FLIM image reveals that the short lifetime is localized in the mitochondria (insert, Figure 2.6A). We previously isolated mitochondria-enriched (P10) and extramitochondrial (S10) fractions of yeast cells expressing Ccp1-GFP,[26] and found using chemical heme staining that mature holoCcp1 is present only in the P10 mitochondrial fraction.[26] Western blotting of the P10 and S10 fractions revealed that 35 ± 5% of Ccp1-GFP is mitochondrial in 7-day cells (Figure 2.6B), which agrees with the FLIM finding that 30% of Ccp1-GFP is present as mature holoCcp1-GFP in mitochondria and 70% as extramitochondrial apoCcp1-GFP in live cells (Figure 2.6A).

2.6) Discussion

2.6.1) Lifetime vs intensity measurements to examine heme binding.

Since we wish to track its maturation, we desired a property of Ccp1-GFP that responds to heme binding but is independent of concentration. We demonstrate here that the fluorescence lifetime of GFP is such a property.

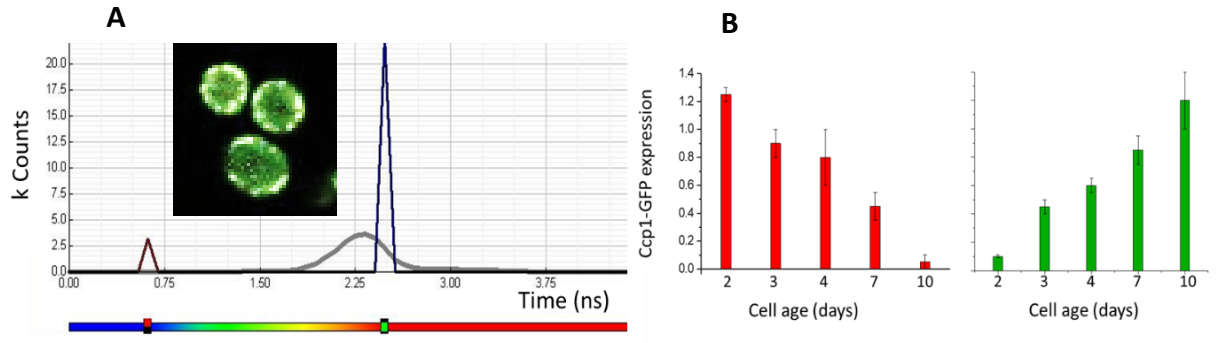

Figure 2.6: FLIM analysis of Ccp1-GFP in 7-day live yeast cells and subcellular localization of Ccp1-GFP. (A) The lifetime histogram obtained by Fast FLIM analysis of 20 cells using SymPhoTime 32 software without background correction. For all pixels, the arrival-time of each photon at the detector with respect to the laser pulse was binned and the lifetime histogram displays an average lifetime of 2.30 ns, which was resolved into fast and slow decaying components with lifetimes of 0.65 and 2.55 ns (red and green squares on color bar) with relative intensities of 13% and 87%, respectively. The results are representative of three independent cultures. The insert shows a FLIM image of representative 7-day cells with mature holoCcp1-GFP localized in the mitochondria (lighter dots; lifetime of 0.65 ns) and extramitochondrial apoCcp1-GFP (green dots, lifetime of 2.55 ns). (B) Plot of mitochondrial (red bars) and extramitochondrial levels (green bars) of Ccp1-GFP vs cell age. Ccp1-GFP expression levels were determined by SDS-PAGE gel electrophoresis and Western blotting of mitochonria-enriched and mitochondria-depleted subcellular fractions. The level of Ccp1-GFP was normalized using the sum of all Coomassie bands in the same lane of the SDS-PAGE gel as a loading control.[26]

ApoCcp1-GFP has a single long lifetime (τ_0 = 2.84 ± 0.01 ns) while holoCcp1-GFP exhibits short (τ_1 = 0.95 ± 0.02 ns) and long (τ_2 = 2.46 ± 0.03 ns) lifetimes. Thus, mixtures of holo- and apoCcp1-GFP can be analyzed using the known values of τ_0, τ_1 and τ_2 to obtain the fractional lifetime amplitudes. The amplitude (a_1) of the well-resolved short lifetime τ_1 increases linearly with the fraction of holoCcp1-GFP in a mixture.

Recently, a number of heme probes with two FPs fused to a heme-binding domain have been used to estimate labile heme concentrations in live cells by ratiometric or FRET (Förster resonance energy transfer) measurements.[40–43] The ratiometric probes were engineered such that only one FP is quenched on heme binding and the ratio of heme-sensitive to heme-insensitive intensity affords a readout of heme concentration independent of probe expression.

Since the heme-bound and heme-free forms of Ccp1-GFP exhibit resolved lifetimes, ratiometric lifetime measurements can be performed on its single fluorophore.

Importantly, we also find that Ccp1-GFP fluorescence lifetimes and their amplitudes (Figure 2.4B) are independent of the pH of the medium. Loss in steady-state fluorescence intensity with decreasing pH (Figures 2.2C, S2.8A,B), and parallel absorption changes (Figure S2.7C,D), arise because of a shift in ground-state equilibrium between the deprotonated, fluorescent form B of GFP (with 488-nm absorption) and its protonated, nonfluorescent form A (with 394-nm absorption).[28,88] Some loss of signal due to protonation will not invalidate ratiometric lifetime measurements on a single FP but the two FPs selected for ratiometric fluorescence intensity measurements should have pK_a values significantly lower than the pH of the medium to avoid errors due to ground-state protonation of the sensing or reference FP.

2.6.2) The GRRIPGLIN linker adopts compact and extended conformations

Heme quenching of GFP fluorescence in holoCcp1-GFP is ascribed to FRET. Analysis of FRET in holoCcp1-GFP (Figure S2.10, Table S2.1, S2.2) predicts heme-fluorophore separations of 39 ± 2 and 61 ± 2 Å. Values of 40 and 65 Å are estimated from a cartoon with the nine-residue GRRIPGLIN linker in helical and extended conformations, respectively (Figure 2.7). Two populations of conformations with limited variation in heme-fluorophore separation within each population would explain the observation of two discrete fluorescence lifetimes for holoCcp1-GFP. Conformations with a non-extended or helical linker are assigned the shorter lifetime τ_1 that is efficiently quenched by heme while those with an extended linker are assigned the longer lifetime τ_2, reflecting reduced quenching. Based on the relative magnitudes of α_2 (~60%) vs α_1 (~40%), the extended-linker conformations of Ccp1-GFP are marginally favored over compact conformations. Also, α_1 and α_2 show little pH dependence (Figure 2.4B), revealing that the populations of the compact and extended conformations remain relatively constant over the physiologic pH range.

The limited flexibility of the GRRIPGLIN linker in Ccp1-GFP arises in part from its central Pro. This residue provides stiffness and the absence of an amide hydrogen precludes H- bonding with other residues, thereby reducing interactions between the linker and the protein domains.[93] Polar Asn, on the other hand, may participate in H-bonding with other linker residues and/or with the protein domains and decrease their separation, while Leu and Ile increase the linker's propensity to adopt a helical formation. The positive charge on the adjacent Arg residues may decrease electrostatic repulsion in compact conformations between the GFP and Ccp1 domains, which both have low pIs (6.04 for GFP and 5.1 for Ccp1). The Arg residues also likely increase

the solvent accessibility of the linker[93] and indeed trypsin releases protease-resistant free GFP[94] from the fusion within 180 min (Figure S2.11).

Notably, apoCcp1-GFP exhibits one lifetime τ_0, which is the same as that of free GFP. Since no GFP quenching occurs in apoCcp1-GFP, fluorescence measurements (lifetimes or intensities) provide no information on the conformations of the apo-sensor. The fluorescence anisotropy of Ccp1-GFP is independent of heme binding (Figure S2.12), suggesting that there are no major conformational differences between its apo- and holoforms.

2.6.3) Fraction of mature Ccp1 in live 7-Day cells

Previous work in our group indicated that Ccp1 exits the mitochondria of respiring yeast in its apoform.[26] For example, we estimated by heme and Western blotting of subcellular fractions that only 35 ± 5% of mature holoCcp1-GFP remains in the mitochondria of cells chromosomally expressing the fusion protein from 7-day cultures (Figure 2.6B). Hence, we expected 35 ± 5% mature holoCcp1-GFP in 7-day cells, which was confirmed by FLIM (Figure 2.6A).

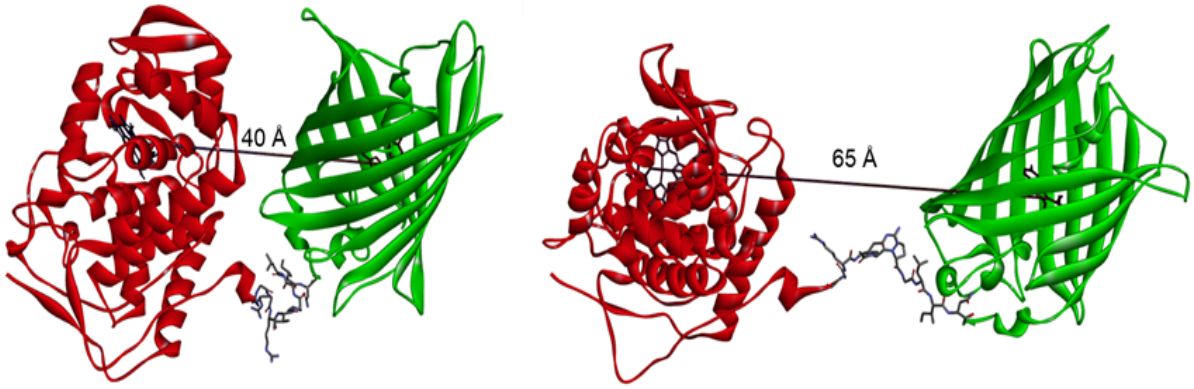

Figure 2.7. Cartoons prepared using Discovery Studio Visualizer of holoCcp1-GFP with the GRRIPGLIN linker in helical and extended conformations. The backbones of Ccp1 (PDB 1ZBY) and GFP (PDB 1EMA) are represented by red and green ribbons, respectively, and the linker (gray), Ccp1 heme (purple) and GFP fluorophore (black) are shown as sticks. The linker also was prepared in Discovery Studio Visualizer and joined to the C-terminus of Ccp1 and the N-terminus of GFP. The distance between the heme Fe and C1 of the fluorophore imidazole is indicated in the figure for each linker conformation. Based on the average fluorescence lifetimes of holoCcp1-GFP (τ_1 = 0.98 ± 0.07 ns, τ_2 = 2.51 ± 0.04 ns), FRET analysis predicts average heme-fluorophore separations of 39 ± 1.5 and 61 ± 1.5 Å (Table S2.1).

This good agreement between the biochemical and FLIM analysis of subcellular fractions[26] affirms that FLIM imaging of live cells can harness the power of ratiometric *lifetime*

measurements to directly and accurately indicate the fraction of an endogenous protein in its mature, heme-bound form.

A critical property of the Ccp1-GFP fusion examined here is that its GRRIPGLIN linker prevents 100% GFP fluorescence quenching by Ccp1-bound heme. In other sensors, such as circularly permutated $Cytb_{562}$-EGFP with a heme-fluorophore separation of 17 Å, EGFP fluorescence is completely quenched on heme binding to $Cytb_{562}$,[36] rendering its heme-bound form spectroscopically silent, which precludes ratiometric fluorescence lifetime analysis. To convert $Cytb_{562}$-EGFP into a quantitative heme sensor in cells, it was necessary to fuse EGFP to a second FP that was not quenched on heme binding to $Cytb_{562}$.[40] A similar approach would be required to quantify Ccp1 heme binding if holoCcp1-GFP were nonfluorescent. Instead, the relative amplitude a_1 of the well-resolved quenched lifetime τ_1 of holoCcp1-GFP provides a highly accurate ratiometric measure of heme binding to Ccp1 and of its mature form with heme bound in live cells. In sum, the resolution of fluorescence lifetimes enables a FP-fusion to function as a single-fluorophore ratiometric probe and dispenses with the need for a reference FP. This is important when selecting a probe for tracking heme-protein maturation in live cells since two FP tags are more likely than one to interfere with a protein's normal localization, processing and function. Hence, time-resolved fluorescence measurements offer more promise than intensity measurements for examining heme-protein maturation in live cells.

2.7) Conclusions

We demonstrate here that ratiometric fluorescence lifetime measurements on a Ccp1-GFP fusion reliably quantify heme binding to Ccp1 *in vitro* and *in vivo*. Crucial in the implementation of this technology is the use of a linker such as GRRIPGLIN that prevents complete fluorescence quenching by heme. Fortuitously, GRRIPGLIN also successfully links GFP to the C-terminal of most yeast ORFs so tracking the maturation of many yeast heme proteins may be possible using the current approach.

Finally, we note that heme staining can establish if heme is associated with a protein in whole-cell lysates or in subcellular fractions.[26] However, heme might repartition between proteins upon cell disruption so direct monitoring of a protein's heme status in live cells is desirable. This had not been reported until now for an *endogenous* protein chromosomally expressed under its natural promoter. Thus, we hope that our results will guide similar studies of heme-protein maturation in live cells in the future as well as the mapping of intracellular heme trafficking.

2.8) Supplementary information

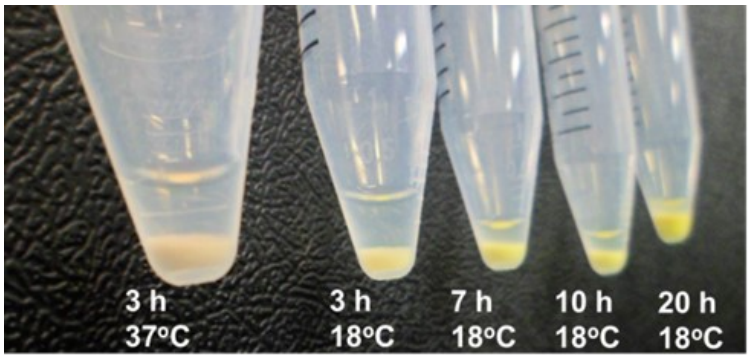

Figure S2.1. Time and temperature dependence of fluorophore maturation in Ccp1-GFP-His$_6$. Maturation of the GFP fluorophore is complete after 20 h at 18 °C. Note that maturation is not seen in the sample incubated at 37 °C for 3 h. See details of protein expression in the main text.

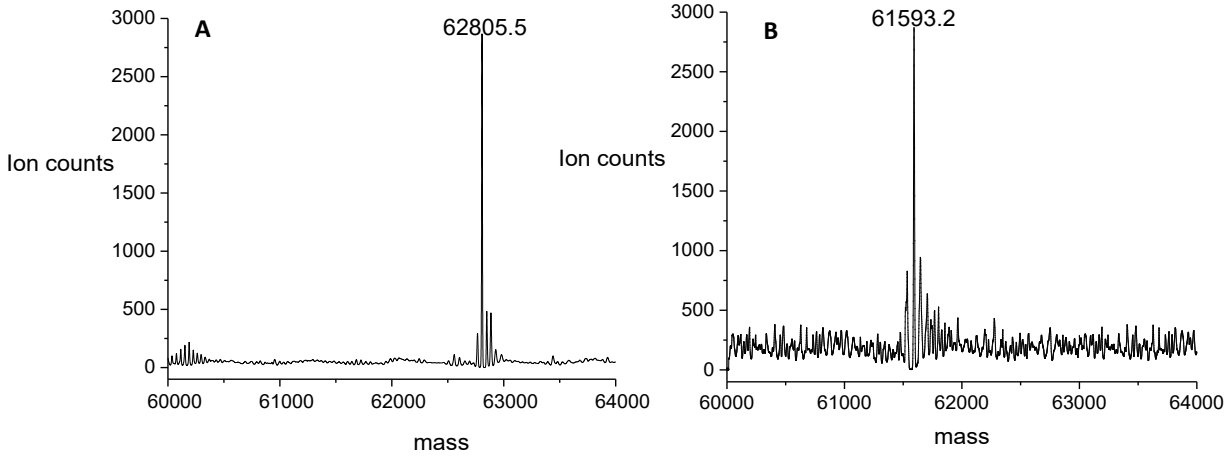

Figure S2.2. Deconvolved ESI mass spectrum of recombinant apoCcp1-GFP before and after His$_6$ tag removal. Spectra of: (A) Ni-NTA-purified apoCcp1-GFP-His$_6$ and (B) apoCcp1-GFP. To record the mass spectra, a 5-μL aliquot of 2 μM protein in 20 mM KPi plus 100 μM DTPA (pH 7.0) was injected onto a 2.1 x 150-mm C_3 column (Agilent) attached to an Agilent 1100 HPLC. Protein was eluted at 0.2 mL/min into the ESI source of a QToF2 mass spectrometer (Waters) using an acetonitrile gradient in 0.1% aqueous formic acid (0–95% acetonitrile in 15 min then 95% acetonitrile for 5 min). The Q-ToF2 parameters were: capillary +3.5 kV, cone +48 V, source temperature 80 °C, desolvation temperature 300°C, resolution 10,000, m/z range 500–2000. Using apomyoglobin as mass calibrant (Sigma), the mass accuracy was 72 ppm (avg mass: theoretical = 16,951.49 u; observed = 16,952.71 u).
The theoretical mass of Ccp1-GFP-His$_6$ is 62,801.4 u based on its sequence (https://web.expasy.org/compute_pi/) and a 20-u mass loss[95,96] on reaction of S65, Y66 and G67 to form the GFP fluorophore.[97] The observed mass of apoCcp1-GFP-His$_6$ was 62,805.5 ± 1.0 (65 ppm error), confirming that GFP was in its mature form. Removal of the His$_6$ tag (GSLEH$_6$) decreases the mass by 1,209.2 u to give a theoretical of 61,592.2 u vs an observed mass of 61,593.2 ± 0.7 u for apoCcp1-GFP (18 ppm error).

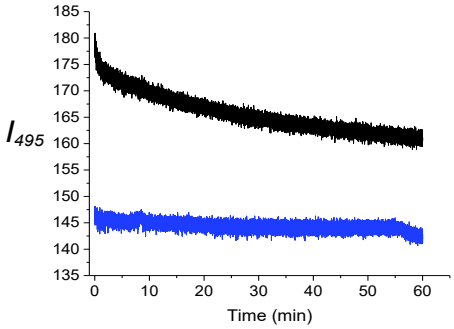

Figure S2.3. Room-temperature steady-state fluorescence at 495-nm of Ccp1-GFP over 60 min ± NaCl. Emission from 0.4 μM Ccp1-GFP in 20 mM MES pH 6.5, 100 μM DTPA without (black line) and with 100 mM NaCl (blue) as monitored following excitation at 488 nm using the Kinetics Module of the Cary Eclipse spectrofluorometer with a 15-W Xenon flash lamp with 1–1.5 μS flash duration. The emission intensity was captured every 0.1 s with 5-nm slits and the PMT at 600 V. Note that Cl^- binds near the GFP fluorophore and quenches fluorescence by electrostatically inhibiting its deprotonation, which lowers the concentration of the deprotonated, fluorescent form.[97] This property of FPs is exploited in halide-ion sensing.[27]

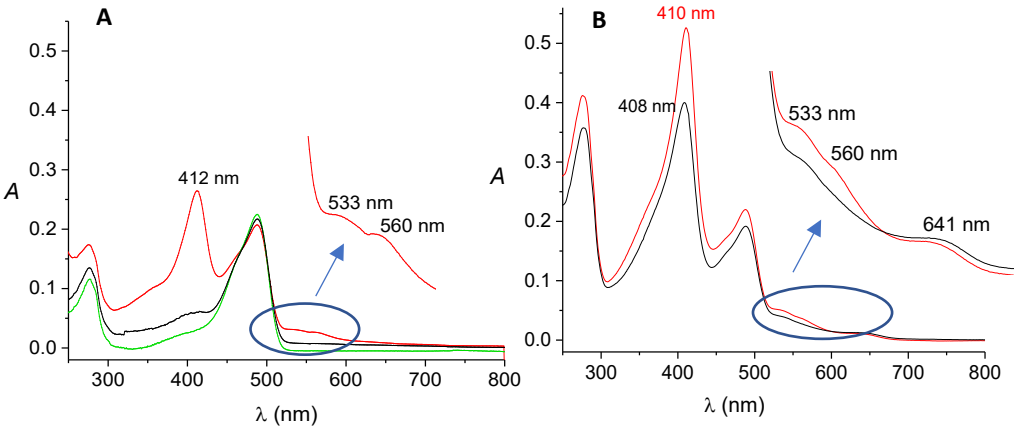

Figure S2.4. Effects of the His_6 tag on heme absorption of GFP and holoCcp1-GFP. (A) UV-vis spectra of: (A) 3 μM GFP-His_6 (green trace), GFP-His_6 + heme (red trace) and GFP + heme (black trace). (B) 5 μM holoCcp1-GFP-His_6 (red line) and holoCcp1-GFP (black line). The inserts show a 20X expansion of the visible regions. Spectra were recorded in 20 mM MES with 100 mM NaCl and 100 μM DTPA (pH 6.5) after removal of excess heme on a DEAE column as outlined under *Materials and Methods* of the main text.

Panel A: Adding heme to GFP-His_6 gives bands at 533 and 560 nm indicative of 6-coordinate heme. **Panel B:** holoCcp1-GFP-His_6 also exhibits bands at 533 and 560 nm as well as a band at 641 nm, which is assigned to the 5-coordinate heme of Ccp1. After any excess heme is removed by DEAE, holoCcp1-GFP and holoCcp1-GFP-His_6 exhibit Soret maximum at 408 and 410 nm plus a 408/280 ratio of 1.1 and 1.3, respectively, indicative of heme binding to the His_6 tag.

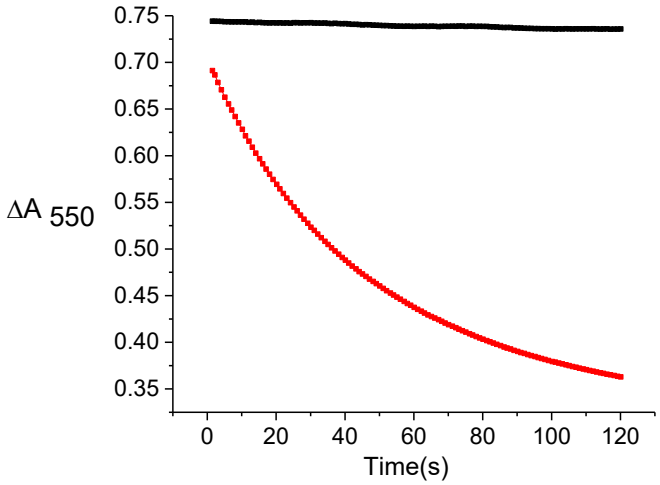

Figure S2.5. Ferrocytochrome c oxidizing activity of apoCcp1-GFP (black line) and holoCcp1-GFP (red line). Ferricytochrome was < 90% reduced with sodium dithionite and added to the assay solution (180 μM H_2O_2 and 1.3 mg/mL Ccp1 in 100 mM KPi, pH 7.0, 10 mM EDTA) to a final concentration of 54 μM in a 1-cm cuvette.[37] ΔA_{550} on ferrocytochrome c oxidation was recorded for 1-2 min, and the activity was determined from the initial slope ($\Delta A/s = \Delta\varepsilon_{550}\, b\, C/s$; $\Delta\varepsilon_{550}$ = 19.6 $mM^{-1}\, cm^{-1}$)[37] for holoCcp1-GFP (- 7.92 X $10^{-3}\, s^{-1}$) and apoCcp1-GFP (-1.3 X $10^{-5}\, s^{-1}$). These values fall within the range we previously found for holoCcp1.[74]

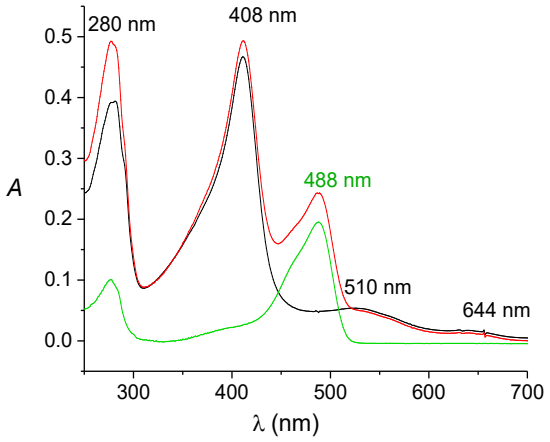

Figure S2.6. Sum of the absorption spectra of GFP and holoCcp1. The room-temperature UV-vis spectrum of 5 μM GFP (green trace) was added to that of 5 μM holoCcp1 (black trace) to predict the spectrum of holoCcp1-GFP (red trace). Proteins were dissolved in 10 mM KPi, 10 mM MES with 100 mM NaCl and 100 μM DTPA (pH 7.0) and spectra were recorded in a 1-cm pathlength.

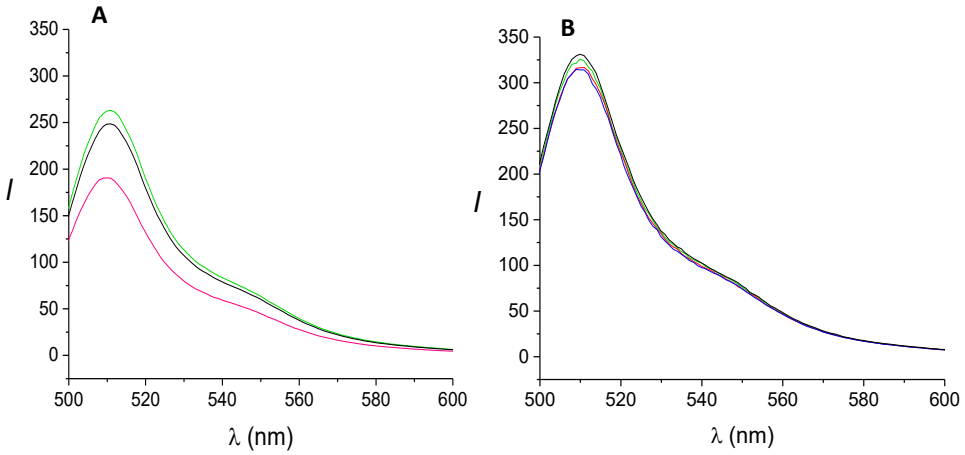

Figure S2.7. Effects of heme and heme proteins on the steady-state fluorescence of GFP and GFP-His$_6$. Emission spectra of: (A) GFP (green line), GFP-His$_6$ (green line; note the emission of both samples is identical), GFP plus heme (black line) and GFP-His$_6$ plus heme (red line) in 10 mM KPi, 10 mM MES (pH 7.0); (B) GFP-His$_6$ (green trace), GFP-His$_6$ plus holoCcp1 (black trace), GFP-His$_6$ plus holomyoglobin (red trace), and GFP-His$_6$ plus bovine serum albumin (blue trace) in 20 mM KPi (pH 7.0). All proteins were 0.4 μM, and 100 mM NaCl plus 100 μM DTPA also were present in all samples. BSA serves as a non-heme-protein control. Heme was added (as hemin protoporphyrin IX chloride) in 1.1 molar excess to the 1-cm cuvettes where indicated. Spectra were recorded at room temperature with 488-nm excitation and 5-nm slits (see caption to Figure 2.2 of the main text).

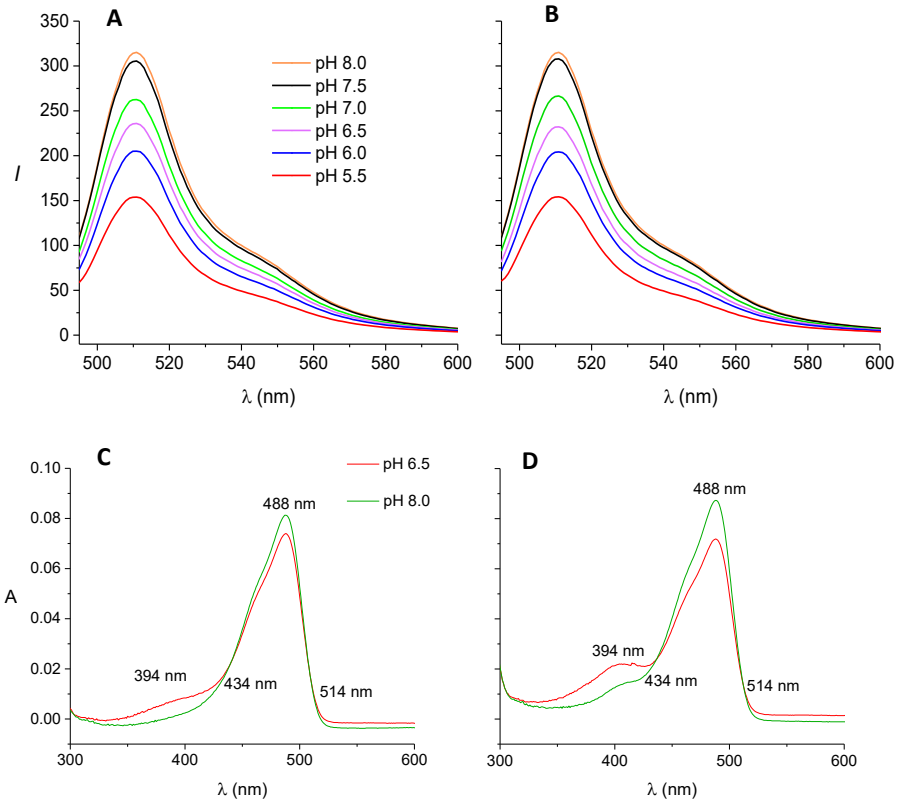

Figure S2.8. Changes in the steady-state fluorescence and absorption of GFP and apoCcp1-GFP due to the pH-sensitive equilibrium between the nonfluorescent A and fluorescent B ground states of the fluorophore. The emission spectrum following 488-nm excitation of 0.4 μM: (A) GFP-His$_6$ and (B) apoCcp1-GFP-His$_6$ in 10 mM KPi, 10 mM MES with 100 mM NaCl and 100 μM DTPA. The absorption spectrum at pH 6.5 (red trace) and 8.0 (green trace) of: (C) GFP-His$_6$ and (D) apoCcp1-GFP-His$_6$ in a 1-cm cuvette at room temperature. To adjust the pH, HCl or NaOH was added to 2 μM protein in 20 mM KPi, 100 μM DTPA (no NaCl here). The 394-nm band of the protonated form A of GFP, which is nonfluorescent,[95] grows in at the expense of the 488-nm band of the deprotonated, fluorescent state B as the pH is decreased. Also, weak heme absorption can be seen at ~ 400 nm in panel D since apoCcp1-GFP-His$_6$ is isolated with trace heme. Fluorescence spectra were recorded as outlined in the caption to Figure 2.2C of the main text.

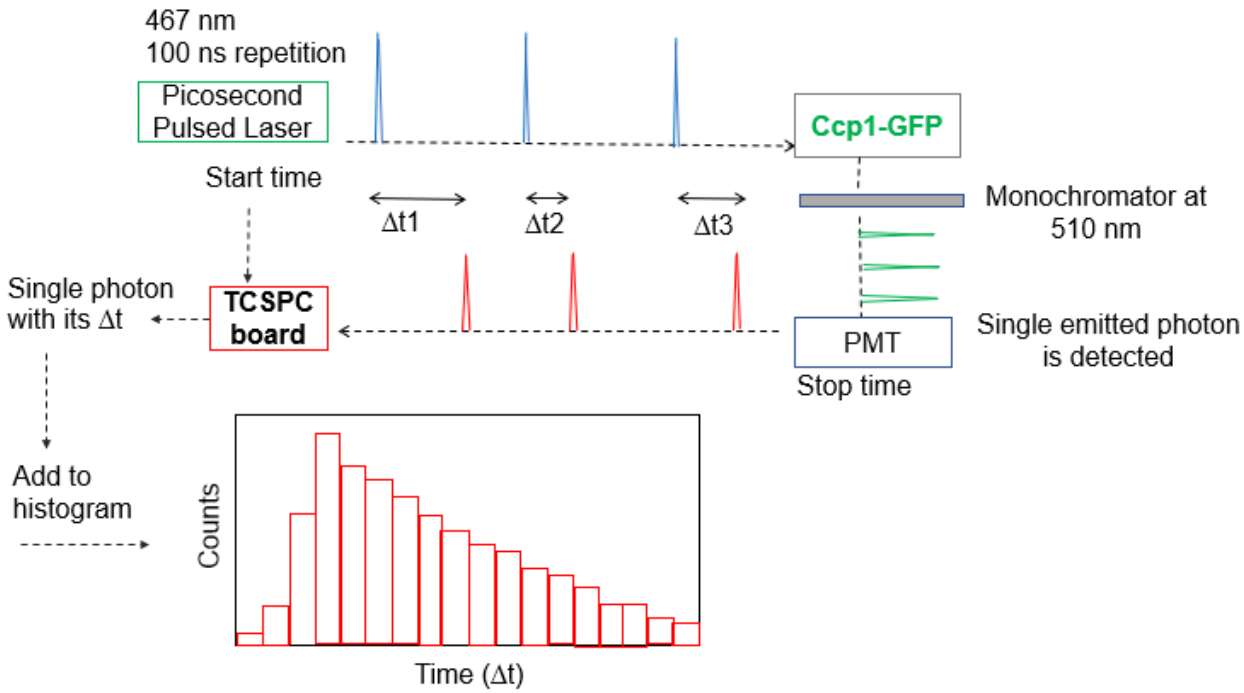

Figure S2.9. Time-correlated single photon counting (TCSPC). Short (470 ps) laser pulses at 467 nm (blue spikes) excite the sample (Ccp1-GFP), which emits photons at 510 nm (green spikes) that are detected by the PMT. The Δt (time difference between the laser pulse and the PMT signal) is recorded by the TCSPC board for each photon emitted, and the fluorescence lifetime decay is given by a histogram of photon counts vs Δt. The instrumental response function (IRF) is measured by substituting LUDOX (colloidal silica), which scatters the laser light (to remove any background), for the sample.

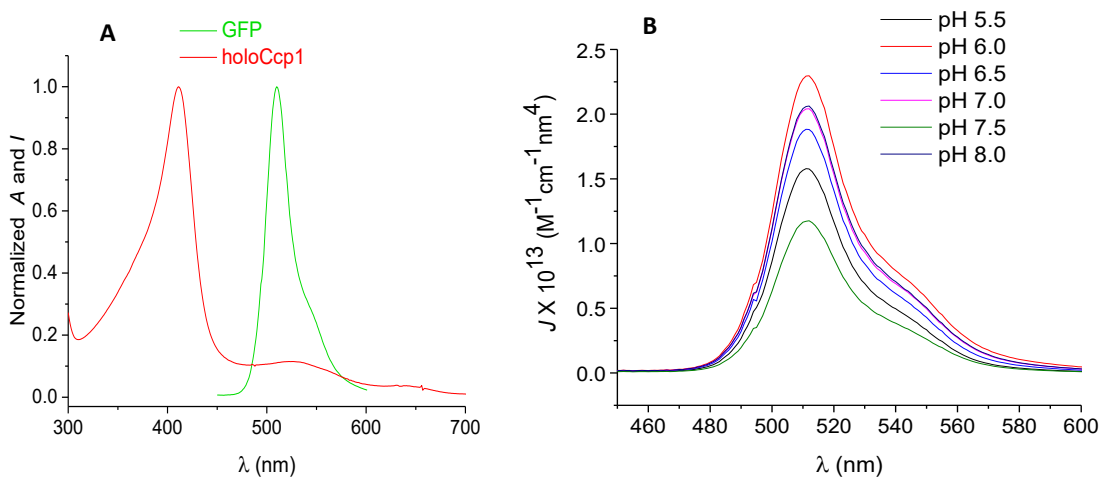

Figure S2.10. Overlap of GFP emission with holoCcp1 absorption and plot of spectral overlap integrals. (A) Emission spectrum of 0.4 μM GFP and absorption spectrum of 3 μM holoCcp1 at pH 6.5 in a 1-cm cuvette at room temperature. (B) Spectral overlap integral J ($M^{-1}cm^{-1}nm^4$) vs λ between GFP emission and holoCcp1 absorption at pH 5.5–8.0. All samples were prepared in 10 mM KPi, 10 mM MES with 100 mM NaCl and 100 μM DTPA. The pH was adjusted with NaOH or HCl.

The visible heme bands at 510 and 644 nm of holoCcp1 (Figure S2.6) overlap GFP emission at 510 nm (Figure S2.10A). Table S2.1 lists the value of J, the overlap integral, summed over all wavelengths between the GFP donor and Ccp1-heme acceptor for each pH. The average value over the pH range examined is 7.32 x 101^4 M^{-1} cm^{-1} nm^4. This yields an average R_o of 43.80 Å (Table S2.2) using Hink's method,[98] which assumes values of 0.67 for k (random orientation of the donor and acceptor transition dipoles) and 1.4 for the refractive index (n) of the medium between the donor and acceptor. R_0 was calculated by filling in the following information into the template[98] in Hink's method: the emission spectrum of the donor (GFP), the absorption spectrum of the acceptor (heme of holoCcp1), the extinction coefficient of heme at its lambda max and the quantum yield of GFP (0.64).[79] From the FRET efficiency and τ_1 and τ_2 of holoCcp1-GFP, the heme-fluorophore separation ***r*** can be calculated from the following equations:

$$E = 100\left(1 - \frac{\tau_n}{\tau_0}\right)$$

$$r = \sqrt[6]{\frac{R_0{}^6 - ER_0{}^6}{E}}$$

Table S2.1 summarizes the values of E and r calculated at each pH for both τ_1 and τ_2. For E_1 = 0.66 ± 0.03 and E_2 = 0.12 ± 0.01 the average values of r are 39 ± 2 and 61 ± 2 Å, respectively. These distances correspond closely to the separation expected between the heme and GFP fluorophore with the GRRIPGLIN linker in helical and extended conformations, respectively (Figure 2.7 of the main text).

Table S2.1. Average separation (*r*) between GFP fluorophore and Ccp1 heme in holoCcp1-GFP at pH 5.5–8.0 [a]

pH	8.0	7.5	7.0	6.5	6.0	5.5	Average
τ_2 (ns)	2.57	2.54	2.51	2.49	2.49	2.48	2.51 ± 0.04
τ_1 (ns)	1.09	1.04	1.00	0.97	0.93	0.86	0.98 ± 0.07
a_2	66	64	63	62	61	58	62 ± 2.5
a_1	34	36	37	38	39	42	38 ± 2.5
E_2	0.11	0.12	0.12	0.13	0.13	0.14	0.12 ± 0.01
E_1	0.62	0.64	0.65	0.66	0.68	0.70	0.66 ± 0.03
r_2 (Å)	64	60	61	60	62	57	61 ± 1.5
r_1 (Å)	41	39	40	39	40	37	39 ± 1.5

[a] Average values of τ and fractional amplitude a for three independent samples of holoCcp1-GFP at each pH. Lifetimes were measured by TCSPC (see Figure 2.3 of the main text). *E* and *r* values were calculated from the equations given above.

Table S2.2. Spectral overlap integral *J* between GFP emission and holoCcp1 absorption at pH 5.5–8.0

pH	Spectral overlap integrand (J) $M^{-1}cm^{-1}nm^4$	R_0 Å
5.5	5.79×10^{14}	42.19
6.0	8.93×10^{14}	45.36
6.5	7.06×10^{14}	43.61
7.0	7.82×10^{14}	44.36
7.5	6.41×10^{14}	42.91
8.0	7.94×10^{14}	44.48
Average	$7.32 \times 10^{14} \pm 1.04$	43.80 ± 1.05

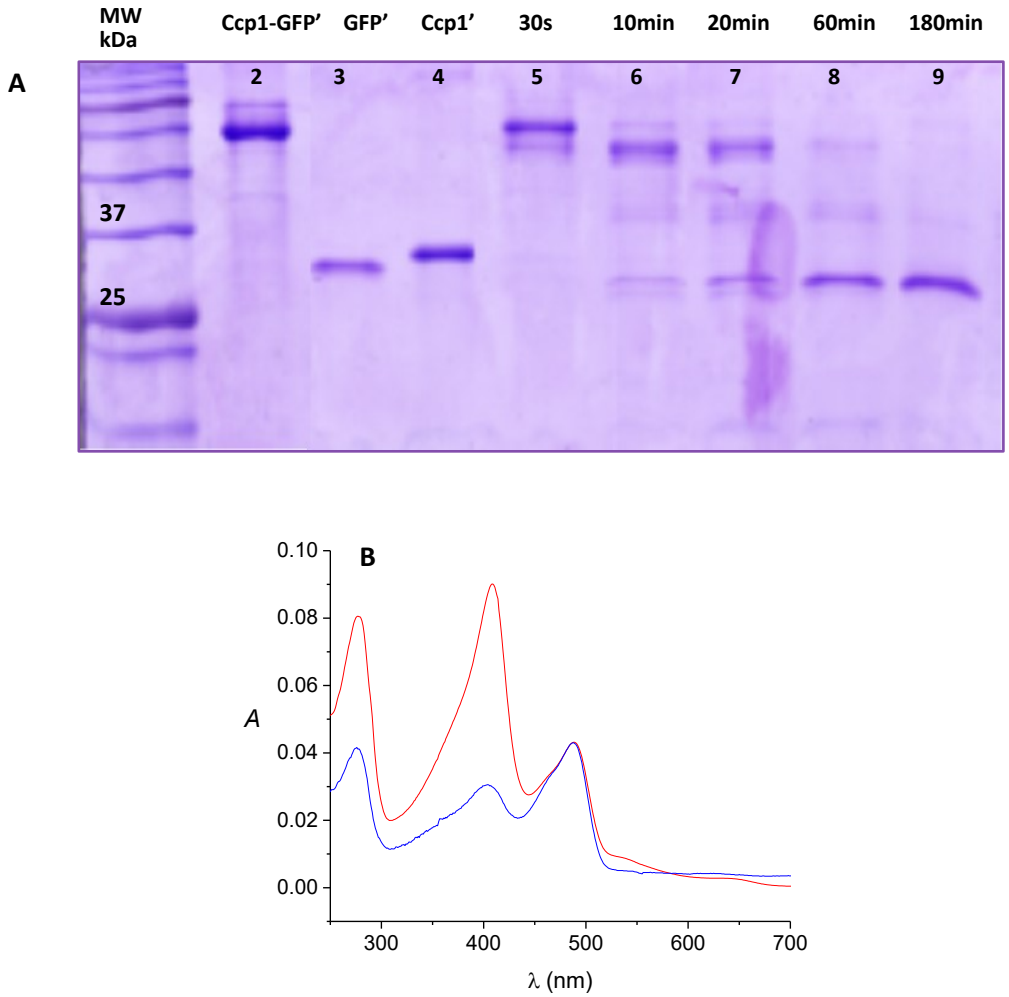

Figure S2.11. Tryptic digestion of holoCcp1-GFP-His$_6$ releases intact GFP. (A) A 25-μL aliquot of 1 μM holoCcp1-GFP-His$_6$ (lane 2, labeled Ccp1-GFP'), GFP-His$_6$ (lane 3, labeled GFP'), holoCcp1-His$_6$ (lane 4, labeled Ccp1'), and a 30-s, 10–180-min tryptic digests of 1 μM holoCcp1-GFP-His$_6$ (lanes 5–9) were loaded on a 12% SDS-page gel. Tryptic digestion was performed with 1:50 tryspin : protein at 37 °C in 20 mM KPi, pH 7.4, 100 μM DTPA. (B) UV-vis spectrum of the 30-s (red trace) and 180-min (blue trace) tryptic digests of holoCcp1-GFP-His$_6$. The 180-min digest was added to a 10 x 2-cm P10 column to remove molecules < 5 kDa by gel filtration before its spectrum was recorded. Also, 500 μL of Ni-NTA resin was added to 100 μL of the 30-s digest but protein remained in the supernatant, indicating that the His$_6$ tag was rapidly cut by trypsin.

Note that the main species in the 180-min digest (lane 9) appears just slightly lower in the gel than GFP-His$_6$ (lane 3), indicating that it is tag-free GFP, which is resistant to trypsin, as confirmed by no loss of GFP absorption at 488-nm in panel B (blue vs red trace). In contrast, no holoCcp1 remains in the 180-min digest (lane 9) but the remaining Soret absorption (panel B, blue trace) suggests that some of the digestion products of Ccp1 bind heme.

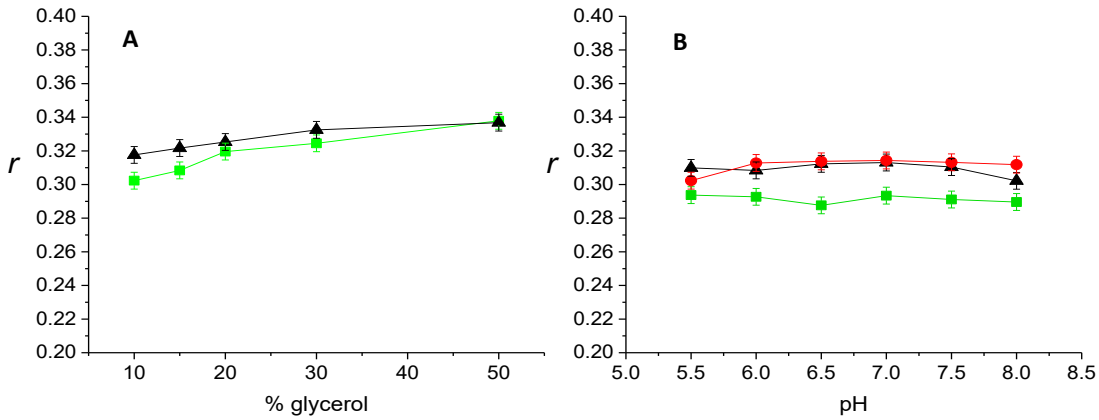

Figure S2.12. Steady-state anisotropy (*r*) of GFP-His$_6$ and Ccp1-GFP-His$_6$ vs glycerol concentration and pH. Steady-state anisotropy in a 1-cm cuvette of: (A) GFP-His$_6$ ■ and apoCcp1-GFP-His$_6$ ▲ at pH 6.5 at 10 ºC vs glycerol concentration; and (B) GFP-His$_6$ ■, apoCcp1-GFP-His$_6$ ▲, and holoCcp1-GFP-His$_6$ ● vs pH in buffer at room temperature. For each sample, 0.8 μM protein (A_{488} ≤ 0.05) was added to 10 mM KPi, 10 mM MES, 100 mM NaCl, 100 μM DTPA and the pH was adjusted with NaOH or HCl. The fluorescence intensity at 508 nm parallel ($I_{\parallel}$) and perpendicular ($I_{\perp}$) to the direction of the polarized excitation beam (488 nm) was measured using mechanical polarizers at 2-nm spectral resolution on a Quantamaster QM4 fluorometer (Photon Technology International).
The experimental anisotropy ***r*** is calculated from:

$$r = \frac{I_{\parallel} - I_{\perp}}{I_T}$$

Here $I_T = I_{\parallel} + 2I_{\perp}$. The Perrin equation relates the experimental anisotropy ***r*** to the intrinsic anisotropy ($\boldsymbol{r_0}$), the fluorescence lifetime τ and the rotational lifetime θ:

$$r = \frac{r_0}{1+\tau/\Theta}$$

The observed value of $\boldsymbol{r_0}$ (i.e., ***r*** in 50% glycerol; panel A) is 0.338 ± 0.002 (*n* = 3) for both GFP and apoCcp1-GFP in agreement with the reported value (0.33 ± 0.01) for GFPS65T over the range of pH 4.5 to pH 8.0.[99] Thus, from our values of τ (2.84 ns; Figure 2.4 of the main text) and r_0, we calculate θ = 20.84 ns for GFP (*r* = 0.294 ± 0.003; 0% glycerol) in agreement with the reported value of 20 ns,[89] and θ = 46.27 ns for apoCcp1-GFP (*r* = 0.315 ± 0.002; 0% glycerol). Since the rotational lifetime θ of apoCcp1-GFP is more than double that of free GFP, we assume that the GFP moiety is not freely tumbling around the linker but rather the fusion protein tumbles as a whole. Also, since τ_2 of holoCcp1-GFP is close to τ_0 of apoCcp1-GFP (Figure 2.4 of the main text), both exhibit the same ***r*** values (panel B). Notably, for each protein, ***r*** is essentially independent of pH as is τ (Figure 2.4 of the main text). Thus, at no pH does GFP rotate independently in apo- or holoCcp1-GFP. This is consistent with a semi-rigid linker.

2.9) Additional supplemental information

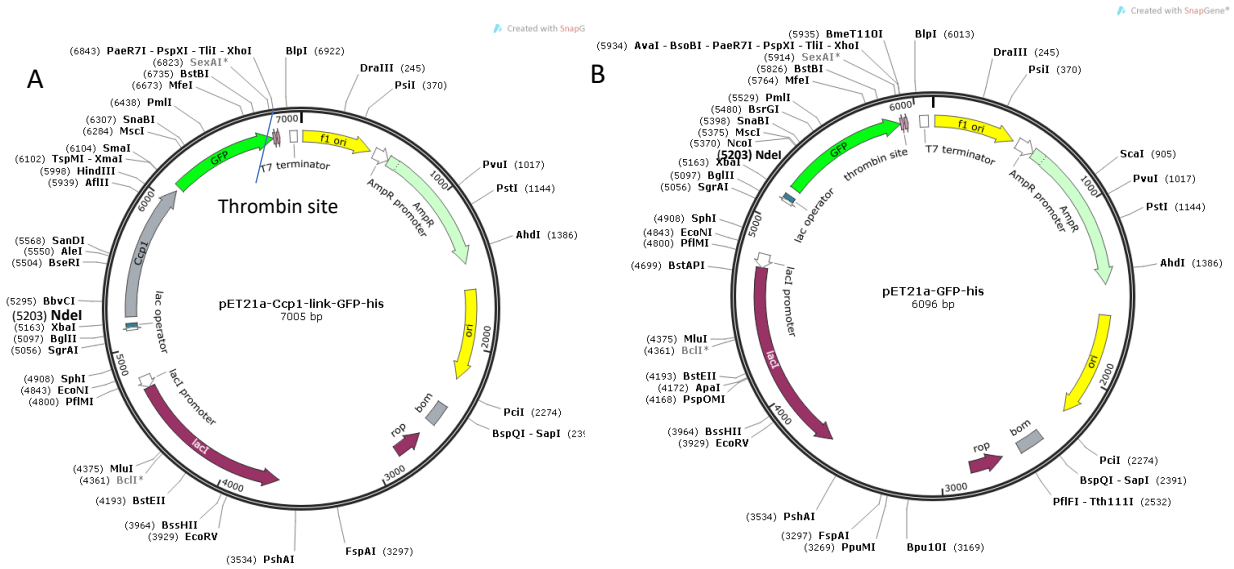

Figure A2.1. The vector map of (A) pET21a-Ccp1-GFP-His$_6$ and (B) pET21a-GFP-His$_6$. (A) The sequence encoding Ccp1-GFP in *S. cerevisiae* (GFP-tagged ORF YKR066C) was amplified by PCR and cloned into *Nde*I and *Xho*I sites of the pET21a vector (Section 2.4.2). (B) The sequence encoding GFP only in *S. cerevisiae* (GFP-tagged ORF YKR066C) was amplified by PCR and cloned into *Nde*I and *Xho*I sites of the pET21a vector (Section 2.4.2). This vector expresses C-terminally His$_6$-tagged protein with a thrombin cleavage site before the His$_6$ tag to allow its proteolytic removal. These maps were created by TopGene Technologies (Montreal, QC) using SnapGene.

DNA and amino acid sequence of Ccp1-GFP-His$_6$ and GFP-His$_6$

Table A2.1. DNA and amino acid sequence of mature Ccp1-GFP-His$_6$ [a]

TTTTGTTTAACTTTAAGAAGGAGATATACATATGACTACACCGCTCGTTCATGTCGCCTCTGTCGAAA
AAGGGAGGTCATACGAGGACTTCCAAAAGGTGTACAATGCGATTGCACTCAAGCTGAGGGAAGAT
GACGAATATGACAACTATATAGGCTATGGGCCCGTATTAGTCCGTCTTGCTTGGCACACTTCAGGG
ACCTGGGACAAGCACGACAATACAGGCGGGTCATACGGTGGTACATACAGATTCAAAAAGGAGTTT
AACGATCCATCCAATGCGGGCTTGCAGAATGGCTTCAAGTTCCTGGAGCCCATTCACAAAGAGTTT
CCCTGGATCTCCTCGGGTGATCTGTTCAGTCTAGGGGGTGTCACTGCCGTGCAGGAAATGCAGGG
TCCCAAGATTCCATGGAGATGTGGTAGAGTCGACACGCCAGAGGATACTACCCCTGACAACGGGA
GACTGCCTGACGCTGATAAAGACGCTGACTATGTCAGAACATTTTTTCAAAGACTTAATATGAATGA
CAGAGATGTAGTTGCTCTTATGGGGGCTCACGCTCTGGGCAAGACCCACTTGAAGAACTCTGGATA
CGAAGGGCCATGGGGAGCCGCTAACAACGTCTTTACCAATGAGTTTTACTTGAACTTGCTGAATGA
AGACTGGAAATTGGAAAAGAACGACGCGAACAACGAACAGTGGGACTCTAAGAGCGGCTACATGA
TGCTGCCCACTGATTATTCTTTGATTCAGGATCCCAAGTACTTAAGCATTGTGAAAGAATACGCTAA
TGACCAGGACAAGTTCTTCAAGGATTTTTCCAAAGCTTTTGAAAAACTGTTGGAGAACGGTATCACT
TTCCCTAAAGACGCGCCCAGTCCATTTATTTTCAAGACTTTAGAGGAACAAGGTTTAGGTCGACGGA
TCCCCGGGTTAATTAACAGTAAAGGAGAGGAACTTTTCACTGGAGTTGTCCCAATTCTTGTTGAATT
AGATGGTGATGTTAATGGGCACAAATTTTCTGTCAGTGGAGAGGGTGAAGGTGATGCAACATACGG
AAAACTTACCCTTAAATTTATTTGCACTACTGGAAAACTACCTGTTCCATGGCCAACACTTGTCACTA
CTTTCACTTATGGTGTTCAATGCTTTTCAAGATACCCAGATCATATGAAACGGCATGACTTTTTCAAG
AGTGCCATGCCCGAAGGTTATGTACAGGAAAGAACTATATTTTTCAAAGATGACGGGAACTACAAG
ACACGTGCTGAAGTCAAGTTTGAAGGTGATACCCTTGTTAATAGAATCGAGTTAAAAGGTATTGATT
TTAAAGAAGATGGAAACATTCTTGGACACAAATTGGAATACAACTATAACTCACACAATGTATACATC
ATGGCAGACAAACAAAAGAATGGAATCAAAGTTAACTTCAAAATTAGACACAACATTGAAGATGGAA
GCGTTCAACTAGCAGACCATTATCAACAAAATACTCCAATTGGCGATGGCCCTGTCCTTTTACCAGA
CAACCATTACCTGTCCACACAATCTGCCCTTTCGAAAGATCCCAACGAAAAGAGAGACCACATGGT
CCTTCTTGAGTTTGTAACAGCTGCTGGGATTACACATGGCATGGATGAACTATACCTGGTGCCGCG
CGGCAGCCTCGAGCACCACCACCACCACCACTGA

Amino acid sequence of mature Ccp1-GFP-His$_6$[a]

MTTPLVHVASVEKGRSYEDFQKVYNAIALKLREDDEYDNYIGYGPVLVRLAWH**T**SGTWDKHD
NTGGSYGGTYRFKKEFNDPSNAGLQNGFKFLEPIHKEFPWISSGDLFSLGGVTAVQEMQGPK
IPWRCGRVDTPEDTTPDNGRLPDADKDA**D**YVRTFFQRLNMNDR**D**VVALMGAHALGKTHLKN
SGYEGPWGAANNVFTNEFYLNLLNEDWKLEKNDANNEQWDSKSGYMMLPTDYSLIQDPKYL
SIVKEYANDQDKFFKDFSKAFEKLLENGITFPKDAPSPFIFKTLEEQGL**GRRIPGLIN**SKGEELF
TGVVPILVELDGDVNGHKFSVSGEGEGDATYGKLTLKFICTTGKLPVPWPTLVTTF**T**YGVQCF
SRYPDHMK**R**HDFFKSAMPEGYVQERTIFFKDDGNYKTRAEVKFEGDTLVNRIELKGIDFKED
GNILGHKLEYNYNSHNVYIMADKQKNGIKVNFKIRHNIEDGSVQLADHYQQNTPIGDGPVLLPD
NHYLSTQSALSKDPNEKRDHMVLLEFVTAAGITHGMDELYLVPRGSLEHHHHHH

[a] Mature yeast Ccp1 isoform 2 (T53, D152) with a E167D mutation, nine-residue linker, *Aequorea Victoria* GFP (S65T, Q80R) minus M1 and C-terminal K238 resudues, thrombin cleavage site + His$_6$ tag. Instead of mitochondrial target sequencing, **M** was added to start of mature Ccp1 sequence. Ccp1 isoform 1 (I53,G152) has been isolated form other yeast strains.[100]

Note: The DNA of Ccp1-GFP-His$_6$ was sequenced by TopGene Technologies (Montreal, QC).

Table A2.2. DNA and amino acid sequence of GFP-His$_6$

ATGAGTAAAGGAGAGGAACTTTTCACTGGAGTTGTCCCAATTCTTGTTGAATTAGATGGTGATGTTA
ATGGGCACAAATTTTCTGTCAGTGGAGAGGGTGAAGGTGATGCAACATACGGAAAACTTACCCTTA
AATTTATTTGCACTACTGGAAAACTACCTGTTCCATGGCCAACACTTGTCACTACTTTCACTTATGGT
GTTCAATGCTTTTCAAGATACCCAGATCATATGAAACGGCATGACTTTTTCAAGAGTGCCATGCCCG
AAGGTTATGTACAGGAAAGAACTATATTTTTCAAAGATGACGGGAACTACAAGACACGTGCTGAAGT
CAAGTTTGAAGGTGATACCCTTGTTAATAGAATCGAGTTAAAAGGTATTGATTTTAAAGAAGATGGA
AACATTCTTGGACACAAATTGGAATACAACTATAACTCACACAATGTATACATCATGGCAGACAAAC
AAAAGAATGGAATCAAAGTTAACTTCAAAATTAGACACAACATTGAAGATGGAAGCGTTCAACTAGC
AGACCATTATCAACAAAATACTCCAATTGGCGATGGCCCTGTCCTTTTACCAGACAACCATTACCTG
TCCACACAATCTGCCCTTTCGAAAGATCCCAACGAAAAGAGAGACCACATGGTCCTTCTTGAGTTTG
TAACAGCTGCTGGGATTACACATGGCATGGATGAACTATACCTGGTGCCGCGCGGCAGCCTCGAG
CACCACCACCACCACCACTGA

Amino acid sequence of GFP-His$_6$

MSKGEELFTGVVPILVELDGDVNGHKFSVSGEGEGDATYGKLTLKFICTTGKLPVPWPTLVTTF**T**YGVQ
CFSRYPDHMK**R**HDFFKSAMPEGYVQERTIFFKDDGNYKTRAEVKFEGDTLVNRIELKGIDFKEDGNILG
HKLEYNYNSHNVYIMADKQKNGIKVNFKIRHNIEDGSVQLADHYQQNTPIGDGPVLLPDNHYLSTQSALS
KDPNEKRDHMVLLEFVTAAGITHGMDEL**YLVPRGSLEHHHHHH**

Note: The DNA of GFP-His$_6$ was sequenced by TopGene Technologies (Montreal, QC).

Chapter 3: Spatiotemporal tracking in live cells of a protein post-translationally modified by insertion of noncovalent heme

3.1) Preface

The work presented in Chapter 3 corresponds to the following manuscript in preparation: Dastpeyman S, Cosa G, and English AM (2020). Spatiotemporal tracking in live cells of a protein post-translationally modified by insertion of noncovalent heme. Target journal: The Journal of the American Chemical Society. SD prepared the samples, collected and analyzed the data with helpful discussion, and prepared a draft of the manuscript. GC contributed to data analysis. AME conceived the experiment and contributed to the discussions, data analysis, writing, editing, and revisions of the manuscript.

3.2) Abstract of the manuscript

Heme proteins drive vital biological processes, including respiration, antioxidant stress and xenobiotic metabolism. However, the extent and reversibility of post-translational modification by covalent or noncovalent heme insertion have not been tracked for any protein in a eukaryotic cell to date. While probing the physiological function of cytochrome c peroxidase (Ccp1) in yeast, we found an accumulation of apoCcp1 in the mitochondria-depleted subcellular fraction at the expense of holoCcp1 in the mitochondria-enriched fraction by immuno- and heme-blotting of lysates from respiring cells. This disrupts the prevailing view that nuclear-encoded immature Ccp1 is targeted to mitochondria for maturation, including heme insertion, to produce a mitochondrial peroxidase with ferrocytochrome c oxidizing activity to detoxify respiration-derived H_2O_2. To address the discrepancy between this view and our findings and to eliminate possible artifacts of cell lysis, we sought to monitor apo- and holoCcp1 in live cells. Here we track Ccp1 fused to green fluorescent protein (GFP) in live cells chromosomally expressing the fusion under control of Ccp1's native promotor using fluorescence lifetime imaging microscopy (FLIM). FLIM reveals that Ccp1-GFP resides in the mitochondria of newly respiring (two-day) cells with 96 ± 3 % of Ccp1 in its holoform. In contrast, after five days of respiratory metabolism, 56 ± 8 % of Ccp1 has lost its heme and resides outside the mitochondria. Parallel FLIM experiments on yeast expressing Sod1-GFP, a nonheme-binding control, expose *time-invariant* fluorescence. This first spatiotemporal tracking in live cells of the heme-bound vs heme-free forms of an endogenous protein unleashes unprecedented opportunities to expand our knowledge of heme-protein function with and without heme bound and to map intracellular heme trafficking.

3.3) Introduction

Heme is an essential prosthetic group in many proteins involved in electron transfer, respiration, metabolism of xenobiotics, antioxidant defense, cell signaling and transcription and translation.[101–105] The final step in heme biosynthesis occurs in the mitochondrial matrix and heme is delivered to the proteins that require it by unknown pathways.[106] Free heme is insoluble in aqueous media and binds non-specifically to proteins and lipids and promotes their oxidation.[31,106] Hence, heme binding to its target proteins and intracellular heme trafficking must be tightly regulated. Despite its importance as a prosthetic group and its potential toxicity, there is essentially no information on how the heme status of proteins vary under normal physiological conditions in eukaryotic cells. Such information is crucial in identifying new moonlighting functions of the apoforms of heme proteins. It also is necessary in characterizing dysregulation of heme homeostasis, which is associated with cancer,[107] diabetes,[107] cardiovascular disease,[108] age-related neurodegeneration including Alzheimer's disease,[109–111] and in designing possible treatments.

Studies to date of heme-protein association in live cells were designed to measure labile heme levels. Typically, the cells of interest were transformed with a high-expression plasmid that overexpresses a heme sensor consisting of two fluorescent proteins (FPs) fused to a heme binding domain (HBD).[40,41,43] The intracellular labile heme concentration is estimated from the extent of heme binding to the HBD of known heme affinity.[40,41,43] The emission of one FP (e.g., EGFP) significantly overlaps with heme absorption and is efficiently quenched by Förster resonance energy transfer (FRET) when heme binds to the HBD as demonstrated for the cytochrome b_{562}-EGFP fusion *in vitro*.[36–38] The emission from the second FB is heme-insensitive (e.g., mKATE2), which enables ratiometric correction for variations in sensor expression and local pH. The latter varies significantly in respiring mitochondria, which have a pH of 7.0 in the intermembrane space vs 8.0 in the matrix due to the H^+ gradient created by the ETC.[112]

Our current interest in monitoring the holo- and apoforms of an endogenous heme protein in live cells stems from our studies on the physiological function of cytochrome c peroxidase (Ccp1) in yeast. Nuclear-encoded immature Ccp1 possesses a 68-residue N-terminal mitochondrial targeting sequence that is removed in mitochondria, where noncovalent heme insertion also occurs to give mature holoCcp1 in the mitochondrial intermembrane space (IMS).[19,20] Note that the heme in heme enzymes such as Ccp1 is considered a *prosthetic group* or a coenzyme that *constitutively* binds to a heme protein in contrast to the many coenzymes that transiently bind to proteins. Thus, we view covalent or noncovalent heme binding to Ccp1

as a post-translational modification (PTM), which also serves to distinguish our study from those mentioned above that examined transient heme binding to exogenous sensors.

Since mature holoCcp1 is released in the IMS, the prevailing view is that Ccp1 functions as a mitochondrial peroxidase with ferrocytochrome c oxidizing activity to detoxify respiration-derived H_2O_2.[113] However, subcellular fractionation using differential centrifugation and immuno- and heme-blotting of lysates from respiring cells by our group revealed accumulation of apoCcp1 *without* its 68-residue targeting sequence (i.e., the mature polypeptide) in mitochondria-depleted fractions at the expense of mature holoCcp1 in the mitochondria-enriched fraction.[26] The buildup of extra-mitochondrial apoCcp1 in respiring yeast is inconsistent with holoCcp1 functioning as a mitochondrial peroxidase that removes H_2O_2 produced during respiration.[113] Thus, heme repartitioning on cell disruption became a concern so we set our sights on tracking the holo- and apoforms of Ccp1 in live cells.

Since heme is a highly efficient quencher of green fluorescent protein (GFP), we turned our attention to yeast cells in which GFP is fused to the Ccp1 open reading frame.[27] These cells chromosomally express Ccp1 C-terminally fused to GFP by a nine-residue linker (GRRIPGLIN) under control of the native Ccp1 promotor and have been well characterized.[114] For example, previous studies by us and others have shown that immature Ccp1-GFP is correctly targeted to the mitochondria[26] and processed like native Ccp1.[19] As with native apoCcp1, we also found accumulation of extra-mitochondrial apoCcp1-GFP by immunoblot analysis of subcellular fractions from respiring cells expressing apoCcp1-GFP.[26]

We already have demonstrated in Chapter 2 the suitability of Ccp1-GFP as a probe of noncovalent heme insertion into Ccp1 in the test tube by characterizing its time-resolved fluorescence.[114] Heme quenching of the fluorescence lifetime of GFP is independent of Ccp1-GFP concentration and solution pH, plus the amplitude of the short lifetime (~1 ns) of holoCcp1-GFP accurately predicts its percentage in mixtures with the apoform.[114] Exploiting these favorable fluorescence characteristics, here we directly visualize Ccp1-GFP with and without heme in live yeast cells by fluorescence lifetime imaging microscopy (FLIM). This first spatiotemporal tracking in live cells of an endogenous protein in both its heme-bound and heme-free forms not only contributes to redefining Ccp1's physiological function, it also demonstrates that a protein that constitutively binds heme and is classified as "heme-dependent" can lose its heme and perform new functions in cells. Additionally, our results highlight the potential power of FLIM in mapping intracellular heme trafficking, which is poorly characterized in eukaryotic cells.[115]

3.4) Experimental section

3.4.1) Yeast strains

Wild-type *Saccharomyces cerevisiae* cells in the BY4741 genetic background (MATa *his3*Δ1 *leu*2Δ0 *met*15Δ0 *ura*3Δ0) were purchased from the European *Saccharomyces cerevisiae* Archive for Functional Analysis (EUROSCARF). *S. cerevisiae* strains expressing Ccp1-GFP (Clone YKR066C; plate # GFP(+)21, well # D12) and Sod1-GFP (CuZn-superoxide dismutase fused to GFP; Clone YJR104C; plate # GFP(+)33, well # F8) in the same genetic background (BY4741; CCP1:GFP-HIS3MX6 or BY4741; SOD1:GFP-HIS3MX6) were purchased from the Yeast GFP Clone Collection (Invitrogen Life Sciences; avaiable now from Thermo Fisher Scientific). The GRRIPGLIN linker is present in both fusion proteins.

3.4.2) Materials

Fluorescent MitoTracker Red CMXRos, a mitochondria-selective probe, was purchased from ThermoFisher. Yeast Nitrogen Base Without Amino Acids (Y0626), Yeast Synthetic Drop-Out Medium Supplements Without Histidine (Y1751), histidine (H7750), D-(+)-glucose, microscope slides (25x75x1 mm), coverslips (22x22x1 mm), sodium phosphate dibasic and monobasic were purchased from Sigma Aldrich.

3.4.3) Yeast growth and live-cell staining for microscopy

Yeast autofluorescence was minimized by growing cells in synthetic complete medium with 2% D-(+)-glucose (SCD).[92] Following the supplier's instructions, the SCD medium was prepared from 6.7 g of Y0626, 2 g of Y1751 and 20 g of D-(+)-glucose in 1.0 L. Additionally, 0.080 g of His (H7750) was added per 1.92 g of Y1751 for growth of WT yeast but not for the strains expressing Ccp1-GFP and Sod1-GFP, which are His-prototrophic since they have the *HIS3MX6* module.[27]

WT cells, cells expressing Sod1-GFP and Ccp1-GFP from frozen glycerol stocks (-80 ºC) were steaked on SCD-agar medium (2% agar) and incubated for 2 days at 30 ºC. Single colonies were selected and transferred to 10 mL of SCD liquid medium (no agar) in 50-mL Falcon tubes. The pre-cultures were grown for 22 h at 30 ºC with shaking at 225 rpm, diluted to an initial OD_{600} of 0.01 in 100 mL of SCD and grown at 30 ºC/ 225 rpm in 500-mL Erlenmeyer flasks at a flask-to-medium ratio of 1:5. After 3 days, cells were transferred to 0.85% NaCl and maintained at 30 ºC / 225 rpm at flask-to-medium ratio of 1:5 for 7 days. Cells from 2- and 7-day cultures were spun at 2000 g for 5 min and pellets were washed with PBS (10 mM sodium phosphate buffer with 150 mM NaCl, pH 7.4), diluted to OD_{600} ~ 0.2 in PBS, and stained with 0.25 μM MitoTracker for 30 min in the dark at room temperature. Samples were spun at 2000 g for 5 min, resuspended

in PBS, 6-μL aliquots were placed on the microscope slides and sealed with coverslips painted at the corners with transparent nail polish.

3.4.4) Fluorescence microscopy and TCSPC FLIM

Fluorescence and bright-field images of cells were acquired at McGill University (ABIF) on a Zeiss LSM 710 laser scanning confocal microscope with a 63X (1.4 NA) Plan-Apochromat objective (Figure S3.1A). GFP (476 nm) and MitoTracker (543 nm) were excited by 25 mW Ar and 1 mW HeNe lasers operating at 50% and 5% maximum power, respectively and fluorescence at 493 – 531 nm (GFP) and 548 – 683 nm (MitoTracker) was recorded through point laser scanning confocal (LSM 710, Zeiss Canada). Bright-field images were obtained on illumination from below the sample with white light from a halogen lamp (Figure S3.1A).

FLIM images also were acquired on the LSM 710 microscope using the PicoQuant TCSPC FLIM Kit (Figure S3.1B; Section 2.4.6).[114] Briefly, this included a 250 ps-pulsed laser diode (with 50 MHz repetition rate) emitting at 473 nm, a GFP emission filter (520 ± 17 nm), a SPAD and time-correlated single-photon counting (TCSPC) electronics (Picoharp 300) set to record a maximum of 1250 counts/ms. Note that photon-count rates were < 5% of the excitation rate to prevent pulse pile-up. The laser power at the sample was < 2.5 μW to minimize GFP photobleaching and SPAD saturation. Photon arrival times at the SPAD with respect to the laser pulse were tracked by TCSPC, which was synchronized with the scanning of the objective to assign each photon to a pixel. Repetitive scans were performed at 3 μs per pixel and a frame size of 512 × 512 pixels (corresponding to an area of 67.34 x 67.34 μm). A total of 382 frames in ~ 5 min were recorded to obtain good photon statistics for the entire FLIM image (~10^4 photons were counted at the peak time-bin per frame) and the resulting FLIM image was generated using SymPhoTime 32 software (PicoQuant). This software plots photon arrival times in each pixel to create FLIM images that quickly reveal the distribution of decay components in the sample, and bins these times to generate arrival-time histograms. The TCSPC data for specific regions of interest (ROI) were exported from SymPhoTime to OriginPro2016 (Originlab) for tail fitting by n-exponentials since the number of photons per ROI was not enough to be analyzed by SymPhoTime. Thus, photons summed from more than 50 ROI were analyzed by OriginPro2016.

3.4.5) Determination of fluorescence liftimes and amplitides for Ccp-GFP in cells from the FLIM data

The photophysical characterization of Ccp1-GFP *in vitro* (Section 2.5.3) shows that holoCcp1-GFP has two fluorescence lifetimes (τ_1 and τ_2) and apoCcp1-GFP has one lifetime (τ_0).[114] Yeast autofluorescence was determined for WT cells (Section 3.5.4), and following

subtraction of autofluorescence from the GFP signal, we found two lifetimes (τ_1 and τ_2) for GFP in mitochondria and one lifetime (τ_0) for GFP outside of mitochondria using mono- and biexponential mathematical models (ExpDecay1 and 2, OriginPro2016, respectively). This is consistant with the results we obtained on blotting cell lysates for Ccp1 and heme, when holoCcp1 and apoCcp1 were found in mitochondria-enriched and mitochondria-depleted fractions, respectively.[26] The three lifetimes (τ_1, τ_2 and τ_0) were fixed and a triexponential model (ExpDecay3, OriginPro2016) was fitted to the FLIM data from whole cells to calculate accurate lifetime amplitudes. The amplitude of the short lifetime (τ_1) of Ccp1-GFP in each ROI is used to estimate percentage holoCcp1 from the standard plot as outlined previously (Section 2.5.5).[114]

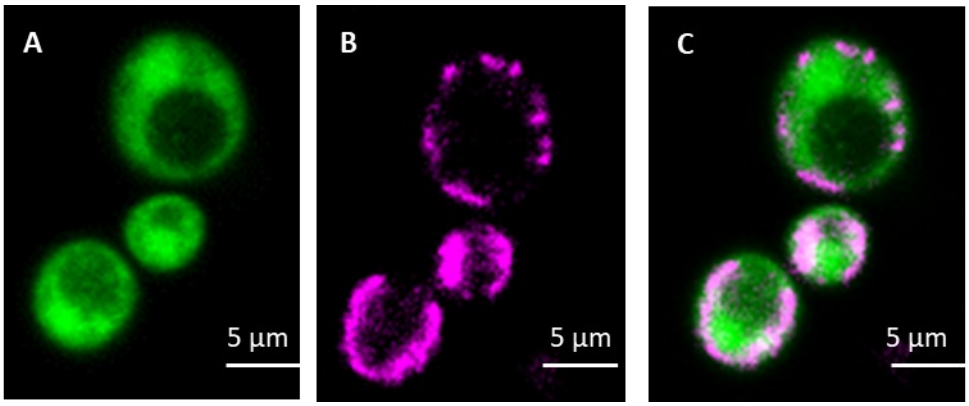

Figure 3.1. **Fluorescence intensity images of 2-day live yeast cells expressing Sod1-GFP.** (A) GFP fluorescence at 493 – 531 nm (ex 473 nm) and (B) MitoTracker fluorescence at 548 – 683 nm (ex 543 nm) colored in magenta to localize mitochondria. (C) Merge of GFP and MitoTracker fluorescence (white) reveals that Sod1-GFP is both mitochondrial and extramitochondrial (green). Cells were grown for 2 days (OD_{600} ~ 2.5) in SCD medium and a confocal fluorescence microscope (Zeiss LSM 710) was used to capture these images.

3.5) Results

3.5.1) FLIM of 2- and 7-day cells expressing Sod1-GFP

We specifically selected 2- and 7-day cells because subcellular fractionation suggested that Ccp1 is largly mitochondrial in 2-day cells but a large fraction is extramitochondrial in 7-day cells.[26] CuZn-superoxide dismutase (Sod1) is a highly abundant protein in the cytosol,[116] mitochondrial intermembrane space[116,117] and nucleus[116] of eukaryotic cells. Since Sod1 is not known to bind heme, yeast chromosomally expressing Sod1-GFP (with the same GRRIPGLIN linker found in Ccp1-GFP) under the native Sod1 promoter were first investigated by FLIM. Sod1-

GFP serves as a valuable control to examine any spatiotemporal variation in the time-resolved fluorescence of GFP fused to a nonheme protein in live cells.

Fluorescence microscopy confirms that Sod1 is a highly abundant protein in both the mitochondrial and extramitochondrial regions of 2-day yeast cells (Figure 3.1). The FLIM image (Figure 3.2A) displays short (red) and long GFP lifetimes (green), which are randomly distributed throughout the cells, giving rise to yellow pixels in regions of higher fluorescence intensity. Binning of photon-arrival times over 6 cells reveals mean arrival times (t_m) of 1.72 and 2.90 ns with a ratio of 30/70 (Figure 3.2B). Thus, the FLIM analysis mode of the SymPhoTime software indicates that Sod1-GFP in 2-day cells possesses short and long fluorescence lifetimes.

Since Sod1-GFP is highly expressed in yeast under the Sod1 promoter, we also could monitor its fluorescence in crude cell lysates. Sod1-GFP in diluted mitochondria-depleted subcellular fractions emits with a maximum at 510 nm (Figure S3.2A) and exhibits fluorescence lifetimes measured by TCSPC spectroscopy of 1.70 ± 0.1 and 3.0 ± 0.1 ns with relative amplitudes of 28 ± 2 and 72 ± 2% (Figure S3.2B). Thus, both FLIM and TCSPC spectroscopy yield similar lifetimes and amplitudes for Sod1-GFP.

3.5.2) Analysis of mitochondrial and extramitochondrial Sod1-GFP in 2- and 7-day cells

We next examined Sod1-GFP fluorescence in mitochondrial and extramitochondrial subcellular regions. Live cells of the expected shape and of similar size, and with unsaturated GFP and MitoTracker signals were selected from the confocal images and turned into masks using macro programming in FIJI-Win64 (NIH, Bethesda USA) (Figure 3.3). The whole-cell masks were then imported into SymPhoTime (described in S3.8.1) and superimposed on the FLIM image, and the TCSPC data from the selected cells were saved. Making masks of cells in FIJI is fast because many cells can be masked at the same time. Well-defined small mitochondrial regions from the same cells were masked by macro programming and superimposed on the FLIM image. Slight spatial deviations (~ 1 mm) between the confocal intensity (recorded in < 30 s) and FLIM images (recorded in 5 min) were noted so mitochondrial and extramitochondrial regions were directly masked on the FLIM images using SymPhoTime (Figure 3.4). This eliminated any spatial deviations but was more time consuming since each tiny mitochondrial or extramitochondrial region had to be masked separately. The TCSPC data from the masked whole cells and the masked mitochondrial and extramitochondrial regions were saved and separately exported to Excel and summed for fitting by an exponential tailfit model in OriginPro2016 (Figure 3.5 and Table 3.1).

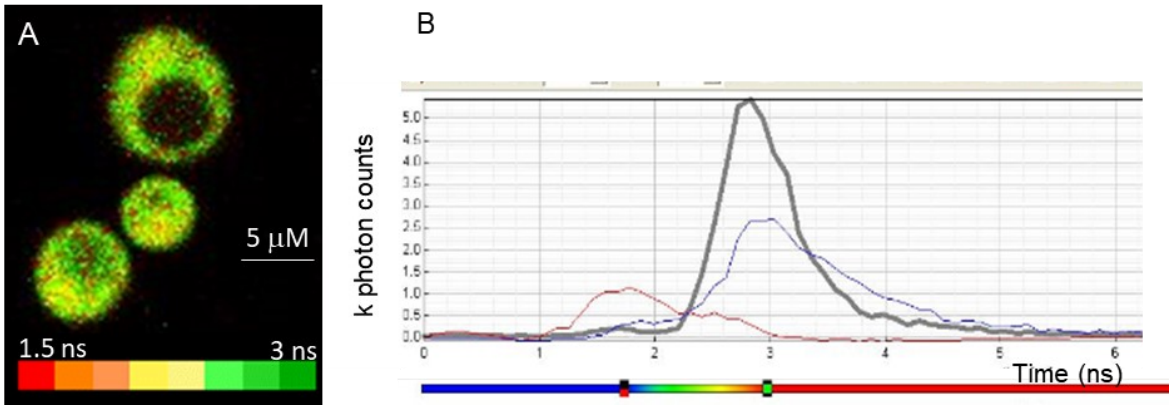

Figure 3.2. **FLIM of 2-day live yeast cells expressing Sod1-GFP following 473-nm laser excitation.** (A) The confocal FLIM image of emission at 520 ± 17 nm showing a random distribution of red, green and yellow dots in the cells. (B) Screen capture of the arrival-time (*t*) histogram obtained by FLIM analysis of six cells. Each *t* value (i.e., the time a photon arrives at the detector following the laser pulse) was binned using SymPhoTime software without background correction or cell selection. The mean arrival time (t_m) of 2.82 ns (grey trace) is the average of t_{m1} and t_{m2} values of 1.72 and 2.90 ns (red and green squares on color bar) with relative intensities of 30% (red trace) and 70% (blue trace), respectively. Thus, the dots in panel A correspond to Sod1-GFP molecules with short (red) and long (green) fluorescence lifetimes. The yellow dots in regions of higher fluorescence intensity signify merged red and yellow dots, signaling the random distribution in cells of Sod1-GFP molecules with short and long fluorescence lifetimes. The results are representative of cells expressing Sod1-GFP from three independent cultures.

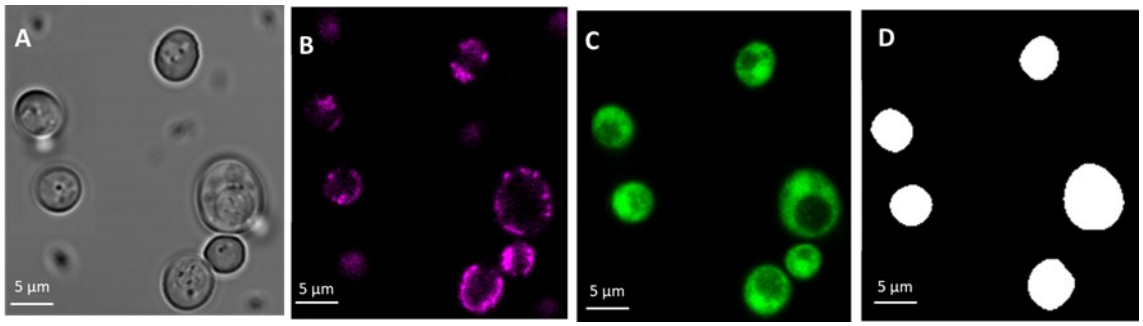

Figure 3.3. Selection of 2-day live yeast cells expressing Sod1-GFP. (A) Bright-field, (B) MitoTracker and (C) GFP channels were examined to avoid selection of damaged cells. (D) The whole-cell mask of selected cells prepared using macro programming in FIJI-Win64 (Section 3.8.1). Images recorded on a confocal microscope (Zeiss LSM 710; Section 3.4.4 and Figure S3.1A) show the transmitted white light, MitoTracker fluorescence at 548 – 683 nm (ex 543 nm), and GFP fluorescence at 493 – 531 nm (ex 473 nm). Cells were grown for 2 days (OD_{600} ~ 2.5) in SCD medium.

Under our growth conditions (2% glucose), yeast begin to respire during their second day in culture and we found that apoCcp1 accumulates in the mitochondria-free subcellular fraction following switch of cells to respiratory metabolism.[26] Hence, Ccp1-GFP fluorescence lifetimes in older cells is of interest so we also performed FLIM analysis of Sod1-GFP-expressing cells from 7-day cultures. In sum, we found that both mitochondrial and extramitochondrial Sod1-GFP exhibit lifetimes of 1.48 ± 0.15 ns (τ_1) and 2.62 ± 0.14 ns (τ_2) with fractional amplitudes (α_1, α_2) of 30 ± 2.5 and 70 ± 2.5 %, respectively, in ~ 100 live cells from a combination of 2- and 7-day cultures (Table 3.1).

Based on these results, we confidently conclude that the time-resolved fluorescence of our nonheme-binding control, Sod1-GFP, does not change with cell age or with subcellular location. Interestingly, Table 3.1 reveals that τ_2 for GFP is smaller in cells (~2.6 ± 0.1 ns) vs in diluted cell lysates (~3.0 ± 0.1 ns). It has been reported that GFP's fluorescence lifetime can vary with environmental factors such as changes in the local refractive index.[118–120] For example, GFP-Rac2 and GFP-gp91(phox), which are cytosolic and membrane-bound subunits of human phagocytic NADPH oxidase,[32] have fluorescence lifetimes of 2.70 and 2.31 ns, respectively.

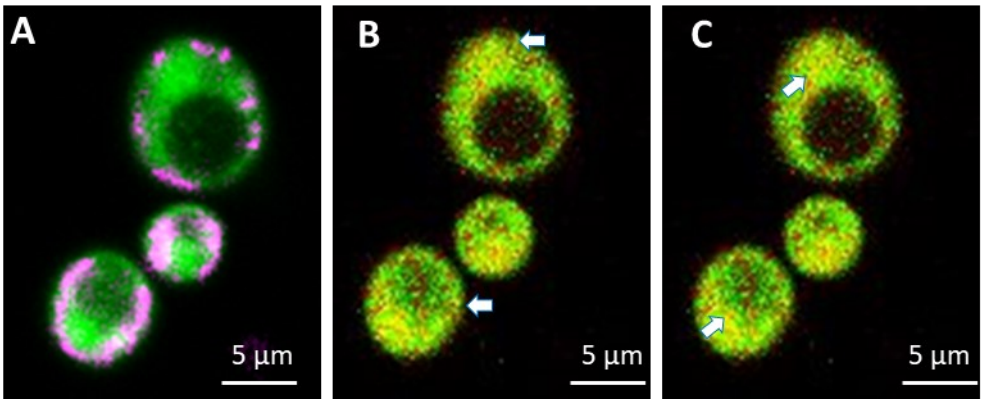

Figure 3.4. **Selection of mitochondrial and extramitochondrial regions in 2-day cells expressing Sod1-GFP and stained with MitoTracker.** (A) Fluorescence intensity image showing GFP (green) and MitoTracker (magenta) signals. Guided by the MitoTracker signal, the white arrows point to typical (B) mitochondrial and (C) extramitochondrial regions selected in the corresponding FLIM image. The data from selected regions were exported from SymPhoTime and imported into OriginPro for analysis.

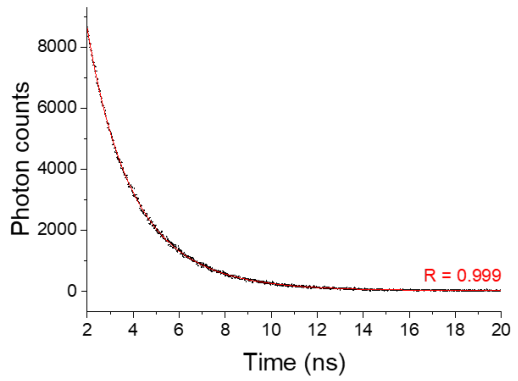

Figure 3.5. Biexponential decay of extramitochondrial Sod1-GFP fluorescence in 2-day live cells. The TCSPC data from 15 extramitochondrial masks (1120 pixels) from 2-day cells expressing Sod1-GFP were summed in Excel and imported into OriginPro. A biexponential tailfit model (ExpDecay2) was fitted to the summed data, yielding fluorescence lifetimes of 1.40 ns (29%) and 2.49 ns (71%) (Section 3.8.1). The same results were observed for 7-day cells expressing Sod1-GFP (Table 3.1). Data are representative of cells selected from 3 independent 2-day (OD_{600} ~ 2.5; total of ~ 50 cells) and 7-day (OD_{600} ~4.5; total of ~ 50 cells) cultures.

Table 3.1. Fluorescence lifetimes and fractional amplitudes of Sod1-GFP vs location in 2- and 7-day live cells[a]

Culture age	Sod1-GFP location	τ_1 (ns)	% a_1	τ_2 (ns)	% a_2
2 days	Whole cell	1.51 ± 0.20	31 ± 2	2.65 ± 0.15	69 ± 2
2 days	Mitochondria	1.41 ± 0.14	29 ± 3	2.57 ± 0.12	71 ± 3
2 days	Extramitochondria	1.42 ± 0.15	29 ± 2	2.56 ± 0.20	71 ± 2
7 days	Whole cell	1.55 ± 0.14	31 ± 2	2.70 ± 0.14	69 ± 2
7 days	Mitochondria	1.47 ± 0.15	31 ± 3	2.68 ± 0.13	69 ± 3
7 days	Extramitochondria	1.54 ± 0.13	30 ± 3	2.63 ± 0.10	70 ± 3
Average τ_n and a_n values [b]		1.48 ± 0.15	30 ± 2.5	2.62 ± 0.14	70 ± 2.5
τ_n and a_n τ values in cell lysates [c]		1.70 ± 0.10	28 ± 2	3.0 ± 0.10	72 ± 2
t_{m1} and t_{m2} values (2-day cells) [d]		1.70 ± 0.15	30 ± 2	2.90 ± 0.15	70 ± 2

[a] [a] Live cells expressing Ccp1-Sod were selected from 3 independent 2-day (OD_{600} ~ 2.5; total of ~50 cells) and 7-day (OD_{600} ~4.5; total of ~50 cells) cultures and were analyzed by FLIM as described in Figures 3.3 to 3.5.

[b] Average of all the τ_n and a_n values recorded for the 100 cells from a combination of 2- and 7-day cultures.

[c] Average τ_1 and τ_2 values measured at room temperature and pH 7.4 by TCSPC for Sod1-GFP in diluted mitochondria-depleted subcellular fractions prepared from lysed cells from 2- and 7-day cultures (Figure S3.2B).

[d] Mean arrival times (t_m) and relative intensities from FLIM analysis of six whole cells from 2-day cultures without background correction or cell selection (Figure 3.2).

3.5.3) Localization of Ccp1-GFP in 2- and 7-day live cells

We previously found by subcellular fractionation using Western blotting that Ccp1-GFP, like native Ccp1, is located in the mitochondria of 2-day cells but also is extramitochondrial in 7-day cells.[26] Here, we first examined Ccp1-GFP's cellular location by epifluorescence microscopy, which provides more fluorescence intensity per pixel than confocal microscopy, an advantage for low-abundant proteins such as Ccp1-GFP. Figure 3.6 (top panels) shows that GFP and MitoTracker, a mitochondrial probe, co-localize in 2-day cells. In contrast, Ccp1-GFP is both mitochondrial and extramitochondrial in 7-day cells (Figure 3.6, bottom panels), which corroborates its dual localization found by Western blotting.[26]

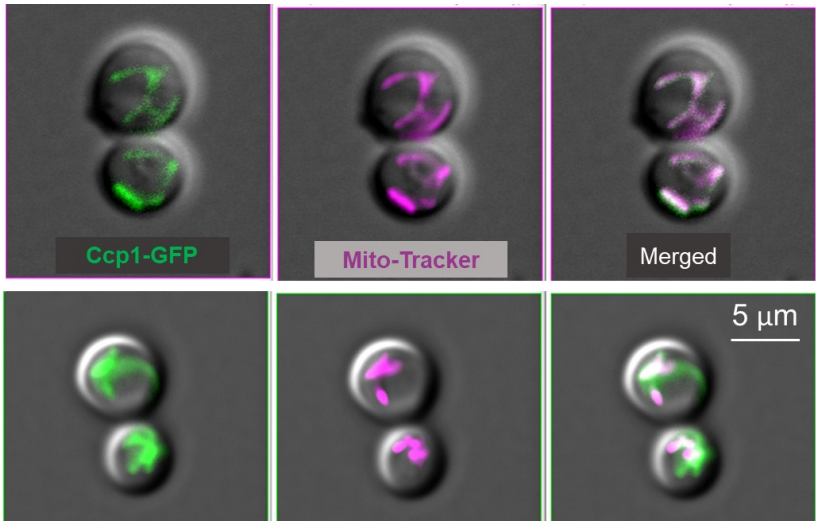

Figure 3.6. Localization of Ccp1-GFP in 2- and 7-day live cells. GFP (green) and MitoTracker (magenta) fluorescence plus merged fluorescence (white) in 2-day (top panels) and 7-day cells (bottom panels) imaged in transmitted DIC (differential interference contrast) with a halogen lamp. Images were acquired on an inverted epifluorescence microscope (Model Leica DMI6000 B) with a 63x/1.6 NA objective and a high-resolution CCD camera (Hamamatsu Orca R2). A mercury lamp plus filter sets (Semrock) for GFP (ex 472 ± 15; em 520 ± 17 nm) and MitoTracker (ex 562 ± 20; em 624 ± 20 nm) allowed selective fluorescence monitoring over 800 ms. Each panel contain ten images separated by 0.3 µm along the Z-axis, which were Z-stacked and displayed using FIJI-Win 64. Cells were grown in SCD medium for 2 days (OD_{600} ~ 2.5) and 7 days (OD_{600} ~ 4.5).

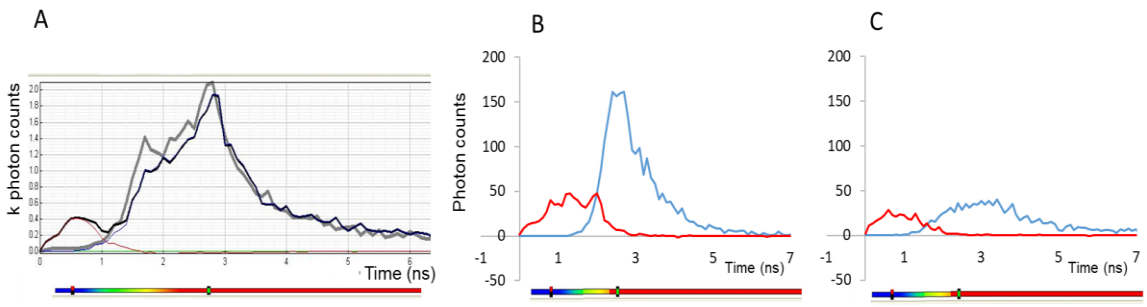

Figure 3.7. FLIM analysis of WT cells vs those expressing Ccp1-GFP. Screen capture of arrival-time histograms of: (A) 20 cells expressing Ccp1-GFP from a 2-day culture with a mean arrival time (t_m) of 2.53 ns (grey trace), average t_{m1} and t_{m2} values of 0.68 and 2.68 ns (red and green squares on color bar) with relative intensities of 20% (red trace) and 80% (blue trace), respectively. The combined red and blue traces is shown in dark blue; (B) 3 cells expressing Ccp1-GFP from a 7-day culture with average t_{m1} and t_{m2} values of 0.75 ns and 2.55 ns (red and green squares on color bar) with relative intensities of 30% (red trace) and 70% (blue trace), respectively; and (C) 3 WT cells from a 7-day culture with average t_{m1} and t_{m2} values of 0.55 ns and 2.65 ns (red and green squares on color bar) with relative intensities of 45% (red trace) and 55% (blue trace), respectively. Data are representative of cells expressing Ccp1-GFP and WT cells from 3 independent cultures. FLIM analysis was performed as outlined in the caption to Figure 3.2.

Our next goal was to monitor apo- and holoCcp1 inside and outside the mitochondria of live cells and compare the results with those from our heme blotting of the subcellular fractions.[26] Chapter 2 reports that, *in vitro*, apoCcp1-GFP exhibits a single excited-state lifetime of 2.84 ± 0.01 ns (τ_0) whereas holoCcp1-GFP displays lifetimes of 0.95 ± 0.02 (τ_1) and 2.46 ± 0.03 ns (τ_2) with fractional amplitudes of 38 ± 2% and 62 ± 1.5% (a_1 and a_2), respectively.[114] Furthermore, standard plots of fractional amplitude a_1 vs percentage of Ccp1-GFP in its holoform are linear (Figure S3.4),[114] which enables the tracking by FLIM of the relative amounts of apo- and holoCcp1-GFP in live cells.

3.5.4) Yeast autofluorescence interferes with Ccp1-GFP lifetime measurements

The arrival-time histograms from the FLIM analysis show t_{m1} values (0.68 and 0.75 ns) for Ccp1-GFP in 2- and 7-day cells (Figure 3.7A, B) that are considerably shorter than τ_1 (0.95 ns) of holoCcp1-GFP *in vitro*[114] (Table 3.2). A comparison of Figure 3.7B vs 3.7C reveals that yeast autofluorescence contributes significantly to t_{m1} of Ccp1-GFP and must be subtracted to accurately fit the GFP signal. By analyzing 100 wild-type cells, we noted that autofluorescence gives rise to a constant number of photons per pixel in each time channel (Figure S3.3 and Table S3.1). Hence, we confidently subtracted this contribution from GFP fluorescence in cells expressing Ccp1-GFP.

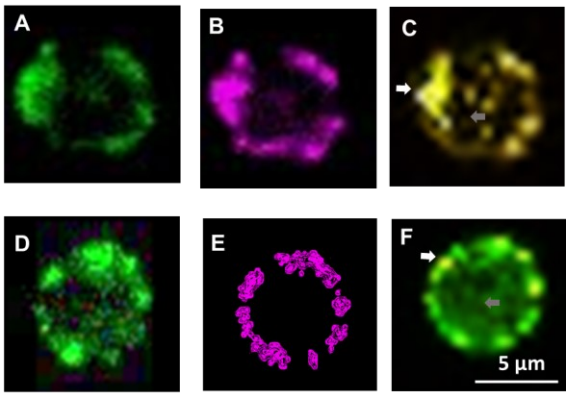

Figure 3.8. **Selection of mitochondrial and extramitochondrial regions in 2- and 7-day live cells expressing Ccp1-GFP.** Fluorescence intensity images showing (A, D) GFP (green) and (B, E) MitoTracker signals (magenta) in 2- (top panels) and 7-day cells (bottom panels). Guided by the MitoTracker signal, the white and grey arrows point to typical mitochondrial and extramitochondrial regions, respectively, that were selected from the corresponding FLIM images (C, F). Data from these regions were exported from SymPhoTime and imported into OriginPro for analysis.

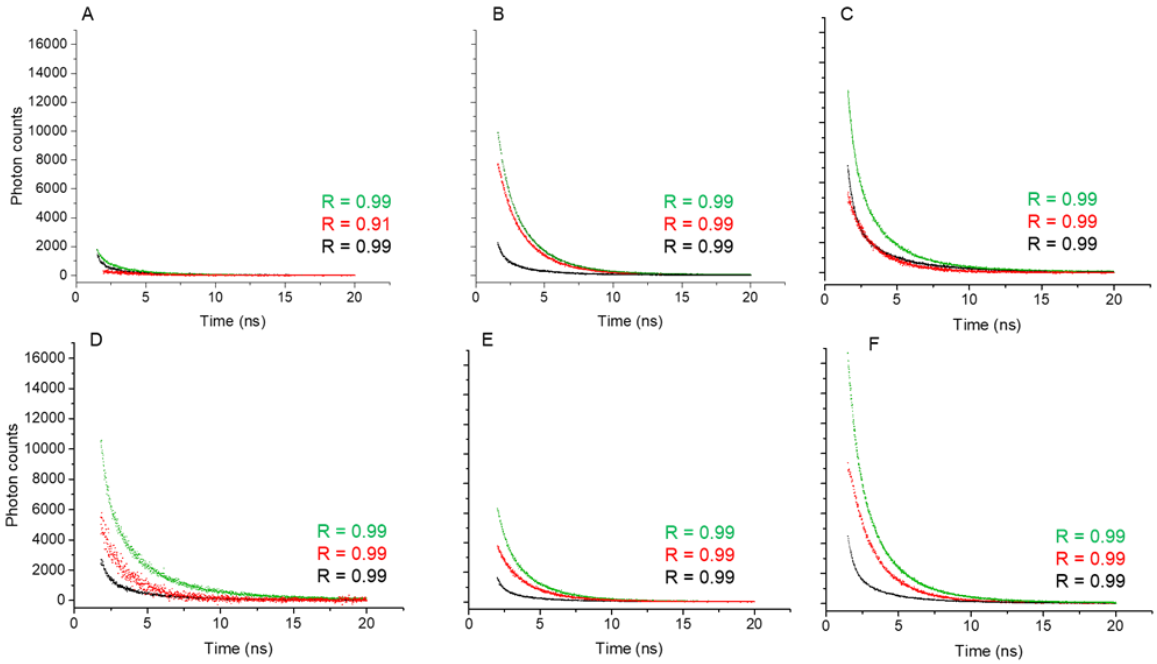

Figure 3.9. **Corrected GFP fluorescence in live yeast cells expressing Ccp1-GFP.** Panels show the summed autofluorescence from 25 WT cells (black dots), the summed fluorescence from 25 cells expressing Ccp1-GFP (green dots), and the corrected GFP fluorescence after subtraction of autofluroescence (red dots). TCSPC data are shown separately for: (A, D) ~ 4000 pixels from extramitochondrial regions of (A) 2-day and (D) 7-day cells; ~ 4000 pixels from mitochondrial regions of (B) 2-day and (E) 7-day cells; and ~ 10000 pixels from (C) 2-day and (F) 7-day whole cells. The FLIM analysis was performed as described in Section 3.4.5. The fluorescence lifetimes and amplitudes calculated from the corrected Ccp1-GFP fluorescence are listed in Table 3.2. Data are representative of 100 cells expressing Ccp1-GFP and 100 WT cells from 3 independent 2-day (OD_{600} ~ 2.5) and 7-day (OD_{600} ~4.5) cultures.

3.5.5) Spatiotemporal distribution of holo- and apoCcp1-GFP in live cells

Following correction for autofluorescence, GFP fluorescence was found to decay mono- and biexponentially in the extramitochondrial and mitochondrial regions, respectively, of live cells expressing Ccp1-GFP (Figure 3.8; Figure 3.9A,B and D,E). From a linear standard plot of α_1 vs % holoCcp1-GFP (Figure S3.4),[114] we can extract the fraction of Ccp1-GFP with bound heme using the α_1 values from the corrected decay curves in Figure 3.9.

Essentially all mitochondrial Ccp1-GFP is in the holoform whereas the extramitochondrial fluorescence monoexponentially decays with a lifetime close to τ_0, indicating that Ccp1-GFP outside the mitochondria is free of heme (Table 3.2). The corrected fluorescence from whole cells is the combination of that from mitochondrial and extramitochondrial Ccp1-GFP. From the FLIM images (Figure 3.10), we can readily see that 2-day cells, which appear yellow (merge of red and green), contain a significantly larger fraction of holoCcp1-GFP than 7-day cells, which appear bright green. To determine the actual percentage of holoCcp1-GFP, the corrected fluorescence from 100 whole cells selected from three independent cultures (i.e., 50 cells from 2-day and 50 cells from 7-day cultures) was fit by triexponential decay with τ_0, τ_1, and τ_2 fixed at the values measured for cells of the same age (Table 3.2 and Figure 3.9C,F).

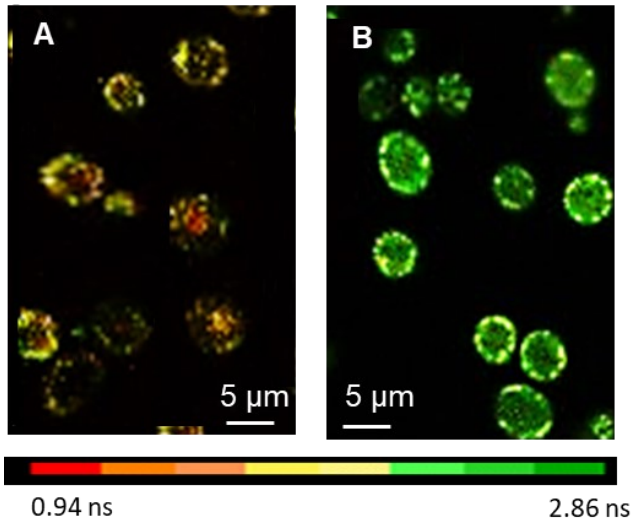

Figure 3.10. The FLIM image of 2-day vs 7-day Ccp1-GFP-expressing cells. The yellow color of (A) 2-day cells (merge of red and green) indicate that they contain a significantly higher percentage of holoCcp1-GFP than (B) 7-day cells, which appear bright green. The calcaulted percentages of holoCcp1-GFP are given in Table 3.2. FIJI software was used to enhance and display these images.

From the standard curve (Figure S3.4) and an average a_1 value of 38 ± 1%, we find 96 ± 3 % holoCcp1 in 2-day whole cells (Table 3.2). This drops to 44 ± 8 % holoCcp1-GFP in 7-day whole cells, which exhibit an average a_1 value of 18 ± 3 % (Table 3.2). From previous Western and heme blotting of subcellular factions, we reported a relatively constant level of Ccp1-GFP in cells from 1–10 day cultures but the fraction of mitochondrial holoCcp1-GFP dropped from 93 ± 2 % in 2-day cells to 35 ± 5 % in 7-day cells and 10 ± 2 % in 10-day cells.[22] Thus, the FLIM results on live cells corroborate the biochemical data. Similar Western blotting of WT cells revealed that the fraction of mitochondrial holoCcp1-GFP dropped from 92 ± 2 % in 2-day cells to 22 ± 5 % in 7-day cells and 5 ± 2 % in 10-day cells.[22] The data for 7-day cells suggest that WT Ccp1 may exit mitochondria slightly faster than Ccp1-GFP but clearly tagging Ccp1 does not significantly impact its cellular location.

3.6) Discussion

3.6.1) FLIM uncovers spatiotemporal invariance in Sod1-GFP's time-resolved fluorescence in live cells

Sod1-GFP with the GRRIPGLIN linker exhibits fluorescence lifetimes (1.48 ± 0.15 and 2.62 ± 0.14 ns) and amplitudes (30 ± 2.5 and 70 ± 2.5 %) that are independent of its subcellular location and remain the same in 2- and 7-day live cells (Table 3.1). GFP fluorescence is quenched by Cu^{II} (which has visible absorption from 450 to 750 nm) with an R_0 of 21 Å.[121] Assuming the same R_0 for Sod1-GFP, FRET analysis (see caption to Figure S2.10) predicts a Cu^{II}-GFP fluorophore separation of ~ 24 Å in molecules with the shorter lifetime and a separation of ~ 43 Å in molecules with the longer lifetime. To examine possible distances between Cu^{II} and the GFP fluorophore, we fused the C-terminus of chain A of the Sod1 homodimer to the N-terminus of GFP *in silico*. With the linker in helical and extended conformations espoused for holoCcp1-GFP (Figure 2.7; Section 2.6.2),[114] the Cu^{II} of chain B is 24 and 43 Å from imidazole C1 of the fluorophore, respectively (Figure S3.5), as predicted by the FRET analysis. Thus, we assume that in live cells our nonheme-binding Sod1-GFP control exists as an equilibrium mixture of compact and extended conformations that does not change with subcellular location or cell age since the lifetime amplitudes remain constant (a_1 and a_2 values; Table 3.1). Furthermore, a_1 and a_2 are the same in buffer as in cells (Table 3.1), indicating that Sod-GFP's extended-compact conformational equilibrium also does not shift in these environments. However, the lifetime amplitudes do change for Ccp1-GFP (Table 3.2; Section 3.5.5).

Table 3.2. Ccp1-GFP location, fluorescence lifetimes, fractional amplitudes and % holoform in 2- and 7-day live cells [a]

Culture age	Ccp1-GFP location	τ_1 (ns)	% a_1	τ_2 (ns)	τ_0 (ns)	% $a_0 + a_2$	% holoform
2 days	Mitochondria	0.94 ± 0.09	38 ± 1.9	2.38 ± 0.12		62 ± 1.9 (a_0 = 0)	100
2 days	Extra-mitochondria				2.57 ± 0.10	100 (a_2 = 0)	0
2 days	Whole cell	0.94 [b]	38 ± 1.0	2.38 [b]	2.57 [b]	62 ± 1.0	96 ± 3
7 days	Mitochondria	0.98 ± 0.08	38 ± 2.0	2.55 ± 0.12		62 ± 2.0 (a_0 = 0)	100
7 days	Extra-mitochondria				2.61 ± 0.05	100 (a_2 = 0)	0
7 days	Whole cell	0.98 [b]	18 ± 3.0	2.55 [b]	2.61 [b]	82 ± 3.0	44 ± 8
Average τ_n and a_n values [c]		0.96 ± 0.02	23 ± 18	2.46 ± 0.1	2.59 ± 0.02	77 ± 18	
τ_n and a_n values *in vitro* [d]		0.95 ± 0.08	38 ± 1.5	2.46 ± 0.03	2.84 ± 0.10	62 ± 1.5 (a_0 = 0)	100
t_{m1} and t_{m2} values (2-day cells) [e]		0.68	20	2.68		80	

[a] Live cells expressing Ccp1-GFP were selected from 3 independent 2-day (OD_{600} ~ 2.5; total of ~50 cells) and 7-day (OD_{600} ~4.5; total of ~50 cells) cultures and were analyzed by FLIM as described in Figures 3.8 to 3.10. The GFP fluorescence was corrected for yeast autofluorescence as outlined in Section 3.4.4.

[b] These lifetimes were fixed at values measured for the mitochondrial and extramitoncondrial regions of cells of the same age. Since τ_0 and τ_2 are not resolved by FLIM, $a_0 + a_2$ are considered as a sum for whole cells.

[c] Average of all the τ_n and a_n values recorded for 100 cells irrespective of culture age. The overall variation in lifetime amplitues (SD ± 18) for cells expressing Ccp1-GFP is much higher than that for cells expressing Sod1-GFP (SD ± 2.5) (Table 3.1).

[d] Fluorescence lifetimes measured for recombinant holoCcp1-GFP (τ_1, τ_2) and apoCcp1-GFP (τ_0) *in vitro* (Section 2.5.4).[114]

[e] Mean arrival times (t_m) and relative intensities measured without background correction or cell selection for 20 whole cells from 2-day cultures (Figure 3.7A).

3.6.2) FLIM reliably tracks PTM of Ccp1-GFP by heme insertion in live cells

Our knowledge of PTM by noncovalent heme incorporation into target constitutive heme proteins is very limited. We do know that immature Ccp1 is produced and targeted to mitochondria even in absence of heme biosynthesis.[21,22] When yeast are exposed to oxygen and heme biosynthesis is turned on, apoCcp1 immediately matures to holoCcp1.[21,22] Unlike Ccp1,[21] nuclear encoded Cta1, the peroxisomal and mitochondrial heme catalase in yeast,[122] is synthesized under O_2/heme control,[21,123] suggesting that apoCta1 matures (i.e., acquires heme) after apoCcp1. In fact, we recently demonstrated that Ccp1-derived heme is recruited for Cta1 maturation in mitochondria.[26]

Additionally, our biochemical analysis of subcellular fractions of respiring yeast suggested that both apoCcp1 and apoCcp1-GFP, but not their holoforms, exit mitochondria.[26] Also, mature holoCcp1 does not enter isolated mitochondria,[124] so it appears that apoCcp1 has the conformational flexibility[124] to diffuse through the outer mitochondrial membrane but not conformationally more rigid holoCcp1.[125] The present FLIM results confirm that Ccp1 loses its heme and that apoCcp1 exits the mitochondria in live, respiring cells.

The partitioning in yeast of holoCcp1 and apoCcp1 inside and outside the mitochondria, respectively, provides a prodigious opportunity to characterize the time-resolved fluorescence of both holoCcp1-GFP and apoCcp1-GFP in live cells. Remarkably, we find that a_1, the amplitude of the short lifetime τ_1 of holoCcp1-GFP, is the same (38 ± 2%) in the mitochondria of 2- and 7-day live cells and in the test tube (Table 3.2). Thus, Ccp1-GFP lifetime quenching on heme acquisition is same in both environments and our standard plot of a_1 vs % holoCcp1-GFP, which we prepared for the recombinant fusion *in vitro* (Figure S4.3), is valid in live cells and provides an accurate determination of the percentage of holoCcp1-GFP in whole cells from the measured a_1 value (Table 3.2).

3.6.3) The GRRIPGLIN linker adopts similar conformations in cells and *in vitro*

The amplitude a_1 of the short lifetime τ_1 (Table 3.1 and 3.2) reports on the populations of the compact conformations of Sod1-GFP (Figure S3.5) and holoCcp1-GFP (Figure 2.7).[114] Based on the observed a_1 values, the GRRIPGLIN linker exhibits similar flexibility in the intracellular environment as in buffer.[114] We speculate that the higher compact population of holoCcp1-GFP (~38%) vs Sod1-GFP (~30%) reflects more favorable electrostatic interactions between Ccp1 (pI 5.1) and GFP (pI 6.0) vs Sod1 (pI 5.6). Also, Sod1 is a homodimer, which may lead to steric hindrance in compact conformations of its GFP fusion. On the other hand, favourable electrostatic interaction between GFP and the electropositive cavity around the

active-site Cu^{II} of Sod1[126] might contribute to stabilization of the more compact conformations of Sod1-GFP. Since all yeast open-reading frames (ORFs) have been C-terminally linked to GFP by GRRIPGLIN,[114] it will be informative to examine α_1 values for fusions of other yeast heme and metalloproteins.

3.6.4) FLIM vs biochemical determination of protein PTM by noncovalent-heme insertion

Heme may repartition between proteins and/or heme proteins may repartition between different subcellular locations on cell lysis. Thus, it is critical to use a technique such as FLIM to directly probe heme-protein maturation in live cells. FLIM also offers technical advantages over the biochemical approach of Western and heme blotting of subcellular fractionation: (i) spatiotemporal changes in heme maturation can be tracked in live cells in real time; (ii) heme maturation of one or more fusion proteins can be simultaneously probed in all cell compartments; (iii) no antibodies are used, avoiding issues of antibody selectivity; and (iv) fewer cells and (v) less time are required. In the current study, we exploited the respiration-induced exit of apoCcp1-GFP from mitochondria to compare the percentages of holoCcp1-GFP in 2- and 7-day cells determined by FLIM (96 ± 3 vs 44 ± 8 %, Table 3.2) and biochemically (93 ± 2 vs 35 ± 5%). The agreement within experimental error between the two techniques suggests little or no loss of holoCcp1-GFP from mitochondria or no heme acquisition by extramitochondrial apoCcp1-GFP on cell lysis. Nonetheless, lysis may cause heme repartitioning and subcellular relocalization of other proteins, so biochemical data should be confirmed on a case-by-case basis by live-cell FLIM imaging.

3.6.5) Fluorescence lifetime vs intensity imaging of live cells to monitor PTM by heme insertion

Fluorescence lifetimes are independent of variation in protein expression, pH, sample absorption, sample thickness, photobleaching, and are not influenced by instrument settings such excitation power and detector gain. These variables affect intensity-based measurements so ratiometric intensity corrections are necessary. Such corrections require fusing the protein of interest to a heme-sensitive fluorescence protein (FP) plus a second heme-insensitive reference FP. This increases the probability that the normal expression, subcellular localization and function of the test protein will be altered. In contrast, ratiometric lifetime measurements can be performed with a single FP, which is less likely to interfere with the test protein's normal role in the cell.

3.7) Conclusions

FPs have served in cells as localization probes,[27] and as sensors of pH,[28] chloride,[29–31] and Ca^{2+} ions[32,33] *in vivo* and of Zn^{2+}, Cu^{2+}, Cd^{2+} and Ni^{2+} ions *in vitro.*[34,35] Here we demonstrate

that GFP lifetime quenching enables accurate spatiotemporal tracking in live cells of PTM by insertion of noncovalent heme. Specifically, we found by live-cell FLIM imaging that holoCcp1-GFP and apoCcp1-GFP are mitochondrial and extramitochondrial, respectively, in respiring yeast. These results support our biochemical data from cell lysates for both Ccp1-GFP and native Ccp1,[26] which affirms the absence of heme repartitioning involving Ccp1 on cell disruption. We also confirmed that Ccp1-GFP behaves similarly to native Ccp1 with respect to respiration-induced heme loss and relocalization. In fact, Ccp1-GFP's relocalization following heme release was highly advantageous in establishing FLIM as a reliable tool to track when, where and how much of a protein is modified by heme insertion in live cells.

Our results also demonstrate for the first time that a fusion protein adopts similar conformations in cells and *in vitro*. Furthermore, both Sod1-GFP and holoCcp1-GFP exhibit similar values of a_1 (the amplitude of the more quenched lifetime), suggesting similar populations of the compact conformation of the GRRIPGLIN linker. Should this hold true in general for GFP fusions with a GRRIPGLIN linker (membrane proteins are likely exceptions), we could quickly measure a_1 to estimate the fraction of a heme protein in its holoform in selected cellular locations. Mapping spatiotemporal changes in the a_1 values of different heme proteins would in turn map heme trafficking in cells under normal and pathological conditions as well as expand our knowledge of the functions of heme-binding proteins in their heme-free forms.

3.8) Supplementary information

3.8.1) Importing masks from FIJI-Win64 into SymPhoTime 32

ROIs for FLIM analysis were selected from the confocal images using a macro written by Dr. Chris Law (CMCI, Concordia University) for FIJI-Win64. This macro allows up to 10 cells to be selected at the same time vs a single cell by the SymPhoTime software (PicoQuant). Briefly, the in-house macro creates masks of cells or subcellular regions based on fluorescent intensity. The masks were resized and rotated to match the data generated by the FLIM software (SymPhoTime), and exported as a text image, with each pixel in the ROI expressed as 1, and every other pixel expressed as 0. Replacement of the tab character "\t" by a single space was performed in Wordpad++, because "\t" is not recognized by SymPhoTime. The ROI mask was then imported into SymPhoTime and superimposed on the FLIM image. TCSPC data from ROI masks from multiple cells were exported from SymPhoTime into Excel for summation and exported from Excel into OriginPro2016 (OriginLab). Fitting of an exponential tailfit model to the summed TCSPC data in Origin yielded fluorescence lifetimes and amplitudes after autofluorescence subtraction (Figure 3.9 and S3.3) where necessary.

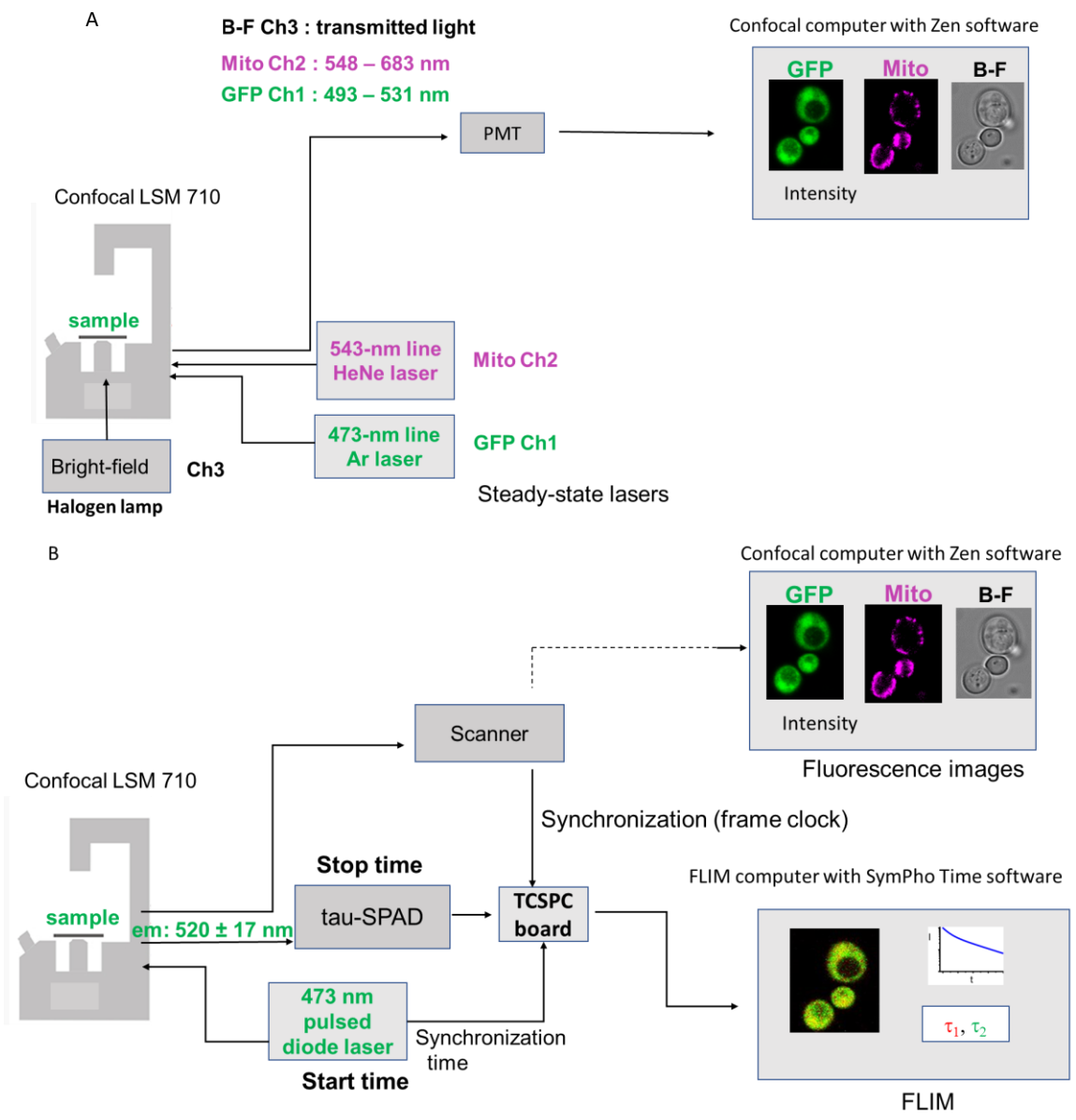

Figure S3.1. Experimental setup for confocal fluorescence microscopy and FLIM of live yeast cells. (A) Setup for GFP localization in live cells by confocal microscopy. A halogen lamp illuminates the sample and the transmitted light is recorded by Zen software (Zeiss) to give the bright field image. Mitotracker (em 548-683 nm) and GFP (em 493-531) are sequentially excited by 543-nm HeNe and 473-nm Ar lasers and the signals are recorded by the Zen software. (B) Set-up to measure GFP lifetimes in live cells by TCSPC FLIM. GFP is excited by a 473-nm pulsed diode laser and the photons emitted at 520 ± 17 nm per Δt (time delay between the laser pulse and photon arrival at the tau-SPAD) are counted in each pixel by the TCSPC board. A histogram of photon counts vs Δt gives the fluorescence lifetimes. The objective scanner is synchronized with the TCSPC to assign each photon to a pixel and build up the FLIM image using SymPho time software. See details in Section 3.4.4.

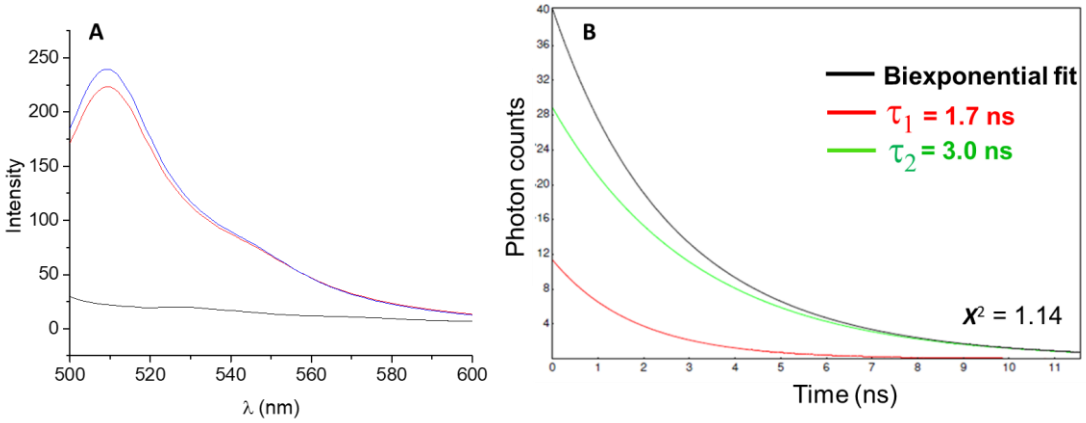

Figure S3.2. Fluorescence intensity and lifetimes of Sod1-GFP in diluted extramitochondrial subcellular fractions prepared from yeast. The mitochondria-depleted subcellular fractions (S10) from WT cells and those expressing Sod1-GFP were diluted into homogenization buffer (pH 7.4) to give an absorbance of ~ 0.05 at 488 nm in 1-cm cuvettes for fluorescence measurements. (A) Steady-state fluorescence spectrum upon excitation at 488 nm of Sod1-GFP from 2- (blue trace) and 7-day (red trace) cells and the signal (black trace) from 7-day WT cells. Spectra were recorded at room temperature on a Cary Varian Eclipse spectrofluorometer (Model FL0812M000) at 600 nm/min with 10-nm slits with the PMT at 600 V and represent the average of 10 scans. (B) The time-resolved fluorescence at 510 nm measured by TCSPC (black trace) following excitation at 467 nm with a 0.47-ns laser pulse of Sod1−GFP from 2-day cells. The data were fitted by biexponential decay (χ^2 = 1.14) and the two components extracted from the biexponential fit (black trace) with τ_1 = 1.7 ns, α_1 = 0.30 (red trace) and τ_2 = 3.0 ns α_2 = 0.70 (green trace). Similar lifetimes were obtained for 7-day cells, and the average values are given in Table 3.2 for cells from 3 independent cultures. Data analysis was performed with FluoFit software (PicoQuant) as described in Section 2.5.3.[114]

Subcellular fractionation was performed as described previously.[26] Aliquots (50 mL) of WT and Sod1-GFP-expressing cells from 2- (OD_{600} ~ 2.5) and 7-day cultures (OD_{600} ~ 4.5) were harvested by centrifugation at 2000 g for 10 min, pellets were washed with 100 mL of distilled water, spun at 2000 g for 5 min, resuspended in DTT buffer (100 mM Tris-H_2SO_4 with 10 mM DTT, pH 9.4, preheated to 30 ºC) with incubated for 10 min at 30 ºC with stirring at 80 rpm, and harvested by centrifugation at 2000 g for 10 min. To break the cell wall, cells were washed with with Zymolyase buffer (1.2 M sorbitol and 20 mM PBS, pH 7.4) and spun at 2000 g for 5 min. Then 4 mL of Zymolyase buffer (with 3 mg Zymolyase 20T per 1 g cells) was added, cells were incubated for 45 min at 30º C, and the resulting spheroplasts were harvested by centrifugation at 2000 g for 5 min at 4º C. In order to break the cell memberane, pellets were homogenized mechanically in 6.5 mL per 1 g cells of homogenization buffer (0.6 M sorbitol, 1 mM EDTA, 1 mM PMSF in 10 mM Tris HCl, pH 7.4 plus 1x proteinase inhibitor cocktail per 225 mL) for 10 cycles/15 strokes and cell debris was pelleted by centrifugation at 2000 g for 5 min. The supernatants were recentrifuged at at 10000 g to give the mitochondria-depleted supernatant (S10) examined here and the mitochondria-enriched pellet (P10). Sorbitol, EDTA, PMSF (phenylmethylsulfonyl fluoride), and EDTA-free Protease Inhibitor Cocktail were purchased from Sigma; Zymolyase 20T was from Thermo Fisher Scientific.

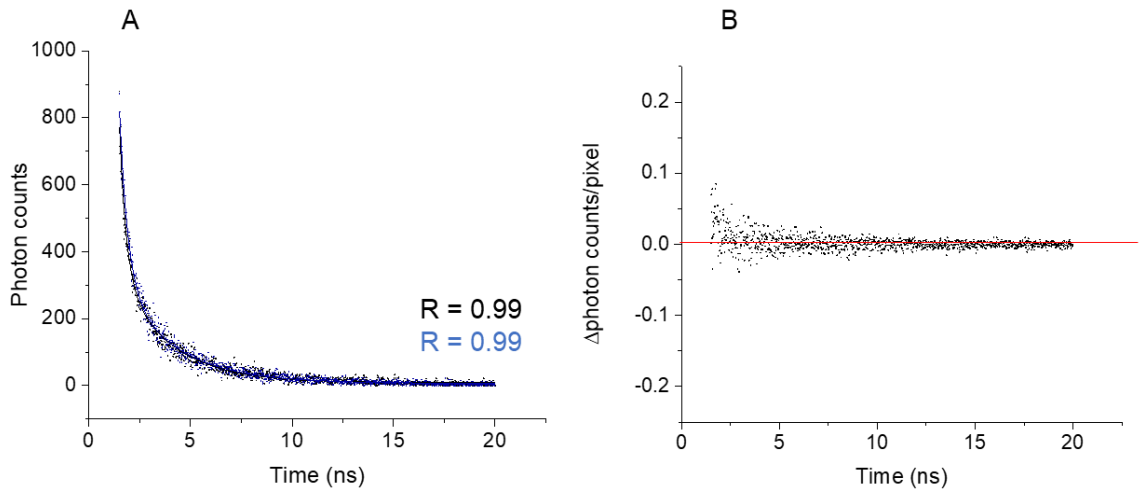

Figure S3.3. **FLIM analysis of the autofluorescence of WT live yeast cells.** (A) The TCSPC data from 50 extramitochondrial masks (1911 pixels) prepared from 25 WT cells from a 2-day culture (black dots) overlayed on the TCSPC data from 50 extramitochondrial masks (1893 pixels) from a second batch of 25 WT cells (blue dots) from a different 2-day culture. Both cultures were grown under the same conditions (Section 3.4.3) at the same time and their FLIM data were recorded on the same day. A biexponential tailfit model (ExpDecay2) was fitted to the summed data (see Section 3.8.1), yielding autofluorescence lifetimes of 0.48 ± 0.09 ns (67 ± 2.5%) and 2.91 ± 0.29 ns (35 ± 2.5%) (Table S3.1). (B) Difference in the number of photons in each of 1150 time channels (16-ps channels) per pixel between first and second batches of cells. The difference gives points (black dots) very close to the red line drawn at y = 0. Note that dividing the number of photons per time channel by the total number of pixels gives a value < 1.

Panel B reveals that the autofluorescence intensity varies negligibly between WT cells, allowing a constant autofluorescence signal to be subtracted from the GFP signal in cells expressing Ccp1-GFP (Figure 3.9). Autofluorescence was analyzed (as described in Figure 3.7) separately for mitochondrial and extramitochondrial regions of WT cells from 2- (OD_{600} ~ 2.5) and 7-day cultures (OD_{600} ~ 4.5) as well as for whole cells. Notably, autofluorescence exhibits lifetimes independent of cell region and age (Table S3.1).

Table S3.1. Lifetimes and fractional amplitudes of autofluorescence from WT cells [a]

Culture age	Cellular region [b]	τ_1 (ns)	% a_1	τ_2 (ns)	% a_2
2-days	Whole cell	0.50 ± 0.03	59 ± 2.6	3.02 ± 0.04	41 ± 2.6
2-days	Mitochondria	0.47 ± 0.05	54 ± 5.0	3.00 ± 0.16	46 ± 5.0
2-days	Extramitochondria	0.48 ± 0.09	67 ± 2.5	2.91 ± 0.29	35 ± 2.5
7-days	Whole cell	0.53 ± 0.10	62 ± 1.0	3.10 ± 0.26	38 ± 1.0
7-days	Mitochondria	0.54 ± 0.10	60 ± 5.0	3.10 ± 0.19	40 ± 5.0
7-days	Extramitochondria	0.53 ± 0.10	61 ± 4.1	3.10 ± 0.10	39 ± 4.1
Average values of τ_n and a_n		0.51 ± 0.03	61 ± 4.2	3.04 ± 0.08	40 ± 3.6

[a] Live WT cells were selected (as shown in Figure 3.3) from 3 independent 2-day (OD_{600} ~ 2.5; total of ~50 cells) and 7-day (OD_{600} ~4.5; total of ~50 cells) cultures and their autofluoresncence was analyzed by FLIM.

[b] Mitochondrial and extramitochondrial ROIs were selected as shown in Figure 3.4 and 3.8.

Table S3.2. Lifetimes and fractional amplitudes of uncorrected fluorescence from Ccp1-GFP-expressing cells[a]

Culture age	Cellular location [b]	τ_1 (ns)	% a_1	τ_2 (ns)	% a_2	τ_0 (ns)	% $a_0 + a_2$ [c]
2-days	Whole cell	0.67 ± 0.06	47 ± 6.0	2.66 ± 0.15	-	2.77 ± 0.20	53 ± 6.0
2-days	Mitochondria	0.75 ± 0.06	41 ± 4.0	2.66 ± 0.21	59 ± 4.0	-	-
2-days	Extramitochondria	0.49 ± 0.08	60 ± 5.0	2.62 ± 0.08	40 ± 5.0	-	-
7-days	Whole cell	0.70 ± 0.01	39 ± 1.0	2.69 ± 0.20	-	2.79 ± 0.20	61 ± 1.0
7-days	Mitochondria	0.69 ± 0.10	39 ± 2.5	2.57 ± 0.15	61 ± 2.5	-	-
7-days	Extramitochondria	0.58 ± 0.10	52 ± 3.1	2.60 ± 0.25	49 ± 3.1	-	-

[a] Live cells expressing Ccp1-GFP were selected (as shown in Figure 3.3) from 3 independent 2-day (OD_{600} ~ 2.5; total of ~50 cells) and 7-day (OD_{600} ~4.5; total of ~50 cells) cultures and were analyzed by FLIM as described in Figures 3.8 to 3.10. The GFP fluorescence lifetimes are *not* corrected for yeast autofluorescence.

[b] Mitochondrial and extramitochondrial ROIs were selected as shown in Figure 3.4 and 3.8.

[c] Since τ_0 and τ_2 are not resolved by FLIM, $a_0 + a_2$ are considered as a sum for whole cells.

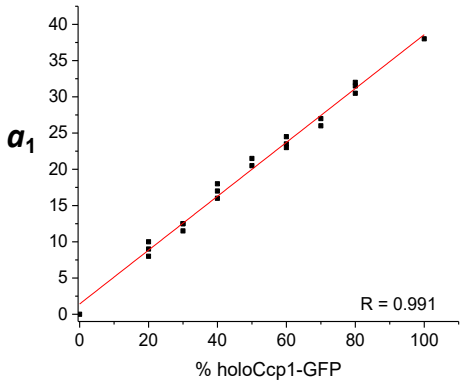

Figure S3.4. The amplitude a_1 of the fluorescence lifetime τ_1 of holoCcp1-GFP vs its mole percent in solution with apoCcp1-GFP. To generate this standard plot, solutions were prepared containing 0-100% mole percent of recombinant apo- and holoCcp1-GFP (0.8 μM total Ccp-GFP in each sample) in 10 mM KPi, 10 mM MES, 100 mM NaCl and 100 μM DTPA (pH 6.5). The time-resolved fluorescence of the solutions was recorded by TCSPC and fit by exponential decay as described in Figure 2.3. The red line shows the linear fit (y = ax + b) to a_1 (expressed as a percentage) vs mole percent of holoCcp1-GFP using the data from Figure 2.5.[114] The excellent fit of the data by a straight line indicates that the percentage of Ccp1-GFP with heme bound can be confidently determined from a_1.

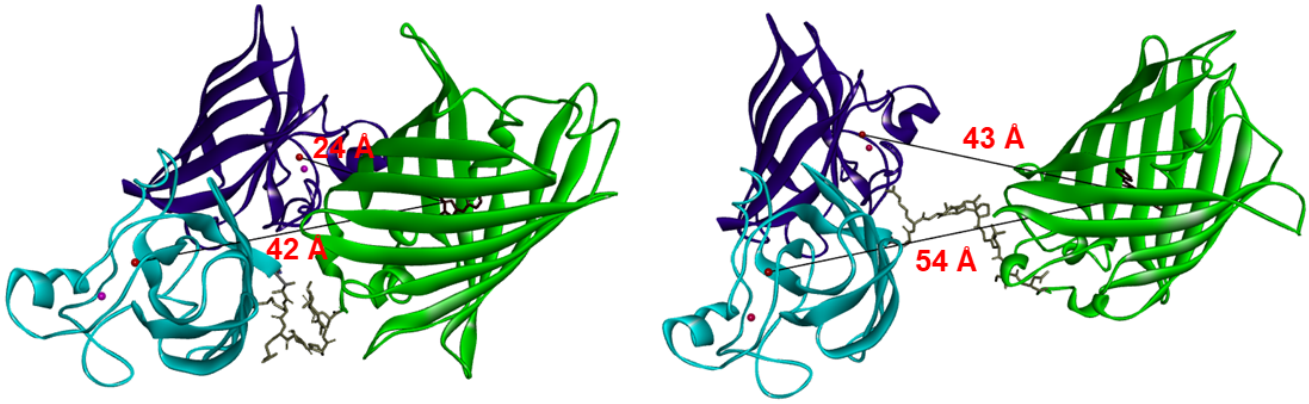

Figure S3.5. Sod1-GFP with the GRRIPGLIN linker in helical and extended conformations. The C-terminus of chain A of the Sod1 homodimer (chain A, cyan ribbon; chain B, blue ribbon) is fused via the GRRIPGLIN linker (grey sticks) to the N-terminus of GFP (green ribbon). The GFP fused to chain B of Sod1 is omitted for clarity. The distances of the active-site Cu^{II} (red dot) of both chain A and B from the imidazole C1 of the fluorophore (black sticks) are indicated for helical (left) and extended conformations of the linker (right). The active-site Zn^{II} is shown as a magenta dot in each Sod1 chain. The linker was prepared and the graphic was generated in Discovery Studio Visualizer using Sod1 (PDB 1F1G) and GFP coordinates (PDB 1EMA). Based on the average fluorescence lifetimes of Sod1-GFP in live cells (τ_1 = 1.48 ± 0.15 ns, τ_2 = 2.62 ± 0.14 ns; Table 3.1), FRET analysis predicts Cu^{II}–fluorophore separations of 24 ± 1 and 43 ± 1 Å, which correspond to the shortest distances marked in the compact (left) and extended conformations (right) of Sod1-GFP (Section 3.6.1).

Chapter 4: Characterizing the H_2O_2 stimulon in *Saccharomyces cerevisiae* cells with normal and amplified H_2O_2 sensing

4.1) Preface

The work presented in Chapter 4 will contribute to a manuscript in preparation: Dastpeyman S, Jiang H, and English AM. Characterizing the H_2O_2 stimulon in *Saccharomyces cerevisiae* cells with normal and amplified H_2O_2 sensing. SD prepared the samples, interpreted the MS data with helpful discussions, and prepared a draft of the manuscript. HJ developed the LC-MS/MS method with helpful discussions and performed the LC-MS/MS analysis. AME conceived the experiment and contributed to the discussions, editing and revisions of the manuscript.

4.2) Abstract of the manuscript

Cytochrome c peroxidase (Ccp1), independently of its peroxidase activity, functions in H_2O_2 sensing and signaling in yeast. A mutant *Saccharomyces cerevisiae* strain (referred to here as W191F) in the BY4741 genetic background producing the peroxidase-inactive Ccp1W191F variant of Ccp1 exhibits amplified H_2O_2 sensing. Also, fermenting W191F cells are more viable than wild-type (WT) cells when challenged with exogenous H_2O_2. To understand this differential response at the proteome level, we performed LC-MS/MS-based label-free quantitative proteomics analysis of exponentially growing fermenting yeast. Following exposure to a sublethal dose (0.4 mM) of H_2O_2, we identified 201 and 141 responsive proteins in WT cells after 10 and 60 min, respectively, compared to 220 and 468 responsive proteins in W191F cells. Thus, W191F strain exhibited a significantly more expansive and prolonged proteomic response to H_2O_2 than WT cells. In both strains changes in protein expression revealed upregulation of antioxidant enzymes and heat shock proteins (HSPs), as well as a switch of cellular activity from biosynthesis to defense such as the redirection of carbohydrate metabolism to trehalose biosynthesis and NADPH regeneration. However, amplified H_2O_2 sensing by Ccp1W191F is linked to stronger stimulation of Ctt1 and HSPs, more protein degradation, less protein and amino-acid biosynthesis, more trehalose biosynthesis following H_2O_2 challenge of fermenting W191F vs WT cells.

4.3) Introduction

Reactive oxygen species (ROS), such as hydrogen peroxide (H_2O_2), superoxide radical anion ($O_2^{-\cdot}$), and the highly reactive hydroxyl radical ($OH^{-\cdot}$), attack biomolecules, which can lead to loss of function and cell death.[47] Cells produce various antioxidant enzymes including superoxide dismutases to catalyze $O_2^{-\cdot}$ removal, and peroxidases and catalases to metabolize H_2O_2. Cooperation between antioxidant enzymes is required to buffer the amount of ROS in cells. In addition to upregulating antioxidant enzymes, cells regulate other proteins to combat ROS stress. In 1998, Godon et al.[66] studied the H_2O_2 stimulon in *S. cerevisiae* strain YPH98 challenged with 0.2 – 0.8 mM H_2O_2 using 2-D gel/radiography. They quantified 400 proteins, including 115 responsive (upregulated and downregulated) proteins: 12 antioxidant enzymes, 12 heat shock/chaperon proteins, 12 proteases and proteasome subunits, 24 proteins associated with the translation apparatus and ribosome biogenesis, 25 enzymes participating in carbohydrate metabolism and 30 enzymes implicated in amino acid metabolism.[66] Mapping of these 115 proteins unto cellular processes indicated that H_2O_2 challenge caused cells to increase antioxidant enzyme expression, decrease protein synthesis, increase protein degradation, and increase NADPH regeneration.[66] Total protein extracts (~ 200 μg) were labeled with ^{35}S-Met to quantify proteins by radioimaging of the 2-D gels so proteins without sulfur-containing residues (e.g., HSP26) were not detected.

In another study, label-free 2-D gel electrophoresis and tandem mass spectrometry (MS/MS) were used to identify the cellular response of the diploid yeast BY4743 to linoleic acid hydroperoxide (LoaOOH) challenge. The focus here was on the role of the major oxidative-stress regulator, the transcription factor, yeast AP-1 (YAP1),[127] which is engaged in detoxifying lipid oxidants and their unsaturated breakdown fragments. Less LoaOOH-responsive proteins were found in cells that did not express YAP1 (*yap1Δ*) than in WT cells, which showed a total of 102 LoaOOH-responsive proteins.[127]

Another group studied the yeasts, *Candida glabrata* and *Candida albicans*,[128–130] and their response to alkaline pH.[131] They quantified 1500-2000 proteins using MS-based label-free proteomics from ~30 μg of total protein extracts.[131] Label-free quantitative proteomics is a rapid tool for the reproducible and high-quality quantitative analyses of small amounts of protein extracts.[132] In contrast, labeling with stable isotopes (^{14}N and ^{15}N) allowed quantitation of ~2300 proteins from the WT and glucose repressed *S. cerevisiae* strains, [133] but labeling requires more sample processing, such as modifying growth conditions, to obtain mixtures of label-free and

labeled cultures under similar conditions. Also, only samples that were physically mixed in the same run can be straightforwardly compared.

Hence, here we exploit the advantages of label-free proteomics to elucidate the role of Ccp1 signaling and the impact of its W191F mutation on the H_2O_2 stimulon. Our research group identified Ccp1 as a novel yeast H_2O_2 sensor,[24] and found its W191F variant, which is devoid of peroxidase activity, to be a better H_2O_2 sensor.[24] Plus the viability of fermenting W191F cells is higher than that of WT cells challenged with 0.4 mM H_2O_2. Thus, our goal was to characterize the H_2O_2-responsive proteins in both strains. Specifically, using LC-MS/MS-based label-free, peptide-centric proteomics, we assessed the changes in global protein expression in *S. cerevisiae* (BY4741 strain) with normal (WT cells) and amplified H_2O_2 sensing (W191F cells) in response to 0.4 mM H_2O_2. We identified ~1700 proteins and report that Ccp1 mutation has a significant impact on the H_2O_2 stimulon in yeast at 10- and 60-min H_2O_2 post-challenge. Figure 4.1 summarizes the protocol used in this study.

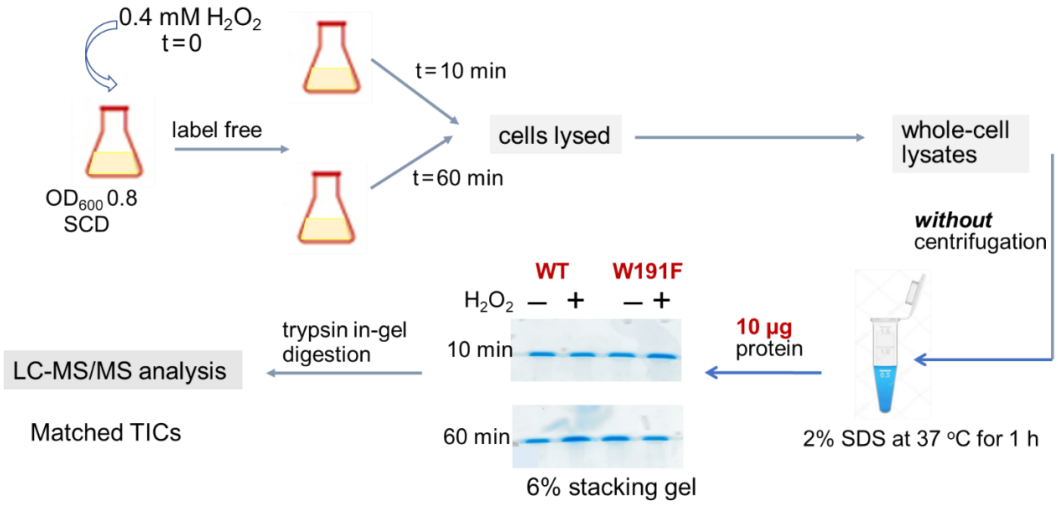

Figure 4.1. Overview of LC-MS/MS-based label-free proteomics analysis of WT and W191F cells following H_2O_2 challenge. *S. cerevisiae* cells grown in SCD to OD_{600} ~ 0.8 (16 h) were challenged with sublethal 0.4 mM H_2O_2 at t = 0 and harvested at t = 10 and 60 min. NaCl (1 mM) was added to control cultures (Section 4.4.2). Cells were lysed and proteins (~10 µg) were concentrated in single bands on 6% stacking gels (Section 4.4.3; Figure 4.3). The bands were cut from the gels, the proteins in-gel digested with trypsin (Section 4.4.4), and an equal amount of digest was analyzed for each sample by LC-MS/MS (Section 4.4.5). Proteins in 24 samples were identified and quantified as outlined in Sections 4.5.1 and 4.5.3.

4.4) Experimental Section

4.4.1) Materials

Suppliers of (bio)chemicals were as follows: sequencing grade modified trypsin from porcine pancreas (T6567), yeast synthetic drop-out medium supplements without histidine (Y1751), histidine (H7750), yeast nitrogen base without amino acids (Y0626), D-(+)-glucose, acid-washed glass beads (425-600 µm), ethylenediaminetetraacetic acid (EDTA), phenylmethylsulfonyl fluoride (PMSF), DL-dithiothreitol (DTT), iodoacetamide, formic acid (FA), ammonium bicarbonate, potassium phosphate monobasic, potassium phosphate dibasic, ammonium persulfate (APS), sodium dodecyl sulfate (SDS), and cOmplete™ EDTA-free Protease Inhibitor Cocktail tablets (Sigma Aldrich); Bio-SafeTM Coomassie stain and 30% Acrylamide/Bis Solution (Bio-Rad); BLUeye prestained protein ladder (FroggaBio); hydrogen peroxide 30%, tetramethylethylenediamine (TEMED), HPLC-grade acetonitrile (ACN), and HPLC-grade water (Thermo Fisher Scientific). All other chemicals were the purest grades available.

4.4.2) Yeast strains, growth conditions and challenge with H_2O_2

Wild-type (WT) *S. cerevisiae* cells in the BY4741 genetic background (MATa his3Δ1 leu2Δ0 met15Δ0 ura3Δ0) were purchased from the European *S. cerevisiae* Archive for Functional Analysis (EUROSCARF). The DNA template for catalytically inactive mature Ccp1(W191F) (*mCCP1*^{W191F}) was kindly provided by Professor Yi Lu (Department of Chemistry, University of Illinois, Urbana, IL, USA) and *mCCP1* was replaced by *mCCP1*^{W191F} in the chromosome under control of the *CCP1* promoter by homologous recombination as our group described previously.[24] Thus, W191F cells have the *CCP::CCP1*^{W191F} mutation in the same genetic background as WT cells.[24,134,135]

WT and W191F cells from frozen glycerol stocks (-80 ºC) were steaked on SCD-agar medium (0.67% yeast nitrogen base without amino acids, 1.92 g/L yeast synthetic drop-out medium supplements without histidine, 0.08 g/L histidine, 2% D-glucose, and 2% agar) and incubated for 2 days at 30 ºC. Single colonies were selected and transferred to 10 mL of SCD liquid medium (no agar) in 50-mL Falcon tubes. The pre-cultures were grown for 22 h at 30 ºC with shaking at 225 rpm, diluted to an initial OD_{600} of 0.01 in 100 mL of SCD and grown at 30 ºC/ 225 rpm in 500-mL Erlenmeyer flasks for 3 days. Aliquots (~200 - 500 µL) were removed from the cultures and their OD_{600} was immediately recorded on a diode-array spectrophotometer (Agilent, Model 8453) to monitor growth (Figure 4.1).

A stock solution of 100 mM H_2O_2 was prepared in autoclaved 0.85% NaCl. At the early log-phase (OD_{600} ~ 0.8), the 100-mL cultures were divided into 50-mL aliquots, 200 µL of stock

H_2O_2 was added to one aliquot to give final concentrations of 0.4 mM H_2O_2 plus 1 mM NaCl, and 200 µL of vehicle only (autoclaved 0.85% NaCl) was added to the control aliquot. At 10 and 60 min post-challenge, the H_2O_2-challenged and control cultures were collected and spun at 2000 g (Figure 4.2). Pellets were washed 2X with 100 mM potassium phosphate pH 7.4 (KPi) and stored at -80 °C for analysis.

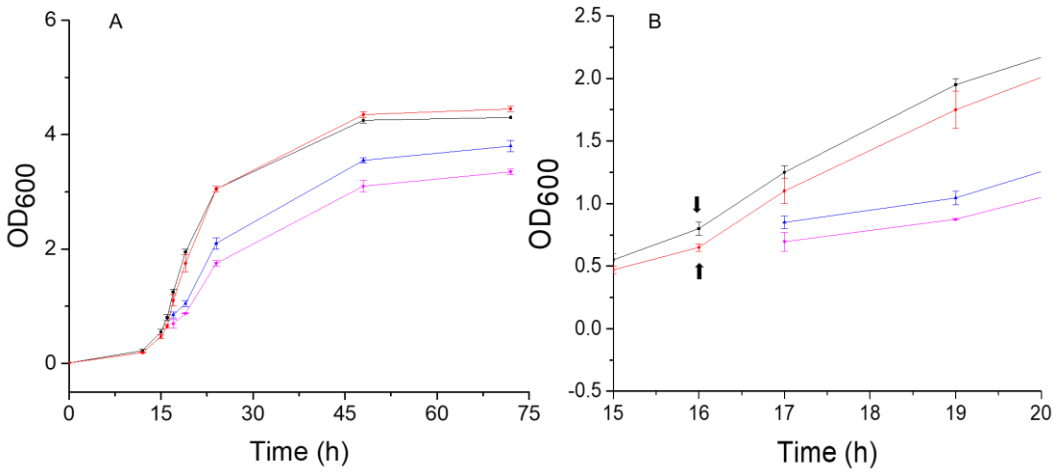

Figure 4.2. Growth curves over three days of unchallenged and H_2O_2-challenged WT and W191F cells. Growth of cultures with an initial OD_{600} ~ 0.01 in SCD medium over 3 days at 30 °C with shaking at 225 rpm. After 16 h (OD_{600} ~ 0.8) 0.4 mM H_2O_2 was added to one aliquot and vehicle only (0.85% NaCl) was added to the second aliquot (control). (A) OD_{600} of control WT (black), control W191F (red), H_2O_2-challenged WT (blue), and H_2O_2-challenged W191F cultures (pink) recorded on a diode-array spectrophotometer (Agilent) in 1-cm cuvettes at RT. (B) The x- and y-scale are expanded in the range of the OD_{600} values at 15, 16, 17 and 19 h, corresponding to 1 h pre- and 0, 1 and 3 h post-challenge with H_2O_2, respectively. Data points represent the mean and standard deviation for 3 independent cultures and H_2O_2 or vehicle was added at the black arrows. The details of culture preparation and challenge are given in Section 4.4.2. Note that to obtain accurate and linear OD_{600} readings (i.e., values within 0.1 - 0.9), aliquots removed from the cultures were diluted in the cuvettes as needed with 1 mM NaCl.

4.4.3) Cell lysis, SDS-PAGE analysis and concentration of proteins from whole-cell lysates

Cells (~ 50 µL) frozen at -80 °C (Section 4.4.2) were thawed on ice, washed 2X in 100 mM KPi (pH 7.4) and resuspended in 200 µL of lysis buffer (100 mM KPi with 1 mM EDTA, 1 mM PMSF, and one cOmplete protease inhibitor tablet per 50 mL buffer) at RT. Glass beads (200 µL) were added and cells were disrupted by vortexing 8 x 30 s at 30-s intervals and cells were placed on ice between agitation. The whole-cell lysates were *not* subjected to centrifugation at this step to avoid loss of insoluble proteins. Aliquots (10 µL) of lysate were suspended in 10 µL of water plus 5 µL of 5X loading buffer (250 mM Tris-Cl pH 6.80 with 10%

SDS, 25% bromophenol blue, 50% glycerol, and 500 mM DTT), and solubilized in this final SDS concentration of 2% by incubating for 1 h at 37 °C. SDS-PAGE analysis was performed to ensure that the lysates have similar protein profiles. The 12% SDS-PAGE gels (10 x 10 cm) were stained with Coomassie blue for 30 min (following Bio-rad's instructions), and destaining in dd-water for 1 h revealed that the protein profiles were the same for all samples (Figure 4.3A).

Proteins in 10 μL of the diluted whole-cell lysates (10 μL of lysate in 10 μL of water plus 5 μL of 5X loading buffer) were concentrated in single bands separated by an empty lane to avoid cross-contamination on a 6% 10 x 10 cm stacking gel (1.6 mL of 30 % acrylamide, 80 μL of 10% APS; 8 μL TEMED, 40 μL of 10% SDS, 1 mL of 1 M tris, and 5.4 mL dd-H_2O, pH 6.8) (Figure 4.3B). The stacking gel was stained with Coomassie blue for 30 min and destained in dd-water overnight. Aliquots of protein ladder (Figure 4.3C) also were concentrated in a 6% stacking gel to estimate visually the amount of protein per 10 μL of lysate.

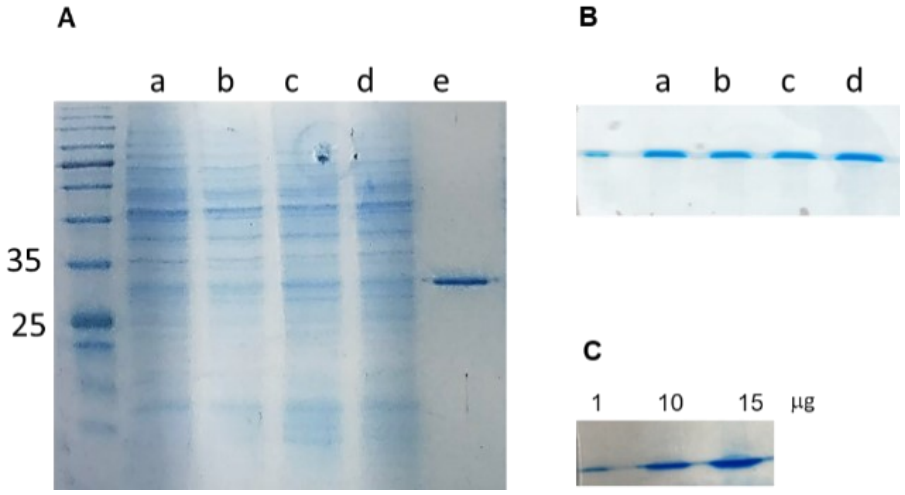

Figure 4.3. SDS-PAGE analysis of cell lysates and concentration of whole-cell proteins in one band. (A) 12% SDS-PAGE gel showing protein profiles in 20 μL of 2.5X diluted whole-cell lysates of: (lane a) WT/10, (lane b) WT/10pc, (lane c) W191F/10 and (lane d) W191F/10pc cells, where /10 and /10pc (pc, post challenge) signify that vehicle and 0.4 mM H_2O_2, respectively, were added to the cultures 10 min before cells were harvested. The first lane shows the protein ladder (3 μg) and (lane e) purified recombinant Ccp1 (0.6 μg). (B) Proteins in the same 2.5X diluted whole-cell lysates (10 μL) analyzed in panel A were concentrated in lanes a-d of a 6% stacking gel and protein ladder (1 μg) was added to the first lane. (C) The indicated quantities of protein ladder in a 6% stacking gel. From panel C, we estimate ~10 μg of total protein per lane a-d of panel B. Whole-cell lysates of cells harvested at 60 min after treatment (i.e., WT/60, WT/60pc, W191F/60 and W191F/60pc cells) were analyzed similarly (data not shown). SDS-PAGE analysis was performed as outlined in Section 4.4.3.

4.4.4) Protein in-gel digestion with trypsin

Bands from the 6% stacking gels were cut into ~1 x 1 mm pieces, transferred to 1.5-mL Eppendorf tubes, and in-gel digestion was performed following a standard protocol provided by Dr Heng Jiang (CBAMS). Briefly, protein thiols were reduced with 10 mM DTT and alkylated with 50 mM iodoacetamide at RT for 30 min. The gels were washed 4X with 25 mM NH_4HCO_3 in increasing amounts (5–50%) of aqueous ACN, incubated in 100% ACN, dried in a Speed Vac (Savant) at 43 ^oC, and rehydrated in 25 mM aqueous NH_4HCO_3. Proteins were in-gel digested with 1:20 (w/w) trypsin:protein overnight at 30 ^oC, the gel pieces were incubated for 15 min at RT in peptide-extraction solution (60% aqueous ACN, 0.5% FA), and the extracted peptides were collected in 1.5-mL Eppendorf tubes, and dried in the Speed Vac at 43 ^oC.

4.4.5) LC-MS/MS analysis, database searching and protein identification

The tryptic peptides (10 μg) were resuspended in 100 μL of solubilization solution (2% aqueous ACN, 1% FA) for LC-MS/MS analysis on an EASY nLC II LC coupled to a LTQ Orbitrap Velos ETD mass spectrometer equipped with a nanospray ion source (Thermo Fisher Scientific). A 2-μL aliquot of each sample was injected onto a 10 cm × 100 μm column packed in-house with Michrom Magic C18 stationary phase (5-μm particle diameter and 300-Å pore size) and equilibrated with mobile phase A (3% aqueous ACN, 0.1% FA). Peptides were eluted at RT from the column at a flow rate of 400 nL/min using a 90-min gradient of solution A and B (97% aqueous ACN, 0.1% FA). The mobile phase was initially 2% B and was ramped up to 8% B by 15 min, 16% B by 48 min, 24% B by 65 min, 32% B by 70 min, 54% B by 77 min, 87% B by 81 min and maintained at 87% B for 3 min followed by 2% B for 6 min to assure all eluted peptides arrived at the detector.[136]

The MS1 spectra of the peptides (~ 272,500 spectra in total) were surveyed from 400 to 1400 m/z at 60,000 resolution (at m/z 400) in the Orbitrap. The dynamic exclusion duration was set to 30 s with a 10-ppm tolerance around the selected precursor ion (peptide) with monoisotopic precursor selection enabled. The ten most abundant precursor ions with charge state +2 or higher were selected for sequencing and peptides were fragmented by collision-induced dissociation (CID) at 35% optimized collision energy with 10 ms activation. The starting m/z of MS2 was automatically determined based on m/z value of the precursor ion and the MS2 sectra were recored in the linear trap with a mass accuracy of 0.5 Da. The MS data were processed using Proteome Discoverer v2.3 (Thermo Fisher Scientific) with the SEQUEST search engine.

Sequence information was obtained for ~11,000 unique tryptic peptides, that is peptides found in only one protein in the database, and proteins were identified from these peptides.

Searches against tryptic peptides in the UniProt *S. cerevisiae* database (Proteome ID: UP000002311S) were performed with a peptide mass tolerance of 10 ppm and dynamic modifications were accepted on Met (oxidation, +15.995 Da) and Cys residues (carbamidomethyl, +57.021 Da). Protein identification is based on ≥ 1 unique peptides with high confidence scores (false discovery rate <1%) and only proteins with high or medium confidence scores (false discovery rate < 5%) are reported (Table S4.1).

4.4.6) Calculation of protein abundance and protein abundance ratio (Ratio) from peptide intensities

The label-free, peptide-centric, quantitative proteomics approached adopted here first requires normalization at the peptide level. Peptide abundances were summed for each sample and the sums were rescaled to the maximum of the 24 values in Proteome Discoverer v2.3. The normalized abundance of a protein is estimated from the *sum* of the rescaled abundances of its unique peptides.

The 24 samples are categorized based on strain (WT or W191F), biological replicate (A, B, C), ± H_2O_2 challenge, 10 or 60 min post-challenge (pc). For example, sample WT-A/10pc corresponds to biological replicate A of WT cells harvested at 10 min post H_2O_2 challenge and its matched control is sample WT-A/10. The averages of the three biological replicates are designated as WT/10, WT/10pc, W191F/10, W191/10pc, etc.

Since a H_2O_2-challenged sample and its control are prepared from the same culture (Figure 4.4), the nested pairwise quantification approach in Proteome Discoverer v2.3. was used to quantify the fold-change in protein abundance from its unique peptides on challenge as defined by Eq 4.1 (called “Ratio” here). Protein Ratios are derived from peptide Ratios (Eq 4.2). For example, protein X was identified based on 3 unique peptides (Figure 4.4) and the Ratio for each peptide was calculated separately for the three biological replicates to give Ratio A, Ratio B, and Ratio C and the median Ratio. Unique peptides 1, 2 and 3 have median Ratios of 2.00, 1.83 and 2.10, respectively (Figure 4.4). Finally, the Ratio of protein X (Eq 4.2) is taken as of the median of the 3 median Ratios for its unique peptides, which is 2.00 (Figure 4.4). A coefficient of variation (CV%) of 12 ± 10 % was observed for peptide Ratios between the 3 biological replicates (Table S4.1).

4.4.7) Principal component analysis (PCA)

PCA is a statistical procedure that removes possible correlation between variables by transforming a set of observed variables into a set of linearly uncorrelated variables called principal components. The PCA of proteomics (PCAP)[137] method is applied to proteomics data

Equation 4.1:

$$\text{Ratio for protein X} = \frac{\text{Abundance of protein X with } H_2O_2 \text{ challenge}}{\text{Abundance of protein X in control}} = 2.00$$

Equation 4.2:

$$\text{Ratio for peptide N} = \frac{\text{Abundance of peptide N with } H_2O_2 \text{ challenge}}{\text{Abundance of peptide N in control}}$$

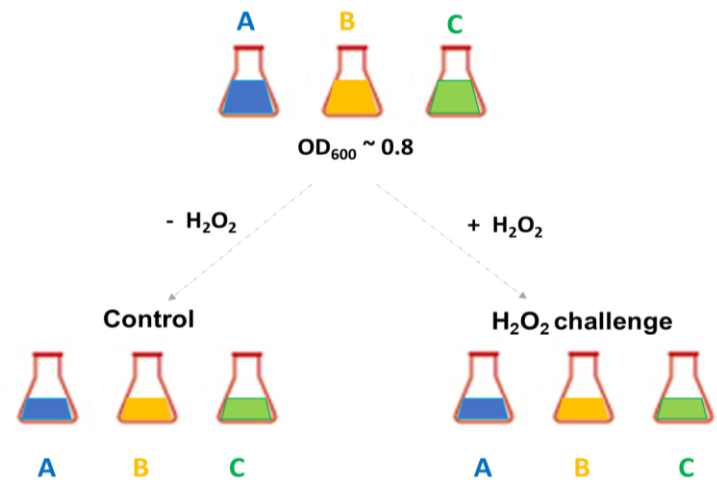

Protein X	A control	A + H_2O_2	Ratio A	B control	B + H_2O_2	Ratio B	C control	C + H_2O_2	Ratio C	Median Ratio
Peptide 1 abundance	50	100	**2.00**	40	85	**2.12**	60	105	**1.75**	*2.00*
Peptide 2 abundance	70	125	**1.76**	50	105	**2.20**	60	110	**1.83**	1.83
Peptide 3 abundance	30	58	**1.93**	40	84	**2.10**	50	112	**2.24**	2.10

Figure 4.4. Calculating the abundance Ratio for protein X from the abundance of its unique peptides. Control and H_2O_2-challenged samples from biological replicates **A**, **B**, and **C** were prepared as outlined in Section 4.4.2. Protein X is identified from its unique peptides 1-3 using LC-MS/MS. The Ratio of each unique peptide (Eq 4.2) is calculated using the nested pairwise quantification approach in Proteome Discoverer v2.3 for each replicate to give Ratio **A**, Ratio **B**, and Ratio **C**, and their median values are listed in the last column. The Ratio of protein X (Eq 4.1) is the median of the median Ratios, which is 2.00 here.

to highlight specific proteins whose expression differs significantly under various conditions.[137–139] Thus, PCAP provides a simple interpretation of proteomics data,[140] and SIMCA (Soft Independent Modeling of Class Analogy) 14 (Umetrics) was used for PCAP analysis in the current research.

4.4.8) Protein annotation

Proteome Discoverer v2.3 provides protein annotation information from a number of databases including: (1) Gene Ontology (GO) database (molecular functions, cellular components, and biological processes); (2) Reactome, KEGG™ PATHWAY, and WikiPathways (pathway annotation); (3) Entrez Gene (gene identification) and (4) UniProt™ (post-translational modification). Note that in the remainder of this chapter the *S. cerevisiae* gene names given in the databases and in Tables 4.4 – 4.10, S4.1, S4.2 and A4.1 (Appendix I) are substituted as abbreviations for the proteins.

4.5) Results

4.5.1) Normalized protein abundances in the 24 samples

Tryptic digests of all cellular proteins concentrated in a single gel band (Section 4.4.3, Figure 4.3) were analyzed by LC-MS/MS (Section 4.4.5). The total ion current (TIC) was similar for all 24 samples (data not shown), confirming that the quantity of digest loaded onto the LC was closely matched for all samples as required in label-free proteomics. Close to 1700 proteins were identified in each lysate (Table 4.1).

Table 4.1. The number of identified and quantified proteins per sample from the three biological replicates

Sample [a]	# protein ID [b]	# protein Ratio [c]
WT/10	1694	1429
WT/10pc	1706	1522
W191F/10	1708	1413
W191F/10pc	1691	1561
WT/60	1681	1505
WT/60pc	1693	1535
W191F/60	1698	1498
W191F/60pc	1708	1575

[a] Sample notation is defined in Section 4.4.6 and Figure 4.5. [b] Number of proteins identified (Section 4.4.5) and quantified (Section 4.4.6) all of the sample's three biological replicates. [c] Number of proteins with a Ratio (Eq 4.1) > 0.67 but < 1.5 identified in all of the sample's three biological replicates (Section 4.4.6 and 4.5.3).

Individual protein abundances were normalized (Section 4.4.6) to eliminate variation between the samples. Such fine-tuning is needed before further data analysis when using label-free quantitation. The box plot in Figure 4.5 reveals that all 24 samples are closely matched with respect to individual protein abundances as expected since most yeast proteins do not respond to challenge with H_2O_2. Thus, given our precision in total protein extraction based on TICs (data not shown) and in observed individual protein abundances (e.g., median Log A = 5.2 ± 0.05, Figure 4.5), we can confidently mine the data for proteins that do respond to H_2O_2 challenge.

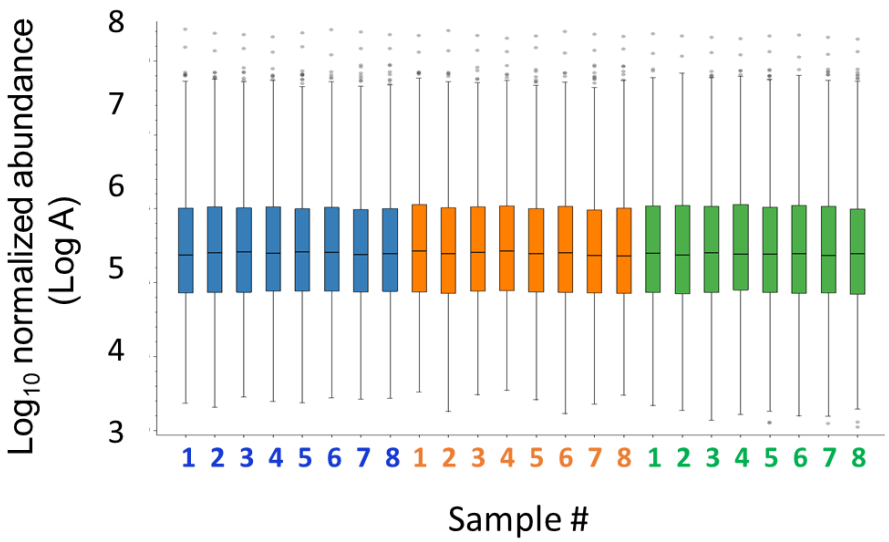

Figure 4.5. Box plot of Log normalized protein abundance (Log A) in the 24 whole-cell lysates. Log A in each of the three biological replicates (**A**, **B**, **C**) examined for lysates from (1) WT/10, (2) WT/10pc, (3) WT/60, (4) WT/60pc, (5) W191F/10, (6) W191F/10pc, (7) W191F/60 and (8) W191F/60pc cells (see Figure 4.3 for cell notation). Normalization at the peptide level was first performed and the normalized abundance plotted here for each of the ~ 1700 individual proteins quantified (Table 4.1) is the sum of the normalized abundances of its unique peptides (Section 4.4.6). The minimum (3.4 ± 0.05), median (5.2 ± 0.05), maximum (7.8 ± 0.05) and interquartile range (4.52 ± 0.05 – 6.74 ± 0.05) of the Log A values are closely matched, indicating that the majority of proteins were expressed at the same level and that protein extraction was highly reproducible for the 24 samples.

4.5.2) PCA of individual protein abundances in the 24 samples

A scores plot is the projection of the samples onto the PCs in two dimensions, which indicates similarity between samples. The x- and y-axis display the selected PCs and here the samples are represented by data points that are each linked to the abundances of ~ 1700 individual proteins per sample. In the PC2 vs PC1 scores plot, the biological replicates of both

the H_2O_2-challenged (triangles) and control samples (circles) separate along the x-axis and are differentiated by PC1. The grouping of the data points reveals surprisingly large differences between replicate C vs replicates A and B for each sample (Figure 4.6A), indicating that differences in some individual protein abundances are greater between replicates than between samples. For example, samples WT-A/10 and WT-B/10 are less similar to their replicate WT-C/10 than to WT-A/60, W191F-A/10, W191F-B/10, W191F-A/60 and W191F-B/60. This likely reflects the interday precision in the LC-MS/MS analysis since biological replicates A and B (16 samples) were run on two consecutive days but replicates C (8 samples) were run a week later.

Nonetheless, exposure to H_2O_2 separates the samples along the y-axis (PC2) and the longitudinal pattern of the data points is similar for the treated and control samples (Figure 4.6A). Thus, the PC2 vs PC1 scores plot implies that the same features change on H_2O_2 challenge in the three replicates. Notably, the W191F/60 replicates show the largest change with respect to PC2 and the response of each to H_2O_2 is similar (dashed lines, Figure 4.6A). In contrast, the WT/60 and WT/60pc replicates separate much less along PC2 except for WT-B/60, which appears to be an outlier.

Figure 4.6B reveals that PC3 separates WT and W191F cells. Since H_2O_2-challenged and control samples are separated by PC2 (Figure 4.6A), in the PC3 vs PC2 scores plot the 24 whole-cell lysates split into four clusters of six samples each, encompassing both the 10- and 60-min time points: WT/10 and 60, WT/10pc and 60pc, W191F/10 and 60, and W191F/10pc and 60pc (Figure 4.6B).

A loadings plot unveils those variables that have the largest effect on a given PC. Thus, a PC3 vs PC2 loadings plot (Figure 4.6C) was prepeared to determine which protein abundances (variables) contribute to the clustering in Figure 4.6B. Each green square in Figure 4.6C represents an individual protein abundance measured across all samples. Squares that lie physically close to 0,0 represent proteins with abundances that vary little between the samples so these variables weakly influence PC2 and PC3. Green squares far from 0,0 represent protein abundances that strongly influence PC2 and/or PC3 and define the main differences between clusters. At a glance, we note that proteins with antioxidant activities such as CCP1, peroxiredoxins (TSA1, AHP1, PRX1), thioredoxin-1 (TRX1), thioredoxin reductase 1 (TRR1), glutathione peroxidase-like peroxiredoxin 2 (GPX2), and glutathione S-transferase omega-like 2 (ECM4) have large positive loadings on both PC2 and PC3, which positions them within the WT/10pc and 60pc cluster. On the other hand, catalase T (CTT1) and sulfiredoxin (SRX1), which also are antioxidant enzymes, and a number of heat shock proteins (HSP26, HSP42, HSP78,

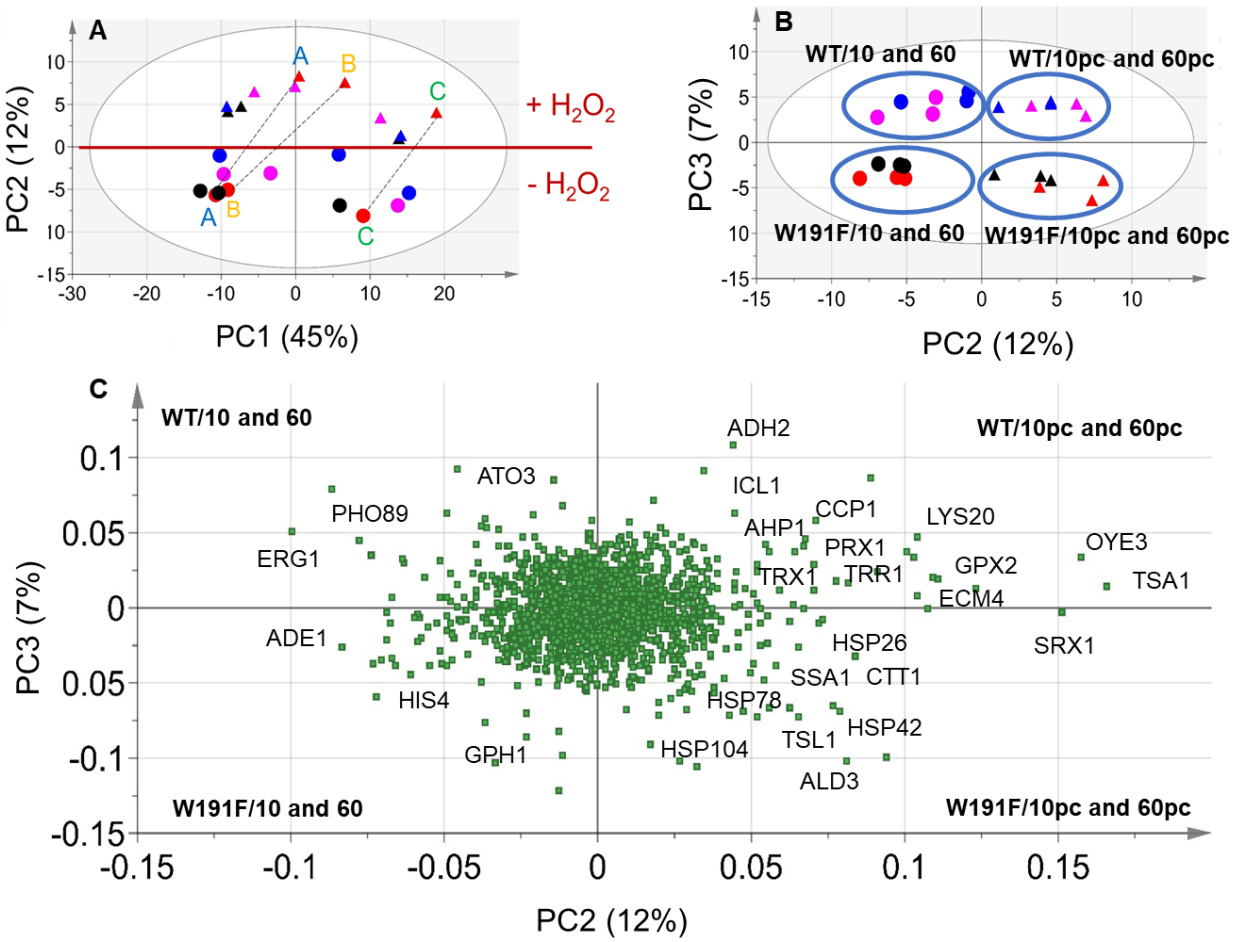

Figure 4.6. PCA scores and loadings plots for protein abundance in the 24 whole-cell lysates. (A) Scores plot of PC2 vs PC1 for biological replicates **A**, **B**, and **C**. The data points (controls: **WT/10** ●, **WT/60** ●, **W191F/10** ●, **W191F/60** ●; H_2O_2-challenged samples: **WT/10pc** ▲, **WT/60pc** ▲, **W191F/10pc** ▲, and **W191F/60pc** ▲) are each linked to the abundances of ~1700 proteins per sample. The dashed lines point out the similar large fold-change between the three **W191F/60** ● / **W191F/60pc** ▲ replicate pairs. (B) Scores plot of PC2 vs PC3 reveals clustering of the 24 samples based on treatment (± H_2O_2) along PC2 and strain (WT vs W191F cells) along PC3 (see text). (C) Loadings plot of PC2 vs PC3 highlights significant differences in the abundance of specific protein between the four clusters identified in panel B. Each variable ■ represents an individual protein measured across all 24 samples. Proteins are labelled by their gene names as follows: Alcohol dehydrogenase 2 (ADH2), cytochrome c peroxidase (CCP1), peroxiredoxins (TSA1, AHP1, PRX1); thioredoxin-1 (TRX1), thioredoxin reductase 1 (TRR1), glutathione peroxidase-like peroxiredoxin 2 (GPX2), glutathione S-transferase omega-like 2 (ECM4), catalase T (CTT1), sulfiredoxin (SRX1), heat shocks proteins (HSP26, HSP42, HSP78, HSP104, SSA1); isocitrate lyase (ICL1), homocitrate synthase (LYS20), NADPH dehydrogenase 3 (OYE3), trehalose synthase complex regulatory subunit TSL1 (TSL1), aldehyde dehydrogenase [NAD(P)+] (ALD3); glycogen phosphorylase (GPH1), histidine biosynthesis trifunctional protein (HIS4), phosphor-ribosylaminoimidazole-succinocarboxamide synthase (ADE1), squalene monooxygenase (ERG1), phosphate permease PHO89 (PHO89); ammonia transport outward protein 3 (ATO3). PCA was performed using SIMCA 14.

HSP104 and SSA1) have significant negative loadings on PC3 and fall within the W191F/10pc and 60pc cluster (Figure 4.6C).

Thus, from the PCA we see that the largest variation in the abundances of individual proteins is between the biological replicates, which are separted by PC1 with 45% of the variance. PC2 with 12% variance separates H_2O_2-challenged from unchallenged samples while PC3 with 7% variance separates samples from cells mutated in Ccp1 vs WT cells.

4.5.3) Variation in protein Ratio between technical and biological replicates

The reproducibility of the LC-MS/MS measurements was examined by Dr Heng Jiang (CBAMS) using a single quality control (QC) sample. This was prepared by mixing whole-cell lysates of yeast (W303-B strain) grown to OD_{600} 1.0 in YPD at 20 ºC, 30 ºC, and 35 ºC. The cells were lysed using acid-washed glass beads, the lysates were mixed, centrifuged at 5000 g, soluble proteins in the supernatants were concentrated in single gel bands, in-gel digested by trypsin (as outlined in Section 4.4.4), and the QC digest was divided into aliquots 1-6. The tryptic peptides in different combinations of the QC aliquots were analyzed by LC-MS/MS (Section 4.4.5), and the abundance ratio between technical replicate *a* and replicate *b* ($Ratio_{a,b}$, Eq 4.3) was determined for ~1000 proteins with at least one unique peptide using nested pairwise quantification (Section 4.4.6).

Equation 4.3:

$$Ratio_{a,b} \text{ of protein X} = \frac{\text{abundance of protein X from technical replicate } a}{\text{abundance of protein X from technical replicate } b}$$

Table 4.2. Protein $Ratio_{a,b}$ from technical replicates[a]

Technical replicate *a* vs *b*	# Quantified proteins	Range of protein abundance ($Ratio_{a,b}$) (*p value* > 0.05)
3 vs 6	951	$0.83 < Ratio_{a,b} < 1.2$
2,3 vs 5,6	1019	$0.83 < Ratio_{a,b} < 1.2$
1,2,3 vs 4,5,6	1047	$0.83 < Ratio_{a,b} < 1.2$

[a] These data were obtained by Dr Heng Jiang (CBAMS) for W303-B cells (see text) on the same day.

$Ratio_{a,b}$ was found to be within the range 0.83 - 1.2 for technical replicates performed on single QC aliquots and on their binary and ternary mixtures on the same day (Table 4.2). Thus, protein Ratios between 0.83 and 1.2 (*p-value* > 0.05) are due to intraday variation in the MS measurements and cannot be assigned any biological significance.

Since technical replicates do not take into consideration variation during cell growth, cell harvesting, protein extraction, tryptic digestion or peptide extraction from gel bands, it also is necessary to examine the reproducibility of biological replicates. The variation in the abundance ratio of individual proteins (Ratio) between biological replicates must be known before we can assume that mutation or cell treatment results in protein up- or downregulation. Thus, we quantified $Ratio_{A,B}$ (Eq 4.4) between biological replicates A and B of sample WT-A/10 and WT-B/10 using the nested pairwise quantification approach (Section 4.4.6).

Equation 4.4:

$$\text{Ratio}_{A,B} \text{ for protein X} = \frac{\text{Abundance of protein X in biological replicate A}}{\text{Abundance of protein X in biological replicate B}}$$

Then, we calculated $Ratio_{B,C}$ and $Ratio_{A,C}$ for WT-B/10, WT-C/10 and WT-A/10, WT-C/10 pairs, respectively, and averaged $Ratio_{A,B}$, $Ratio_{B,C}$ and $Ratio_{A,C}$ for each protein ($Ratio_{avg}$). We found for ~1500 proteins that $0.67 < Ratio_{avg} < 1.5$ for the WT/10 samples. We then measured $Ratio_{avg}$ for WT/60, WT/10pc, WT/60pc, and for the corresponding W191F samples. In each case, we found $0.67 < Ratio_{avg} < 1.5$ (*p-value* > 0.05) for 1505 ± 58 proteins (Table 4.1).

A previous study using 2-D gel/autoradiography[2] also observed 0.67 < Ratio < 1.5 for 400 protein spots between 2 biological replicates of the yeast strain YPH98. Another group using 2-D gel/LC-MS/MS found 0.5 < Ratio < to 2 between biological replicates of the diploid yeast, BY4743.[127] Based on our $Ratio_{avg}$ values, we consider any protein with Ratio ≥ 1.5 (*p-value* < 0.05) to be stimulated and any protein with Ratio ≤ 0.67 (*p-value* < 0.05) to be repressed after H_2O_2 challenge. The significant deviation of $Ratio_{avg}$ from 1.00 for many proteins exposes that the biological replicates are the biggest source of variability in our dataset as also seen in the PCA of individual protein abundances (Figure 4.6A) but not in Figure 4.5 since this plots normalized abundance.

4.5.4) Protein Ratios in WT and W191F cells after H_2O_2 challenge

The Ratio (defined by Eq 4.1) of each protein was examined in WT and W191F cells and the results are summarized in Table 4.3. Overall, sublethal H_2O_2 challenge of early log-phase cells results in significant changes in the expression of certain proteins, especially in WT cells. However, we observed dramatically more H_2O_2-responsive proteins in W191F cells harvested 60 min after challenge (Table 4.3).

Table 4.3. Number of stimulated and repressed proteins following H_2O_2 challenge plus the range and average of their Ratios [a]

Cells	Time pc (min)	# Stimulated Proteins [b]	Range (avg) of Ratio [c]	# Repressed proteins [b]	Range (avg) [c]
WT	10	114	1.51 – 39 (5.33)	87	0.05 – 0.66 (0.49)
WT	60	102	1.51 – 54 (5.27)	39	0.09 – 0.66 (0.47)
W191F	10	95	1.51 – 14 (2.94)	125	0.04 – 0.66 (0.43)
W191F	60	149	1.51 – 41 (2.83)	319	0.04 – 0.66 (0.44)

[a] WT and W191F cells were challenged with 0.4 mM H_2O_2 and harvested at 10 and 60 min post challenge (pc) as outlined in Section 4.4.2. The protein Ratio (as defined by Eq 4.1) was calculated by the nested pairwise quantification approach (Section 4.4.6 and Figure 4.4) for the indicated number of stimulated and repressed proteins in each sample.
[b] Any protein with a Ratio ≥ 1.5 (*p-value* < 0.05) is considered to be stimulated and any protein with a Ratio ≤ 0.67 (*p-value* < 0.05) is considered to be repressed (Section 4.5.3).
[c] Range of Ratio values and average Ratio (in brackets) of stimulated and repressed proteins.

Godon et al.[66] observed 115 H_2O_2-responsive proteins in fermenting yeast YPH98 cells in response to 0.2–0.8 mM H_2O_2 using 2-D gels. Their focus on cellular H_2O_2 adaptation mechanisms has offered considerable insight into thiol-based cytosolic H_2O_2 sensors.[66] However, our group has shown that fermenting *ccp1Δ* and W191F yeast cells (BY4741 strain) mount weak and strong cellular defenses to 0.4 mM H_2O_2, respectively.[24] Thus, we wished to identify the H_2O_2-responsive proteins in WT and W191F cells. Where known, we classify the H_2O_2-responsive proteins based on their functions (Table S4.2) into six categories considered by Godon et al.,[66] (i) proteins with antioxidant defense function, (ii) heat-shock proteins, (iii) protease and proteasome subunits, (iv) proteins involved in translation apparatus and ribosome biogenesis, (v) enzymes involved in carbohydrate metabolism, and (vi) enzymes involved in sulfur, amino acid metabolism and purine and pyrimidine synthesis. Additionally, we collected NADPH or NADP+ dehydrogenase enzymes in (vii) category. In the following sections, we present the H_2O_2-responsive proteins we found in each category.

(i) Proteins with antioxidant defense function

This class of 19 H_2O_2-responsive proteins (Table 4.4), which can be divided further into 14 thiol-based proteins and 5 metal/heme-based proteins,[66] comprise the major antioxidant enzymes such as CCP1, CTT1, SOD1, SOD2, TSA1, TSA2, TRX2, TRR1, TRR2, GPX2, and SRX1. Our results are in accord with the findings on the H_2O_2 stimulon in YPH98 cells using 2-D gels.[66]

More antioxidant proteins are upregulated in WT vs W191F cells in response to H_2O_2 (Table 4.4). Specifically, 15 and 16 proteins are upregulated in WT/10pc and WT/60pc compared to 9 and 12 in W191F/10pc and W191F/60pc, respectively. Notably, CCP1 shows ~ 6-fold increase in WT/60pc vs ~ 2-fold increase in W191F/60pc whereas CTT1 shows essentially the opposite behaviour. These protein Ratios (Table 4.4) are consistent with the PC2 vs PC3 loadings plot (Figure 4.6C) where the abundance of CCP1 falls within the WT/10pc and 60pc cluster and that of CTT1 within the W191F/10pc and 60pc cluster. Also, we previously reported higher catalase activity in fermenting W191F (BY4741) cells compared to WT,[24] and Godon et al. showed ~ 6-fold increase in CCP1 level in response to 0.2 mM H_2O_2 and ~ 15-fold increase in CTT1 in response to 0.8 mM H_2O_2 in YPH98 cells.[66]

Table 4.4. Ratios of proteins with antioxidant defense function following H_2O_2 challenge [a]

Gene name	Protein name	WT [b] R_{10}	WT [b] R_{60}	W191F [b] R_{10}	W191F [b] R_{60}
a) thiol-based proteins					
GRX2	Glutaredoxin-2	2.11	3.20	1.62	2.0
GPX2	Glutathione peroxidase-like peroxiredoxin 2	3.22	7.20	2.13	3.22
ECM4	Glutathione S-transferase omega-like 2	8.03	7.53	2.71	1.20
GTT1	Glutathione S-transferase 1	1.21	0.98	1.12	2.21
AHP1	Peroxiredoxin AHP1	2.10	4.90	1.41	2.52
PRX1	Peroxiredoxin PRX1	5.05	4.12	1.22	1.84
TSA1	Peroxiredoxin TSA1	1.61	2.41	1.12	0.91
TSA2	Peroxiredoxin TSA2	37.9	55.1	13.2	23.3
SRX1	Sulfiredoxin	8.52	4.51	1.22	41.1
TRR1	Thioredoxin reductase 1	4.05	5.32	1.49	1.48
TRR2	Thioredoxin reductase 2	3.58	1.79	1.71	3.22
TRX1	Thioredoxin-1	1.12	1.33	0.72	0.48
TRX2	Thioredoxin-2	3.52	6.53	1.53	2.72
GRE2	NADPH-dependent methylglyoxal reductase GRE2	5.62	7.68	4.12	5.59
b) metal/ heme-based proteins					
CTT1	Catalase T	2.33	1.59	3.12	7.01
CCP1	Cytochrome c peroxidase	6.52	5.66	2.12	2.52
SOD1	Superoxide dismutase [Cu-Zn]	1.12	2.13	1.01	1.34
SOD2	Superoxide dismutase [Mn]	2.33	2.02	1.24	0.95
CUP1-2, CUP1-1	Copper metallothionein 1-2	0.47	0.85	0.57	0.72

[a] Protein Ratio (Eq 4.1) calculated by the nested pairwise quantification approach (Section 4.4.6 and Figure 4.4). We consider any protein with a Ratio ≥ 1.5 (*p-value* < 0.05) to be stimulated and any protein with a Ratio ≤ 0.67 (*p-value* < 0.05) to be repressed (Section 4.5.3).

[b] R_{10} and R_{60} are the protein Ratios measured at 10 and 60 min post H_2O_2 challenge of WT and W191F cells.

(ii) Heat-shock proteins (HSPs)

Godon et al.[66] reported that HSP104, HSP12, HSP42, and HSP78 were strongly upregulated (2- to 15-fold) on challenge of YPH98 cells with 0.8 mM H_2O_2. We identified these HSPs but some were not stimulated on challenge of WT BY4741 cells with 0.4 mM H_2O_2 (Table 4.5).. HSP26 and HSP42 were upregulated 3- and 2-fold, respectively in WT/10pc (Table 4.5) but both returned to the unstimulated level in WT/60pc. However, HSP26, which mainly suppresses unfolded protein aggregation,[141–143] remains strongly upregulated (10.5-fold) in W191F/60pc, In fact, all 8 HSPs are upregulated in W191F/60pc and 5 in W191F/10pc (Table 4.5). Godon et al. reported that HSPs and CCT1 exhibit a similar dose-response profile to 0.2–0.8 mM H_2O_2 in YPH98 cells,[66] with maximum response to 0.8 mM H_2O_2.[66] We observed the maximum response of HSPs and CTT1 in W191F/60pc (Table 4.4 and 4.5) and HSPs and CTT1 fall within the W191F/10pc and 60pc cluster of the loadings plot (Figure 4.6C). Thus, HSP and CTT1 expression may be similarly regulated.

Table 4.5. Ratios of heat-shock proteins (HSPs) following H_2O_2 challenge [a]

Gene name	Protein name	WT [b] R_{10}	WT [b] R_{60}	W191F [b] R_{10}	W191F [b] R_{60}
HSP26	Heat shock protein 26	3.02	1.33	1.72	10.5
HSP42	Heat shock protein 42	1.92	0.95	2.32	3.01
HSP78	Heat shock protein 78	1.15	1.44	1.43	2.02
HSP82	ATP-dependent molecular chaperone HSP82	1.13	1.25	1.33	2.32
HSP104	Heat shock protein 104	1.34	1.32	1.91	3.80
SSA1	Heat shock protein SSA1 (HSP 70 family)	1.41	1.42	1.49	2.02
SSA2	Heat shock protein SSA2 (HSP 70 family)	1.42	0.96	1.83	1.95
STI1	Heat shock protein STI1	1.20	0.99	1.62	1.71

[a] Protein Ratio (Eq 4.1) calculated by the nested pairwise quantification approach (Section 4.4.6 and Figure 4.4). We consider any protein with a Ratio ≥ 1.5 (*p-value* < 0.05) to be stimulated and any protein with a Ratio ≤ 0.67 (*p-value* < 0.05) to be repressed (Section 4.5.3).

[b] R_{10} and R_{60} are the protein Ratios measured at 10 and 60 min post H_2O_2 challenge of WT and W191F cells.

(iii) Protease and proteasome subunits

This group of 11 proteins (Table 4.6) are not H_2O_2-responsive in WT cells within our cut-off (Section 4.5.3) but a number are weakly upregulated in W191F/60pc (Table 4.6).

(iv) Protein translation apparatus and ribosome biogenesis

With a few exceptions, the 19 proteins in these two subgroups[66] exhibit little or no H_2O_2 response (Table 4.7). GAR1 is significantly stimulated in both WT/10pc and W191F60pc while CAF20 is significantly stimulated in WT/60pc but repressed in W191F/60, which contains the most repressed proteins (Table 4.7).

Table 4.6. Ratios of proteasome subunits following H_2O_2 challenge [a]

Gene name	Protein name	WT [b] R_{10}	WT [b] R_{60}	W191F[b] R_{10}	W191F[b] R_{60}
RPT2	26S proteasome regulatory subunit 4 homolog	1.42	1.02	1.46	1.54
RPT5	26S proteasome regulatory subunit 6A	1.52	0.99	1.07	0.99
RPN5	26S proteasome regulatory subunit rpn5	1.25	0.95	1.05	1.62
RPN7	26S proteasome regulatory subunit RPN7	1.42	1.01	1.16	1.65
RPN12	26S proteasome regulatory subunit rpn12	1.51	0.99	0.91	0.80
PRE2	20S proteasome subunit beta type-5	1.25	0.99	1.17	1.72
PRE6	20S proteasome subunit alpha type-4	1.06	1.18	0.76	0.47
PRE8	20S proteasome subunit alpha type-2	1.38	1.00	1.26	1.61
SCL1	20S proteasome subunit alpha type-1	1.13	1.18	1.16	1.56
PUP1	20S proteasome subunit beta type-2	1.14	1.07	1.02	1.68
PUP3	20S proteasome subunit beta type-3	1.19	1.18	0.91	0.64

[a] Protein Ratio (Eq 4.1) calculated by the nested pairwise quantification approach (Section 4.4.6 and Figure 4.4). We consider any protein with a Ratio ≥ 1.5 (*p-value* < 0.05) to be stimulated and any protein with a Ratio ≤ 0.67 (*p-value* < 0.05) to be repressed (Section 4.5.3).

[b] R_{10} and R_{60} are the protein Ratios measured at 10 and 60 min post H_2O_2 challenge of WT and W191F cells.

(v) Proteins involved in carbohydrate metabolism

This class contains 22 H_2O_2-responsive proteins in 5 subgroups [66] (Table 4.8). Enzymes involved in glycolysis and the TCA cycle were significantly upregulated in WT/10pc but not in WT/60pc with the exception of TDH1 (Table 4.8). A number of enzymes of the pentose phosphate pathway and trehalose synthesis showed the opposite trend, being upregulated in WT/60pc but not in WT/10pc, whereas one of the two H_2O_2-responsive enzymes in glycerol metabolism (GUT2) was upregulated in WT/10pc and the other (GPT2) in WT/60pc. Only PYC1

of the TCA cycle showed any significant change (upregulation) in W191F/10pc and this enzyme plus GPD1 of glycerol metabolism and three enzymes involved in trehalose synthesis were upregulated in W191F/60pc.

Table 4.7. Ratios of proteins involved in the protein-translation apparatus and ribosome biogenesis following H_2O_2 challenge [a]

Gene name	Protein name	WT [b] R_{10}	WT [b] R_{60}	W191F[b] R_{10}	W191F[b] R_{60}
a) translation apparatus					
CAF20	Cap-associated protein CAF20	0.54	2.32	0.74	0.32
CAF40	Protein CAF40	0.86	1.03	1.07	0.63
HCR1	Eukaryotic translation initiation factor 3 subunit J	1.08	0.61	1.15	1.45
RPS30B; RPS30A	40S ribosomal protein S30-B	1.7	1.37	1.62	0.68
RPL22A	60S ribosomal protein L22-A	0.46	0.92	0.68	0.91
RPL13B	60S ribosomal protein L13-B	0.44	1.11	0.81	0.34
RPL13A	60S ribosomal protein L13-A	0.47	1.75	0.77	0.28
RPL37B	60S ribosomal protein L37-B	1.58	1.25	1.31	1.18
RPL24A	60S ribosomal protein L24-A	1.56	0.86	1.33	1.11
RPS10B	40S ribosomal protein S10-B	1.88	0.68	0.79	0.79
b) ribosome biogenesis					
GAR1	H/ACA ribonucleoprotein complex subunit 1	3.52	0.27	0.75	2.36
NOP10	H/ACA ribonucleoprotein complex subunit 3	0.99	0.64	0.99	0.97
NOP4	Nucleolar protein 4	0.82	0.63	0.96	1.21
UTP9	U3 small nucleolar RNA-associated protein 9	0.90	1.03	0.84	0.49
UTP15	U3 small nucleolar RNA-associated protein 15	0.89	0.96	0.87	0.62
UTP21	U3 small nucleolar RNA-associated protein 21	1.23	0.90	0.82	0.44
UTP25	U3 small nucleolar RNA-associated protein 25	0.58	1.08	1.07	0.85
LSM2	U6 snRNA-associated Sm-like protein LSm2	1.07	0.90	0.67	0.40
HRR25	casein kinase I homolog HRR25	1.56	1.37	1.23	0.92

[a] Protein Ratio (Eq 4.1) calculated by the nested pairwise quantification approach (Section 4.4.6 and Figure 4.4). We consider any protein with a Ratio ≥ 1.5 (*p-value* < 0.05) to be stimulated and any protein with a Ratio ≤ 0.67 (*p-value* < 0.05) to be repressed (Section 4.5.3).

[b] R_{10} and R_{60} are the protein Ratios measured at 10 and 60 min post H_2O_2 challenge of WT and W191F cells.

Table 4.8. Ratios of proteins involved in carbohydrate metabolism following H_2O_2 challenge [a]

Gene name	Protein name	WT [b] R_{10}	WT [b] R_{60}	W191F [b] R_{10}	W191F [b] R_{60}
a) pentose phosphate pathway					
GND1	6-phosphogluconate dehydrogenase, decarboxylating 1	1.25	1.65	1.01	1.15
ZWF1	Glucose-6-phosphate 1-dehydrogenase	1.81	1.89	1.13	1.29
GND2	6-phosphogluconate dehydrogenase, decarboxylating 2	0.95	1.82	1.12	1.59
SOL3	6-phosphogluconolactonase 3	0.62	1.40	0.89	0.51
b) glycolysis					
ALD3	Aldehyde dehydrogenase [NAD(P)+] 2	1.00	0.87	2.14	10.51
ALD4	Potassium-activated aldehyde dehydrogenase	2.15	1.00	1.24	1.36
TDH1	Glyceraldehyde-3-phosphate dehydrogenase 1	1.88	2.76	1.28	1.52
TDH3	Glyceraldehyde-3-phosphate dehydrogenase 3	0.88	1.01	0.55	1.01
SFA1	S-(hydroxymethyl)glutathione dehydrogenase	1.90	1.37	1.52	1.30
ADH6	NADP-dependent alcohol dehydrogenase 6	1.86	1.74	1.00	0.96
ADH2	Alcohol dehydrogenase 2	3.84	0.99	1.41	1.10
ACS1	acetyl-coenzyme A synthetase 1	3.19	0.98	1.37	1.23
c) TCA cycle					
ICL1	Isocitrate lyase	2.21	1.04	1.36	1.36
PYC1	pyruvate carboxylase 1	1.76	1.21	1.70	1.91
d) glycerol metabolism					
GUT2	Glycerol-3-phosphate dehydrogenase	1.63	0.96	1.23	0.87
DAK1	Dihydroxyacetone kinase 1	1.08	1.25	1.07	1.56
GPT2	glycerol-3-phosphate O-acyltransferase 2	1.66	1.95	1.58	1.52
GPD1	Glycerol-3-phosphate dehydrogenase [NAD(+)] 1	1.00	1.25	1.30	1.66
HOR2; GPP2	Glycerol-1-phosphate phosphohydrolase 2	0.80	0.85	1.11	1.52
e) trehalose synthesis					
TSL1	Trehalose synthase complex regulatory subunit TSL1	1.23	1.90	1.44	2.63
TPS1	Alpha,alpha-trehalose-phosphate synthase [UDP-forming] 56 kDa subunit	1.27	1.27	1.26	1.81
TPS2	Trehalose-phosphatase	1.16	1.17	1.46	2.01
PGM2	Phosphoglucomutase 2	1.27	1.61	0.97	1.27

[a] Protein Ratio (Eq 4.1) calculated by the nested pairwise quantification approach (Section 4.4.6 and Figure 4.4). We consider any protein with a Ratio ≥ 1.5 (*p-value* < 0.05) to be stimulated and any protein with a Ratio ≤ 0.67 (*p-value* < 0.05) to be repressed (Section 4.5.3).

[b] R_{10} and R_{60} are the protein Ratios measured at 10 and 60 min post H_2O_2 challenge of WT and W191F cells.

(vi) Proteins involved in sulfur and amino-acid metabolism plus purine and pyrimidine synthesis

This group of 20 H_2O_2-responsive proteins is categorized into three subgroups (Table 4.9).[66] W191F/10pc and W191F/60pc show a large number of repressed proteins, the most highly repressed being ADE17, an enzyme in purine and pyridine synthesis. Less repression is observed in WT cells. LYS20 is significantly stimulated in both WT and W191F cells as well as YPH98 cells,[66] and ARO9 is the only other enzyme stimulated in W191F cells, whereas a number of different enzymes are weakly stimulated in WT cells (Table 4.9).

Table 4.9. Ratios of proteins involved in sulfur and amino-acid metabolism plus purine and pyridine synthesis following H_2O_2 challenge [a]

Gene name	Protein name	WT [b] R_{10}	WT [b] R_{60}	W191F [b] R_{10}	W191F [b] R_{60}
a) sulfur metabolism					
CYC1	Cytochrome c iso-1	1.46	1.66	0.96	1.07
b) amino-acid metabolism					
BNA3	Probable kynurenine-oxoglutarate transaminase BNA3	0.96	2.04	0.96	0.63
SER3	D-3-phosphoglycerate dehydrogenase 1	0.51	0.55	0.42	0.51
SHM2	Serine hydroxymethyl transferase	0.89	0.67	0.32	0.26
ARO9	Aromatic amino acid aminotransferase 2	2.22	1.14	1.38	2.69
BAT2	Branched-chain-amino-acid aminotransferase	1.64	1.29	1.09	0.92
LYS20	Homocitrate synthase	6.96	4.91	3.15	2.18
CAR2	Ornithine aminotransferase	1.58	0.97	1.03	0.98
HIS1	ATP phosphoribosyl transferase	0.84	0.89	0.95	0.54
HIS4	Histidine biosynthesis trifunctional protein	0.67	0.73	0.48	0.39
c) purine and pyrimidine synthesis					
HAM1	Inosine triphosphate pyrophosphatase	1.08	1.67	1.13	0.64
ADE17	Bifunctional purine biosynthesis	0.67	0.32	0.08	0.09
AAH1	Adenine deaminase	0.57	0.93	0.69	0.82
APT2	Adenine phosphoribosyl transferase 2	0.58	2.19	0.92	0.57
ADE1	Phosphoribosyl aminoimidazole-succinocarboxamide synthase	0.74	0.72	0.26	0.22
ADE 2	Phosphoribosyl aminoimidazole carboxylase	0.98	0.73	0.46	0.38
ADE 4	Amido phosphoribosyl transferase	0.93	0.82	0.45	0.50
ADE 5,7	Bifunctional purine biosynthetic protein ADE5,7	0.89	0.73	0.49	0.48
ADE6	Phosphoribosyl formyl glycinamidine synthase	0.75	0.89	0.66	0.58
ADE8	Phosphoribosyl glycinamide formyl transferase	0.77	1.012	0.48	0.59

[a] Protein Ratio (Eq 4.1) calculated by the nested pairwise quantification approach (Section 4.4.6 and Figure 4.4). We consider any protein with a Ratio ≥ 1.5 (*p-value* < 0.05) to be stimulated and any protein with a Ratio ≤ 0.67 (*p-value* < 0.05) to be repressed (Section 4.5.3).

[b] R_{10} and R_{60} are the protein Ratios measured at 10 and 60 min post H_2O_2 challenge of WT and W191F cells.

(vii) NADPH/NADP$^+$ dehydrogenases and reductases

Since Godon et al. reported that carbohydrate metabolism is redirected to NADPH regeneration on H_2O_2 challenge of YPH98 cells,[66] we examined the expression of NADPH/NADP$^+$-dependent dehydrogenases and reductases (Table 4.10). Most of these enzymes are weakly stimulated and two, OYE2 and GRE2, are highly stimulated in WT and W191 cells at both time points after challenge (Table 4.10).

Table 4.10. Ratios of NADPH/NADP$^+$-dependent proteins following H_2O_2 challenge [a]

Gene name	Protein name	WT [b] R_{10}	WT [b] R_{60}	W191F [b] R_{10}	W191F [b] R_{60}
OYE2	NADPH dehydrogenase 2	2.18	1.42	2.03	1.71
OYE3	NADPH dehydrogenase 3	13.3	8.76	5.14	10.70
UGA2	Succinate-semialdehyde dehydrogenase [NADP(+)]	2.30	1.90	2.02	2.30
YDL124W	NADPH-dependent alpha-keto amide reductase	1.67	2.10	1.01	1.08
GRE2	NADPH-dependent methylglyoxal reductase GRE2	5.6	7.7	4.1	5.6

[a] Protein Ratio (Eq 4.1) calculated by the nested pairwise quantification approach (Section 4.4.6 and Figure 4.4). We consider any protein with a Ratio ≥ 1.5 (*p-value* < 0.05) to be stimulated and any protein with a Ratio ≤ 0.67 (*p-value* < 0.05) to be repressed (Section 4.5.3).

[b] R_{10} and R_{60} are the protein Ratios measured at 10 and 60 min post H_2O_2 challenge of WT and W191F cells.

4.6) Discussion

LC-MS/MS-based, label-free, peptide centric, quantitative proteomics has been used to rapidly examine the yeast proteome and quantify 1500 - 2000 proteins.[131] Here we exploited this technology to elucidate at the proteome level the role of CCP1 on the H_2O_2 stimulon in the yeast strain BY4741 by studying the impact of its mutation into the hyper sensor, CCP1W191F. The abundance of over 1700 individual proteins was determined in 24 whole-cell lysates and the abundance ratio (Ratio) of over 1500 proteins was calculated in H_2O_2-challenged cells and their matched controls using nested pairwise quantitation. Table 4.11 classifies 120 ± 20 proteins that were stimulated or repressed in WT and W191F cells. The number of H_2O_2-responsive proteins varies somewhat between the two cell types. In particular, it appears that W191 cells mount a more persistent H_2O_2 response (shaded columns in Table 4.11). In the following sections, we discuss the roles of key proteins that fall within the categories listed in Table 4.11 and compare our H_2O_2 stimulon to that reported for YPH98 cells.[66]

Table 4.11. Classification of stimulated and repressed proteins in WT and W191F cells at 10 and 60 min post H_2O_2 challenge [a,b]

# proteins / Category	stimulated WT/10pc	repressed WT/10pc	stimulated WT/60pc	repressed WT/60pc	stimulated W191F/10 pc	repressed W191F/10 pc	stimulated W191F/60 pc	repressed W191F/60 pc
i) antioxidant enzymes	15	1	16	0	9	1	12	1
ii) heat shock proteins	2	0	0	0	5	0	8	0
iii) proteasome subunits	2	0	0	0	0	0	7	1
iv) translation apparatus/ ribosome biogenesis	6	5	2	2	1	0	1	8
v) carbohydrate metabolism	11	1	8	0	4	1	11	1
vi) amino acid metabolism	4	3	5	2	1	9	2	14
vii) NADPH/ / $NADP^+$ dependent enzymes	5	0	4	0	4	0	4	0

[a] WT and W191F cells (BY4741 strain) were challenged with 0.4 mM H_2O_2 as outlined in Section 4.4.2 and harvested 10 or 60 min post challenge (pc).

[b] Classification of stimulated (Ratio ≥ 1.5) and repressed proteins (Ratio ≤ 0.67) in each sample relative to the untreated control from Tables 4.4 - 4.10. The protein Ratio is defined by Eq 4.1. See Section 4.4.6 and Figure 4.5 for cell notation; for example, WT/10pc indicates WT cells harvested at 10 min pc.

4.6.1) H_2O_2-metabolizing enzymes

Figure 4.7 summarizes the abundance of four H_2O_2-metabolizing enzymes, two thiol-based (TSA1, TSA2) and two heme-based (CCP1, CTT1), in H_2O_2-challenged WT and W191F cells and their matched controls. The most striking observation is the significantly larger stimulation by H_2O_2 of TSA1 and TSA2 in WT compared to W191F cells. In fact, the TSA1 abundance in W191F/10 matches that of WT/10pc although previously TSA1 mRNA was found to be significantly induced by 0.2 mM H_2O_2 in W191F cells in the CEN.PK2 genetic background grown in YPD.[44] Clearly, TSA1 mRNA upregulation fails to translate to the protein level, underscoring the importance of proteomics in fully elucidating cellular defense mechanisms. Of the two heme-based enzymes, CCP1 is highly stimulated in WT cells vs CTT1 in W191F cells. We previously reported higher CTT1 activity in fermenting W191F vs WT cells.[24]

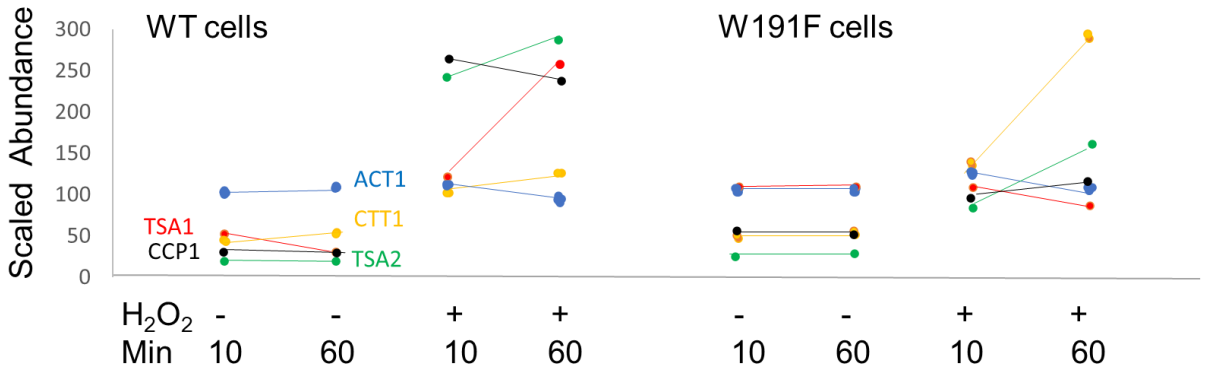

Figure 4.7. Trend chart for four H_2O_2-metabolizing enzymes in WT and W191F cells challenged with H_2O_2 and their matched controls. Actin (ACT1) is plotted as a non-H_2O_2-responsive control. Peroxiredoxins, TSA1 and TSA2, catalase T (CTT1), and cytochrome c peroxidase (CCP1) in WT/10, WT/60, WT/10pc, WT/60pc (left) and in W191F/10, W191F/60, W191F/10pc, W191F/60pc (right). Cell notation is given in Section 4.4.6 and Figure 4.5. The abundance of each protein is scaled between the 8 samples to an average of 100. The trend chart was produced by Proteome Discoverer v2.3.

Higher basal CTT1 and TSA1 levels may supress the stimulation of other antioxidant proteins in W191F cells (Table 4.4). Even after 60 min, antioxidant enzymes are more upregulated in WT vs W191F cells with the notable exception of SRX1 (Ratio ~41 in W191F/60pc; Table 4.4), which falls within the W191F/10pc and 60pc cluster in the loadings plot in Figure 4.6C. SRX1 increases in response to DNA replication stress[144] and it functions as an antioxidant enzyme by reducing cysteine-sulfinic acid groups in TSA1.[145] Thus, efficient cycling of TSA1 between its inactivated sulfinic form and active sulfhydryl form may obviate the need for its stimulation by H_2O_2 in W191F cells. SRX1 with a pI of 9.25 (www.yeastgenome.org) was not detected in the analysis of the H_2O_2 stimulon using 2-D gels as these fail to detect proteins with a pI > 7.5.[66]

TSA1, TSA2, AHP1, and PRX1, [60–62] major peroxiredoxins (or thioredoxin peroxidases), are all stimulated to varying degrees (Table 4.4). TSA2 is the most highly upregulated antioxidant enzyme in WT/10pc and 60 pc with Ratios of 38 and 55 (Table 4.4). It also is highly stimulated in W191F/10pc and 60pc (Ratios 13 and 23; Table 4.4) and Godon et al.[66] reported the maximum response (Ratio > 15) for TSA2 (YDR453)[66] in YPH98 cells. Hence, although basal expression of TSA1 is significantly higher than that of TSA2 but TSA2 is stimulated much more potently by H_2O_2.

The thioredoxins, TRX1 and TRX2, act as reducing substrates for TSA1 and other peroxiredoxins. TRX1 abundance did not change significantly in WT/10pc or 60pc and it was downregulated in W191F/60pc. On the other hand, TRX2 is upregulated, particularly in WT cells with 2.5-fold more stimulation in WT/60pc than W191F/60pc (Table 4.4). Godon et al.[66] reported that TRX is stimulated in YPH98 cells challenged with H_2O_2 but TRX1 and TRX2 were not resolved in the 2-D gels because they have the same MW (11.2 kDa) and pI (4.93) (www.yeastgenome.org).[66] We also observed some upregulation of cytosolic thioredoxin reductase 1 (TRR1) and mitochondrial thioredoxin reductase 2 (TRR2), which is associated with antioxidant defense,[146] in both WT and W191F cells but TRR2 was not detected in 2-D gels.[66]

The omega class of glutathione S-transferases[147] play neuroprotective roles,[148] and here we observe that glutathione S-transferase omega-like 2 (ECM4[149] or GTO2[147]) is highly stimulated in WT but less in W191F cells. ECM4 was not detected in the 2-D gels[66] so four thiol-based H_2O_2-responsive proteins, TRX1, TRX2, ECM4 and TRR2, were successfully quantified by LC-MS/MS but not in 2-D gels.[66]

4.6.2) Heat shock proteins (HSPs) are more upregulated in W191F cells

HSPs play an important role in cell protection under stress conditions.[150–152] Most HSPs are molecular chaperones that aid in protein (re)folding and proteolytic degradation of abnormal proteins. Amplified H_2O_2 sensing by CCP1W191F upregulates HSP26 10-fold in W191F/60pc. HSP26 is the best-characterized member of the family of HSPs in *S. cerevisiae*.[141–143,153] Like other HSPs, HSP26 forms large oligomeric complexes of 24 subunits[154] and suppresses the aggregation of target proteins.[143,155] HSP42, an important player in protein homeostasis under physiological and stress conditions,[155] is upregulated in both W191F/10pc and W191F/60pc. HSP104, a disaggregase that cooperates with Hsp70 family members Ssa1p and Ssa2p to refold denatured proteins,[156–159] also is significantly upregulated in W191F/60pc. Table 4.5 reveals little significant stimulation of HSPs in WT/10pc and none in WT/60pc, which contrasts with the 8 upregulated HSPs in W191F/60pc (Table 4.11).

Godon et al.[66] showed that HSP12, HSP42, HSP78, and HSP104 were upregulated by 0.8 mM H_2O_2 challenge in fermenting WT YPH98 cells. (HSP26 has no sulfur-containing residues so it was not detected in 2-D gels with ^{35}S labeling.[66]) Furthermore, they found that HSP104 was stimulated 0-, 2.5- and 15-fold by 0.2, 0.4 and 0.8 mM H_2O_2, revealing the heightened sensitivity of YPH98 cells to H_2O_2 as its concentration is increased.[66]

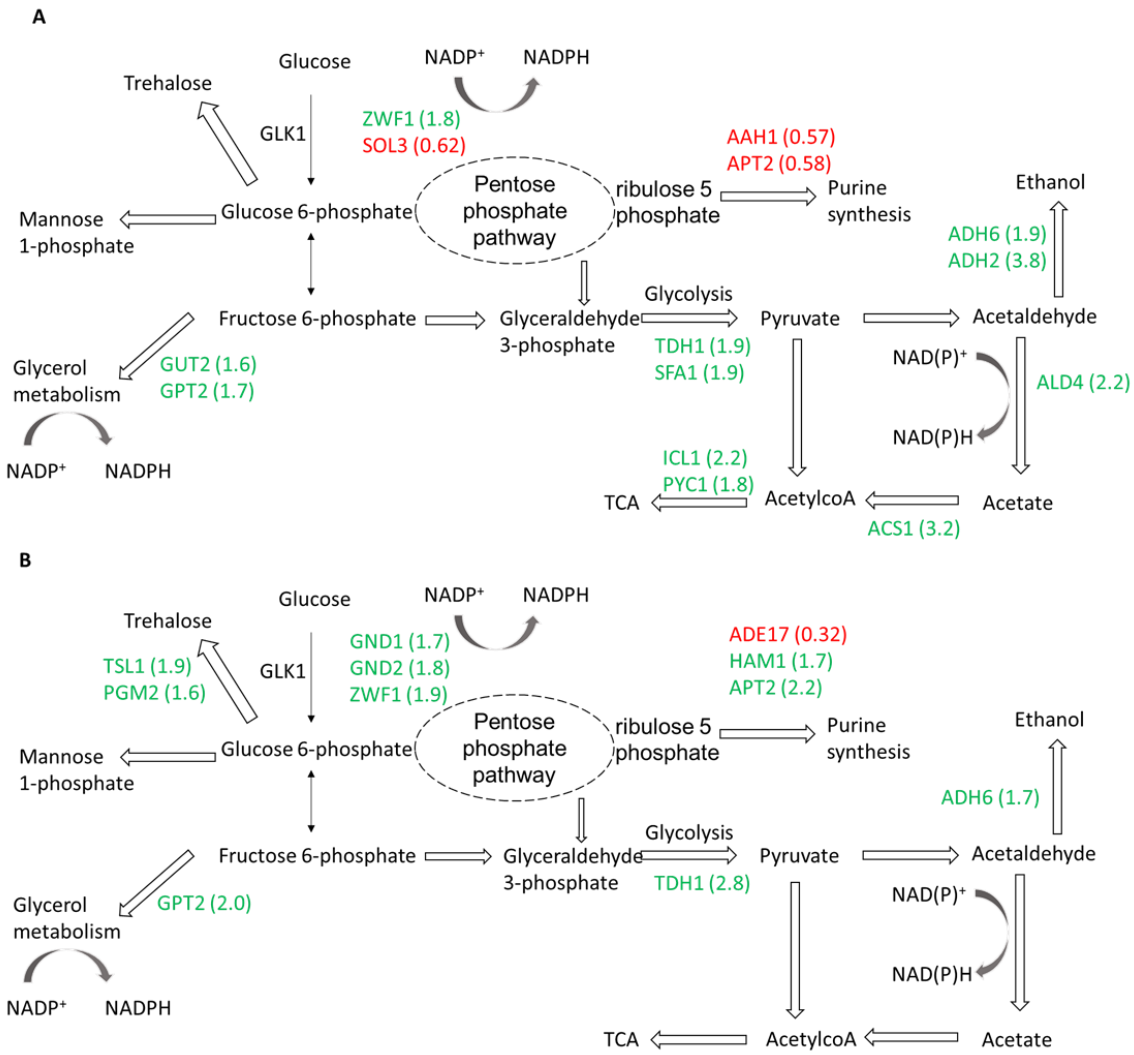

Figure 4.8. H_2O_2-responsive enzymes in carbohydrate metabolism pathways in WT cells. (A) WT/10pc and (B) WT/60pc (see cell notation in Section 4.4.6 and Figure 4.5). The gene names of the enzymes stimulated (**green**) and repressed (**red**) following the challenge of WT cells with 0.4 mM H_2O_2 are indicated as well as the protein Ratios (Eq 4.1) for their protein products. The protein Ratio of glucokinase-1 (GLK1, Table A4.1) did not change after H_2O_2 challenge. Full protein names are given in Table 4.8 and 4.9, and their functions are listed in Table S4.2. This scheme is adapted from Godon et al. [66]

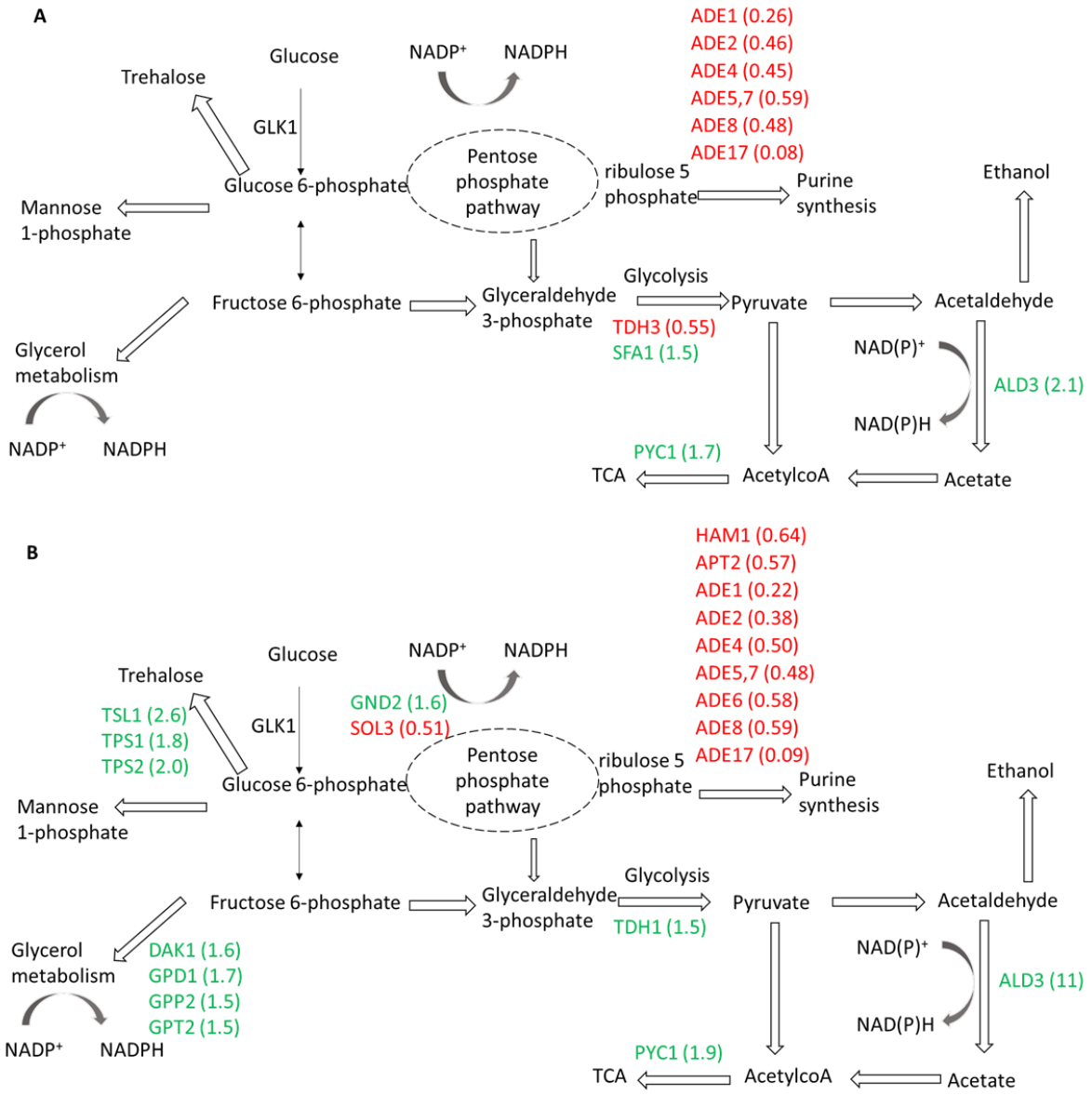

Figure 4.9. H_2O_2-responsive enzymes in carbohydrate metabolism pathways in W191F cells. (A) W191F/10pc and (B) W191F/60pc (see cell notation in Section 4.4.6 and Figure 4.5). The gene names of the enzymes stimulated (**green**) and repressed (**red**) following the challenge of W191F cells with 0.4 mM H_2O_2 are indicated as well as the protein Ratios (Eq 4.1) for their protein products. The protein Ratio of glucokinase-1 (GLK1, Table A4.1) did not change after H_2O_2 challenge. Full protein names are given in Table 4.8 and 4.9, and their functions are listed in Table S4.2. This scheme is adapted from Godon et al. [66]

4.6.3) H_2O_2-challenge impacts protein degradation and biosynthesis more in W191F cells

The proteasome removes damaged or unwanted proteins by proteolysis. We see no significant change in the abundance of the proteasome subunits in WT cells but seven subunits are weakly stimulated (Ratios 1.54–1.72) and one weakly repressed (Ratio 0.47) in W191F/60pc (Table 4.6). The stronger repression in W191F/60pc vs WT/60pc of proteins participating in the translational apparatus and in ribosome biogenesis (Table 4.7 and 4.11) suggests greater H_2O_2-induced repression of protein synthesis in the mutant strain.

This is corroborated by the much larger number of repressed proteins associated with amino-acid plus purine and pyrimidine synthesis in W191F/60pc vs WT/60pc (Table 4.9 and 4.11). Notably, two proteins involved in *de novo* purine synthesis, ADE1 and particularly ADE17, are among the most repressed proteins in W191F cells. LYS20 (homocitrate synthase), which is highly upregulated in WT cells (Table 4.9) also functions in DNA repair.[160,161] Taken together, the response of HSPs, the proteasome subunits, the translational apparatus, ribosome biogenesis, and amino-acid, purine, pyrimidine biosynthesis to 0.4 mM H_2O_2 indicates stronger protein protection, more protein degradation, and less protein biosynthesis in W191F vs WT cells.

4.6.4) Redirecting carbohydrate to NADPH production and trehalose biosynthesis

The Ratio of glucokinase-1 (GLK1), which converts D-glucose to D-glucose 6-phosphate in the presence of ATP and is key in glucose uptake,[162] did not change after H_2O_2 challenge. The utilization of D-glucose-6-phosphate is mapped into different pathways: (i) glycolysis, (ii) pentose phosphate pathway, (iii) glycerol metabolism, and (iv) trehalose biosynthesis (Figure 4.8 and 4.9). Vital products of the pentose phosphate pathway are NADPH and the ribulose-5-phosphate sugar used to make DNA and RNA. The NADPH generating enzymes include ZWF1, SOL3, GND1, and GND2 (Figures 4.8 and 4.9). ZWF1, GND1, and GND2 are upregulated in WT cells (Table 4.8), which will increase NADPH generation. Ribulose-5-phosphate is isomerized to ribose-5-phophate for purine and pyrimidine synthesis but numerous enzymes are repressed in this pathway, particularly in W191F cells (Table 4.9 and 4.11). Hence, downregulation of purine/pyrimidine synthesis will redirect ribulose-5-phosphate to the pentose phosphate pathway to regenerate more NADPH. Also, ribulose-5-phosphate can be converted to glyceraldehyde-3-phosphate to generate NAD(P)H via acetyl CoA biosynthesis in the glycolysis pathway.

A notable H_2O_2-responsive protein in the glycolysis pathway is glyceraldehyde-3-phosphate dehydrogenase (GAPDH).[163] *S. cerevisiae* has three GAPDH isoenzymes, TDH1, TDH2, and TDH3.[163] Reportedly,TDH2 and TDH3 are mainly detected in fermenting cells[164]

whereas TDH1 shows low expression in fermenting[165,166] vs respiring cells.[164,167] Quantification by Western blotting[168] detected no change in TDH2 or TDH3 levels in fermenting BY4741 cells (OD_{600} ~ 0.5) exposed to steady-state 0.16 mM H_2O_2 for 60 min but 0.5 mM H_2O_2 repressed both isoforms. Also, Godon et al.[66] observed using 2-D gels that TDH2 and TDH3 are repressed In fermenting YPH98 cells challenged with bolus 0.2, 0.4, and 0.8 mM H_2O_2. TDH1 was not identified in these studies[66,168] but surprisingly we identified TDH1 (6 unique peptides / 29% sequence coverage), TDH2 (3 unique peptides / 9% sequence coverage), and TDH3 (5 unique peptides / 18% sequence coverage) (Table 4.12 and A4.1). However, TDH2 was not responsive to 0.4 mM H_2O_2 in the fermenting (OD_{600} ~ 0.8) cells examined in this study (Table A4.1). TDH1 is slightly upregulated in WT/10pc while TDH3 was slightly repressed in W191F/10pc (Table 4.8). Importantly, it has been reported that in fermenting BY4741 cells challenged with 0.5 mM H_2O_2, GAPDH was recognized as the major target of S-glutathionylation, which reversibly inactivated the enzyme[168] and redirectedthe carbohydrate flux to NADPH production.[168] This post-translational modification could also occur under our H_2O_2-challenge conditions and significantly alter the carbohydrate flux with little change in TDH1/2/3 expression.

Table 4.12: Sequence of unique peptides of GAPDH isoforms TDH1/2/3

Gene name	Peptide FDR confidence[a]	Unique peptide sequence [b]
TDH1	High	[K].GTVSHDDKHIIIDGVK.[I]
TDH1	High	[K].IDVAVDSTGVFK.[E]
TDH1	High	[K].LISWYDNEYGYSAR.[V]
TDH1	High	[K].VVITAPSSSAPMFVVGVNHTK.[Y]
TDH1	High	[R].VVDLIEYVAK.[A]
TDH1	High	[R].YKGTVSHDDKHIIIDGVK.[I]
TDH2	High	[K].IATFQER.[D]
TDH2	High	[R].KNVEVVALNDPFISNDYSAYMFK.[Y]
TDH2	High	[R].YAGEVSHDDKHIIVDGHK.[I]
TDH3	High	[K].HIIVDGKK.[I]
TDH3	High	[K].KIATYQER.[D]
TDH3	High	[K].VINDAFGIEEGLMTTVHSLTATQK.[T]
TDH3	High	[R].IALSRPNVEVVALNDPFITNDYAAYMFK.[Y]
TDH3	High	[R].YAGEVSHDDKHIIVDGKK.[I]

[a] Only peptides with FDR (false discovery rate) < 1% (high confidence) are reported.

[b] The residues in square brackets are N- and C-terminal in the protein sequence to the trypsin cut sites indicated by the periods.

Glucose-derived fructose 6-phosphate also can be consumed in the glycerol metabolism pathway to generate NADPH (Figure 4.8 and 4.9). Four enzymes in this pathway are weakly upregulated in W191/60pc, two in WT/10pc and one in WT/60pc (Table 4.8 and 4.11). Since evidence suggests that H_2O_2 challenge modifies carbohydrate metabolism to produce more NADPH,[66] we ask how NADPH protects cells against this challenge. In erythrocytes, for example, catalase serves as a NADPH reservoir.[169] Each monomer of the catalase tetramer binds a NADPH,[169] which is not essential for catalase activity (2 $H_2O_2 \rightarrow O_2$ and 2 H_2O) but protects the enzyme against inactivation by H_2O_2.[169,170] CTT1 is stimulated in both WT and W191F cells (Table 4.4) so more NADPH is needed to avoid CTT1 inactivation on H_2O_2 challenge. Also, NADPH is an essential cofactor for thioredoxin reductase (TRR1, TRR2; Table 4.4) and glutathione reductase (GLR1, Table A4.1), critical enzymes in cellular thiol-dependent redox control and antioxidant defense.[37-39] Moreover, a number of NADPH/$NADP^+$-dependent proteins were significantly stimulated after H_2O_2 challenge (Table 4.10). The high upregulation of OYE3 [171] and GRE2[172,173] in both WT and W191F cells presumably combats increases in small toxic aldehydes and ketones generated by H_2O_2 attack on unsaturated lipids.

Additionally, glucose 6-phosphate can be diverted to the trehalose biosynthesis pathway (Figure 4.8 and 4.9). Trehalose (α-D-glucopyranosyl-(1→1)-α-D-glucopyranoside) is a nonreducing disaccharide made of two glucose units and synthesised in fungi, bacteria, and plants in response to lack of water, high salinity, temperature changes, and oxidative and heavy metal stress.[174,175] For example, trehalose defends proteins against degradation and membranes against fusion in stressed plants.[176] Trehalose biosynthesis is also upregulated by heat shock and osmotic stress,[177,178] and its assembly is linked with thermo-tolerance.[179] Enzymes in the trehalose pathway (Figure 4.8 and 4.9) are significantly more stimulated in W191F/60pc vs WT/60pc (Table 4.8). Since no stimulation is observed in WT/10pc and W191F/10pc, increased trehalose production may occur at a later stage in the H_2O_2 stress response.

In sum, mapping the H_2O_2-responsive proteins onto carbohydrate metabolic pathways (Figure 4.8 and 4.9) indicates that fermenting BY4741 cells reprogram their carbohydrate metabolism to produce more NADPH and trehalose to deal with exogenous H_2O_2. This accords with the previous conclusion on the H_2O_2 stimulon in fermenting YPH98 cells.[66]

4.6.5) Advances enabled by LC-MS/MS over 2-D gel/autoradiography

Over 20 years ago, Godon et al. first studied the H_2O_2 stimulon in the YPH98 strain of *S. cerevisiae* using 2-D gel/autoradiography.[66] They used ~200 µg of sample and quantified only soluble and highly abundant proteins. We are the first group to study the H_2O_2 stimulon in *S.*

cerevisiae (BY4741 strain) by label-free proteomics. This allows us to directly compare all samples with each other between different runs unlike SILAC (stable isotope labeling by amino acids in cell culture) or TMT (tandem mass tags).

Sample preparation also is minimized using label-free LC-MS/MS proteomics. Minimizing sample processing enhances the reproducibility of the data obtained from the many samples required for functional proteomics. For example, five samples were run in one 6% stacking gel but a separate 2-D gel is required for each sample for 2-D gel/autoradiography. LC-MS/MS sample preparation takes 3 days vs over 10 days for 2-D gel/autoradiography,[66] which requires radioactive isotopes but not LC-MS/MS. The identification and quantification of proteins are independent of the isoelectric point (pI) and MW of proteins in peptide-centric bottom-up LC-MS/MS, but not in 2-D gel/autoradiography. Notably, key antioxidant proteins (TDH1, SRX1, HSP26, TRX1, TRX2, ECM4, TRR2) could not be quantified by ^{35}S-Met on 2-D gels[66] but were quantified here by LC-MS/MS.

Approximately 1000 protein spots were identified by 2-D gel/autoradiography [66] vs 1700 by LC-MS/MS (Table 4.1). Only 400 protein spots were quantified by 2-D gel/autoradiography vs ~1500 proteins by LC-MS/MS. Assuming ~ 5000 protein-coding genes in the *S. cerevisiae* genome,[180] 8% of proteins were quantified by 2-D gel/autoradiography vs 30% by LC-MS/MS. Here we used data dependent acquisition (DDA) but the number of peptides, and hence proteins, identified and quantified might be increased using data independent acquisition (DIA), which can be considered in future work. Additionally, we performed shotgun proteomics only so it should be possible to increase unique peptide coverage for low-abundance proteins using targeted analysis.

Less H_2O_2-responsive proteins (115) were identified using 2-D gel/autoradiography[66] than by LC-MS/MS (201 proteins in WT and 468 in W191F cells; Table 4.3). Using similar functional categories as Godon et al.[66] (Tables 4.4–4.10), 103 H_2O_2-responsive proteins are discussed in this chapter. Further analysis and discussion of all 468 H_2O_2-responsive proteins will better describe how the H_2O_2 stimulon is regulated by the H_2O_2 sensing/signaling functions of CCP1 and its W191F variant.

4.7) Conclusions

Since the W191F variant of CCP1 is identified as an amplified H_2O_2 sensor, we studied the impact of this single mutation on the H_2O_2 stimulon in fermenting yeast using label-free LC-MS/MS. WT and W191F cells exhibit surprising variation in their response to challenge with a sublethal dose of H_2O_2 (0.4 mM) as seen from mapping the functions of 103 H_2O_2-responsive proteins. More upregulation of CTT1 and HSPs, more protein degradation, less protein and

amino-acid biosynthesis, more trehalose biosynthesis and possibly more NADPH generation via glycerol metabolism occur following challenge of fermenting W191F vs WT cells. Some H_2O_2-responsive proteins show an early response (10pc) in WT cells vs a delayed response (60pc) in W191F cells, suggesting that perhaps higher basal levels of active TSA1 and CTT1 and/or stronger CTT1 stimulation (Figure 4.6) due to amplified H_2O_2 sensing retard the onset of other protective responses in W191F relative to WT cells. One striking difference in their reponse to H_2O_2 is that W191F cells do not upregulate TSA1 but highly upregulate SRX1 to efficiently recycle TSA1 between its H_2O_2-inactivated sulfinic form and active sulfhydryl form. On the other hand, SRX1 is stimulated much less in WT cells, which upregulate TSA1 and also TSA2. Such observations underline the complexity of stress responses.

The present study confirms previous findings using 2-D gels.[66] Like YPH98 cells,[66] fermenting WT and W191F BY4741 cells respond to exogenous H_2O_2 largely by switching from protein biosynthesis to cellular defense (increased NADPH generation and trehalose synthesis). As a matter of interest, we questioned if the YPH98 strain is more H_2O_2 resistant than BY4741 strain. Taking catalase activity as a H_2O_2-resistance indicator, challenge with 0.25 mM H_2O_2 for 30 min (28 ^{o}C and 180 rpm) increased this activity 2-fold more in fermenting YPH250 vs YPH98 cells,[181] while challenge with 0.20 mM H_2O_2 for 1.5 h (30 ^{o}C and 225 rpm) increased this activity 3-fold more in fermenting YPH250 vs BY4741 cells.[182] Hence, resistance to H_2O_2 stress between WT YPH98 and BY4741 strains appears to be similar. However, the CTT1 Ratios (Table 4.4) predict, as our lab reported,[24] that fermenting W191F cells are more H_2O_2-resistant than WT cells.

Finally, the results of this chapter underline the complexity of yeast systems biology and highlight the power of label-free, peptide centric, quantitative proteomics using LC-MS/MS. This rapid and reliable technology sheds light on how yeast adapt to H_2O_2 challenge at the proteome level, and it offers great promise in unraveling complexity in future functional proteomics studies.

4.8) Supplementary information

Table S4.1. CV of protein Ratios (Eq 4.1), protein and peptide FDR confidence, sequence coverage and number of unique peptide for the 103 H_2O_2-responsive proteins in Tables 4.4 – 4.10

Gene name	CV% WT R_{10} [a]	CV% WT R_{60} [a]	CV% W191F R_{10} [a]	CV% W191F R_{60} [a]	Protein FDR confidence [b]	Peptide FDR confidence [b]	Sequence Coverage % [c]	# Unique peptides [d]
GRX2	10.51	13.08	21.62	13.09	High	High	26	3
GPX2	3.24	0	14.62	5.86	High	High	31	3
ECM4	16.77	16.44	22.02	15.55	High	High	9	2
GTT1	1.71	18.86	8.42	4.88	High	High	14	3
AHP1	3.04	20.94	13.76	1.53	High	High	47	7
PRX1	0.36	9.95	2.78	2.94	High	High	39	10
TSA1	7.51	14.92	17.09	1.93	High	High	63	15
TSA2	1.26	21.52	19.88	16.4	High	High	48	10
SRX1	22.88	35.44	40.52	21.98	High	High	55	4
TRR1	5.42	8.06	18.87	11.91	High	High	60	15
TRR2	44.57	34.38	0.03	5.48	High	High	12	2
TRX1	1.08	1.85	10.94	5.4	High	High	30	3
TRX2	46.69	34.29	2.62	2.82	High	High	66	7
GRE2	9.68	19.99	18.09	3.17	High	High	16	4
CTT1	15.09	26.15	15.57	0.91	Medium	High	2	1
CCP1	5.29	25.34	1.01	1.53	High	High	43	12
SOD1	16.99	28.26	1.64	5.1	High	High	60	6
SOD2	27.95	15.58	12.1	24.98	High	High	32	5
CUP1-2, CUP1-1	3.45	0.88	3.7	2.75	High	High	31	1
HSP26	11.67	47.83	10.21	4.12	High	High	54	8
HSP42	12.23	20.14	27.38	6.06	High	High	22	5
HSP78	10.95	8.16	11.15	7.52	High	High	13	8
HSP82	0.86	21.07	7.49	4.23	High	High	49	45
HSP104	1.27	13.64	3.61	1.94	High	High	46	37
SSA1	15.16	3.45	0.76	1.31	High	High	65	37
SSA2	17.74	6.07	10.45	16.82	High	High	56	35
STI1	1.65	16.05	1.02	10.62	High	High	33	15
RPT2	16.63	9.18	4.80	5.25	High	High	15	5
RPT5	0.54	11.98	26.78	0.56	High	High	28	8
RPN5	15.97	17.99	5.67	17.27	High	High	15	7
RPN7	21.88	23.02	0.83	9.36	High	High	13	6

RPN12	18.59	14.43	9.18	13.64	High	High	14	3
PRE2	1.29	29.13	3.53	16.83	High	High	17	4
PRE6	17.89	39.38	0.91	2.34	High	High	21	3
PRE8	3.87	7.19	5.01	5.29	High	High	22	4
SCL1	1.64	0.31	3.67	20.7	High	High	27	6
PUP1	23.66	8.96	3.52	9.67	High	High	8	2
PUP3	26.27	10.86	7.85	19.63	High	High	21	3
CAF20	15.55	19.19	43.95	15.28	High	High	19	1
CAF40	32.81	29.51	20.96	13.66	High	High	11	3
HCR1	3.82	11.42	0.01	13.46	High	High	7	2
RPS30B; RPS30A	9.75	18.43	4.41	5.23	High	High	16	1
RPL22A	4.25	28.18	0.75	34.87	High	High	47	3
RPL13B	1.14	32.25	22.83	0.45	High	High	52	11
RPL13A	2.95	24.27	28.64	1.10	High	High	52	11
RPL37B	36.28	11.84	3.69	17.76	High	High	23	2
RPL24A	15.93	19.22	10.17	4.06	High	High	34	8
RPS10B	39.07	1.21	25.88	14.26	High	High	47	5
GAR1	26.63	1.25	15.52	16.95	High	High	6	1
NOP10	9.95	20.79	12.29	45.56	Medium	High	16	1
NOP4	2.43	21.09	0.61	43.46	High	High	9	4
UTP9	0.29	4.04	5.85	9.25	High	High	10	5
UTP15	18.23	2.72	24.96	2.43	High	High	2	1
UTP21	13.46	0.63	24.19	2.47	High	High	5	4
UTP25	1.57	2.96	3.77	4.85	High	High	5	3
LSM2	16.63	32.75	30.29	0.62	High	High	36	3
HRR25	24.66	31.45	17.28	33.69	High	High	2	1
GND1	3.38	4.76	5.82	9.70	High	High	64	29
ZWF1	0.30	12.21	6.90	8.62	High	High	38	14
GND2	27.74	24.53	35.88	18.91	High	High	23	11
SOL3	11.52	6.03	16.4	9.92	High	High	10	2

ALD3	3.87	14.55	9.61	18.13	High	High	20	8
ALD4	1.65	5.90	1.41	1.69	High	High	65	28
TDH1	4.36	32.29	2.50	7.58	High	High	29	6
TDH3	5.22	7.42	6.60	8.90	High	High	18	5
SFA1	8.02	17.12	11.2	3.37	High	High	5	2
ADH6	21.34	4.60	8.78	31.31	High	High	29	7
ADH2	14.03	8.52	1.76	6.57	High	High	52	15
ACS1	10.33	7.76	20.51	35.33	High	High	12	8
ICL1	8.94	41.17	11.09	33.25	High	High	8	4
PYC1	20.86	3.28	3.86	3.93	High	High	34	34
GUT2	12.57	7.71	0.08	0.46	High	High	16	10
DAK1	0.85	10.11	14.76	0.01	High	High	32	12
GPT2	24.34	40.17	9.84	27.78	High	High	9	6
GPD1	16.58	15.23	3.72	13.19	High	High	14	5
HOR2; GPP2	4.10	16.22	19.38	1.70	High	High	29	6
TSL1	12.14	6.84	1.34	11.31	High	High	20	6
TPS1	1.86	9.72	16.9	0.93	High	High	31	10
TPS2	8.66	18.08	1.44	1.79	High	High	14	10
PGM2	4.86	14.63	1.78	1.94	High	High	21	10
CYC1	6.68	12.34	0.62	5.57	High	High	38	6
BNA3	41.05	19.17	35.91	12.88	High	High	7	2
SER3	1.62	0.85	3.10	5.27	High	High	21	8
SHM2	6.84	7.96	0.24	0.32	High	High	59	27
ARO9	19.68	1.50	4.42	3.48	High	High	5	2
BAT2	1.30	9.59	2.99	14.92	High	High	23	6
LYS20	21.9	4.57	1.03	42.5	High	High	45	16
CAR2	1.62	3.47	11.1	6.30	High	High	41	12
HIS1	12.3	0.14	7.19	2.96	High	High	30	6
HIS4	11.59	19.41	1.11	0.43	High	High	9	5
HAM1	2.68	3.62	13.68	6.66	High	High	12	2

AAH1	1.79	33.27	2.57	29.55	High	High	12	4
APT2	3.6	35.49	26.39	5.3	High	High	6	1
ADE1	7.78	2.63	1.10	1.70	High	High	41	10
ADE 2	6.73	2.72	3.35	2.13	High	High	15	6
ADE 4	1.47	20.69	0.07	3.29	High	High	23	9
ADE 5,7	3.49	5.20	0.08	0.53	High	High	35	20
ADE6	2.26	0.13	0.02	1.45	High	High	19	19
ADE8	12.32	31.0	4.16	4.97	High	High	8	2
ADE17	1.74	4.25	0.11	0.43	High	High	43	20
OYE2	8.07	12.54	1.01	7.76	High	High	44	16
OYE3	17.37	25.35	17.51	76.9	High	High	21	7
UGA2	17.49	18.55	3.70	5.50	High	High	3	1

[a] Coefficient of variation of protein Ratio (Eq 4.1) between the biological replicates for each sample (WT/10pc, WT/60pc, W191F/10pc , W191F/60pc; see Section 4.4.6 and Figure 4.5 for cell notation). For example, column 2 gives the CV% of the Ratios (R_{10}) of biological replicates A, B and C of WT/10pc. Considering three biological replicates, we find 0.67 < Ratio < 1.5 (*p value* > 0.05) for ~ 1500 proteins for each sample, which gives CV% ~ 56%. Thus, Ratios with CV% < 56% are acceptable. The 103 H_2O_2-responsive proteins discussed in this chapter have an average CV% of 12 ± 10%.

[b] Protein or peptide false discovery rate; only proteins with FDR < 5% (high and medium confidence) and only peptides with FDR < 1% (high confidence) are reported.

[c] The percentage of residues in a protein sequence that are present in its peptides observed by MS.

[d] Number of unique peptides observed for each protein; i.e., peptides that are unique to this protein in the *S. cerevisiae* proteome.

Table S4.2. Functions of H_2O_2 responsive proteins in groups i-vii

Gene name	Protein function
(i) proteins with antioxidant defense function	
GRX2	Response to stimulus; antioxidant activity[1]
GPX2	Response to stimulus; antioxidant activity,[1] TP53 regulates metabolic genes,[1] glutathione metabolism[2] and Glutathione-Glutaredoxin Redox Reaction
ECM4	Antioxidant activity[1]
GTT1	Antioxidant activity, [1] glutathione metabolism,[2] glutathione-glutaredoxin redox reaction.[4]
AHP1	Response to stimulus; antioxidant activity,[1] TP53 regulates metabolic genes,[2] and detoxification of reactive oxygen species[3]
PRX1	Response to stimulus; antioxidant activity[1]
TSA1	Response to stimulus; antioxidant activity[1] TP53 regulates metabolic genes; detoxification of reactive oxygen species[3]
TSA2	Response to stimulus; antioxidant activity[1] TP53 regulates metabolic genes; detoxification of reactive oxygen species[3]
SRX1	Response to stimulus; antioxidant activity[1]
TRR1	Response to stimulus; antioxidant activity[1]
TRR2	Response to stimulus; antioxidant activity[1]
TRX1	Response to stimulus; antioxidant activity,[1] TP53 regulates metabolic genes; oxidative stress Induced senescence; detoxification of reactive oxygen species[3]
TRX2	Response to stimulus; antioxidant activity,[1] TP53 regulates metabolic genes; oxidative stress Induced senescence; detoxification of reactive oxygen species[3]
GRE2	MAPK signaling pathway – yeast[2]
CTT1	Response to stimulus; antioxidant activity,[1] MAPK signaling pathway - yeast; biosynthesis of antibiotics; longevity regulating pathway[3]
CCP1	Response to stimulus; antioxidant activity[1]
SOD1	Response to stimulus; antioxidant activity,[1] longevity regulating pathway,[2] detoxification of reactive oxygen species[3]
SOD2	Response to stimulus; antioxidant activity[1] longevity regulating pathway,[2] transcriptional activation of mitochondrial biogenesis; detoxification of reactive oxygen species[3]
CUP1-2, CUP1-1	Response to stimulus; antioxidant activity; catalytic activity; metal ion binding[1]
(ii) heat shock proteins	
HSP26	Response to stimulus,[1] protein processing in endoplasmic reticulum[2]
HSP42	Protein processing in endoplasmic reticulum[2]

HSP78	Response to stimulus[1]
HSP82	Response to stimulus,[1] protein processing in endoplasmic reticulum transport,[2] the NLRP3 inflammasome; HSP90 chaperone cycle for steroid hormone receptors (SHR); HSF1 activation; attenuation phase; eNOS activation[3]
HSP104	Response to stimulus,[1] longevity regulating pathway - multiple species[2]
SSA1	Spliceosome; longevity regulating pathway - multiple species; protein processing in endoplasmic reticulum; Endocytosis[2]
SSA2	Spliceosome; longevity regulating pathway - multiple species; protein processing in endoplasmic reticulum; Endocytosis[2]
STI1	HSP90 chaperone cycle for steroid hormone receptors (SHR)[3]
(iii) protease and proteasome subunits	
RPT2	Proteasome degradation,[2-4] p53-dependent G1 DNA damage response, MAPK6/MAPK4 signaling, ubiquitin mediated degradation of phosphorylated Cdc25A, ubiquitination degradation.[3]
RPT5	Proteasome degradation,[2-4] p53-dependent G1 DNA damage response, MAPK6/MAPK4 signaling, ubiquitin mediated degradation of phosphorylated Cdc25A, ubiquitination degradation.[3]
RPN5	Proteasome degradation,[2-4] p53-dependent G1 DNA damage response, MAPK6/MAPK4 signaling, ubiquitin mediated degradation of phosphorylated Cdc25A, ubiquitination degradation.[3]
RPN7	Proteasome degradation,[2-4] p53-dependent G1 DNA damage response, MAPK6/MAPK4 signaling, ubiquitin mediated degradation of phosphorylated Cdc25A, ubiquitination degradation.[3]
RPN12	Proteasome degradation,[2-4] p53-dependent G1 DNA damage response, MAPK6/MAPK4 signaling, ubiquitin mediated degradation of phosphorylated Cdc25A, ubiquitination degradation.[3]
PRE2	Proteasome degradation,[2-4] p53-dependent G1 DNA damage response, MAPK6/MAPK4 signaling, ubiquitin mediated degradation of phosphorylated Cdc25A, ubiquitination degradation.[3]
PRE6	Proteasome degradation,[2-4] p53-dependent G1 DNA damage response, MAPK6/MAPK4 signaling, ubiquitin mediated degradation of phosphorylated Cdc25A, ubiquitination degradation.[3]
PRE8	Proteasome degradation,[2-4] p53-dependent G1 DNA damage response, MAPK6/MAPK4 signaling, ubiquitin mediated degradation of phosphorylated Cdc25A, ubiquitination degradation.[3]
SCL1	Proteasome degradation,[2-4] p53-dependent G1 DNA damage response, MAPK6/MAPK4 signaling, ubiquitin mediated degradation of phosphorylated Cdc25A, ubiquitination degradation.[3]
PUP1	Proteasome degradation,[2-4] p53-dependent G1 DNA damage response, MAPK6/MAPK4 signaling, ubiquitin mediated degradation of phosphorylated Cdc25A, ubiquitination degradation.[3]

PUP3	Proteasome degradation,[2-4] p53-dependent G1 DNA damage response, MAPK6/MAPK4 signaling, ubiquitin mediated degradation of phosphorylated Cdc25A, ubiquitination degradation.[3]
(iv) protein translation apparatus and ribosome biogenesis	
CAF20	Regulation of biological process,[1] translation factors[4]
CAF40	RNA degradation[2]
HCR1	RNA transport,[2] translation factors[4]
RPS30B; RPS30A	Ribosome,[2] ribosomal scanning and start codon recognition; GTP hydrolysis and joining of the 60S ribosomal subunit,[3] cytoplasmic ribosomal proteins[4]
RPL22A	Formation of a pool of free 40S subunits; SRP-dependent cotranslational protein targeting to membrane; GTP hydrolysis and joining of the 60S ribosomal subunit,[3] cytoplasmic Ribosomal Proteins[4]
RPL13B	Formation of a pool of free 40S subunits; SRP-dependent cotranslational protein targeting to membrane; GTP hydrolysis and joining of the 60S ribosomal subunit,[3] cytoplasmic ribosomal Proteins[4]
RPL13A	Formation of a pool of free 40S subunits; RP-dependent cotranslational protein targeting to membrane; GTP hydrolysis and joining of the 60S ribosomal subunit,[3] cytoplasmic ribosomal proteins[4]
RPL37B	Cytoplasmic ribosomal proteins[4]
RPL24A	Formation of a pool of free 40S subunits; RP-dependent cotranslational protein targeting to membrane; GTP hydrolysis and joining of the 60S ribosomal subunit[3]
RPS10B	Response to stimulus,[1] cytoplasmic ribosomal proteins[4]
GAR1	Ribosome biogenesis in eukaryotes[2]
NOP10	Ribosome biogenesis in eukaryotes[2]
NOP4	Ribosome biogenesis in eukaryotes[2]
UTP9	Ribosome biogenesis in eukaryotes[2]
UTP15	Ribosome biogenesis in eukaryotes,[2] Major pathway of rRNA processing in the nucleolus and cytosol[3]
UTP21	Ribosome biogenesis in eukaryotes,[2] Major pathway of rRNA processing in the nucleolus and cytosol[3]
UTP25	Major pathway of rRNA processing in the nucleolus and cytosol[3]
LSM2	RNA degradation; Spliceosome,[2] mRNA decay by 5' to 3' exoribonuclease; mRNA Splicing - Minor Pathway[3]
HRR25	Response to stimulus,[1] ribosome biogenesis in eukaryotes[2]
(v) carbohydrate metabolism enzymes	

GND1	Response to stimulus,[1] pentose phosphate pathway (hexose monophosphate shunt),[2,3] carbon metabolism,[2,4] biosynthesis of antibiotics,[2] non-oxidative branch of the pentose pathway; oxidative branch of the pentose phosphate pathway[4]
ZWF1	Response to stimulus,[1] pentose phosphate pathway (hexose monophosphate shunt),[2,3] carbon metabolism,[2,4] biosynthesis of antibiotics,[2] non-oxidative branch of the pentose pathway; oxidative branch of the pentose phosphate pathway,[4] TP53 regulates metabolic genes[3]
GND2	Pentose phosphate pathway (hexose monophosphate shunt)[2,3] carbon metabolism,[2,4] biosynthesis of antibiotics,[2] non-oxidative branch of the pentose pathway; oxidative branch of the pentose phosphate pathway[4]
SOL3	Pentose phosphate pathway[2-4]
ALD3	Glycolysis / gluconeogenesis,[2,4] Panothenate and Coenzyme A Biosynthesis[4]
ALD4	Pentose and glucuronate interconversions,[2] glycolysis / gluconeogenesis,[2,4] fructose catabolism,[3] principle pathways of carbon metabolism [4]
TDH1	Glycolysis / gluconeogenesis,[2,4] biosynthesis of antibiotics; carbon metabolism,[2] principle pathways of carbon metabolism [4]
TDH3	Glycolysis / gluconeogenesis,[2,4] biosynthesis of antibiotics; carbon metabolism,[2] principle pathways of carbon metabolism[4]
SFA1	Glycolysis / gluconeogenesis; fatty acid degradation; biosynthesis of antibiotics; carbon metabolism[2]
ADH6	Biosynthesis of antibiotics; glycolysis / gluconeogenesis; pentose and glucuronate interconversions[2]
ADH2	Glycolysis / gluconeogenesis,[2,4] biosynthesis of antibiotics,[2] principle pathways of carbon metabolism[4]
ACS1	Carbon metabolism; glycolysis / gluconeogenesis, [2,4] propanoate metabolism; biosynthesis of antibiotics; pyruvate metabolism[2]
ICL1	Glyoxylate and dicarboxylate metabolism,[2] principle pathways of carbon metabolism,[2,4] TCA Cycle[4]
PYC1	Citrate cycle (TCA cycle); principle pathways of carbon metabolism[2,4]
GUT2	Glycerophospholipid metabolism,[2] triglyceride catabolism,[3] principle pathways of carbon metabolism; aerobic glycerol catabolism; anaerobic respiration[4]
DAK1	Fructose and mannose metabolism; glycerolipid metabolism[2]
GPT2	Glycerolipid metabolism; glycerophospholipid metabolism[2]
GPD1	Glycerophospholipid metabolism,[2] aerobic glycerol catabolism[3]
HOR2; GPP2	Glycerolipid metabolism[2]
TSL1	Response to stimulus,[1] starch and sucrose metabolism,[2] trehalose biosynthesis[4]

TPS1	Response to stimulus,[1] starch and sucrose metabolism,[2] trehalose biosynthesis[4]
TPS2	Response to stimulus,[1] starch and sucrose metabolism, [2] trehalose biosynthesis[4]
PGM2	Starch and sucrose metabolism; amino sugar and nucleotide sugar metabolism,[2] galactose metabolism,[2,3] glycogen synthesis; glycogen breakdown,[3] starch and cellulose Biosynthesis; lactose degradation[4]
(vi) enzymes involved in sulfur, amino acid metabolism and purine and pyrimidine synthesis	
CYC1	Transporter activity,[1] sulfur metabolism,[2] transcriptional activation of mitochondrial biogenesis; release of apoptotic factors from the mitochondria; detoxification of reactive oxygen species[3]
BNA3	Tryptophan metabolism,[2,3] amino acid synthesis and interconversion (transamination); phenylalanine and tyrosine catabolism,[3] tryptophan degradation Via kynurenine; de novo NAD Biosynthesis[4]
SER3	Biosynthesis of amino acids; glycine, serine, and threonine metabolism; biosynthesis of antibiotics,[2] serine Biosynthesis[3,4]
SHM2	Biosynthesis of amino acids; one carbon pool by folate; biosynthesis of secondary metabolites; glycine, serine, and threonine metabolism; Carbon metabolism; glyoxylate and dicarboxylate metabolism[2]
ARO9	Phenylalanine, tyrosine and tryptophan biosynthesis,[2] lysine catabolism; tryptophan catabolism[3]
BAT2	Biosynthesis of amino acids; valine, leucine and isoleucine degradation; cysteine and methionine metabolism; pantothenate and CoA biosynthesis[2]
LYS20	Cell organization and biogenesis; metabolic process; response to stimulus,[1] lysine biosynthesis,[2,4] biosynthesis of antibiotics; pyruvate metabolism[2]
CAR2	Metabolic process, response to stimulus,[1] arginine and proline metabolism; biosynthesis of antibiotics,[2] amino acid synthesis and interconversion (transamination),[3] arginine degradation[4]
HIS1	Biosynthesis of secondary metabolites; histidine metabolism; biosynthesis of amino acids; metabolic pathways[2]
HIS4	Histidine metabolism; biosynthesis of secondary metabolites; biosynthesis of amino acids; metabolic pathways[2]
HAM1	Purine metabolism [2,3]
ADE17	Purine metabolism,[2] super pathway of histidine, purine, and pyrimidine[4]
AAH1	Purine metabolism,[2] purine salvage,[3] purine fermentation [4]
APT2	Purine metabolism,[2] purine salvage; neutrophil degranulation [3]
ADE1	Purine metabolism; biosynthesis of secondary metabolites; metabolic pathways; biosynthesis of antibiotics [2]
ADE 2	Purine metabolism; biosynthesis of secondary metabolites; metabolic pathways [2]

ADE 4	Purine metabolism; alanine, aspartate and glutamate metabolism; biosynthesis of secondary metabolites; metabolic pathways; biosynthesis of antibiotics [2]
ADE 5,7	Biosynthesis of secondary metabolites; Metabolic pathways; Biosynthesis of antibiotics; Purine metabolism [2]
ADE6	Biosynthesis of secondary metabolites; metabolic pathways; biosynthesis of antibiotics; purine metabolism [2]
ADE8	One carbon pool by folate; Biosynthesis of secondary metabolites; Metabolic pathways; Biosynthesis of antibiotics; Purine metabolism [2]
(vii) NADPH or NADP+ dependent enzymes.	
OYE2	Cell death; metabolic process; catalytic activity; nucleotide binding; protein binding[1]
OYE3	Cell death; metabolic process; catalytic activity; nucleotide binding; protein binding[1]
UGA2	Response to stimulus,[1] metabolic pathways; alanine, aspartate, glutamate, butanoate, tyrosine metabolism; nicotinate and nicotinamide metabolism; lysine degradation [2]
YDL124W	Response to stimulus; metabolic process; catalytic activity[1]
GRE2	MAPK signaling pathway – yeast[2]

Protein annotations reported by Proteome Discoverer v2.3, which accessed the following sources: [1]The Gene Ontology (GO) database, [2] KEGG Pathways, [3] Reactome Pathways, and [4] Wiki Pathways as outlined in Section 4.4.8.

Chapter 5: Investigating at the molecular level why the W191F variant of Ccp1 is a more efficient peroxide sensor protein than Ccp1

5.1) Preface

Data production, analysis and interpretation, writing and revisions of the text were performed by SD. AME contributed to the data analysis, discussion, editing and revisions of the text.

5.2) Abstract

Cytochrome c peroxidase (Ccp1) is a heme-based H_2O_2 sensor in yeast and catalytically inactive Ccp1W191F performs as an amplified H_2O_2 sensor in these cells. However, the reason for better H_2O_2 sensing/singling by Ccp1W191F compared to Ccp1 is not known. Ccp1 can reduce up to 10 M eq of H_2O_2 by endogenous electron donation from its residues in the absence of its biological donor, cytochrome c (Cyt c^{II}). The heme-mediated oxidation of Ccp1 by up to 10 M eq of H_2O_2 in the absence of Cyt c^{II} was previously studied by LC-MS/MS, which identified 24 residues as electron donors. Consumption of 10 M eq H_2O_2 by recombinant Ccp1W191F has been confirmed but its polypeptide has not been characterized afterwards. Here Ccp1 and Ccp1W191F are compared after reaction with 1, 5 and 10 M eq of H_2O_2, and the results reveal that the variants use different strategies to reduce H_2O_2. Unlike Ccp1, both 1 and 10 M eq of H_2O_2 resulted in a similar fraction of Ccp1W191F dimerization as monitored by SDS-PAGE and in similar changes in its Soret absorption. Also, Ccp1W191F, which is devoid of cytochrome c peroxidase (CCP) activity, slowly consumes H_2O_2 by catalase-like activity when presented with 10 M eq of H_2O_2, whereas Ccp1 exhibits no catalase activity under this condition. Its lack of CCP activity and its weak catalase activity, which would not compete with other H_2O_2-metabolizing enzymes, may contribute to Ccp1W191F's amplified H_2O_2 sensing/signaling in cells.

5.3) Introduction

During aerobic respiration, incomplete reduction of O_2 produces reactive oxygen species (ROS).[183] High levels of ROS damage cellular components[49] and are associated with the pathophysiology of many disorders such as cancer, diabetes, and neurogenerative diseases.[184] Thus, ROS levels must be tightly controlled to achieve levels that are favorable to the organism.

The ROS of interest here is H_2O_2, which is an important signaling molecule at low levels.[185] The prevailing view is that Ccp1, which is nuclear encoded but targeted to the intermembrane space of mitochondria in *S. cerevisiae*,[2] protects the electron-transport chain

from respiratory-derived H_2O_2. Ccp1 efficiently catalyzes the two-electron reduction of H_2O_2 to water using electrons obtained from the oxidation of two molecules of Cyt c^{II}. During this catalytic cycle, Ccp1 is converted to higher oxidation state intermediates, namely Compound I (CmpdI; Fe^{IV}, $W191^{+\bullet}$) and Compound II (CmpdII; Fe^{IV}).[10] An electron from the heme of Cyt c^{II} is transferred to the heme of Ccp1 to reduce Fe^{IV} to Fe^{III}. In the absence of Cyt c^{II}, Ccp1 transfers electrons from its own residues to its oxidized heme.[74] Repeated two-electron reduction of H_2O_2 by Ccp1 requires repeated intramolecular electron transfer from its residues to the oxidized heme. This generates new transient radicals in Ccp1's polypeptide and in studies performed *in vitro*, a total of 24 oxidized residues in Ccp1 were identified by LC-MS/MS.[74]

We found that Ccp1's polypeptide also is oxidized in respiring cells.[26] Additionally, heme is released from Ccp1 in cells following oxidation of its proximal H175.[26] Furthermore, Ccp1's heme is recruited for maturation of catalase A (Cta1).[24] In fact, we observed that when heme-free Ccp1 exits mitochondria in 7-day respiring cells (Chapter 3), Cta1 activity increases.[26] W191 is a critical residue since it is located on the electron-transfer pathway between Ccp1's heme and that of Cyt c.[2,186] Mutation of W191 to redox-inactive phenylalanine (F) gives the W191F variant, which exhibits negligible Cyt c^{II}-oxidizing ability.[187] However, Ccp1W191F is viewed as an amplified peroxide sensor[24] since fermenting cells expressing this variant (W191F cells) upregulate cytosolic catalase T (Ctt1) activity more than WT cells when challenged with exogenous H_2O_2.[24] We compared the H_2O_2 stimulon of fermenting WT and W191F cells using label-free LC-MS/MS (Chapter 4) and found that hyper sensing by Ccp1W191F produces a dramatically more sustained response. In this chapter, we aimed to answer at the molecular level why Ccp1W191F is a more efficient peroxide sensor protein than WT Ccp1 by comparing how reaction with H_2O_2 modifies their heme and polypeptide. Specifically, we characterized recombinant Ccp1W191F vs WT Ccp1 following reaction with 0, 1, 5, and 10 M eq of H_2O_2.

5.4) Experimental Section

5.4.1) Materials

Suppliers of (bio)chemicals were as follows: horse heart myoglobin (Mb), sequencing grade modified trypsin from porcine pancreas, hemin from bovine, acid-washed glass beads (212-300 µm), bovine catalase, diethylaminoethyl cellulose (DEAE)-Sepharose, DL-dithiothreitol (DTT), iodoacetamide with purity > 99%, 3,5-dibromo-sulphanilic acid sodium salt, 2,2'-azino-bis(3-ethylbenzthiazoline-6-sulfonic acid) (ABTS), horseradish peroxidase (HRP), anhydrous sodium acetate and glacial acetic acid (Sigma-Aldrich), thrombin with technical grade (Calbiochem), tryptone (EMD Millipore), yeast extract (Bioshop), Bio-SafeTM Coomassie stain (Bio-Rad), BLUeye Prestained Protein Ladder (FroggaBio), cOmplete His-tag purification Ni-

IMAC resin (Roche), diethylenetriamine pentaacetate or DTPA (ICN Biomedicals Inc.), hydrogen peroxide 30%, HPLC grade acetonitrile (ACN), formic acid (FA) and HPLC grade water (Thermo Fisher Scientific).

5.4.2) Reaction of H_2O_2 with WT Ccp1 and Ccp1W191F

Protein stock solutions of 5 μM were prepared in 20 mM potassium phosphate buffer pH 7.5 with 200 μM DTPA (KPi/DTPA) to suppress trace-metal catalyzed oxidation. Protein concentrations were determined spectrophotometrically using ε_{408} = 98 mM^{-1} cm^{-1} for Ccp1[86] and ε_{411} = 109 mM^{-1} cm^{-1} for Ccp1W191F.[188] A stock H_2O_2 solution (1 mM) was prepared in the same buffer and 5 μM protein was reacted with 0, 1, 5 and 10 M eq of H_2O_2. Protein and H_2O_2 were stirred at RT for 1 h in the dark, and the presence of residual H_2O_2 was probed by adding HRP and ABTS and monitoring HRP-catalysed ABTS oxidation by H_2O_2, which gives a product that absorbs at 405 nm.[189]

5.4.3) LC-MS conditions

Solutions of 5 μM oxidized Ccp1 and Ccp1W191F were diluted 2.5-fold into KPi/DTPA and 5-μL aliquots were loaded onto a reversed-phase Zorbax 300SB-CN column equilibrated with 5% aqueous ACN/0.1 % FA at RT on an Agilent 1200 HPLC. Samples were eluted from the column at a flow rate of 0.2 mL/min with a 5–95% ACN gradient over 5 min into the ESI source of a QTof3 mass spectrometer (Waters Micromass). Mass analysis was performed using the following parameters: capillary voltage 3.5 kV, cone voltage 80 V, RF lens 50 V, source temperature 80 °C and desolvation temperature 350 °C. Protein envelopes were deconvoluted by the MassLynx4 (Waters) to obtain protein masses.

5.4.4) Measurement of oxygen evolution

Oxygen evolution was measured with an Oxygraph-2k multisensor (OROBOROS Instruments). This instrument has two 2.0-mL chambers equipped with polarographic oxygen sensors (POS). Each POS consists of a gold cathode and a silver-silver chloride anode enclosed by an oxygen-permeable membrane. The chambers were rinsed extensively with KPi/DTPA and once the O_2 concentration stabilized, 1 μM recombinant Ccp1 or Ccp1W191F, followed by 10 μM H_2O_2 in the same buffer, were added and the O_2 concentration was monitored for a further 20 min.

5.4.5) Recombinant His_6-Ccp1 and His_6-Ccp1W191F overexpression and purification

Two pET15b-derived vectors, pHis-CCP and pHis-CCP(W191F), that express N-terminally His_6-tagged Ccp1 and Ccp1W191F were previously engineered as outlined in Figure S5.1. BL21(DE3) cells were transformed with pHis-CCP and both BL21(DE3) and BL21(DE3)pLysS cells were transformed with pHis-CCP(W191F) (Figure S5.1; Section S5.8.1).

Protein expression was monitored using SDS-PAGE gel and the best expressing clones were used to inoculate 500 mL of LB medium with 100 µg/mL ampicillin plus 34 µg/mL chloramphenicol for the BL21(DE3)pLysS strain. Cells were incubated at 37 °C with stirring at 250 rpm until they reached OD_{600} 0.4–0.6 (~2 h). To induce His_6-Ccp1 or His_6-Ccp1W191F overexpression, 250 µL of 0.5 mM IPTG was added, and cells were incubated at 18 °C/225 rpm for 1 day. The cultures were centrifuged at 10000 g for 10 min, the supernatant was discarded, and the pellets were stored at - 80 °C for protein purification.

Cells were lysed by 3 freeze/thaw cycles in liquid nitrogen and a water bath at 37 °C. The lysate was added to 25 mL of loading buffer (100 mM HEPES with 500 mM NaCl and 10 mM imidazole, pH 7.5). Following 15 x 10 s sonication cycles, the cell debris was removed by centrifugation at 12000 g at 4 ºC for 20 min, 1 mL of Ni-IMAC resin was added to 10 mL of supernatant and rotated end-over-end at 4 °C for 1 h. After centrifugation at 2500 g for 5 min, the resin was washed sequentially with loading buffer containing 10 and 25 mM imidazole at 4 °C for 5 min. His_6-Ccp1 and His_6-Ccp1W191F were eluted from the resin by adding 500 mM imidazole to the loading buffer and incubating twice for 20 min at 4 °C with end-over-end rotation. The eluates were dialyzed twice against KPi/DTPA at 4 °C overnight. The UV-Vis spectra of the purified proteins recorded on a Cary 100 spectrophotometer (Agilent) showed a peak at 280 nm but no heme absorbance as expected,[114] indicating that His_6-Ccp1 and His_6-Ccp1W191F were isolated in their apoforms. The proteins were stored at -80 °C until further use.

Previously, we showed His_6-tag interference with heme loading of apoCcp1 (Section 2.5.1)[114] so the tag was removed from His_6-Ccp1 and His_6-Ccp1W191F using 5 U of thrombin per mg of protein as described previously (Section 2.4.3).[114] Ni-IMAC resin was added (200 µL to ~ 1 mg protein) to bind free His_6 and the supernatants containing the tag-free proteins were transferred to Eppendorf tubes. His_6-tag removal was confirmed by LC-MS (Section 2.4.3).

5.4.6) Formation of the holoforms of Ccp1 and Ccp1W191F

ApoCcp1 and apoCcp1W191F were incubated with 1.1 M eq hemin for 15 min at 4 °C with end-over-end rotation to form the holoproteins. Any unbound hemin was removed on a 0.8 x 4 cm DEAE Sepharose column equilibrated with 20 mM MES buffer (pH 6.5) and the holoproteins were eluted by adding 500 mM NaCl to the buffer (Section 2.4.3).[114] Note that in the remainder of this chapter, Ccp1 and Ccp1W191F refer to the holoproteins, unless otherwise indicated.

5.4.7) Synthesis of 3,5-dibromo-4-nitrosobenzenesulphonate (DBNBS) - a spin trap

DBNBS was synthesized as outlined previously.[190] Briefly, a solution of 3,5-dibromo-sulphanilic acid sodium salt (0.706 g, MW 367.95, 1.92 mmol), anhydrous sodium acetate (0.164

g), and 1.58 mL of 30% aqueous H_2O_2 in 6 mL of glacial acetic acid was gently heated in a 10-mL beaker until the solution was clear.[190] The solution was covered with aluminium foil with a few holes and left standing at RT in the dark. DBNBS crystals appeared after 45 days and these were washed with 5 mL of anhydrous diethyl ether followed by 5 mL of cold ethanol.[190] The yield of DBNBS (0.219 g, MW 343.7, 0.64 mmol) was 33% vs the reported yield of 30-33%,[190] and it showed the expected mass spectrum (Figure 5.6).

5.5) Results

5.5.1) BL21(DE3)pLysS cells overexpressed His_6-Ccp1W191F better than BL21(DE3) cells

The best host and conditions for His_6-Ccp1W191F expression from the pHis-CCP(W191F) vector were evaluated using 5-mL cultures. A 2.5-mL aliquot was induced with IPTG for protein overexpression (Section 5.4.5) and the other 2.5 mL served as a non-induced control. After 3 h, cells were centrifuged at 2000 g, the pellet was resuspended in 200 µL of 100 mM KPi (pH 7) with 100 µg/mL lysozyme, and cells were lysed using glass beads by repeatedly (8X) vortexing for 30 s with 30-s intervals on ice. Whole-cell lysates (25 µL) were solubilized at 37 ºC for 1 h by incubation with 5 µL of 5X loading buffer (100 mM Tris-Cl pH 6.8, 4% SDS, 0.2% bromophenol blue, 20% glycerol, 200 mM β-mercaptoethanol), and His_6-Ccp1W191F expression in whole-cell lysates was checked by SDS-PAGE gel analysis. Figure 5.1 shows negligible background expression of His_6-Ccp1W191F in cells with the pLysS plasmid but after IPTG-induction, His_6-Ccp1W191F is highly expressed in BL21(DE3)pLysS cells whereas no induction above background is seen in BL21(DE3) cells.

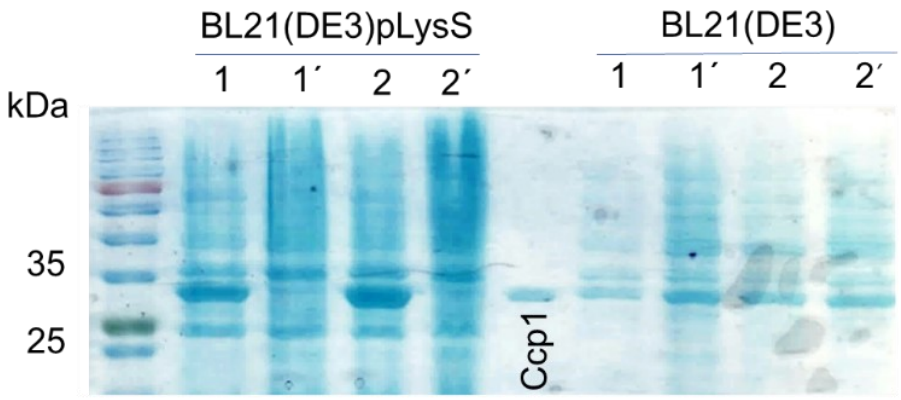

Figure 5.1. Overexpression of His_6-Ccp1W191F in *E. coli* cells. SDS-PAGE gel analysis of whole-cell lysates from BL21(DE3)pLysS and BL21(DE3) *E. coli* cells transformed with pHis-CCP(W191F). Lanes 1 and 2 are the IPTG-induced lysates and lane 1´ and 2´ are the control, non-induced lysates. Purified WT His_6-Ccp1 was run in the middle lane as a MW marker.

Low His_6-Ccp1W191F expression suggests that this protein is toxic to BL21(DE3) cells. BL21(DE3)pLysS cells are commonly used for the expression of toxic proteins with T7 promoter-based expression systems such as pET vectors (Instruction manual: Agilent Technologies and Promega). Typical yields of His_6-Ccp1W191F were ~ 60 mg/L in BL21(DE3)pLysS cells vs ~ 0.5 mg/L in BL21(DE3) cells. The yield of His_6-Ccp1 was ~ 60 mg/L in BL21(DE3) cells.

5.5.2) Spectrophotometric titration of apoCcp1W191F with heme

After removal of the His_6 tag, WT Ccp1's heme-binding stoichiometry is 1:1.[84,191] The heme titration of tag-free apoCcp1W191F was spectrophotometrically monitored at 411 nm,[188] and the heme-binding stoichiometry is confirmed to also be 1:1 from the deflection point in the plot of A_{411} vs [hemin] added (Figure 5.2).

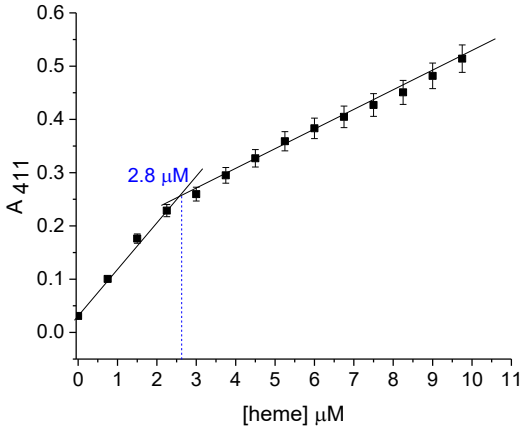

Figure 5.2. Spectrophotometric titration of tag-free apoCcp1W191F with heme. The titration was performed in KPi/DTPA in a 1-cm quartz cuvette at RT on a Beckman Coulter DU800 UV-Visible spectrophotometer. The titrant was 500 μM hemin in 0.1 M aqueous NaOH. A_{411} values were corrected for dilution after each 1.0-μL aliquot of hemin was added. The lines through the data points were manually drawn and extrapolation of their crossover point to the x-axis (dotted line) indicates that 2.8 μM of apoCcp1W191F binds 2.8 μM of hemin. The data are the average plus standard deviation of 3 individual experiments.

5.5.3) Spectrophotometric monitoring of Ccp1 and Ccp1W191F oxidation by H_2O_2

The absorption spectrum of untreated Ccp1 in KPi/DTPA shows a Soret maximum at 408 nm (Figure 5.3A).[84] Immediately upon addition of 1 M eq of H_2O_2, the Soret red shifts to 418 nm (Figure 5.3A), signaling Cmpd I formation.[74] The Soret intensity drops by ~15% over the next hour with a slight blue shift to 417 nm (Figure 5.3B). The spectrum of Ccp1 oxidized with 10 M eq of H_2O_2 initially resembles that of Cmpd I with a Soret at 418 nm and visible absorption bands at 530 and 560 nm characteristic of oxyferryl heme[10] (Figure 5.3A). However over 1 h, the Soret

drops in intensity by ~ 40% and blue shifts to 412 nm plus the 530 and 560-nm bands also lose intensity (Figure 5.3B).[74]

Before H_2O_2 addition, Ccp1W191F shows a Soret maximum at 411 nm[10,188,192] vs 408 nm in Ccp1 (Figure 5.3C vs. A). Upon addition of 1 M eq of H_2O_2, the Soret blue shifts to 416 nm[192,193] (Figure 5.3C) and bands appear at 530 and 560 nm, consistent with oxyferryl heme formation.[10]

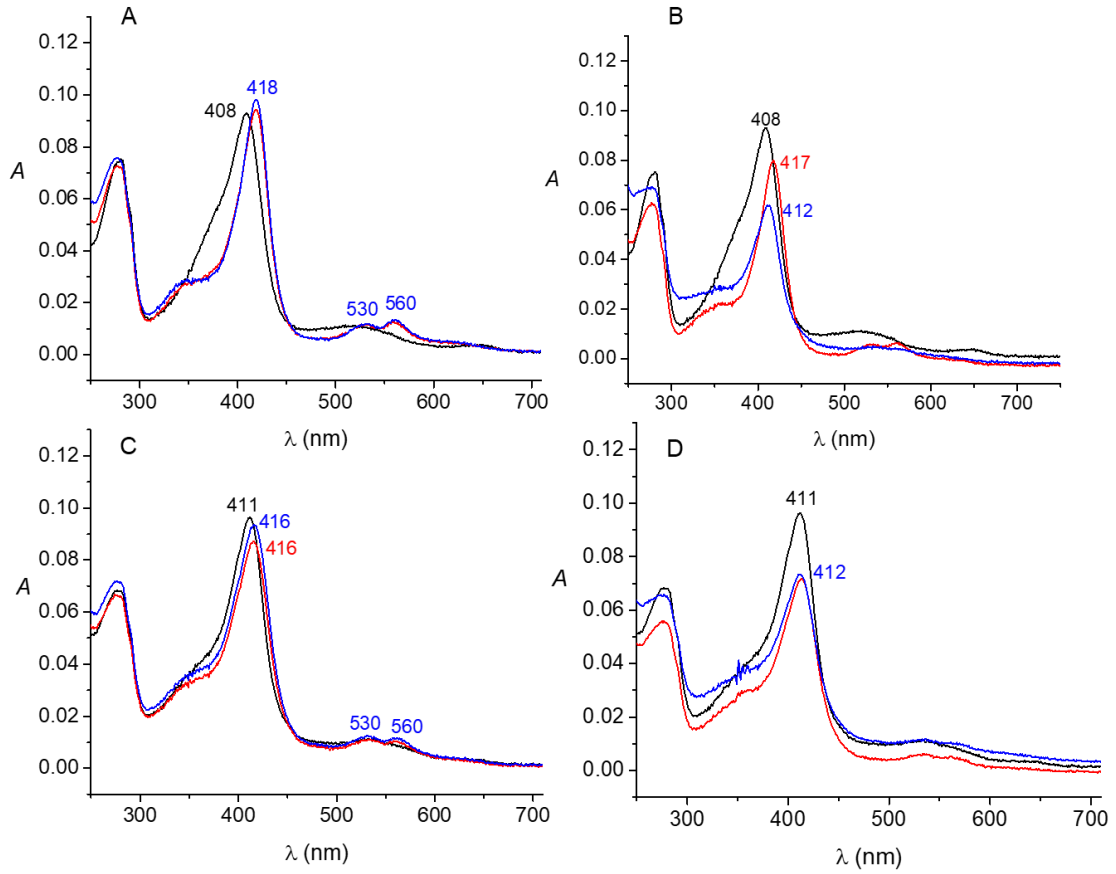

Figure 5.3. UV-Vis absorption spectra of Ccp1 and Ccp1W191F before and after H_2O_2 addition. Spectra in 1-cm quartz cuvette at RT of 1 μM protein in KPi/DTPA after the addition of 0 (black traces), 1.0 (red traces) and 10 M eq of H_2O_2 (blue traces). Ccp1 spectra at: (A) t = 0 and (B) t = 1 h. Ccp1W191F spectra at: (C) t = 0 and (D) t = 1 h. Results are representative of three independent experiments. The noise in the spectra around 350 nm is due to the lamp switchover in the Cary 100 spectrophotometer (Agilent).

Ccp1W191F oxidized with 10 M eq of H_2O_2 shows a similar spectrum with a Soret maximum at 416 nm[192] (Figure 3C). After 1-h incubation both samples show the same Soret, which has lost ~ 25% of its intensity and blue shifted to 412 nm (Figure 5.3D). Notably, the addition of 10 M eq of H_2O_2 does not lead to greater loss of Soret intensity as seen for WT Ccp1 (Figure 5.3B). One reason for this could be the slower rate of H_2O_2 consumption by Ccp1W191F (20 min) vs

holoCcp1 (5 min).[194] It also signals that the variants consume H_2O_2 by different mechanisms as explored in the following sections.

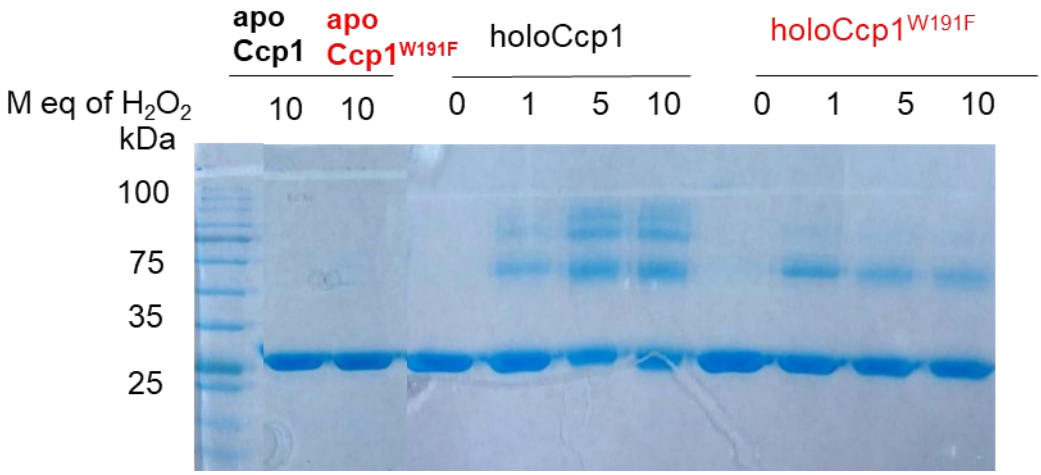

Figure 5.4. SDS-PAGE analysis of H_2O_2-induced cross-linking of Ccp1 and Ccp1W191F. The apo- and holoproteins (5 μM) were reacted with the indicated H_2O_2 concentration in KPi /DTPA for 1 h at RT and analyzed by 12% SDS-PAGE with Coomassie staining. The apoproteins treated with 10 M eq of H_2O_2 remain monomeric (~34 kDa) as are untreated holoCcp1 and holoCcp1W191F. Dimer bands (~68 kDa) are visible in holoCcp1 and holoCcp1W191F reacted with 1 M eq of H_2O_2. Trimer (102 kDa) and tetramer bands (136 kDa) appear in holoCcp1 but not holoCcp1W191F reacted with 5 and 10 M eq of H_2O_2. The gel is representative of three experiments.

5.5.4) H_2O_2-induced cross-linking of holoCcp1 and holoCcp1W191F

Following reaction with H_2O_2, Ccp1 and Ccp1W191F were analyzed by SDS-PAGE (Figure 5.4). This figure shows that H_2O_2 cross-linking of the proteins is heme mediated since the apoproteins undergo no detectable cross-linking. In contrast, dimerization of a fraction (~ 5%) of holoCcp1 and holoCcp1W191F occurs in their reaction with 1 M eq of H_2O_2. Reaction with 5 and 10 M eq of H_2O_2 induces significant trimerization and tetramerization of holoCcp1 but not of holoCcp1W191F, which also undergoes no further dimerization on reaction with > 1 M eq of H_2O_2 (Figure 5.4). Thus, H_2O_2-induced cross-linking of holoCcp1W191F appears to shut down following its reaction with ≤ 1 M eq of H_2O_2, which signals an abrupt switch in the mechanism of H_2O_2 consumption by this variant.

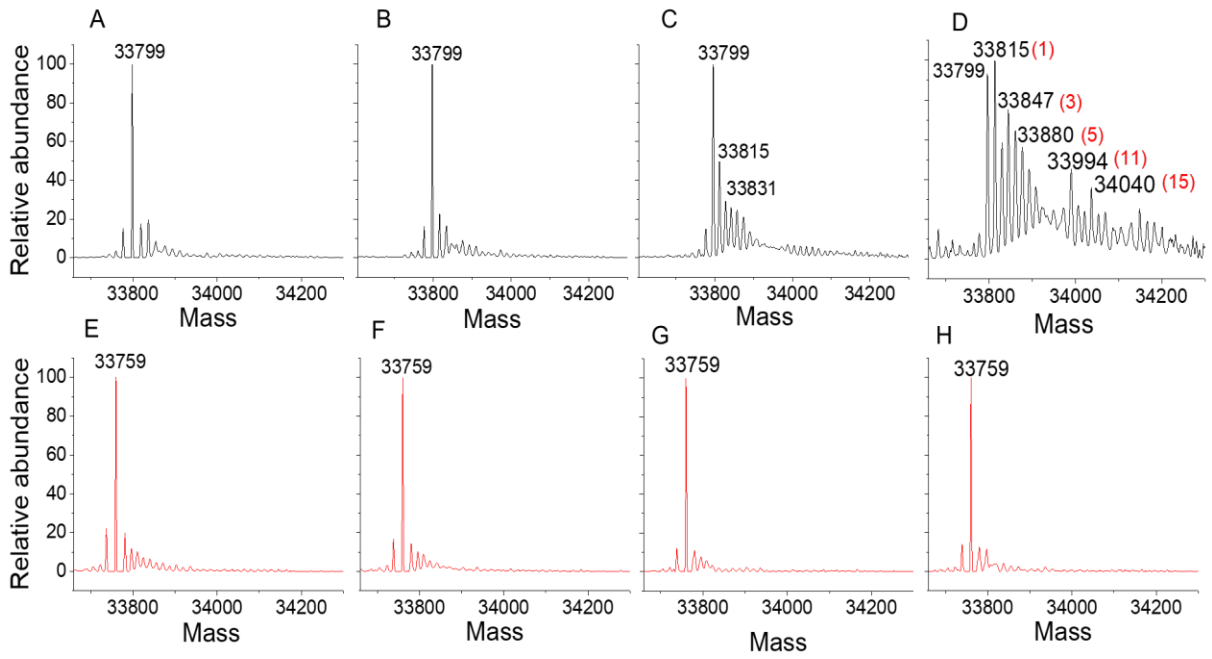

Figure 5.5. Deconvolved mass spectra of Ccp1 and Ccp1W191F after reaction with H_2O_2. Mass spectra of Ccp1 (top panels) and Ccp1W191F (bottom panels) reacted with (A, E) 0, (B, F) 1, (C, G) 5, and (D, H) 10 M eq of H_2O_2. Proteins (5 μM) and H_2O_2 were stirred in KPi/DTPA at RT for 1 h in the dark (Section 5.4.2), diluted 2.5-fold into KPi/DTPA and 5-μL aliquots were injected into the LC-MS (Section 5.4.3). The Q-Tof3 was mass calibrated using apomyoglobin (calc avg mass 16,951.49 u; obs avg mass 16,952.66; mass error 69 ppm). The obs masses of untreated Ccp1 (33,799 u; 38 ppm error) and Ccp1W191F (33759 u; 9.5 ppm error) agree well with those calculated (33,797.71 and 33,758.68 u) using ExPASy (https://web.expasy.org/compute_pi/). Ccp1 reacted with 5 and 10 M eq of H_2O_2 (panels C and D) shows 1 to > 15 (as indicated in red font in panel D) incremental mass shifts of +16 u but not Ccp1W191F (panels G and H).

5.5.5) LC-MS analysis of Ccp1 and Ccp1W191F after reaction with H_2O_2

Following reaction with 5 and 10 M eq of H_2O_2, the mass spectra of Ccp1 (33799 ± 1 u) exhibit new peaks with incremental mass shifts of +16 u (Figure 5.5, top panels). We assign these peaks to oxidized forms of the protein that have incorporated one or more oxygen atoms at specific residues. The number of oxidized residues increases with the amount of H_2O_2 added such that Ccp1 treated with 10 M eq of H_2O_2 has incorporated over 15 oxygens (Figure 5.5D). In contrast, the mass spectra of Ccp1W191F (obs mass 33759 ± 1 u) following reaction with 1, 5 or 10 M eq of H_2O_2 are identical (Figure 5.5 F-H). Hence, LC-MS provides no evidence for oxygen incorporation into its residues, which affirms that Ccp1W191F does not consume H_2O_2 by the same mechanism as WT Ccp1.

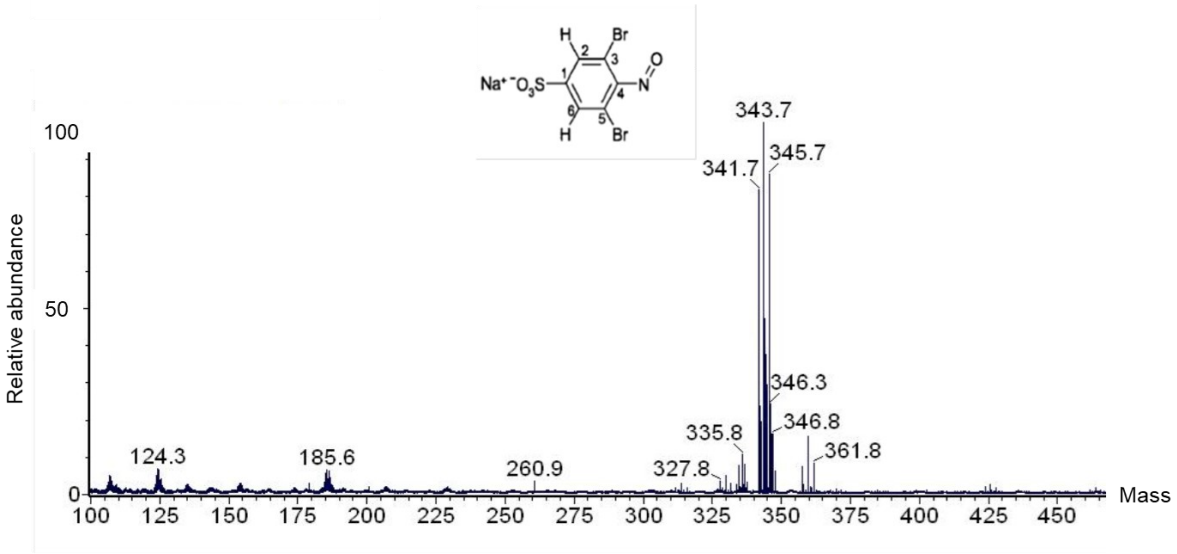

Figure 5.6. Mass spectrum of DBNBS. DBNBS was synthesized as described (Section 5.4.7) and a 1 mM stock solution was prepared in 10 mM ammonium acetate, pH 7.5. The diluted stock (1 μM DBNBS) was directly injected by syringe into the ESI source of a QTof2 (Waters Micromass) operated with the following parameters: negative mode, capillary voltage -3.5 kV, cone voltage 40 V, RF lens 50 V, source temperature 80 °C and desolvation temperature 300 °C. The mass accuracy was found to be 788 ppm with NaI as a mass calibrant (Sigma) (avg mass I: obs = 127.0 u; calc = 126.9 u; https://beta-static.fishersci.ca). In negative mode, the DBNBS anion $(C_6H_2Br_2NO_4S)^-$ with two Br atoms has calculated monoisotopic masses at m/z 341.8 ($^{79}Br^{79}Br$), 343.8 ($^{79}Br^{81}Br$) and 345.8 ($^{81}Br^{81}Br$) (calculated with enviPat Web 2.4; www.envipat.eawag.ch), and peaks were observed at m/z 341.7 (292 ppm error), 343.7 (290 ppm error), and 345.7 (289 ppm error) in agreement with previous results (m/z 342, 344 and 346) using fast atom bombardment (FAB)-MS.[190]

5.5.6) DBNBS spin trapping

Employing the spin trap, 2-methyl-2-nitrosopropane (MNP),[194,195] we trapped spin adducts on Y236, Y153, and one or more of Y36, Y39 and Y42 of oxidized Ccp1, indicating formation of carbon-centered radicals on these tyrosines. We also noted that H_2O_2-induced Ccp1 cross-linking was diminished in the presence of MNP.[194] In contrast, no MNP-spin adducts of oxidized Ccp1W191F were observed and MNP did not compete with its cross-linking.[194]

Another spin trap, DBNBS, has been used previously by our group to identify sites of radical formation in Cyt c.[195] DBNBS is an efficient spin trap[196] with higher solubility than MNP so we used it here in an attempt to trap carbon-centered radicals in Ccp1W191F. Because DBNBS is not commercially available, we synthesized it following the literature procedure (Section 5.4.7)[190] and supported its synthesis by mass spectrometry (Figure 5.6). DBNBS was added to Ccp1W191F or Ccp1, followed by 10 M eq of H_2O_2 plus ascorbate 10 min later to reduce the spin adducts to stable diamagnetic adducts (Figure 5.7).[195]

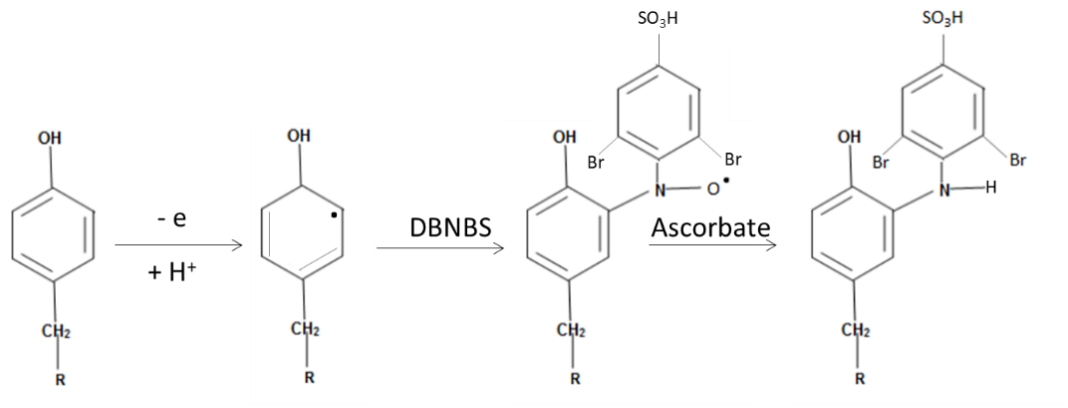

Figure 5.7. Spin-trapping of a tyrosyl radical by DBNBS. The tyrosyl radical has high spin density at the ring ortho carbon (Figure S5.2), which forms a covalent bond with the nitroso N of DBNBS. Ascorbate reduces the spin adduct to a more stable diamagnetic adduct for MS detection.[195] The average (monoisotopic) mass increase in a tyrosyl radical on spin trapping is 343.9 u (341.8 u), and following reduction to the diamagnetic adduct the mass increase is 328.9 u (326.8) u (calculated with www.lfd.uci.edu/~gohlke/molmass). A similar mechanism was proposed for trapping of tyrosyl radicals by MNP.[197] This figure was prepared using ChemDraw.

About 10% of Ccp1 and Ccp1W191F shows a mass increase of 344 and 342 u, respectively, when incubated with DBNBS in the absence of H_2O_2 (Figure 5.8 A, B). This indicates the covalent or noncovalent binding of DBNBS (avg mass = 344 u) to the proteins.[166] However, up to 4 such adducts formed in Ccp1 and 7 in Ccp1W191F when H_2O_2 was present in the reaction (Figure 5.8C, D), which we attribute to DBNBS spin-adduct formation (Figure 5.7). Furthermore, Ccp1, and Ccp1W191F to a lesser extent, form adducts with an avg mass of 329 u, which we attribute to reduction of the spin adducts to diamagnetic adducts (Figure 5.7).

To examine adduct formation at the peptide level, products of the protein/H_2O_2/DBNBS/ascorbate reactions were subjected to tryptic digestion. Following digestion in ammonium bicarbonate at 37 °C for 4 h, peptides were desalted on C18 Zip tips, eluted with 10 µL of 60% aqueous ACN/0.1% FA and dried on a SpeedVac (Savant). Following reconstitution in 0.1% FA, the peptides were injected into the nano-LC-Orbitrap MS/MS (Section 4.4.6). Only native peptides were observed (data not shown), suggesting that the adducts were unstable to tryptic digestion as we reported previously for the DBNBS adducts of Cyt c.[195]

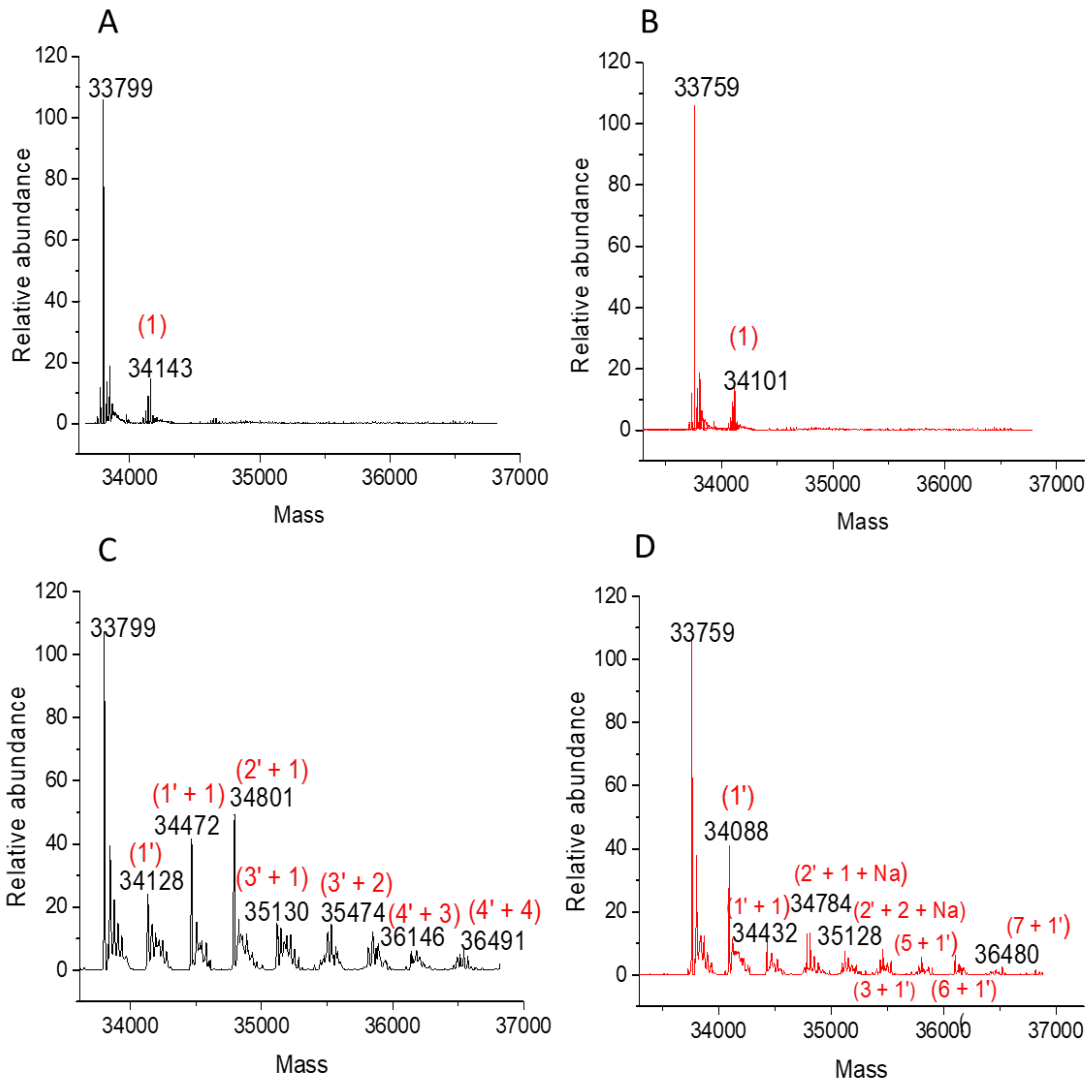

Figure 5.8. LC-MS analysis of spin trapping by DBNBS in the reactions of Ccp1 and Ccp1W191F with 10 M eq of H_2O_2. DBNBS (2.5 mM) was added to 5 μM Ccp1 or Ccp1W191F in KPi/DTPA followed by 50 μM H_2O_2. After 10 min reaction at RT, 5 mM sodium ascorbate was added and the reaction was allowed to continue for 30 min. Control samples were treated the same way except no H_2O_2 was added. All samples were diluted 2.5-fold into KPi/DTPA and 5-μL aliquots were injected onto the LC-MS (Section 5.4.3). The deconvolved mass spectra of: (A) 2 μM Ccp1 (control; no H_2O_2), (B) 2 μM Ccp1W191F (control, no H_2O_2), (C) 2 μM oxidized Ccp1, and (D) 2 μM oxidized Ccp1W191F recorded as described in the caption of Figure 5.5. Panels A and B reveal ~ 10% DBNBS (avg mass = 344 u) adduct formation in the absence of H_2O_2. Panel C and D show that with H_2O_2 present, the proteins form multiple spin and diamagnetic adducts (avg mass = 329 u; indicated by a prime).

5.5.7) Oxygen evolution during the reaction of H_2O_2 with Ccp1 and Ccp1W191F

No H_2O_2 was detected by the HRP/ABTS assay[189] 1 h after 10 M eq of H_2O_2 was added to holoCcp1 or holoCcp1W191F (Figure 5.9). In contrast, no H_2O_2 was consumed by apoCcp1 or apoCcp1W191F (Figure 5.9), indicating that any reactions between the proteins and H_2O_2 is heme mediated.

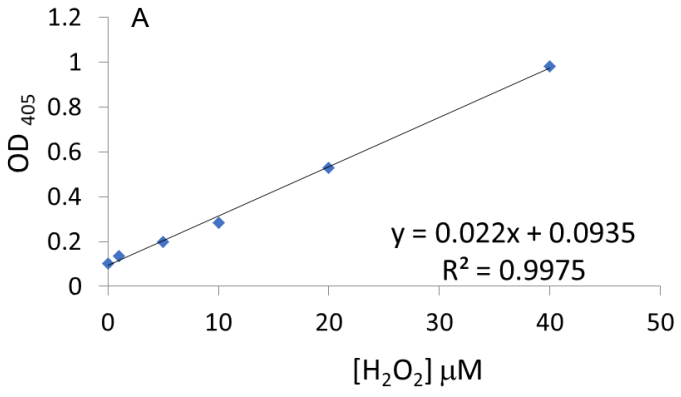

B

	holoCcp1	holoCcp1W191F	apoCcp1	apoCcp1W191F
OD_{405}	0.094 ± 0.005	0.094 ± 0.004	0.313 ± 0.003	0.314 ± 0.005
Residual H_2O_2 (μM)	0	0	10	10

Figure 5.9. Consumption of H_2O_2 by Ccp1 and Ccp1W191F. (A) Standard curve for H_2O_2 determination by the HRP/ABTS assay.[189] Excess ABTS (2 mM) and 5 μM HRP were added to standard solutions containing 0, 1, 5, 10, 20 and 40 μM H_2O_2 and the absorbance at 405 nm of oxidized ABTS was measured after 1 min and is plotted vs [H_2O_2]. (B) H_2O_2 remaining in solution with holoCcp1, holoCcp1W191F, apoCcp1 and apoCcp1W191F as determined from the standard curve in A. H_2O_2 (10 μM) was added to 1 μM apo- or holoprotein in KPi/DTPA at RT, 2 mM ABTS and 5 μM HRP were added after 1 h, and the OD_{405} was recorded immediately to determine the residual H_2O_2. Note that the proteins used in these experiemtns were *not* His_6 tagged.

Catalase activity disproportionates H_2O_2 to H_2O and O_2, using peroxide both as reductant and oxidant.[194] Since Ccp1W191F appears to be less physically modified by H_2O_2, we questioned if it possessed catalase-like activity. O_2 production in the consumption of 10 M eq of H_2O_2 by 1 μM protein was investigated with a polarographic oxygen sensor (Figure 5.10). Ccp1W191F produced 2.3 ± 0.3 μM O_2 from 10 μM H_2O_2 in 20 min but no O_2 evolution was detected in the Ccp1 reaction (Figure 5.10). Theoretically, 5 μM O_2 would be produced in the disproportionation of 10 μM H_2O_2 (10 H_2O_2 → 5 O_2 + 10 H_2O), indicating that Ccp1W191F

partially consumes H_2O_2 by catalase activity. Using an oxygen electrode, our lab previously reported negligible O_2 production from 50 μM H_2O_2 in solutions of 5 μM Ccp1(MI) and Ccp1W191F(MI).[194] This raises the question if the mechanisms of H_2O_2 consumption are concentration dependent or if Ccp1W191F(MI) behaves differently from the Ccp1W191F construct used here (Figure S5.1 and Section S5.8.1). Further experiments are needed to clarify the discrepancy between our current and previous results.

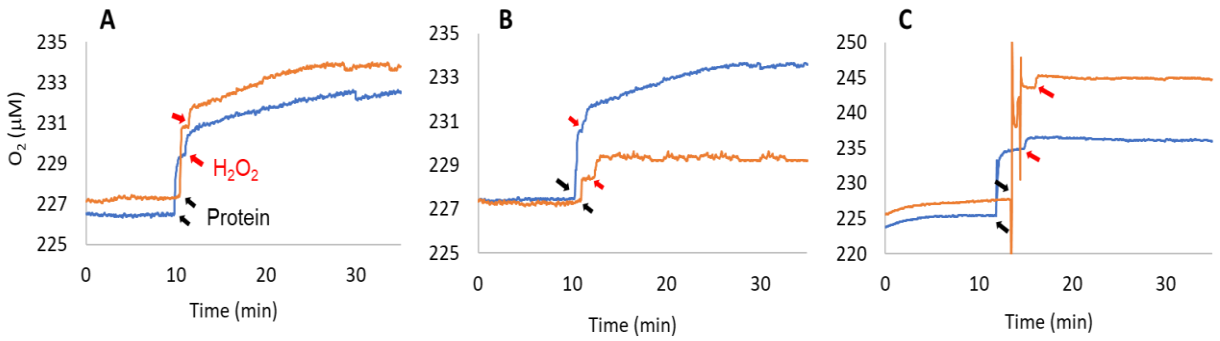

Figure 5.10. O_2 evolution in solutions of 10 M eq of H_2O_2 with Ccp1 and Ccp1W191F. O_2 evolution over ~ 20 min at 22 ºC in the reaction of 10 μM H_2O_2 with1 μM of: (A) Ccp1W191F (both traces), (B) Ccp1W191F (blue trace) and Ccp1 (red trace), and (C) Ccp1 (both traces). KPi/DTPA (1.85 mL) was added to each chamber of the Oxygraph-2k sensor (Section 5.4.4) and, after the background O_2 reading stabilized (~ 10 min), 100 μL of protein (black arrows) followed ~2 - 5 min later by 50 μL of H_2O_2 (red arrows; t = 0) were added by syringe, and O_2 evolution was recorded for ~ 20 min. In panel C (red trace), H_2O_2 was added after the signal stabilized following protein addition. The results are representative of 3 experiments. Note that the proteins used in these experiemtns were *not* His_6 tagged.

5.6) Discussion

Mature holoCcp1 is present in the IMS before yeast synthesize Cta1 or Cyt c.[66,198] Thus, given its ability to reduce up to 10 M eq of H_2O_2 in the absence of its biological partner Cyt c,[74] Ccp1's might serve as the first available mitochondrial antioxidant in response to respiration-derived H_2O_2. Ccp1 also functions as a H_2O_2 sensor, and its W191F variant is an amplified H_2O_2 sensor.[24] However, Ccp1W191F does not accept electrons from Cyt c^{II},[10] and it consumes excess H_2O_2 more slowly *in vitro*.[194] Thus, to understand how Ccp1W191F functions as an amplified H_2O_2 sensor, we explored here how it was modified by H_2O_2.

5.6.1) Heme-mediated H_2O_2-induced modification of residues in Ccp1W191F

LC-MS analysis identified 24 oxidized residues in WT Ccp1 following reaction with H_2O_2 (Figure 5.11). This enabled mapping of hole hopping from the heme to residues in three polypeptide regions,[74] which encouraged us to probe hole hopping in Ccp1W191F. However,

mass spectra of Ccp1W191F following reaction with up to 10 M eq of H_2O_2 do not show oxygen incorporation as found for WT Ccp1 (Figure 5.5). Moreover, analysis of H_2O_2-induced cross-linking suggests limited radical migration from the heme to the protein surface in Ccp1W191F (Figure 5.4). Nonetheless, DBNBS appears to trap a similar number of radicals in oxidized Ccp1W191F and Ccp1 as both proteins form up to seven DBNBS adducts (Figure 5.8). The question remains are all these adducts derived from spin trapping and if so which residues are oxidized in Ccp1W191F?

Upon reaction with H_2O_2, Ccp1W191F forms a transient porphyrin π-cation radical that is quickly transferred to its polypeptide.[192,194,199] A transient Y236 radical was detected by EPR/ENDOR,[200,201] and radical candidates on tryptic petides T_{26} (Y229, Y236) and T_6 (Y36, Y39, Y42) were identified by peptide mapping of the Ccp1W191F cross-linked dimer isolated from its reaction with 10 M eq of H_2O_2.[194] Since DBNBS[195] effectively traps carbon-centered radicals, its adducts (Figure 5.8) may result from trapping some of these tyrosyl radicals, but this requires further investigation.

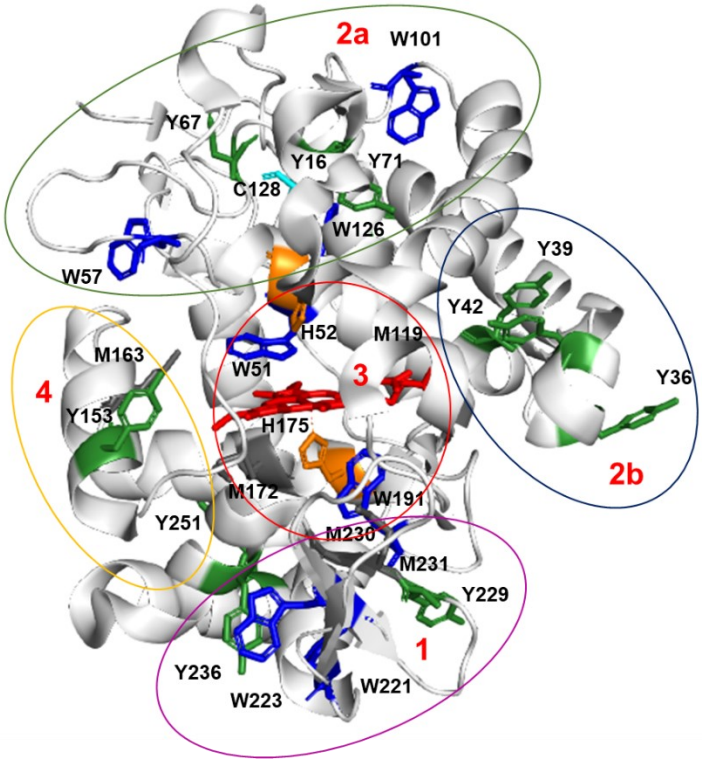

Figure 5.11. Distribution of the 24 residues oxidized during the reaction of WT Ccp1 with 10 M eq of H_2O_2 *in vitro*. PyMOL was used to generate this ribbon cartoon of Ccp1 (PDB 1ZBY) with W (blue), Y (green), H (orange), M (grey) and C (cyan) residues shown as sticks. Discrete zones containing oxidized residues are outlined by circles in magenta (1), green and blue (2a, 2b) and red (3). Residues in zone 4 (yellow circle) experience little oxidation.[74] This figure is adapted from reference. [74]

5.6.2) Ccp1 and Ccp1W191F consume H_2O_2 by different mechanisms

The rate of consumption of 10 M eq of H_2O_2 by Ccp1 and Ccp1W191F was previously compared in our lab using HRP/ABTS.[194] All H_2O_2 was consumed by Ccp1 within 5 min vs 20 min by CcpW191F,[194] suggesting that the two proteins consume the peroxide by different pathways.[194] Here SDS-PAGE reveals more H_2O_2-induced cross-linking of Ccp1 vs Ccp1W191F (Figure 5.4), which further supports different pathways of H_2O_2 decomposition by the two proteins. Direct evidence for this comes from the investigation of O_2 evolution. Ccp1 consumed 10 M eq of H_2O_2 without O_2 evolution[74] but under the same conditions, Ccp1W191F decomposed ~50 % of H_2O_2 by catalase-like activity (Section 5.5.7). In fact, all the experiments performed here to characterize H_2O_2-oxidized Ccp1W191F vs Ccp1 reveal that they are significantly different, which can be attributed to the different mechanisms they employ to consume H_2O_2.

5.7) Conclusions

Fermenting W191F cells have lower basal H_2O_2 levels and higher catalase T (Ctt1) activity than WT cells.[24] Fermenting W191F cells regulate more proteins, including Ctt1 and heat shock proteins, in response to H_2O_2 challenge (Chapter 4). These observations led us to investigate at the molecular level why Ccp1W191F is a better H_2O_2 sensing and signaling protein than WT Ccp1 in cells. We showed here that Ccp1W191F, which has negligible CCP activity,[10] exhibits only weak catalase activity that is unlikely to compete with other H_2O_2-metabolizing enzymes in cells. Thus, our results *in vitro* suggest that Ccp1W191F plays no direct enzymatic role in H_2O_2 regulation in cells. However, the properties of oxidized Ccp1W191F that enable it to perform amplified H_2O_2 sensing and signaling remain elusive. Further experiments, including the characterization of Ccp1W191F isolated from yeast cells, are needed to understand at the molecular level why this variant is a better H_2O_2 sensor.

5.8) Supplementary information

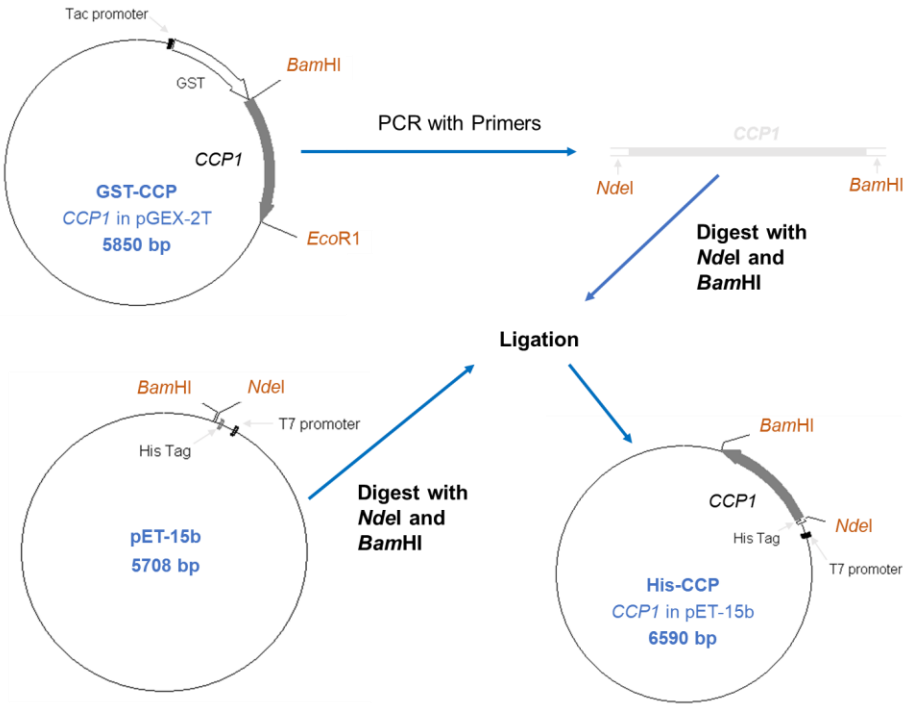

Figure S5.1. pHis-CCP and pHis-CCPW191F vector construction. The cDNA template for mature Ccp1 was excised from the EcoRI-BamHI sites of the pGEX 2T vector (GST-CCP; Iolie C. Bakas, MSc 1999, Concordia) and subcloned in our lab (by Dr. Heng Jiang, 2008) into the NdeI and BamHI sites of the pET15b vector to give pHis-CCP, which expresses N-terminally His_6-tagged mature Ccp1 (isoform 1) plus a thrombin cut site (see Section S5.8.1 below). Removal of the His_6 tag gives a construct of 297 residues with GSH plus M at position (1) of yeast Ccp1.[100]

The pHis-CCP(W191F) vector, with the cDNA for His_6-CCPW191F cloned into the NdeI and BamHI sites of pET15b, was prepared from pHis-CCP by TopGene Technologies (Montreal, QC). I transformed 5 μL of the purified pHis-CCP(W191F) vector into 100 μL of competent BL21(DE3) and BL21(DE3)pLysS *E. coli* cells using standard procedures (www.biodynamics.co.jp/images/prd_ds250/DS255ZipBLhp.pdf). Competent cells including DNA were kept on ice for 20 min, then, following heat-shock at 42 °C for 45 s, cells were immediately placed on ice for 2 min. The cells were added to 0.9 mL of SOC medium (20 g/L tryptone, 5 g/L yeast extract, 0.5 g/L NaCl, 0.186 g/L KCl, 2.4 g/L $MgSO_4$ anhydrous, and 4 g/L glucose) and incubated at 37°C for 1 h with shaking at 250 rpm. The transformed cells were spread on agar plates with 100 μg/mL ampicillin [BL21(DE3)] or 100 μg/ml ampicillin plus 34 μg/mL chloramphenicol [BL21(DE3)pLysS] since pLysS plasmid contains the chloramphenicol resistance marker. The plates were incubated at 37 °C overnight, then checked visually for isolated colonies, which were selected for protein expression as outlined in Section 5.4.5.

S5.8.1) Protein sequence of His_6-Ccp1W191F [a]

GSSHHHHHHSSGLVPRGSHMTPLVHVASVEKGRSYEDFQKVYNAIALKLR
EDDEYDNYIGYGPVLVRLAWH**I**SGTWDKHDNTGGSYGGTYRFKKEFNDPS
NAGLQNGFKFLEPIHKEFPWISSGDLFSLGGVTAVQEMQGPKIPWRCGRV
DTPEDTTPDNGRLPDADKDA**G**YVRTFFQRLNMNDREVVALMGAHALGKTH
LKNSGYEGP**F**GAANNVFTNEFYLNLLNEDWKLEKNDANNEQWDSKSGYMM
LPTDYSLIQD PKYLSIVKEY ANDQDKFFKDFSKAFEKLLE NGITFPKDAPSPFI
FKTLEE QGL.

[a] Mature yeast Ccp1 isoform 1 (**I**53, **G**152).[100] **M** was added at position -1 of the mature Ccp1 sequence. **His_6 tag** is in blue and **F191** is in red. Cleavage of the His_6 tag by thrombin between the undelined R and G residues gives a construct with **GSH**M at the N-terminus as shown in the following sequence:

GSHMTPLVHVASVEKGRSYEDFQKVYNAIALKLR
EDDEYDNYIGYGPVLVRLAWH**I**SGTWDKHDNTGGSYGGTYRFKKEFNDPS
NAGLQNGFKFLEPIHKEFPWISSGDLFSLGGVTAVQEMQGPKIPWRCGRV
DTPEDTTPDNGRLPDADKDA**G**YVRTFFQRLNMNDREVVALMGAHALGKTH
LKNSGYEGP**F**GAANNVFTNEFYLNLLNEDWKLEKNDANNEQWDSKSGYMM
LPTDYSLIQD PKYLSIVKEY ANDQDKFFKDFSKAFEKLLE NGITFPKDAPSPFI
FKTLEE QGL.

The above sequence of His_6-tag free Ccp1(W191F) has a theoretical mass of 33758.68 u as calculated using ExPASy (https://web.expasy.org/compute_pi/). The observed mass of Ccp1(W191F) (33,759; Figure 5.5E) agrees with the theoretical mass within the mass accuracy of the mass spectrometer (Figure 5.5).

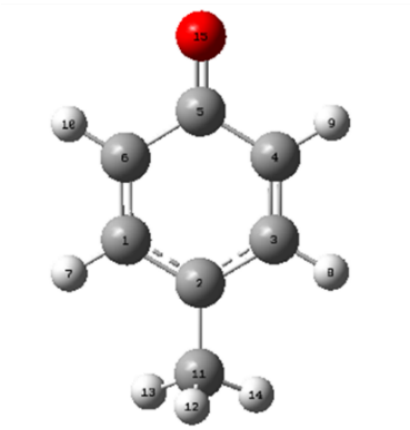

Mulliken atomic spin densities:

1	C	-0.138002
2	C	**0.377161**
3	C	-0.143212
4	C	**0.286837**
5	C	-0.047953
6	C	**0.273959**
7	H	0.004940
8	H	0.004991
9	H	-0.012725
10	H	-0.012158
11	C	-0.026828
12	H	0.024426
13	H	0.009486
14	H	0.003329
15	O	**0.395748**

Sum of Mulliken atomic spin densities = 1.00000

Figure S5.2. Calculation of spin density distribution in the tyrosyl radical. Using the p-cresyl (4-methylphenoxyl) radical as a model, the distribution of Mulliken atomic spin densities on the tyrosyl radical were calculated at the B3LYP/6-31+G(2d,2p) level with Gaussian09 software. Atoms 15, 2, 4, 6 show the highest spin density. The ortho carbons (atoms 4 and 6) are most likely to form stable spin adducts with carbon-centered spin traps such as DBNBS or MNP. Spin trapping at the para carbon (atom 2) will be inhibited by steric effects while trapping at the oxygen (atom 15) will result in an unstable spin adduct. The structure of p-cresyl was created by GaussView 05.

Chapter 6: General conclusions

Over the past 80 years, extensive research has been conducted on yeast Ccp1 as a model heme peroxidase. There is, however, little information on its physiological roles, which depend on its mature form in cells as well as its location. My doctoral research aimed to understand the physiological roles of Ccp1 through ratiometric fluorescence lifetime measurements and proteomics.

Heme insertion, a post-translation modification, is a key step in the maturation of a heme protein. Nevertheless, where and when heme insertion occurs in eukaryotic cells is unknown for most heme proteins. Free heme is insoluble and binds non-specifically to lipids and proteins and promotes oxidations of these biomolecules.[106] Thus, intracellular heme trafficking and heme insertion into target proteins must be tightly regulated. Heme biosynthesis is catalyzed by eight different enzymes, ending in the mitochondrial matrix. [23] Heme is transferred from mitochondria to other compartments via unknown pathways. Our lack of knowledge of heme trafficking is in part due to technical limitations in probing heme transfer between proteins and compartments *in vivo*.

Previous studies from our group suggest that the antioxidant functions of Ccp1 may include the recruitment of its heme for catalase A (Cta1) maturation.[24,26] Cta1 is an antioxidant enzyme that efficiently metabolizes H_2O_2 in yeast. Based on subcellular fractionation and biochemical data, our lab concluded previously that most of Ccp1 is heme-loaded and located in the mitochondria of 2-day respiring cells, whereas more than half of Ccp1 is extramitochondrial and has lost its heme in 7-day respiring cells and Cta1 activity has increased.[26] Accumulation of apoCcp1 outside of mitochondria in respiring yeast cells is at odds with holoCcp1 functioning as a mitochondrial peroxidase that removes the H_2O_2 formed during respiration.[113] However, we were concerned about possible artifactual repartitioning of apo- and holoCcp1 between compartments during subcellular fractionation. **Chapter 2** describes how my research provided a reliable method to track heme-loaded and heme-free forms of Ccp1 in live cells. Ccp1 was fused to GFP by a nine-residue linker (GRRIPGLIN), which was a fortuitous choice since shorter linkers can disrupt heme insertion,[37,38] and/or allow heme to fully quench GFP fluorescence such that the heme-loaded fusion would be invisible in cells.[36] Heme only partially quenches GFP fluorescence in our Ccp1-GFP probe so I could fully characterize heme-loaded and heme-free Ccp1-GFP photophysically to establish its suitability as a tool to track heme binding to Ccp1 in cells. My study reveals that ratiometric fluorescence lifetime measurements on Ccp1-GFP reliably quantify heme binding to Ccp1 *in vitro*.

Next, I tested the suitability of my Ccp1-GFP probe to track the heme status of Ccp1 *in vivo*. In **Chapter 3**, FLIM imaging reveals that holoCcp1-GFP is mitochondrial in fermenting yeast but apoCcp1-GFP is extramitochondrial in respiring yeast. These results confirm our lab's previous biochemical data on the distribution of native Ccp1 in subcellular fractions,[26] as well as our postulation that Ccp1 serves as a heme donor in respiring cells.[26] The heme binding of endogenous proteins in live cells had not been studied previously and our results lead us to hypothesize that apoCcp1 and the apoforms of other heme-binding proteins may have moonlighting functions in live cells. We also speculate by comparing the time-dependent fluorescence of Ccp1-GFP and Sod1-GFP that the percentage (~ 35%) of the GRRIPGLIN linker in a compact conformation remains relatively constant in GFP fusions. Hence, the value of a_1 (amplitude of τ_1, the quenched litetime) in a specific cellular location may be a quantitative readout of the fraction of a heme-protein-GFP fusion in its holoform.

Fermenting WT cells are more sensitive to challenge with exogenous H_2O_2 than W191F cells[24] although the latter possess no CCP activity. Thus, more robust H_2O_2 sensing/signaling is assumed to protect W191F cells rather than CCP activity so we aimed to uncover the impact of the W191F mutation in Ccp1 on the H_2O_2 stimulon in fermenting yeast. **Chapter 4** reveals that WT and W191F cells regulate 201 and 468 proteins, respectively, when challenged with a sublethal dose (0.4 mM) of H_2O_2. Cells adapt to H_2O_2 by upregulation of antioxidant enzymes, heat shock proteins, proteases, trehalose biosynthesis and NADPH production but repress protein and amino acid biosynthesis. Changes in the proteome are more persistent in W191F vs WT cells, which better protects the mutant strain against H_2O_2. The detailed information available from these studies highlights the power of combining LC-MS/MS, a reliable, sensitive and rapid technology, with suitably selected yeast mutants in unraveling the complexity of the H_2O_2 stimulon in eukaryotes.

Chapter 5 investigates *in vitro* at the molecular level why the W191F mutation in Ccp1 converts the protein into a more efficient H_2O_2 sensor protein. The oxidized forms of Ccp1 and Ccp1W191F were characterized following reaction with H_2O_2 in the absence of a reducing substrate such as Cyt c^{II}. Ccp1W191F, which has negligible CCP activity, exhibits weak catalase activity. The latter is not efficient enough to compete with other H_2O_2-metabolizing enzymes in cells so Ccp1W191F may function as a dedicated H_2O_2 sensing/signaling protein.

A Ccp1 homolog is not expressed in human cells, but these cells express vitally important heme peroxidases such as myeloperoxidase (expressed in a subtype of white blood cells),[202] eosinophil peroxidase (expressed in myeloid cells),[203] lactoperoxidase (found in mucosal glands),[204] and pseudoperoxidases such as hemoglobin, myoglobin, and cytoglobin (expressed

in tissues).[205] Elucidation of moonlighting roles (H_2O_2 sensing/signaling, heme donation, regulation of the H_2O_2 stimulon) for these enzymes might shed new light on heme-related pathologies such as heart disease,[108] cancer,[107] Alzheimer's disease,[109–111] and diabetes,[107] which are leading causes of death. Information on how the heme status of a given protein varies under normal physiological conditions is crucial in characterizing its role under pathological conditions and will inform drug design.

Chapter 7: Future work

My research has opened up numerous avenues for further investigation. For example, our proposed method for tracking the heme-loaded and heme-free forms of Ccp1 proved to be successful *in vitro* and *in vivo*. The FLIM results confirm that extramitochondrial apoCcp1 is present in 2- and 7-day cells. Previously, our lab reported that Ccp1 releases its heme and exits mitochondria while the catalase activity of peroxisomal/mitochondrial Cta1 increases. Tracking the heme status of Cta1 fused to GFP in fermenting and respiring yeast cells by FLIM would provide direct evidence for when and where Cta1 is heme loaded. We expect the percentage of holoCta1-GFP to increase with cell age whereas the opposite is reported here for holoCcp1-GFP. These results will provide critical information on how Ccp1's heme is recruited for Cta1. Another intriguing FLIM investigation would be the heme tracking of Ccp1W191F-GFP in live cells. Comparing the results with those in Chapter 3 on cells expressing Ccp1-GFP should provide deeper insights into Ccp1's role as a heme-based sensor protein.

My FLIM study confirmed that apoCcp1 exits respiring mitochondria, which our group has attributed to the protein's oxidation by respiration-derived H_2O_2.[26,206] Thus, I predict that exposure of *fermenting* cells to exogenous H_2O_2 also might trigger the exit of apoCcp1 and apoCcp1W191F from mitochondria, which could be filmed using epifluorescence microscopy on the Leica DMI6000 B microscope. Since only the apoproteins are expected to exit the mitochondria, this study also would indicate the time course of heme release from Ccp1W191F vs Ccp1, which is of interest given the higher resistance of W191F vs WT cells to H_2O_2 challenge.

The proteomics results in Chapter 4 revealed that *cytosolic* Ctt1 is upregulated 3-fold more in fermenting W191F cells compared to the WT strain on H_2O_2 challenge. The heme status of Ctt1 under these conditions is of interest and could be followed using FLIM of cells expressing Ctt1-GFP.

The poor viability of fermenting *ccp1*Δ cells following exposure to exogenous H_2O_2 could be explored using the same label-free proteomics approach outlined in Chapter 4. Are fewer proteins regulated on H_2O_2 challenge in the absence of Ccp1 sensing? Similarly, the H_2O_2 stimulon could be investigated in cells deleted for other antioxidant enzymes such as Cta1 to probe in more detail how the H_2O_2 stress response is coordinated.

The commonly used BY4741 strain of *S. cerevisiae* is deficient in Hap1, which is a regulator of heme protein synthesis. Thus, a comparison of the H_2O_2 stimulon in BY4741, YPH250, and W303 yeast strains would yield valuable insights at the proteome level into heme-based cellular adaptation to H_2O_2.

In my PhD research, I have focused on the H_2O_2 stimulon in yeast but the superoxide stimulon also is of interest. Superoxide could be generated in situ by adding xanthine oxidase/hypoxanthine to the culture medium,[207] and the superoxide stimulon in the BY4741, YPH250, and W303 strains examined by label-free proteomics and compared to the H_2O_2 stimulon.

Finally, in Chapter 5, the oxidized form of recombinant Ccp1W191F after reaction with H_2O_2 was partially characterized *in vitro*. A complementary future experiment would be to characterize Ccp1W191F isolated from respiring yeast cells as performed for WT Ccp1.[26,206]

References

(1) Yonetani, T.; Ray, G. S. Studies on Cytochrome c Peroxidase. I. Purification and Some Properties. *J. Biol. Chem.* **1965**, *240* (11), 4503–4508.

(2) Volkov, A. N.; Nicholls, P.; Worrall, J. A. The Complex of Cytochrome c and Cytochrome c Peroxidase: The End of the Road? *Biochim. Biophys. Acta* **2011**, *1807* (11), 1482–1503.

(3) Goodin, D. B.; Mauk, A. G.; Smith, M. Studies of the Radical Species in Compound ES of Cytochrome c Peroxidase Altered by Site-Directed Mutagenesis. *Proc. Natl. Acad. Sci.* **1986**, *83* (5), 1295–1299.

(4) Goodin, D. B.; Davidson, M. G.; Roe, J. A.; Mauk, A. G.; Smith, M. Amino Acid Substitutions at Tryptophan-51 of Cytochrome c Peroxidase: Effects on Coordination, Species Preference for Cytochrome c, and Electron Transfer. *Biochemistry* **1991**, *30* (20), 4953–4962.

(5) Teske, J. G.; Savenkova, M. I.; Mauro, J. M.; Erman, J. E.; Satterlee, J. D. Yeast Cytochrome c Peroxidase Expression in *Escherichia Coli* and Rapid Isolation of Various Highly Pure Holoenzymes. *Protein Expr. Purif.* **2000**, *19* (1), 139–147.

(6) Savenkova, M. I.; Satterlee, J. D.; Erman, J. E.; Siems, W. F.; Helms, G. L. Expression, Purification, Characterization, and NMR Studies of Highly Deuterated Recombinant Cytochrome *c* Peroxidase. *Biochemistry* **2001**, *40* (40), 12123–12131.

(7) Poulos, T. L.; Freer, S. T.; Alden, R. A.; Edwards, S. L.; Skogland, U.; Takio, K.; Eriksson, B.; Xuong, N.; Yonetani, T.; Kraut, J. The Crystal Structure of Cytochrome c Peroxidase. *J. Biol. Chem.* **1980**, *255* (2), 575–580.

(8) Poulos, T. L. Thirty Years of Heme Peroxidase Structural Biology. *Arch. Biochem. Biophys.* **2010**, *500* (1), 3–12.

(9) Beetlestone, J. The Oxidation of Cytochrome c by Cytochrome c Peroxidase. *Arch. Biochem. Biophys.* **1960**, *89* (1), 5–40.

(10) Miller, M. A.; Vitello, L.; Erman, J. E. Regulation of Interprotein Electron Transfer by Trp 191 of Cytochrome c Peroxidase. *Biochemistry* **1995**, *34* (37), 12048–12058.

(11) Bowman, S. E. J.; Bren, K. L. The Chemistry and Biochemistry of Heme c: Functional Bases for Covalent Attachment. *Nat. Prod. Rep.* **2008**, *25* (6), 1118-1130.

(12) Erman, J. E.; Vitello, L. B. Yeast Cytochrome c Peroxidase: Mechanistic Studies via Protein Engineering. *Biochim. Biophys. Acta BBA - Protein Struct. Mol. Enzymol.* **2002**, *1597* (2), 193–220.

(13) Barrows, T. P.; Poulos, T. L. Role of Electrostatics and Salt Bridges in Stabilizing the Compound I Radical in Ascorbate Peroxidase. *Biochemistry* **2005**, *44* (43), 14062–14068.

(14) Pipirou, Z.; Guallar, V.; Basran, J.; Metcalfe, C. L.; Murphy, E. J.; Bottrill, A. R.; Mistry, S. C.; Raven, E. L. Peroxide-Dependent Formation of a Covalent Link between Trp51 and the Heme in Cytochrome c Peroxidase. *Biochemistry* **2009**, *48* (16), 3593–3599.

(15) Arciero, D. M.; Hooper, A. B. A Di-Heme Cytochrome c Peroxidase from Nitrosomonas Europaea Catalytically Active in Both the Oxidized and Half-Reduced States. *J. Biol. Chem.* **1994**, *269* (16), 11878–11886.

(16) Barrows, T. P.; Bhaskar, B.; Poulos, T. L. Electrostatic Control of the Tryptophan Radical in Cytochrome *c* Peroxidase. *Biochemistry* **2004**, *43* (27), 8826–8834.

(17) Vlasova, I. Peroxidase Activity of Human Hemoproteins: Keeping the Fire under Control. *Molecules* **2018**, *23* (10), 2561-2603.

(18) Kaput, J.; Goltz, S.; Blobel, G. Nucleotide Sequence of the Yeast Nuclear Gene for Cytochrome c Peroxidase Precursor. Functional Implications of the Pre Sequence for Protein Transport into Mitochondria. *J. Biol. Chem.* **1982**, *257* (24), 15054–15058.

(19) Suppanz, I. E.; Wurm, C. A.; Wenzel, D.; Jakobs, S. The M-AAA Protease Processes Cytochrome c Peroxidase Preferentially at the Inner Boundary Membrane of Mitochondria. *Mol. Biol. Cell* **2009**, *20* (2), 572–580.

(20) Michaelis, G.; Esser, K.; Tursun, B.; Stohn, J. P.; Hanson, S.; Pratje, E. Mitochondrial Signal Peptidases of Yeast: The Rhomboid Peptidase Pcp1 and Its Substrate Cytochrome C Peroxidase. *Gene* **2005**, *354* (18), 58–63.

(21) Djavadi-Ohaniance, L.; Rudin, Y.; Schatz, G. Identification of Enzymically Inactive Apocytochrome c Peroxidase in Anaerobically Grown *Saccharomyces Cerevisiae*. *J. Biol. Chem.* **1978**, *253* (12), 4402–4407.

(22) Sels, A. A.; Cocriamont, C. Induced Conversion of a Protein Precursor into Cytochrome C Peroxidase during Adaptation of Yeast to Oxygen. *Biochem. Biophys. Res. Commun.* **1968**, *32* (2), 192–198.

(23) Hoffman, M.; Góra, M.; Rytka, J. Identification of Rate-Limiting Steps in Yeast Heme Biosynthesis. *Biochem. Biophys. Res. Commun.* **2003**, *310* (4), 1247–1253.

(24) Martins, D.; Kathiresan, M.; English, A. M. Cytochrome c Peroxidase Is a Mitochondrial Heme-Based H_2O_2 Sensor That Modulates Antioxidant Defense. *Free Radic. Biol. Med.* **2013**, *65*, 541–551.

(25) Charizanis, C.; Juhnke, H.; Krems, B.; Entian, K. D. The Oxidative Stress Response Mediated via Pos9/Skn7 Is Negatively Regulated by the Ras/PKA Pathway in *Saccharomyces Cerevisiae*. *Mol. Gen. Genet. MGG* **1999**, *261* (4–5), 740–752.

(26) Kathiresan, M.; Martins, D.; English, A. M. Respiration Triggers Heme Transfer from Cytochrome c Peroxidase to Catalase in Yeast Mitochondria. *Proc. Natl. Acad. Sci. U. S. A.* **2014**, *111* (49), 17468–17473.

(27) Huh, W. K.; Falvo, J. V.; Gerke, L. C.; Carroll, A. S.; Howson, R. W.; Weissman, J. S.; O'Shea, E. K. Global Analysis of Protein Localization in Budding Yeast. *Nature* **2003**, *425* (6959), 686–691.

(28) Kneen, M.; Farinas, J.; Li, Y.; Verkman, A. S. Green Fluorescent Protein as a Noninvasive Intracellular PH Indicator. *Biophys. J.* **1998**, *74* (3), 1591–1599.

(29) Jayaraman, S.; Haggie, P.; Wachter, R. M.; Remington, S. J.; Verkman, A. S. Mechanism and Cellular Applications of a Green Fluorescent Protein-Based Halide Sensor. *J. Biol. Chem.* **2000**, *275* (9), 6047–6050.

(30) Wachter, R. M.; Yarbrough, D.; Kallio, K.; Remington, S. J. Crystallographic and Energetic Analysis of Binding of Selected Anions to the Yellow Variants of Green Fluorescent Protein. *J. Mol. Biol.* **2000**, *301* (1), 157–171.

(31) Lakowicz, J. R. Quenching of Fluorescence. In Principles of fluorescence spectroscopy; Springer-Verlag New York Inc.: New York, NY, United States, 2007; pp 308–309.

(32) Miyawaki, A.; Llopis, J.; Heim, R.; McCaffery, J. M.; Adams, J. A.; Ikura, M.; Tsien, R. Y. Fluorescent Indicators for Ca^{2+} Based on Green Fluorescent Proteins and Calmodulin. *Nature* **1997**, *388* (6645), 882–887.

(33) Persechini, A.; Lynch, J. A.; Romoser, V. A. Novel Fluorescent Indicator Proteins for Monitoring Free Intracellular Ca2+. *Cell Calcium* **1997**, *22* (3), 209–216.

(34) Prachayasittikul, V.; Isarankura Na Ayudhya, C. Construction of a Chimeric Histidine6-Green Fluorescent Protein: Role of Metal on Fluorescent Characteristic. *Thammasaltn T J ScT Ech* **2001**, *5* (1), 61–68.

(35) Richmond, T. A.; Takahashi, T. T.; Shimkhada, R.; Bernsdorf, J. Engineered Metal Binding Sites on Green Fluorescence Protein. *Biochem. Biophys. Res. Commun.* **2000**, *268* (2), 462–465.

(36) Arpino, J. A.; Czapinska, H.; Piasecka, A.; Edwards, W. R.; Barker, P.; Gajda, M. J.; Bochtler, M.; Jones, D. D. Structural Basis for Efficient Chromophore Communication and Energy Transfer in a Constructed Didomain Protein Scaffold. *J. Am. Chem. Soc.* **2012**, *134* (33), 13632–13640.

(37) Takeda, S.; Kamiya, N.; Arai, R.; Nagamune, T. Design of an Artificial Light-Harvesting Unit by Protein Engineering: Cytochrome B562–Green Fluorescent Protein Chimera. *Biochemi Biophys. Res Com* **2001**, *289* (1), 299–304.

(38) Takeda, S.; Kamiya, N.; Nagamune, T. A Novel Protein-Based Heme Sensor Consisting of Green Fluorescent Protein and Apocytochrome b(562). *Anal. Biochem.* **2003**, *317* (1), 116–119.

(39) Yantsevich, A. V.; Harnostai, I. N.; Lukashevich, O. P.; Gilep, A. A.; Usanov, S. A. Engineering, Expression, Purification, and Physicochemical Characterization of a Chimeric Protein, Full-Length Cytochrome b(5)-Green Fluorescence Protein (HMWb5--EGFP). *Biochemistry(Moscow)* **2007**, *72* (1), 77–83.

(40) Hanna, D. A.; Harvey, R. M.; Martinez-Guzman, O.; Yuan, X.; Chandrasekharan, B.; Raju, G.; Outten, F. W.; Hamza, I.; Reddi, A. R. Heme Dynamics and Trafficking Factors Revealed by Genetically Encoded Fluorescent Heme Sensors. *Proc. Natl. Acad. Sci. U. S. A.* **2016**, *113* (27), 7539–7544.

(41) Song, Y.; Yang, M.; Wegner, S. V.; Zhao, J.; Zhu, R.; Wu, Y.; He, C.; Chen, P. R. A Genetically Encoded FRET Sensor for Intracellular Heme. *ACS Chem. Biol.* **2015**, *10* (7), 1610–1615.

(42) Yuan, X.; Rietzschel, N.; Kwon, H.; Walter Nuno, A. B.; Hanna, D. A.; Phillips, J. D.; Raven, E. L.; Reddi, A. R.; Hamza, I. Regulation of Intracellular Heme Trafficking Revealed by Subcellular Reporters. *Proc. Natl. Acad. Sci. U. S. A.* **2016**, *113* (35), E5144-52.

(43) Abshire, J. R.; Rowlands, C. J.; Ganesan, S. M.; So, P. T. C.; Niles, J. C. Quantification of Labile Heme in Live Malaria Parasites Using a Genetically Encoded Biosensor. *Proc. Natl. Acad. Sci.* **2017**, *114* (11), E2068–E2076.

(44) Charizanis, C.; Juhnke, H.; Krems, B.; Entian, K.-D. The Mitochondrial Cytochrome c Peroxidase Ccp1 of Saccharomyces Cerevisiae Is Involved in Conveying an Oxidative Stress Signal to the Transcription Factor Pos9 (Skn7). *Mol. Gen. Genet. MGG* **1999**, *262* (3), 437–447.

(45) Wallrabe, H.; Periasamy, A. Imaging Protein Molecules Using FRET and FLIM Microscopy. *Curr. Opin. Biotechnol.* **2005**, *16* (1), 19–27.

(46) Galdieri, L.; Mehrotra, S.; Yu, S.; Vancura, A. Transcriptional Regulation in Yeast during Diauxic Shift and Stationary Phase. *OMICS J. Integr. Biol.* **2010**, *14* (6), 629–638.

(47) Azzi, A. Oxidative Stress: A Dead End or a Laboratory Hypothesis? *Biochem. Biophys. Res. Commun.* **2007**, *362* (2), 230–232.

(48) Harman, D. Aging: A Theory Based on Free Radical and Radiation Chemistry. *J. Gerontol.* **1956**, *11* (3), 298–300.

(49) Berlett, B. S.; Stadtman, E. R. Protein Oxidation in Aging, Disease, and Oxidative Stress. *J. Biol. Chem.* **1997**, *272* (33), 20313–20316.

(50) Wells, P. G.; McCallum, G. P.; Chen, C. S.; Henderson, J. T.; Lee, C. J.; Perstin, J.; Preston, T. J.; Wiley, M. J.; Wong, A. W. Oxidative Stress in Developmental Origins of Disease: Teratogenesis, Neurodevelopmental Deficits, and Cancer. *Toxicol. Sci. Off. J. Soc. Toxicol.* **2009**, *108* (1), 4–18.

(51) Mulligan, V. K.; Chakrabartty, A. Protein Misfolding in the Late-Onset Neurodegenerative Diseases: Common Themes and the Unique Case of Amyotrophic Lateral Sclerosis. *Proteins* **2013**, *81* (8), 1285–1303.

(52) Ogusucu, R.; Rettori, D.; Netto, L. E.; Augusto, O. Superoxide Dismutase 1-Mediated Production of Ethanol- and DNA-Derived Radicals in Yeasts Challenged with Hydrogen Peroxide: Molecular Insights into the Genome Instability of Peroxiredoxin-Null Strains. *J. Biol. Chem.* **2009**, *284* (9), 5546–5556.

(53) Romano, A. D.; Serviddio, G.; de Matthaeis, A.; Bellanti, F.; Vendemiale, G. Oxidative Stress and Aging. *J. Nephrol.* **2010**, *23 Suppl 15*, S29-36.

(54) Klaunig, J. E.; Kamendulis, L. M.; Hocevar, B. A. Oxidative Stress and Oxidative Damage in Carcinogenesis. *Toxicol. Pathol.* **2010**, *38* (1), 96–109.

(55) Giacco, F.; Brownlee, M. Oxidative Stress and Diabetic Complications. *Circ. Res.* **2010**, *107* (9), 1058–1070.

(56) Switala, J.; Loewen, P. C. Diversity of Properties among Catalases. *Arch. Biochem. Biophys.* **2002**, *401* (2), 145–154.

(57) Choen, G.; Rapatz, W.; Ruis, H. Sequence of the *Saccharomyces Cerevisiae* CATI Gene and Amino Acid Sequence of Catalase A Derived from It. *Eur. J. Biochem.* **1988**, *176* (1), 159–163.

(58) Hartig, A.; Ruis, H. Nucleotide Sequence of the *Saccharomyces Cerevisiae* CTT1 Gene and Deduced Amino-Acid Sequence of Yeast Catalase T. *Eur. J. Biochem.* **1986**, *160* (3), 487–490.

(59) Inoue, Y.; Matsuda, T.; Sugiyama, K.; Izawa, S.; Kimura, A. Genetic Analysis of Glutathione Peroxidase in Oxidative Stress Response of *Saccharomyces Cerevisiae*. *J. Biol. Chem.* **1999**, *274* (38), 27002–27009.

(60) Munhoz, D. C.; Netto, L. E. S. Cytosolic Thioredoxin Peroxidase I and II Are Important Defenses of Yeast against Organic Hydroperoxide Insult: Catalases and Peroxiredoxins

Cooperate in the Decomposition of H_2O_2 by Yeast. *J. Biol. Chem.* **2004**, *279* (34), 35219–35227.

(61) Rhee, S. G. Cell Signaling: H_2O_2, a Necessary Evil for Cell Signaling. *Science* **2006**, *312* (5782), 1882–1883.

(62) Rhee, S. G.; Woo, H. A.; Kil, I. S.; Bae, S. H. Peroxiredoxin Functions as a Peroxidase and a Regulator and Sensor of Local Peroxides. *J. Biol. Chem.* **2012**, *287* (7), 4403–4410.

(63) Park, S. G.; Cha, M.-K.; Jeong, W.; Kim, I.-H. Distinct Physiological Functions of Thiol Peroxidase Isoenzymes in *Saccharomyces Cerevisiae*. *J. Biol. Chem.* **2000**, *275* (8), 5723–5732.

(64) Ristow, M.; Zarse, K. How Increased Oxidative Stress Promotes Longevity and Metabolic Health: The Concept of Mitochondrial Hormesis (Mitohormesis). *Exp. Gerontol.* **2010**, *45* (6), 410–418.

(65) Martins, D.; Titorenko, V. I.; English, A. M. Cells with Impaired Mitochondrial H2O2 Sensing Generate Less OH Radicals and Live Longer. *Antioxid. Redox Signal.* **2014**, *21* (10), 1490–1503.

(66) Godon, C.; Lagniel, G.; Lee, J.; Buhler, J. M.; Kieffer, S.; Perrot, M.; Boucherie, H.; Toledano, M. B.; Labarre, J. The H_2O_2 Stimulon in *Saccharomyces Cerevisiae*. *J. Biol. Chem.* **1998**, *273* (35), 22480–22489.

(67) Paulsen, C. E.; Carroll, K. S. Chemical Dissection of an Essential Redox Switch in Yeast. *Chem. Biol.* **2009**, *16* (2), 217–225.

(68) Krems, B.; Charizanis, C.; Entian, K.-D. The Response Regulator-like Protein Pos9/Skn7 Of *Saccharomyces Cerevisiae* Is Involved in Oxidative Stress Resistance. *Curr. Genet.* **1996**, *29* (4), 327–334.

(69) Lee, J.; Godon, C.; Lagniel, G.; Spector, D.; Garin, J.; Labarre, J.; Toledano, M. B. Yap1 and Skn7 Control Two Specialized Oxidative Stress Response Regulons in Yeast. *J. Biol. Chem.* **1999**, *274* (23), 16040–16046.

(70) Wasinger, V. C.; Cordwell, S. J.; Cerpa-Poljak, A.; Yan, J. X.; Gooley, A. A.; Wilkins, M. R.; Duncan, M. W.; Harris, R.; Williams, K. L.; Humphery-Smith, I. Progress with Gene-Product Mapping of the Mollicutes:Mycoplasma Genitalium. *Electrophoresis* **1995**, *16* (1), 1090–1094.

(71) Godovac-Zimmermann, J.; Brown, L. R. Perspectives for Mass Spectrometry and Functional Proteomics. *Mass Spectrom. Rev.* **2001**, *20* (1), 1–57.

(72) Pappireddi, N.; Martin, L.; Wühr, M. A Review on Quantitative Multiplexed Proteomics. *ChemBioChem* **2019**, *20* (10), 1210–1224.

(73) Hu, A.; Noble, W. S.; Wolf-Yadlin, A. Technical Advances in Proteomics: New Developments in Data-Independent Acquisition. *F1000Research.* **2016**, *5*, 419.

(74) Kathiresan, M.; English, A. M. LC-MS/MS Suggests That Hole Hopping in Cytochrome c Peroxidase Protects Its Heme from Oxidative Modification by Excess H_2O_2. *Chem. Sci.* **2017**, *8* (2), 1152–1162.

(75) Dhandayuthapani, S.; Via, L. E.; Thomas, C. A.; Horowitz, P. M.; Deretic, D.; Deretic, V. Green Fluorescent Protein as a Marker for Gene Expression and Cell Biology of Mycobacterial Interactions with Macrophages. *Mol. Microbiol.* **1995**, *17* (5), 901–912.

(76) Heim, R.; Tsien, R. Y. Engineering Green Fluorescent Protein for Improved Brightness, Longer Wavelengths and Fluorescence Resonance Energy Transfer. *Curr. Biol. CB* **1996**, *6* (2), 178–182.

(77) Wurm, C. A.; Jakobs, S. Differential Protein Distributions Define Two Sub-Compartments of the Mitochondrial Inner Membrane in Yeast. *FEBS Lett.* **2006**, *580* (24), 5628–5634.

(78) Tsien, R. Y. The Green Fluorescent Protein. *Annu. Rev. Biochem.* **1998**, *67*, 509–544.

(79) Patterson, G. H.; Knobel, S. M.; Sharif, W. D.; Kain, S. R.; Piston, D. W. Use of the Green Fluorescent Protein and Its Mutants in Quantitative Fluorescence Microscopy. *Biophys. J.* **1997**, *73* (5), 2782–2790.

(80) Heim, R.; Cubitt, A. B.; Tsien, R. Y. Improved Green Fluorescence. *Nature* **1995**, *373* (6516), 663–664.

(81) Yamamoto, S. Purification and Assay of PGH Synthase from Bovine Seminal Vesicles. *Methods Enzymol.* **1982**, *86*, 55–60.

(82) Godin, R.; Liu, H. W.; Cosa, G. Ambient Condition Oxidation in Individual Liposomes Observed at the Single Molecule Level. *Chem Sci* **2014**, *5* (6), 2525–2529.

(83) Owens, C. P.; Du, J.; Dawson, J. H.; Goulding, C. W. Characterization of Heme Ligation Properties of Rv0203, a Secreted Heme Binding Protein Involved in Mycobacterium Tuberculosis Heme Uptake. *Biochemistry* **2012**, *51* (7), 1518–1531.

(84) Yonetani, T. Studies on Cytochrome c Peroxidase. X. Crystalline Apo-and Reconstituted Holoenzymes. *J. Biol. Chem.* **1967**, *242* (21), 5008–5013.

(85) Vitello, L. B.; Huang, M.; Erman, J. E. PH-Dependent Spectral and Kinetic Properties of Cytochrome c Peroxidase: Comparison of Freshly Isolated and Stored Enzyme. *Biochemistry* **1990**, *29* (18), 4283–4288.

(86) Yonetani, T.; Anni, H. Yeast Cytochrome c Peroxidase. Coordination and Spin States of Heme Prosthetic Group. *J. Biol. Chem.* **1987**, *262* (20), 9547–9554.

(87) Volkov, A. N.; Wohlkonig, A.; Soror, S. H.; van Nuland, N. A. Expression, Purification, Characterization, and Solution Nuclear Magnetic Resonance Study of Highly Deuterated Yeast Cytochrome C Peroxidase with Enhanced Solubility. *Biochemistry* **2013**, *52* (13), 2165–2175.

(88) Elsliger, M. A.; Wachter, R. M.; Hanson, G. T.; Kallio, K.; Remington, S. J. Structural and Spectral Response of Green Fluorescent Protein Variants to Changes in pH. *Biochemistry* **1999**, *38* (17), 5296–5301.

(89) Swaminathan, R.; Hoang, C. P.; Verkman, A. S. Photobleaching Recovery and Anisotropy Decay of Green Fluorescent Protein GFP-S65T in Solution and Cells: Cytoplasmic Viscosity Probed by Green Fluorescent Protein Translational and Rotational Diffusion. *Biophys. J.* **1997**, *72* (4), 1900–1907.

(90) Cosa, G.; Focsaneanu, K. S.; McLean, J. R. N.; Scaiano, J. C. Direct Determination of Single-to-Double Stranded DNA Ratio in Solutionapplying Time-Resolved Fluorescence Measurements of Dye–DNA Complexes. *Chem Commun* **2000**, *1*(3), 689–690.

(91) Cosa, G.; Vinette, A. L.; McLean, J. R.; Scaiano, J. C. DNA Damage Detection Technique Applying Time-Resolved Fluorescence Measurements. *Anal. Chem.* **2002**, *74* (24), 6163–6169.

(92) Vasicova, P.; Lejskova, R.; Malcova, I.; Hasek, J. The Stationary-Phase Cells of *Saccharomyces Cerevisiae* Display Dynamic Actin Filaments Required for Processes Extending Chronological Life Span. *Mol. Cell. Biol.* **2015**, *35* (22), 3892–3908.

(93) Chen, X.; Zaro, J. L.; Shen, W. C. Fusion Protein Linkers: Property, Design and Functionality. *Adv. Drug Deliv. Rev.* **2013**, *65* (10), 1357–1369.

(94) Chiang, C. F.; Okou, D. T.; Griffin, T. B.; Verret, C. R.; Williams, M. N. Green Fluorescent Protein Rendered Susceptible to Proteolysis: Positions for Protease-Sensitive Insertions. *Arch. Biochem. Biophys.* **2001**, *394* (2), 229–235.

(95) Reid, B. G.; Flynn, G. C. Chromophore Formation in Green Fluorescent Protein. *Biochemistry* **1997**, *36* (22), 6786–6791.

(96) Zhang, L.; Patel, H. N.; Lappe, J. W.; Wachter, R. M. Reaction Progress of Chromophore Biogenesis in Green Fluorescent Protein. *J. Am. Chem. Soc.* **2006**, *128* (14), 4766–4772.

(97) Heim, R.; Prasher, D. C.; Tsien, R. Y. Wavelength Mutations and Posttranslational Autoxidation of Green Fluorescent Protein. *Proc. Natl. Acad. Sci. U. S. A.* **1994**, *91* (26), 12501–12504.

(98) Hink, M. A.; Visser, N. V.; Borst, J. W.; Hoek, A. V.; Visser, A. J. W. G. Practical Use of Corrected Fluorescence Excitation and Emission Spectra of Fluorescent Proteins in Förster Resonance Energy Transfer (FRET) Studies. *J Fluoresc.* **2003**, *13*, 185–188.

(99) Liu, Y.; Kim, H. R.; Heikal, A. A. Structural Basis of Fluorescence Fluctuation Dynamics of Green Fluorescent Proteins in Acidic Environments. *J. Phys. Chem.* **2006**, *110* (47), 24138–24146.

(100) Jiang, H.; English, A. M. Phenotypic Analysis of the Ccp1Delta and Ccp1Delta-Ccp1W191F Mutant Strains of Saccharomyces Cerevisiae Indicates That Cytochrome c Peroxidase Functions in Oxidative-Stress Signaling. *J. Inorg. Biochem.* **2006**, *100* (12), 1996–2008.

(101) Ponka, P. Cell Biology of Heme. *Am. J. Med. Sci.* **1999**, *318* (4), 241–256.

(102) Yin, L.; Wu, N.; Curtin, J. C.; Qatanani, M.; Szwergold, N. R.; Reid, R. A.; Waitt, G. M.; Parks, D. J.; Pearce, K. H.; Wisely, G. B.; Lazar, M. A. Rev-Erbalpha, a Heme Sensor That Coordinates Metabolic and Circadian Pathways. *Science* **2007**, *318* (5857), 1786–1789.

(103) Tsiftsoglou, A. S.; Tsamadou, A. I.; Papadopoulou, L. C. Heme as Key Regulator of Major Mammalian Cellular Functions: Molecular, Cellular, and Pharmacological Aspects. *Pharmacol. Ther.* **2006**, *111* (2), 327–345.

(104) Hamza, I.; Dailey, H. A. One Ring to Rule Them All: Trafficking of Heme and Heme Synthesis Intermediates in the Metazoans. *Biochim. Biophys. Acta* **2012**, *1823* (9), 1617–1632.

(105) Faller, M.; Matsunaga, M.; Yin, S.; Loo, J. A.; Guo, F. Heme Is Involved in MicroRNA Processing. *Nat. Struct. Mol. Biol.* **2007**, *14* (1), 23–29.

(106) Vincent, S. H.; Grady, R. W.; Shaklai, N.; Snider, J. M.; Muller-Eberhard, U. The Influence of Heme-Binding Proteins in Heme-Catalyzed Oxidations. *Arch. Biochem. Biophys.* **1988**, *265* (2), 539–550.

(107) Shen, J.; Sheng, X.; Chang, Z.; Wu, Q.; Wang, S.; Xuan, Z.; Li, D.; Wu, Y.; Shang, Y.; Kong, X.; Yu, L.; Li, L.; Ruan, K.; Hu, H.; Huang, Y.; Hui, L.; Xie, D.; Wang, F.; Hu, R. Iron Metabolism Regulates P53 Signaling through Direct Heme-P53 Interaction and Modulation of P53 Localization, Stability, and Function. *Cell Rep.* **2014**, *7* (1), 180–193.

(108) Wu, M. L.; Ho, Y. C.; Lin, C. Y.; Yet, S. F. Heme Oxygenase-1 in Inflammation and Cardiovascular Disease. *Am. J. Cardiovasc. Dis.* **2011**, *1* (2), 150–158.

(109) Schipper, H. M.; Song, W.; Zukor, H.; Hascalovici, J. R.; Zeligman, D. Heme Oxygenase-1 and Neurodegeneration: Expanding Frontiers of Engagement. *J. Neurochem.* **2009**, *110* (2), 469–485.

(110) Atamna, H.; Frey, W. H., 2nd. A Role for Heme in Alzheimer's Disease: Heme Binds Amyloid Beta and Has Altered Metabolism. *Proc. Natl. Acad. Sci. U. S. A.* **2004**, *101* (30), 11153–11158.

(111) Atamna, H.; Killilea, D. W.; Killilea, A. N.; Ames, B. N. Heme Deficiency May Be a Factor in the Mitochondrial and Neuronal Decay of Aging. *Proc. Natl. Acad. Sci. U. S. A.* **2002**, *99* (23), 14807–14812.

(112) Feher, J. J. *Quantitative Human Physiology: An Introduction*, Second Edition.; Academic Press series in biomedical engineering; Elsevier/AP, Amsterdam ; Boston, 2017.

(113) Perrone, G. G.; Tan, S. X.; Dawes, I. W. Reactive Oxygen Species and Yeast Apoptosis. *Biochim. Biophys. Acta* **2008**, *1783* (7), 1354–1368.

(114) Dastpeyman, S.; Godin, R.; Cosa, G.; English, A. M. Quantifying Heme−Protein Maturation from Ratiometric Fluorescence Lifetime Measurements on the Single Fluorophore in Its GFP Fusion. *J Phys Chem A* **2020**, *124* (4), 746–754.

(115) Hanna, D. A.; Martinez-Guzman, O.; Reddi, A. R. Heme Gazing: Illuminating Eukaryotic Heme Trafficking, Dynamics, and Signaling with Fluorescent Heme Sensors. *Biochemistry* **2017**, *56* (13), 1815–1823.

(116) Kawamata, H.; Manfredi, G. Import, Maturation, and Function of SOD1 and Its Copper Chaperone CCS in the Mitochondrial Intermembrane Space. *Antioxid. Redox Signal.* **2010**, *13* (9), 1375–1384.

(117) Sturtz, L. A.; Diekert, K.; Jensen, L. T.; Lill, R.; Culotta, V. C. A Fraction of Yeast Cu,Zn-Superoxide Dismutase and Its Metallochaperone, CCS, Localize to the Intermembrane Space of Mitochondria. A Physiological Role for Sod1 in Guarding against Mitochondrial Oxidative Damage. *J. Biol. Chem.* **2001**, *276* (41), 38084–38089.

(118) Tregidgo, C.; Levitt, J. A.; Suhling, K. Effect of Refractive Index on the Fluorescence Lifetime of Green Fluorescent Protein. *J. Biomed. Opt.* **2008**, *13* (3), 031218.

(119) Treanor, B.; Lanigan, P. M.; Suhling, K.; Schreiber, T.; Munro, I.; Neil, M. A.; Phillips, D.; Davis, D. M.; French, P. M. Imaging Fluorescence Lifetime Heterogeneity Applied to GFP-Tagged MHC Protein at an Immunological Synapse. *J. Microsc.* **2005**, *217* (Pt 1), 36–43.

(120) van Manen, H. J.; Verkuijlen, P.; Wittendorp, P.; Subramaniam, V.; van den Berg, T. K.; Roos, D.; Otto, C. Refractive Index Sensing of Green Fluorescent Proteins in Living Cells Using Fluorescence Lifetime Imaging Microscopy. *Biophys. J.* **2008**, *94* (8), L67-L69.

(121) Hotzer, B.; Ivanov, R.; Altmeier, S.; Kappl, R.; Jung, G. Determination of Copper(II) Ion Concentration by Lifetime Measurements of Green Fluorescent Protein. *J. Fluoresc.* **2011**, *21* (6), 2143–2153.

(122) Petrova, V. Y.; Drescher, D.; Kujumdzieva, A. V.; Schmitt, M. J. Dual Targeting of Yeast Catalase A to Peroxisomes and Mitochondria. *Biochem. J.* **2004**, *380* (Pt 2), 393–400.

(123) Zimniak, P.; Hartter, E.; Woloszczuk, W.; Ruis, H. Catalase Biosynthesis in Yeast: Formation of Catalase A and Catalase T during Oxygen Adaptation of Saccharomyces Cerevisiae. *Eur. J. Biochem.* **1976**, *71* (2), 393–398.

(124) Kaput, J.; Brandriss, M. C.; Prussak-Wieckowska, T. *In Vitro* Import of Cytochrome c Peroxidase into the Intermembrane Space: Release of the Processed Form by Intact Mitochondria. *J. Cell Biol.* **1989**, *109* (1), 101–112.

(125) Tsaprailis, G.; Chan, D. W.; English, A. M. Conformational States in Denaturants of Cytochrome c and Horseradish Peroxidases Examined by Fluorescence and Circular Dichroism. *Biochemistry* **1998**, *37* (7), 2004–2016.

(126) Fetherolf, M. M.; Boyd, S. D.; Taylor, A. B.; Kim, H. J.; Wohlschlegel, J. A.; Blackburn, N. J.; Hart, P. J.; Winge, D. R.; Winkler, D. D. Copper-Zinc Superoxide Dismutase Is Activated through a Sulfenic Acid Intermediate at a Copper Ion Entry Site. *J. Biol. Chem.* **2017**, *292* (29), 12025–12040.

(127) O'Doherty, P. J.; Khan, A.; Johnson, A. J.; Rogers, P. J.; Bailey, T. D.; Wu, M. J. Proteomic Response to Linoleic Acid Hydroperoxide in *Saccharomyces Cerevisiae*. *FEMS Yeast Res.* **2017**, *17* (3), 1–11.

(128) Merhej, J.; Delaveau, T.; Guitard, J.; Palancade, B.; Hennequin, C.; Garcia, M.; Lelandais, G.; Devaux, F. Yap7 Is a Transcriptional Repressor of Nitric Oxide Oxidase in Yeasts, Which Arose from Neofunctionalization after Whole Genome Duplication. *Mol. Microbiol.* **2015**, *96* (5), 951–972.

(129) Leger, T.; Garcia, C.; Ounissi, M.; Lelandais, G.; Camadro, J. M. The Metacaspase (Mca1p) Has a Dual Role in Farnesol-Induced Apoptosis in Candida Albicans. *Mol. Cell. Proteomics MCP* **2015**, *14* (1), 93–108.

(130) Leger, T.; Garcia, C.; Collomb, L.; Camadro, J. M. A Simple Light Isotope Metabolic Labeling (SLIM-Labeling) Strategy: A Powerful Tool to Address the Dynamics of Proteome Variations In Vivo. *Mol. Cell. Proteomics MCP* **2017**, *16* (11), 2017–2031.

(131) Lelandais, G.; Denecker, T.; Garcia, C.; Danila, N.; Leger, T.; Camadro, J. M. Label-Free Quantitative Proteomics in Candida Yeast Species: Technical and Biological Replicates to Assess Data Reproducibility. *BMC Res. Notes* **2019**, *12* (1), 470–473.

(132) Léger, T.; Garcia, C.; Videlier, M.; Camadro, J.-M. Label-Free Quantitative Proteomics in Yeast. In *Yeast Functional Genomics*; Devaux, F., Ed.; Methods in Molecular Biology; Springer New York: New York, NY, 2016; Vol. 1361, 289–307.

(133) Usaite, R.; Wohlschlegel, J.; Venable, J. D.; Park, S. K.; Nielsen, J.; Olsson, L.; Yates III, J. R. Characterization of Global Yeast Quantitative Proteome Data Generated from the Wild-Type and Glucose Repression *Saccharomyces Cerevisiae* Strains: The Comparison of Two Quantitative Methods. *J. Proteome Res.* **2008**, *7* (1), 266–275.

(134) Ito, H.; Fukuda, Y.; Murata, K.; Kimura, A. Transformation of Intact Yeast Cells Treated with Alkali Cations. *J. Bacteriol.* **1983**, *153* (1), 163–168.

(135) Sikorski, R. S.; Boeke, J. D. *In Vitro* Mutagenesis and Plasmid Shuffling: From Cloned Gene to Mutant Yeast. *Methods Enzymol.* **1991**, *194*, 302–318.

(136) Mirzahosseini, Z.; Shabani, L.; Sabzalian, M. R.; Dayanandan, S. Comparative Physiological and Proteomic Analysis of A*rabidopsis Thaliana* Revealed Differential Wound Stress Responses Following the Exposure to Different LED Light Sources. *Environ. Exp. Bot.* **2020**, *169*, 103895–103905.

(137) Alonso-Gutierrez, J.; Kim, E.-M.; Batth, T. S.; Cho, N.; Hu, Q.; Chan, L. J. G.; Petzold, C. J.; Hillson, N. J.; Adams, P. D.; Keasling, J. D.; Garcia Martin, H.; Lee, T. S. Principal Component Analysis of Proteomics (PCAP) as a Tool to Direct Metabolic Engineering. *Metab. Eng.* **2015**, *28*, 123–133.

(138) Minafra, L.; Di Cara, G.; Albanese, N. N.; Cancemi, P. Proteomic Differentiation Pattern in the *U937* Cell Line. *Leuk. Res.* **2011**, *35* (2), 226–236.

(139) Verhoeckx, K. C. M.; Bijlsma, S.; de Groene, E. M.; Witkamp, R. F.; van der Greef, J.; Rodenburg, R. J. T. A Combination of Proteomics, Principal Component Analysis and Transcriptomics Is a Powerful Tool for the Identification of Biomarkers for Macrophage Maturation in the *U937* Cell Line. *Proteomics* **2004**, *4* (4), 1014–1028.

(140) Rao, P. K.; Li, Q. Principal Component Analysis of Proteome Dynamics in Iron-Starved *Mycobacterium Tuberculosis*. *J. Proteomics Bioinform.* **2009**, *2* (1), 19–31.

(141) Petko, L.; Lindquist, S. Hsp26 Is Not Required for Growth at High Temperatures, nor for Thermotolerance, Spore Development, or Germination. *Cell* **1986**, *45* (6), 885–894.

(142) Stromer, T.; Fischer, E.; Richter, K.; Haslbeck, M.; Buchner, J. Analysis of the Regulation of the Molecular Chaperone Hsp26 by Temperature-Induced Dissociation: The N-

Terminal Domail Is Important for Oligomer Assembly and the Binding of Unfolding Proteins. *J. Biol. Chem.* **2004**, *279* (12), 11222–11228.

(143) Haslbeck, M.; Walke, S.; Stromer, T.; Ehrnsperger, M.; White, H. E.; Chen, S.; Saibil, H. R.; Buchner, J. Hsp26: A Temperature-Regulated Chaperone. *EMBO J.* **1999**, *18* (23), 6744–6751.

(144) Tkach, J. M.; Yimit, A.; Lee, A. Y.; Riffle, M.; Costanzo, M.; Jaschob, D.; Hendry, J. A.; Ou, J.; Moffat, J.; Boone, C.; Davis, T. N.; Nislow, C.; Brown, G. W. Dissecting DNA Damage Response Pathways by Analysing Protein Localization and Abundance Changes during DNA Replication Stress. *Nat. Cell Biol.* **2012**, *14* (9), 966–976.

(145) Biteau, B.; Labarre, J.; Toledano, M. B. ATP-Dependent Reduction of Cysteine-Sulphinic Acid by S. Cerevisiae Sulphiredoxin. *Nature* **2003**, *425* (6961), 980–984.

(146) Pedrajas, J. R.; Kosmidou, E.; Miranda-Vizuete, A.; Gustafsson, J. A.; Wright, A. P.; Spyrou, G. Identification and Functional Characterization of a Novel Mitochondrial Thioredoxin System in *Saccharomyces Cerevisiae*. *J. Biol. Chem.* **1999**, *274* (10), 6366–6373.

(147) Garcera, A.; Barreto, L.; Piedrafita, L.; Tamarit, J.; Herrero, E. *Saccharomyces Cerevisiae* Cells Have Three Omega Class Glutathione S-Transferases Acting as 1-Cys Thiol Transferases. *Biochem. J.* **2006**, *398* (2), 187–196.

(148) Kim, Y.; Cha, S. J.; Choi, H.-J.; Kim, K. Omega Class Glutathione S-Transferase: Antioxidant Enzyme in Pathogenesis of Neurodegenerative Diseases. *Oxid. Med. Cell. Longev.* **2017**, *2017*, 1–6.

(149) Lussier, M.; White, A. M.; Sheraton, J.; di Paolo, T.; Treadwell, J.; Southard, S. B.; Horenstein, C. I.; Chen-Weiner, J.; Ram, A. F.; Kapteyn, J. C.; Roemer, T. W.; Vo, D. H.; Bondoc, D. C.; Hall, J.; Zhong, W. W.; Sdicu, A. M.; Davies, J.; Klis, F. M.; Robbins, P. W.; Bussey, H. Large Scale Identification of Genes Involved in Cell Surface Biosynthesis and Architecture in Saccharomyces Cerevisiae. *Genetics* **1997**, *147* (2), 435–450.

(150) Morano, K. A.; Grant, C. M.; Moye-Rowley, W. S. The Response to Heat Shock and Oxidative Stress in Saccharomyces Cerevisiae. *Genetics* **2012**, *190* (4), 1157–1195.

(151) Craig, E. A.; Gambill, B. D.; Nelson, R. J. Heat Shock Proteins: Molecular Chaperones of Protein Biogenesis. *Microbiol. Rev.* **1993**, *57* (2), 402–414.

(152) Mager, W. H.; De Kruijff, A. J. Stress-Induced Transcriptional Activation. *Microbiol. Rev.* **1995**, *59* (3), 506–531.

(153) Susek, R. E.; Lindquist, S. L. Hsp26 of *Saccharomyces Cerevisiae* Is Related to the Superfamily of Small Heat Shock Proteins but Is without a Demonstrable Function. *Mol. Cell. Biol.* **1989**, *9* (11), 5265–5271.

(154) Bentley, N. J.; Fitch, I. T.; Tuite, M. F. The Small Heat-Shock Protein Hsp26 of Saccharomyces Cerevisiae Assembles into a High Molecular Weight Aggregate. *Yeast Chichester Engl.* **1992**, *8* (2), 95–106.

(155) Haslbeck, M.; Braun, N.; Stromer, T.; Richter, B.; Model, N.; Weinkauf, S.; Buchner, J. Hsp42 Is the General Small Heat Shock Protein in the Cytosol of Saccharomyces Cerevisiae. *EMBO J.* **2004**, *23* (3), 638–649.

(156) Hasin, N.; Cusack, S. A.; Ali, S. S.; Fitzpatrick, D. A.; Jones, G. W. Global Transcript and Phenotypic Analysis of Yeast Cells Expressing Ssa1, Ssa2, Ssa3 or Ssa4 as Sole Source of Cytosolic Hsp70-Ssa Chaperone Activity. *BMC Genomics* **2014**, *15* (1), 194–206.

(157) Sharma, D.; Masison, D. C. Single Methyl Group Determines Prion Propagation and Protein Degradation Activities of Yeast Heat Shock Protein (Hsp)-70 Chaperones Ssa1p and Ssa2p. *Proc. Natl. Acad. Sci.* **2011**, *108* (33), 13665–13670.

(158) Sharma, D.; Martineau, C. N.; Le Dall, M.-T.; Reidy, M.; Masison, D. C.; Kabani, M. Function of SSA Subfamily of Hsp70 Within and Across Species Varies Widely in Complementing Saccharomyces Cerevisiae Cell Growth and Prion Propagation. *PLoS ONE* **2009**, *4* (8), e6644.

(159) Matsumoto, R.; Akama, K.; Rakwal, R.; Iwahashi, H. The Stress Response against Denatured Proteins in the Deletion of Cytosolic Chaperones SSA1/2 Is Different from Heat-Shock Response in *Saccharomyces Cerevisiae*. *BMC Genomics* **2005**, *6* (1), 141–156.

(160) Scott, E. M.; Pillus, L. Homocitrate Synthase Connects Amino Acid Metabolism to Chromatin Functions through Esa1 and DNA Damage. *Genes Dev.* **2010**, *24* (17), 1903–1913.

(161) Torres-Machorro, A. L.; Aris, J. P.; Pillus, L. A Moonlighting Metabolic Protein Influences Repair at DNA Double-Stranded Breaks. *Nucleic Acids Res.* **2015**, *43* (3), 1646–1658.

(162) Albig, W.; Entian, K. D. Structure of Yeast Glucokinase, a Strongly Diverged Specific Aldo-Hexose-Phosphorylating Isoenzyme. *Gene* **1988**, *73* (1), 141–152.

(163) McAlister, L.; Holland, M. J. Isolation and Characterization of Yeast Strains Carrying Mutations in the Glyceraldehyde-3-Phosphate Dehydrogenase Genes. *J. Biol. Chem.* **1985**, *260* (28), 15013–15018.

(164) Delgado, M. L.; O'Connor, J. E.; Azorín, I.; Renau-Piqueras, J.; Gil, M. L.; Gozalbo, D. The Glyceraldehyde-3-Phosphate Dehydrogenase Polypeptides Encoded by the Saccharomyces Cerevisiae TDH1, TDH2 and TDH3 Genes Are Also Cell Wall Proteins. *Microbiology* **2001**, *147* (2), 411–417.

(165) McAlister, L.; Holland, M. J. Differential Expression of the Three Yeast Glyceraldehyde-3-Phosphate Dehydrogenase Genes. *J. Biol. Chem.* **1985**, *260* (28), 15019–15027.

(166) Randez-Gil, F.; Sánchez-Adriá, I. E.; Estruch, F.; Prieto, J. A. The Formation of Hybrid Complexes between Isoenzymes of Glyceraldehyde-3-phosphate Dehydrogenase Regulates Its Aggregation State, the Glycolytic Activity and Sphingolipid Status in *Saccharomyces Cerevisiae*. *Microb. Biotechnol.* **2020**, *13* (2), 562–571.

(167) Boucherie, H.; Bataille, N.; Fitch, I. T.; Perrot, M.; Tuite, M. F. Differential Synthesis of Glyceraldehyde-3-Phosphate Dehydrogenase Polypeptides in Stressed Yeast Cells. *FEMS Microbiol. Lett.* **1995**, *125* (2–3), 127–133.

(168) Cyrne, L.; Antunes, F.; Sousa-Lopes, A.; Diaz-Berrio, J.; Marinho, H. S. Glyceraldehyde-3-Phosphate Dehydrogenase Is Largely Unresponsive to Low Regulatory Levels of Hydrogen Peroxide in *Saccharomyces Cerevisiae*. *BMC Biochem.* **2010**, *11*, 49–60.

(169) Kirkman, H. N.; Gaetani, G. F. Catalase: A Tetrameric Enzyme with Four Tightly Bound Molecules of NADPH. *Proc. Natl. Acad. Sci. U. S. A.* **1984**, *81* (14), 4343–4347.

(170) Cattani, L.; Ferri, A. The Function of NADPH Bound to Catalase. *Boll. Della Soc. Ital. Biol. Sper.* **1994**, *70* (4), 75–82.

(171) Trotter, E. W.; Collinson, E. J.; Dawes, I. W.; Grant, C. M. Old Yellow Enzymes Protect against Acrolein Toxicity in the Yeast *Saccharomyces Cerevisiae*. *Appl. Environ. Microbiol.* **2006**, *72* (7), 4885–4892.

(172) Heer, D.; Heine, D.; Sauer, U. Resistance of *Saccharomyces Cerevisiae* to High Concentrations of Furfural Is Based on NADPH-Dependent Reduction by at Least Two Oxireductases. *Appl. Environ. Microbiol.* **2009**, *75* (24), 7631–7638.

(173) Jayakody, L. N.; Turner, T. L.; Yun, E. J.; Kong, I. I.; Liu, J.-J.; Jin, Y.-S. Expression of Gre2p Improves Tolerance of Engineered Xylose-Fermenting *Saccharomyces Cerevisiae* to Glycolaldehyde under Xylose Metabolism. *Appl. Microbiol. Biotechnol.* **2018**, *102* (18), 8121–8133.

(174) Jang, I.-C.; Oh, S.-J.; Seo, J.-S.; Choi, W.-B.; Song, S. I.; Kim, C. H.; Kim, Y. S.; Seo, H.-S.; Choi, Y. D.; Nahm, B. H.; Kim, J.-K. Expression of a Bifunctional Fusion of the *Escherichia Coli* Genes for Trehalose-6-Phosphate Synthase and Trehalose-6-Phosphate Phosphatase in Transgenic Rice Plants Increases Trehalose Accumulation

and Abiotic Stress Tolerance without Stunting Growth. *Plant Physiol.* **2003**, *131* (2), 516–524.

(175) Cortina, C.; Culiáñez-Macià, F. A. Tomato Abiotic Stress Enhanced Tolerance by Trehalose Biosynthesis. *Plant Sci.* **2005**, *169* (1), 75–82.

(176) Iturriaga, G.; Suárez, R.; Nova-Franco, B. Trehalose Metabolism: From Osmoprotection to Signaling. *Int. J. Mol. Sci.* **2009**, *10* (9), 3793–3810.

(177) De Virgilio, C.; Hottiger, T.; Dominguez, J.; Boller, T.; Wiemken, A. The Role of Trehalose Synthesis for the Acquisition of Thermotolerance in Yeast. I. Genetic Evidence That Trehalose Is a Thermoprotectant. *Eur. J. Biochem.* **1994**, *219* (1–2), 179–186.

(178) Gounalaki, N.; Thireos, G. Yap1p, a Yeast Transcriptional Activator That Mediates Multidrug Resistance, Regulates the Metabolic Stress Response. *EMBO J.* **1994**, *13* (17), 4036–4041.

(179) Wiemken, A. Trehalose in Yeast, Stress Protectant Rather than Reserve Carbohydrate. *Antonie Van Leeuwenhoek* **1990**, *58* (3), 209–217.

(180) Velculescu, V. E.; Zhang, L.; Zhou, W.; Vogelstein, J.; Basrai, M. A.; Bassett, D. E., Jr; Hieter, P.; Vogelstein, B.; Kinzler, K. W. Characterization of the Yeast Transcriptome. *Cell* **1997**, *88* (2), 243–251.

(181) Bayliak, M.; Semchyshyn, H.; Lushchak, V. Possible Accumulation of Non-Active Molecules of Catalase and Superoxide Dismutase in S. Cerevisiae Cells under Hydrogen Peroxide Induced Stress. *Open Life Sci.* **2007**, *2* (3), 326–336.

(182) Martins, D.; English, A. M. Catalase Activity Is Stimulated by H_2O_2 in Rich Culture Medium and Is Required for H_2O_2 Resistance and Adaptation in Yeast. *Redox Biol.* **2014**, *2*, 308–313.

(183) Stowe, D. F.; Camara, A. K. Mitochondrial Reactive Oxygen Species Production in Excitable Cells: Modulators of Mitochondrial and Cell Function. *Antioxid. Redox Signal.* **2009**, *11* (6), 1373–1414.

(184) Uttara, B.; Singh, A. V.; Zamboni, P.; Mahajan, R. T. Oxidative Stress and Neurodegenerative Diseases: A Review of Upstream and Downstream Antioxidant Therapeutic Options. *Curr. Neuropharmacol.* **2009**, *7* (1), 65–74.

(185) Veal, E. A.; Day, A. M.; Morgan, B. A. Hydrogen Peroxide Sensing and Signaling. *Mol. Cell* **2007**, *26* (1), 1–14.

(186) Guo, M.; Bhaskar, B.; Li, H.; Barrows, T. P.; Poulos, T. L. Crystal Structure and Characterization of a Cytochrome c Peroxidase-Cytochrome c Site-Specific Cross-Link. *Proc. Natl. Acad. Sci. U. S. A.* **2004**, *101* (16), 5940–5945.

(187) Fabrizio, P.; Longo, V. D. The Chronological Life Span of *Saccharomyces Cerevisiae*. *Methods Mol. Biol. Clifton NJ* **2007**, *371*, 89–95.

(188) Mauro, J. M.; Fishel, L. A.; Hazzard, J. T.; Meyer, T. E.; Tollin, G.; Cusanovich, M. A.; Kraut, J. Tryptophan-191 .Fwdarw. Phenylalanine, a Proximal-Side Mutation in Yeast Cytochrome c Peroxidase That Strongly Affects the Kinetics of Ferrocytochrome c Oxidation. *Biochemistry* **1988**, *27* (17), 6243–6256.

(189) Childs, R. E.; Bardsley, W. G. The Steady-State Kinetics of Peroxidase with 2,2'-Azino-Di-(3-Ethyl-Benzthiazoline-6-Sulphonic Acid) as Chromogen. *Biochem. J.* **1975**, *145* (1), 93–103.

(190) Hamilton, L.; Nielsen, B. R.; Davies, C. A.; Symons, M. C.; Winyard, P. G. Purity of Different Preparations of Sodium 3,5-Dibromo-4-Nitrosobenzenesulphonate and Their Applicability for EPR Spin Trapping. *Free Radic. Res.* **2003**, *37* (1), 41–49.

(191) Michel, B.; Bosshard, H. R. Spectroscopic Analysis of the Interaction between Cytochrome c and Cytochrome c Oxidase. *J. Biol. Chem.* **1984**, *259* (16), 10085–10091.

(192) Musah, R. A.; Goodin, D. B. Introduction of Novel Substrate Oxidation into Cytochrome *c* Peroxidase by Cavity Complementation: Oxidation of 2-Aminothiazole and Covalent Modification of the Enzyme. *Biochemistry* **1997**, *36* (39), 11665–11674.

(193) Vitello, L. B.; Erman, J. E.; Mauro, J. M.; Kraut, J. Characterization of the Hydrogen Peroxide - Enzyme Reaction for Two Cytochrome c Peroxidase Mutants. *Biochim. Biophys. Acta BBA - Protein Struct. Mol. Enzymol.* **1990**, *1038* (1), 90–97.

(194) Tsaprailis, G.; English, A. M. Different Pathways of Radical Translocation in Yeast Cytochrome c Peroxidase and Its W191F Mutant on Reaction with H_2O_2 Suggest an Antioxidant Role. *J. Biol. Inorg. Chem. JBIC Publ. Soc. Biol. Inorg. Chem.* **2003**, *8* (3), 248–255.

(195) Filosa, A.; English, A. M. Mass Spectral Analysis of Protein-Based Radicals Using DBNBS: Nonradical adduct formation *versus* spin trapping. *J. Biol. Chem.* **2001**, *276* (24), 21022–21027.

(196) Kaur, H.; Leung, K. H. W.; Perkins, M. J. A Water-Soluble, Nitroso-Aromatic Spin-Trap. *J. Chem. Soc. Chem. Commun.* **1981**, (3),142–143.

(197) Qian, S. Y.; Chen, Y.-R.; Deterding, L. J.; Fann, Y. C.; Chignell, C. F.; Tomer, K. B.; Mason, R. P. Identification of Protein-Derived Tyrosyl Radical in the Reaction of Cytochrome c and Hydrogen Peroxide: Characterization by ESR Spin-Trapping, HPLC and MS. *Biochem. J.* **2002**, *363* (2), 281–288.

(198) Hörtner, H.; Ammerer, G.; Hartter, E.; Hamilton, B.; Rytka, J.; Bilinski, T.; Ruis, H. Regulation of Synthesis of Catalases and Iso-1-Cytochrome c in *Saccharomyces Cerevisiae* by Glucose, Oxygen and Heme. *Eur. J. Biochem.* **2005**, *128* (1), 179–184.

(199) Morimoto, A.; Tanaka, M.; Takahashi, S.; Ishimori, K.; Hori, H.; Morishima, I. Detection of a Tryptophan Radical as an Intermediate Species in the Reaction of Horseradish Peroxidase Mutant (Phe-221 → Trp) and Hydrogen Peroxide. *J. Biol. Chem.* **1998**, *273* (24), 14753–14760.

(200) Fishel, L. A.; Farnum, M. F.; Mauro, J. M.; Miller, M. A.; Kraut, J.; Liu, Y.; Tan, X. L.; Scholes, C. P. Compound I Radical in Site-Directed Mutants of Cytochrome c Peroxidase as Probed by Electron Paramagnetic Resonance and Electron-Nuclear Double Resonance. *Biochemistry* **1991**, *30* (7), 1986–1996.

(201) Scholes, C. P.; Liu, Y.; Fishel, L. A.; Farnum, M. F.; Mauro, J. M.; Kraut, J. Recent ENDOR and Pulsed Electron Paramagnetic Resonance Studies of Cytochrome *c* Peroxidase - Compound I and Its Site-Directed Mutants. *Isr. J. Chem.* **1989**, *29* (1), 85–92.

(202) Klebanoff, S. J. Myeloperoxidase: Friend and Foe. *J. Leukoc. Biol.* **2005**, *77* (5), 598–625.

(203) Yamaguchi, Y.; Zhang, D. E.; Sun, Z.; Albee, E. A.; Nagata, S.; Tenen, D. G.; Ackerman, S. J. Functional Characterization of the Promoter for the Gene Encoding Human Eosinophil Peroxidase. *J. Biol. Chem.* **1994**, *269* (30), 19410–19419.

(204) Pruitt, K. M.; Tenovuo, J. O. The Lactoperoxidase System: Chemistry and Biological Significance; Immunology series; Dekker: New York, 1985.

(205) Schmidt, M.; Gerlach, F.; Avivi, A.; Laufs, T.; Wystub, S.; Simpson, J. C.; Nevo, E.; Saaler-Reinhardt, S.; Reuss, S.; Hankeln, T.; Burmester, T. Cytoglobin Is a Respiratory Protein in Connective Tissue and Neurons, Which Is up-Regulated by Hypoxia. *J. Biol. Chem.* **2004**, *279* (9), 8063–8069.

(206) Kathiresan, M.; English, A. M. LC-MS/MS Proteoform Profiling Exposes Cytochrome c Peroxidase Self-Oxidation in Mitochondria and Functionally Important Hole Hopping from Its Heme. *J. Am. Chem. Soc.* **2018**, *140* (38), 12033–12039.

(207) Youseff, B. H.; Holbrook, E. D.; Smolnycki, K. A.; Rappleye, C. A. Extracellular Superoxide Dismutase Protects Histoplasma Yeast Cells from Host-Derived Oxidative Stress. *PLoS Pathog.* **2012**, *8* (5), e1002713.

Appendix I: List of 1708 proteins identified by label-free proteomics (Pages 148 - 303)

Table A4.1. FDR confidence, sequence coverage, number of unique peptides, 10- and 60-min Ratios (Eq 4.1) for 1708 proteins from WT and W191F cells as determined by Proteome Discoverer v2.3

- See footnotes to Table S4.1.
- Maximum and minimum values accepted by Proteome Discoverer v2.3 for the protein abundance Ratio (Eq 4.1) are 100 and 0.01, respectively.
- No Ratio value is given in the table if no peptide was detected for an identified protein in either the control or H_2O_2-challenged sample.

	Description	Gene name	Protein FDR Confidence	Coverage [%]	# Unique Peptides	WT/10 pc	WT/60 pc	W191F/10 pc	W191F/60 pc
1	Partitioning protein REP1		High	8	3	0.995	1.002	0.977	1.3
2	Partitioning protein REP2		High	11	2	1.395	0.863	0.572	1.173
3	Putative uncharacterized protein YLR154W-F		High	41	1	0.818	1.017	0.719	0.457
4	Putative uncharacterized protein YJL135W		Medium	8	1	0.709	0.841	1.009	0.963
5	Adenine deaminase	AAH1	High	12	4	0.571	0.927	0.69	0.817
6	Alanine/arginine aminopeptidase	AAP1	High	19	11	0.874	0.99	1.011	1.091
7	Aspartate aminotransferase, cytoplasmic	AAT2	High	47	16	1.202	1.074	1.135	1.27
8	ARS-binding factor 2, mitochondrial	ABF2	High	28	5	1.108	0.845	0.882	1.111
9	actin-binding protein	ABP1	High	36	14	1.057	1.139	1.255	1.207
10	tRNA(Thr) (cytosine(32)-N(3))-methyltransferase	ABP140	High	9	4	1.212	0.951	1.178	0.896
11	Acetyl-CoA carboxylase	ACC1	High	53	105	1.473	1.093	1.347	1.344

12	Endo-1,3(4)-beta-glucanase 2	ACF2	High	1	1	0.877	0.01	1.127	0.01
13	acetyl-CoA hydrolase	ACH1	High	26	12	1.058	1.196	0.956	1.084
14	Aconitate hydratase, mitochondrial	ACO1	High	45	30	0.936	0.872	1.043	0.935
15	Homocitrate dehydratase, mitochondrial	ACO2	High	5	3	1.084	1.277	1.079	0.77
16	acetyl-coenzyme A synthetase 1	ACS1	High	12	8	3.19	0.981	1.367	1.233
17	acetyl-coenzyme A synthetase 2	ACS2	High	31	19	1.044	0.976	1.159	1.191
18	Actin	ACT1	High	69	20	1.203	0.895	1.344	1.058
19	phosphoribosylaminoimidazole-succinocarboxamide synthase	ADE1	High	41	10	0.742	0.722	0.269	0.229
20	adenylosuccinate synthetase	ADE12	High	33	11	0.809	0.812	0.441	0.492
21	adenylosuccinate lyase	ADE13	High	42	16	0.983	0.723	0.376	0.41
22	bifunctional purine biosynthesis protein	ADE16	High	22	6	1.024	1.139	1.254	1.239

23	bifunctional purine biosynthesis protein	ADE17	High	43	15	0.674	0.325	0.081	0.093
24	phosphoribosylaminoimidazole carboxylase	ADE2	High	15	6	0.981	0.725	0.462	0.388
25	C-1-tetrahydrofolate synthase, cytoplasmic	ADE3	High	26	17	0.966	0.897	0.783	0.794
26	amidophosphoribosyltransferase	ADE4	High	23	9	0.933	0.815	0.451	0.503
27	Bifunctional purine biosynthetic protein	ADE5,7	High	35	20	0.887	0.73	0.492	0.489
28	Phosphoribosylformylglycinamidine synthase	ADE6	High	19	19	0.749	0.885	0.665	0.585
29	Phosphoribosylglycinamide formyltransferase	ADE8	High	8	2	0.772	1.124	0.488	0.59
30	Alcohol dehydrogenase 1	ADH1	High	65	13	0.834	0.879	0.911	0.701
31	Alcohol dehydrogenase 2	ADH2	High	52	10	3.841	0.996	1.418	1.104
32	Alcohol dehydrogenase 3, mitochondrial	ADH3	High	21	5	1.173	0.874	1.155	1.009
33	NADP-dependent alcohol dehydrogenase 6	ADH6	High	29	7	1.857	1.738	1.006	0.957

34	adenylate kinase	ADK1	High	53	11	1.153	1.055	1.008	0.844
35	Adenosine kinase	ADO1	High	51	13	0.918	1.034	1.142	0.908
36	Probable ATP-dependent permease	ADP1	High	2	2	1.252	1.041	1.072	0.803
37	Regulatory protein ADR1	ADR1	High	6	6	0.812	0.799	1.307	0.907
38	Accumulation of dyads protein	ADY2	High	8	1	100	12.454	100	
39	Protein AFG1	AFG1	High	3	1	0.939	1.323	0.732	0.431
40	ATPase family gene 2	AFG2	Medium	2	1	1.193	1.105	0.01	1.592
41	alanine--glyoxylate aminotransferase 1	AGX1	High	3	1	2.324	2.574	2.155	1.965
42	Hsp90 co-chaperone AHA1	AHA1	High	38	10	1.189	1.033	1.432	1.284
43	Peroxiredoxin AHP1	AHP1	High	47	7	2.072	4.872	1.424	2.484
44	Probable oxidoreductase AIM17	AIM17	High	5	2	1.858	1.562	1.918	3.076

45	Protein AIM2	AIM2	High	9	1	100	1	0.395	0.044
46	Altered inheritance of mitochondria	AIM21	High	2	1	1.035	0.969	1.682	1.491
47	Altered inheritance of mitochondria	AIM24	High	16	4	1.209	0.779	1.015	0.738
48	altered inheritance rate of	AIM29	Low	6	1	0.775	1.179	0.965	1.491
49	Altered inheritance of mitochondria	AIM36	High	5	1	1	1.243	0.12	0.632
50	Probable electron transfer flavoprotein	AIM45	High	15	3	0.832	1.131	1.114	0.445
51	Altered inheritance of mitochondria	AIM46	High	10	2	100	2.036	0.8	0.715
52	Altered inheritance of mitochondria	AIM6	High	9	2	0.617	1.516	0.609	0.479
53	Protein AIM7	AIM7	High	7	1	0.831	1.131	1.232	1.249
54	Altered inheritance of mitochondria	AIM9	High	4	2	1.091	1.186	1.15	1.183
55	Actin-interacting protein 1	AIP1	High	19	8	1.011	1.066	1.117	1.217

56	alanine--tRNA ligase, mitochondrial	ALA1	High	35	30	1.007	0.918	1.052	1.028
57	Aldehyde dehydrogenase [NAD(P)+] 2	ALD3	High	20	8	1.000	0.869	2.144	10.544
58	Potassium-activated aldehyde dehydrogenase, mitochondrial	ALD4	High	65	26	2.151	1	1.24	1.358
59	Aldehyde dehydrogenase 5, mitochondrial	ALD5	High	18	7	0.985	0.873	1.085	1.075
60	Magnesium-activated aldehyde dehydrogenase, cytosolic	ALD6	High	54	25	1.448	1.137	1.144	1.161
61	chitobiosyldiphosphodolichol beta-mannosyltransferase	ALG1	High	2	1	0.794	0.931	1.179	0.718
62	Dol-P-Man:Man(7)GlcNAc(2)-PP-Dol alpha-1,6-mannosyltransferase	ALG12	High	1	1	0.672	1.217	1.418	0.745
63	Alpha-1,3/1,6-mannosyltransferase ALG2	ALG2	High	8	3	1.226	1.053	1.176	0.905
64	dolichyl-phosphate beta-glucosyltransferase	ALG5	High	3	1	1.113	0.826	1.062	1.029
65	dolichyl pyrophosphate Glc1Man9GlcNAc2 alpha-1,3-glucosyltransferase	ALG8	High	2	1	0.725	1.45	1.042	0.96

66	Alpha-1,2-mannosyltransferase ALG9	ALG9	High	6	3	0.801	1.056	1.037	0.925
67	D-arabinono-1,4-lactone oxidase	ALO1	High	13	6	1.095	1.109	1.086	0.697
68	probable alanine aminotransferase, mitochondrial	ALT1	High	2	1			0.935	0.01
69	AMP deaminase	AMD1	High	7	5	1.055	1.154	1.026	0.98
70	mannan polymerase II complex	ANP1	High	2	1	0.889	1.011	0.982	0.744
71	Protein APA1	APA1	High	44	10	0.894	1.041	0.952	0.94
72	vacuolar aminopeptidase 1	APE1; LAP4	High	17	7	1.905	2.817	1.789	3.837
73	Aminopeptidase 2, mitochondrial	APE2	High	20	14	0.856	1.123	1.015	0.863
74	aminopeptidase Y	APE3	High	15	5	0.802	0.877	1.032	0.983
75	Aspartyl aminopeptidase 4	APE4	High	14	5	0.943	1.116	0.783	1.122
76	AP-2 complex subunit beta	APL1	High	5	2	100	0.01	0.621	0.301

77	AP-1 complex subunit beta-1	APL2	High	3	2	1.055	0.962	1.262	1.106
78	AP-2 complex subunit alpha	APL3	High	5	4	1.401	0.853	0.497	0.312
79	AP-1 complex subunit gamma-1	APL4	High	3	2	1.117	1.398	1.161	1.1
80	AP-3 complex subunit delta	APL5	High	1	1	100	12.997	0.573	0.061
81	AP-3 complex subunit beta	APL6	Medium	2	1	1.027	0.926	1.556	1.688
82	AP-3 complex subunit mu	APM3	High	4	1	0.682	0.812	0.977	1.149
83	AP-3 complex subunit sigma	APS3	High	5	1	1.514	100	1.186	1.329
84	Adenine phosphoribosyltransferase 1	APT1	High	22	4	1.064	1.27	1.154	0.663
85	Adenine phosphoribosyltransferase 2	APT2	High	6	1	0.589	2.197	0.917	0.571
86	D-arabinose dehydrogenase [NAD(P)+] heavy	ARA1	High	25	6	1.16	1.243	1.041	1.181
87	ABC transporter ATP-binding protein	ARB1	High	36	16	0.969	0.913	1.01	1.18

88	tRNA-aminoacylation cofactor ARC1	ARC1	High	39	13	1.167	0.946	1.16	1.296
89	Actin-related protein 43864 complex	ARC18	High	11	2	1.193	1.336	0.774	0.833
90	Actin-related protein 43864 complex	ARC35	High	30	8	1.06	1.107	1.09	1.371
91	Actin-related protein 43864 complex	ARC40	High	29	8	0.762	1.075	1.012	1.242
92	N-terminal acetyltransferase A complex	ARD1	High	5	1	1.331	0.791	0.864	0.829
93	ADP-ribosylation factor 1	ARF1	High	56	2	0.739	0.835	1.206	0.678
94	ADP-ribosylation factor 2	ARF2	High	56	2	0.798	1.03	0.853	0.425
95	Argininosuccinate synthase	ARG1	High	25	9	1.401	1.25	1.184	1.053
96	argininosuccinate lyase	ARG4	High	27	8	0.986	0.755	1.145	1.302
97	Arginine biosynthesis bifunctional protein	ARG7	High	3	1				
98	ADP-ribosylation factor-like protein 1	ARL1	High	14	2	0.731	1.025	1.144	0.774

99	Pentafunctional AROM polypeptide	ARO1	High	23	28	0.99	1.035	1.089	0.991
100	chorismate synthase	ARO2	High	28	8	1.428	0.986	1.44	1.211
101	Phospho-2-dehydro-3-deoxyheptonate aldolase, phenylalanine-inhibited	ARO3	High	21	6	1.124	1.083	0.721	0.752
102	Phospho-2-dehydro-3-deoxyheptonate aldolase, tyrosine-inhibited	ARO4	High	39	9	0.981	0.894	1.022	0.952
103	Chorismate mutase	ARO7	High	8	2	0.826	0.919	0.997	1.216
104	Aromatic/aminoadipate aminotransferase 1	ARO8	High	35	14	1.018	1.057	1.105	1.026
105	Aromatic amino acid aminotransferase	ARO9	High	5	2	2.217	1.144	1.386	2.687
106	Actin-related protein 2	ARP2	High	26	8	1.323	0.847	1.259	1.451
107	actin-related protein 3	ARP3	High	22	8	1.074	0.915	1.08	1.376
108	actin-like protein Arp8	ARP8	High	1	1	0.541	9.611	0.01	6.776
109	Probable metalloprotease ARX1	ARX1	High	8	3	0.936	0.921	1.009	1.035

110	Guanine nucleotide-binding protein subunit	ASC1	High	56	13	0.908	0.96	1.028	0.983
111	Histone chaperone ASF1	ASF1	High	23	4	0.994	1.145	1.07	1.312
112	Activator of SKN7 protein	ASK10	High	1	1	1.229	0.977	0.953	1.505
113	Asparagine synthetase [glutamine-hydrolyzing] 1	ASN1	High	25	9	1.12	0.901	1.399	1.361
114	Asparagine synthetase [glutamine-hydrolyzing] 2	ASN2	High	48	18	1.029	1.154	1.099	1.247
115	L-asparaginase 1	ASP1	High	10	3	1.097	0.806	1.603	1.234
116	Alcohol O-acetyltransferase 2	ATF2	Medium	3	1	0.55	9.597	0.851	0.179
117	Autophagy-related protein 27	ATG27	High	5	1	1.141	1.161	8.707	0.626
118	Iron-sulfur clusters transporter ATM1,	ATM1	High	1	1	0.338	1.005	1.795	0.289
119	Ammonia transport outward protein	ATO3	High	7	1	1.157	0.795	0.426	0.214
120	ATP synthase subunit alpha,	ATP1	High	46	27	1.228	0.883	1.121	0.929

121	ATP synthase subunit H,	ATP14	Low	9	1	0.808	1.189	1.247	2.165
122	ATP synthase subunit epsilon,	ATP15	High	39	2	1.007	0.757	1.431	1.072
123	ATP synthase subunit f,	ATP17	High	9	1	0.59	0.724	1.392	0.586
124	ATP synthase subunit beta,	ATP2	High	58	23	1.103	0.963	1.261	0.879
125	ATP synthase subunit g,	ATP20	High	35	3	1.13	0.79	0.851	0.924
126	ATP synthase subunit gamma,	ATP3	High	39	11	1.421	0.989	1.335	0.876
127	ATP synthase subunit 4,	ATP4	High	39	9	1.273	0.936	1.199	0.828
128	ATP synthase subunit 5,	ATP5	High	49	9	1.136	0.798	1.026	0.594
129	ATP synthase subunit A	ATP6	Medium	7	1		0.01	0.01	
130	ATP synthase subunit d,	ATP7	High	25	3	2.427	1.155	0.902	0.408
131	Late secretory pathway protein	AVL9	High	1	1	12.199	8.192	0.376	0.196

132	Vacuolar amino acid transporter	AVT2	Medium	4	1	1.643	1.991	0.984	0.674
133	Vacuolar amino acid transporter	AVT7	High	2	1	0.679	0.917	0.926	0.665
134	Putative protease AXL1	AXL1	Medium	1	1		1	0.447	0.01
135	NADPH-dependent 1-acyldihydroxyacetone phosphate reductase	AYR1	High	26	5	1.054	0.921	0.972	0.763
136	Leu/Val/Ile amino-acid permease	BAP2	High	2	1	0.913	1.674	0.707	1.257
137	Branched-chain-amino-acid aminotransferase, mitochondrial	BAT1	High	46	12	0.899	0.976	1.043	0.919
138	Branched-chain-amino-acid aminotransferase, cytosolic	BAT2	High	23	4	1.634	1.294	1.086	0.915
139	Myosin tail region-interacting protein	BBC1	High	3	2	1.16	1.038	1.119	1.385
140	Serine/threonine-protein kinase BCK1/SLK1/SSP31	BCK1	Medium	0	1				
141	protein BCP1	BCP1	High	7	1		100	0.01	
142	cAMP-dependent protein kinase regulatory	BCY1	High	17	6	1.189	1.032	1.318	1.61

143	(R,R)-butanediol dehydrogenase	BDH1	High	30	8	0.948	1.183	0.949	1.02
144	Bud emergence protein 1	BEM1	Low	1	1	0.721	0.993	0.96	1.458
145	GTPase-activating protein BEM2/IPL2	BEM2	High	2	3	9.92	100	0.778	1.118
146	Geranylgeranyl transferase type-2 subunit	BET2	Low	4	1	1.299	1.026	1.203	1.438
147	nuclear segregation protein Bfr1	BFR1	High	30	13	1.047	0.898	1.103	1.326
148	protein BFR2	BFR2	High	6	3	1.125	0.869	1.126	0.908
149	glucan 1,3-beta-glucosidase	BGL2	High	30	10	2.268	1.043	1.099	0.979
150	Cytochrome b mRNA maturase	BI3	High	2	1	0.991	1.127	0.857	1.075
151	Biotin synthase, mitochondrial	BIO2	High	33	9	0.861	1.029	0.969	0.856
152	adenosylmethionine-8-amino-7-oxononanoate aminotransferase	BIO3	High	15	6	0.712	0.881	0.712	0.825
153	Dethiobiotin synthetase	BIO4	High	16	2	0.77	0.901	0.737	0.349

154	Proteasome activator BLM10	BLM10	High	2	3	0.977	1.044	1.135	1.265
155	Protein BMH1	BMH1	High	58	5	1.082	1.03	1.117	0.904
156	Protein BMH2	BMH2	High	55	3	1.175	0.99	1.24	1.194
157	Ribosome biogenesis protein BMS1	BMS1	High	7	7	0.708	1.156	0.923	1.061
158	3-hydroxyanthranilate 3,4-dioxygenase	BNA1	High	18	2	1.589	1.001	0.915	0.858
159	Probable kynurenine--oxoglutarate transaminase BNA3	BNA3	High	7	2	0.962	2.038	0.957	0.631
160	kynureninase	BNA5	High	4	1	1.413	1.361	0.896	0.807
161	Bud neck protein 5	BNI5	High	2	1	0.878	0.895	1.162	1.249
162	E3 ubiquitin-protein ligase Bre1	BRE1	High	3	2	1.122	0.819	1.201	1.143
163	UBP3-associated protein BRE5	BRE5	High	8	2	1.137	0.955	1.415	1.473
164	ribosome biogenesis protein BRX1	BRX1	High	17	3	0.757	1.162	0.744	0.605

165	Cell cycle arrest protein	BUB3	Low	3	1	0.01	100	0.01	0.01
166	Phosphopantothenate--cysteine ligase CAB2	CAB2	High	6	2	1.059	0.95	1.099	0.957
167	phosphopantetheine adenylyltransferase	CAB4	High	4	1	1.519	0.853	1.319	1.588
168	Cap-associated protein CAF20	CAF20	High	19	1	0.548	2.307	0.744	0.326
169	protein CAF40	CAF40	High	11	3	0.864	1.033	1.071	0.631
170	protein CAJ1	CAJ1	High	21	6	0.827	0.931	1.144	1.316
171	Elongation factor 1-gamma 1	CAM1	High	39	14	1.022	0.906	1.039	1.508
172	F-actin-capping protein subunit beta	CAP2	High	15	3	1.156	0.964	1.276	1.21
173	arginase	CAR1	High	10	3	1.267	1.003	1.04	0.67
174	ornithine aminotransferase	CAR2	High	41	12	1.579	0.975	1.028	0.978
175	Centromere-binding protein 1	CBF1	High	12	3	1.101	1.139	1.255	1.57

176	H/ACA ribonucleoprotein complex subunit	CBF5	High	37	13	0.899	0.86	0.798	0.874
177	Protein CBP3, mitochondrial	CBP3	High	6	2	1.284	1.133	1.02	0.737
178	NADH-cytochrome b5 reductase 1	CBR1	High	32	6	1.131	0.96	0.95	0.837
179	CCA tRNA nucleotidyltransferase, mitochondrial	CCA1	High	3	1	1.318	1	0.445	0.01
180	Protein CCC1	CCC1	High	7	2	1.072	0.694	1.099	1.02
181	cytochrome c peroxidase, mitochondrial	CCP1	High	43	12	6.534	5.737	2.114	2.545
182	glucose-repressible alcohol dehydrogenase transcriptional	CCR4	High	3	2	0.753	100	0.715	0.16
183	Superoxide dismutase 1 copper	CCS1	High	5	1	1.655	1.301	1.843	1.473
184	T-complex protein 1 subunit	CCT2	High	17	7	1.167	0.942	1.044	1.106
185	T-complex protein 1 subunit	CCT3	High	30	14	1.158	0.994	1.129	1.269
186	T-complex protein 1 subunit	CCT4	High	36	14	1.155	1.067	1.081	1.084

187	T-complex protein 1 subunit	CCT5	High	12	6	1.221	0.915	1.116	1.026
188	T-complex protein 1 subunit	CCT6	High	11	4	0.969	1.153	1.068	0.543
189	T-complex protein 1 subunit	CCT7	High	26	11	1.147	0.946	1.202	1.056
190	T-complex protein 1 subunit	CCT8	High	25	12	1.157	0.982	1.183	1.175
191	Covalently-linked cell wall protein	CCW14	High	10	1	1.182	2.594	0.866	0.795
192	Cell division control protein	CDC1	High	2	1	1.234	1.183	1.501	1.003
193	cell division control protein	CDC10	High	10	3	1.276	0.972	1.123	1.246
194	cell division control protein	CDC11	High	3	1	0.469	1.134	0.851	0.265
195	Cell division control protein	CDC12	High	30	12	1.042	0.927	1.136	1.247
196	Pyruvate kinase 1	CDC19	High	81	44	0.889	0.892	0.985	1.062
197	thymidylate synthase	CDC21	High	14	3	1.147	1.187	0.847	0.586

198	Cyclin-dependent kinase 1	CDC28	High	10	2	1.337	0.749	1.374	1.05
199	Cell division control protein	CDC3	High	8	5	0.975	0.966	1.247	1.188
200	Cell division control protein	CDC31	Low	11	1				
201	Eukaryotic translation initiation factor	CDC33	High	25	5	0.947	0.923	1.037	0.689
202	Hsp90 co-chaperone Cdc37	CDC37	High	10	3	1.249	1.442	1.061	0.687
203	General negative regulator of	CDC39	High	6	11	1.121	0.958	1.129	0.819
204	cell division control protein	CDC42	High	20	3	0.94	1.009	1.05	0.914
205	Cell division control protein	CDC48	High	37	27	1.182	1.131	1.181	1.24
206	Cell division control protein	CDC53	High	9	5	1.216	1.349	1.113	0.975
207	Protein phosphatase PP2A regulatory	CDC55	Medium	3	1	1.132	0.75	1.578	1.382
208	Leucine--tRNA ligase, cytoplasmic	CDC60	High	37	30	0.9	0.972	1.095	1.236

209	Cell division control protein	CDC73	High	6	2	1.32	0.942	1.423	1.848
210	phosphatidate cytidylyltransferase	CDS1	High	20	8	0.786	0.857	0.981	0.933
211	mRNA-capping enzyme subunit beta	CET1	High	3	1	0.511	1.728	0.954	0.67
212	Cytoplasmic export protein 1	CEX1	Medium	1	1	1.041	0.957	1.018	0.999
213	Clathrin heavy chain	CHC1	High	30	38	1.1	1.074	1.129	1.12
214	CDP-diacylglycerol--serine O-phosphatidyltransferase	CHO1	High	12	2	0.544	0.786	0.718	0.597
215	phosphatidylethanolamine N-methyltransferase	CHO2	High	8	5	0.857	1.105	0.743	0.495
216	Chitin synthase 1	CHS1	High	2	2	1.082	1.069	1.174	0.34
217	Chitin biosynthesis protein CHS5	CHS5	High	7	4	0.92	1.144	1.076	1.134
218	proteasome-interacting protein CIC1	CIC1	High	9	2	0.818	0.891	0.952	1.222
219	Probable electron transfer flavoprotein	CIR1	High	15	2	1.15	0.926	1.085	0.969

220	Probable electron transfer flavoprotein-ubiquinone	CIR2	High	6	3	0.968	1.01	0.979	0.684
221	Cell wall mannoprotei n CIS3	CIS3	High	11	3	1.149	0.668	0.674	0.771
222	citrate synthase, mitochondria l	CIT1	High	36	15	1.312	1.039	1.01	1.029
223	Casein kinase II subunit	CKA1	Medium	2	1	0.964	0.962	1.224	1.152
224	casein kinase II subunit	CKA2	High	9	3	0.895	0.99	0.968	1.105
225	Casein kinase II subunit	CKB2	High	9	2	1.14	0.931	0.921	1.06
226	Choline kinase	CKI1	High	4	2	1.749	0.853	0.604	0.28
227	mRNA cleavage and polyadenylat ion	CLP1	Medium	2	1	1.461	1.136	1.238	1.4
228	Clustered mitochondria protein 1	CLU1	High	30	31	0.994	0.948	1.118	1.048
229	Calcium/cal modulin-dependent protein kinase I	CMK1	High	8	3	1.099	1.177	1.264	1.234
230	Calcium/cal modulin-dependent protein kinase II	CMK2	High	2	1	1.192	1.009	1.003	1.31

231	Serine/threonine-protein phosphatase 2B catalytic	CMP2	High	4	2	0.982	1.023	1.119	1.314
232	Protein CMS1	CMS1	High	8	2	1.153	0.915	0.902	0.752
233	serine/threonine-protein phosphatase 2B catalytic	CNA1	High	3	1	1.147	100	0.095	1.35
234	Cytochrome c oxidase assembly	COA1	High	12	2	1.228	0.996	0.887	1.05
235	Cofilin	COF1	High	40	5	0.85	1.239	0.97	0.622
236	Conserved oligomeric Golgi complex	COG8	High	2	1	100	100	1.166	0.352
237	coatomer subunit alpha	COP1	High	37	31	0.796	1.061	1.003	0.97
238	hexaprenyl pyrophosphate synthase, mitochondrial	COQ1	High	3	1	0.973	1.125	1.151	0.197
239	Cytochrome b-c1 complex subunit	COR1	High	44	16	1.214	0.918	1.215	0.922
240	Cobalt uptake protein COT1	COT1	High	3	1	1.445	2.644	1.077	0.968
241	Cytochrome c oxidase subunit	COX1	High	3	1	0.493	1.271	0.43	0.266

242	Cytochrome c oxidase subunit	COX12	High	10	1	0.781	0.848	0.857	1.161
243	Cytochrome c oxidase subunit	COX13	High	8	1	0.935	0.955	0.979	0.435
244	Cytochrome c oxidase assembly	COX15	High	6	3	0.752	1.254	1.104	1.038
245	Cytochrome c oxidase subunit	COX2	High	14	3	1.287	1.035	1.307	0.995
246	Cytochrome c oxidase protein	COX20	High	6	1				
247	cytochrome c oxidase subunit	COX4	High	61	5	0.905	0.994	0.896	0.658
248	Cytochrome c oxidase polypeptide	COX5A	High	9	1	1.269	0.923	1.066	0.659
249	Cytochrome c oxidase subunit	COX9	High	14	1	0.843	0.808	0.974	0.709
250	Carbamoyl-phosphate synthase arginine-specific small	CPA1	High	3	1	2.017	0.913	2.549	2.598
251	carbamoyl-phosphate synthase arginine-specific large	CPA2	High	29	25	1.481	1.199	1.531	1.453
252	peptidyl-prolyl cis-trans isomerase	CPR1	High	51	8	0.871	1.301	0.892	0.792

253	Peptidyl-prolyl cis-trans isomerase C,	CPR3	High	30	4	0.733	1.079	0.896	0.843
254	peptidyl-prolyl cis-trans isomerase D	CPR5	High	32	5	1.24	1.139	0.906	0.857
255	Peptidyl-prolyl cis-trans isomerase CPR6	CPR6	High	29	10	1.06	1.158	1.185	1.711
256	carboxypeptidase S	CPS1	High	8	5	1.274	1.237	0.962	0.784
257	Exportin-1	CRM1	High	13	12	0.856	0.987	1.11	0.919
258	coronin-like protein	CRN1	High	6	3	0.892	1.205	1.668	1.197
259	Cruciform DNA-recognizing protein 1	CRP1	High	21	7	0.878	0.979	1.038	1.523
260	importin alpha re-exporter	CSE1	High	7	6	1.05	0.992	1.242	1.059
261	phosphatidyl inositol transfer protein CSR1	CSR1	High	11	3	1.026	0.85	1.118	1.193
262	Copper transport protein 86	CTR86	High	6	3	1.053	1.109	1.179	1.344
263	RNA polymerase-associated protein CTR9	CTR9	High	8	7	0.931	1.121	1.112	1.033

264	Endochitinase	CTS1	High	6	3	1.61	1.053	1.078	0.881
265	catalase T	CTT1	Medium	2	1	2.286	1.625	3.051	7.027
266	ubiquitin-binding protein CUE5	CUE5	High	10	2	0.927	1.071	1.153	0.711
267	Copper metallothionein	CUP1-2; CUP1-1	High	31	1	0.472	0.857	0.572	0.718
268	Protein cwh43	CWH43	High	2	2	1.016	0.938	1.1	0.983
269	Cytochrome c iso-1	CYC1	High	38	6	1.453	1.655	0.96	1.075
270	General transcriptional corepressor CYC8	CYC8	High	2	2	1.163	0.83	1.085	0.944
271	Mitochondrial presequence protease	CYM1	High	1	1	2.797	0.907	1.653	1.537
272	Cystathionine gamma-lyase	CYS3	High	25	7	1.193	1.012	1.08	0.877
273	Cystathionine beta-synthase	CYS4	High	67	29	0.89	0.968	1.087	1.182
274	Cytochrome c1, heme protein,	CYT1	High	37	7	1.031	1.066	1.165	0.701

275	dihydroxyacetone kinase 1	DAK1	High	32	12	1.088	1.258	1.078	1.558
276	ATP-dependent RNA helicase DBP10	DBP10	High	4	3	0.833	1.144	0.883	0.805
277	ATP-dependent RNA helicase dbp2	DBP2	High	26	11	0.901	0.818	0.707	0.793
278	ATP-dependent RNA helicase dbp3	DBP3	High	15	6	0.987	0.928	1.011	0.89
279	ATP-dependent RNA helicase dbp5	DBP5	High	37	13	1.196	0.942	1.29	0.918
280	ATP-dependent RNA helicase DBP6	DBP6	High	6	3	0.869	1.032	0.732	0.421
281	ATP-dependent RNA helicase DBP8	DBP8	Medium	3	1	1.321	0.738	1.372	100
282	ATP-dependent RNA helicase dbp9	DBP9	High	11	5	0.877	0.968	0.908	0.896
283	m7GpppN-mRNA hydrolase	DCP2	High	2	2	1.261	1.098	1.302	1.724
284	M7GpppX diphosphatase	DCS1	High	8	2	1.926	5.668	0.942	0.872
285	Diphosphoinositol polyphosphate phosphohydrolase DDP1	DDP1	High	15	2	0.85	1.004	1.018	0.9

286	ATP-dependent RNA helicase ded1	DED1	High	50	23	0.97	0.878	1.118	1.058
287	Asparagine--tRNA ligase, cytoplasmic	DED81	High	33	17	0.989	0.967	1.124	1.23
288	RNA polymerase II degradation	DEF1	High	10	5	0.837	1.061	1.097	1.34
289	DER1-like family member protein	DFM1	High	10	2	0.834	1.376	0.829	0.816
290	ATP-dependent RNA helicase DHH1	DHH1	High	22	9	1.053	0.926	1.243	0.999
291	vacuolar protein-sorting-associated protein 46	DID2	High	9	2	0.986	1.013	1.003	1.33
292	DOA4-independent degradation protein 4	DID4	High	4	1	0.654	0.942	0.854	1.06
293	dimethyladenosine transferase	DIM1	High	11	3	0.927	0.756	1.109	1.24
294	U3 small nucleolar RNA-associated	DIP2	High	7	5	0.993	0.948	0.788	0.855
295	Exosome complex exonuclease dis3	DIS3	High	5	4	0.929	0.949	0.922	1.314
296	D-lactate dehydrogenase [cytochrome] 1,	DLD1	High	9	4	1.349	1.165	1.336	0.834

297	D-2-hydroxyglutarate--pyruvate transhydrogenase DLD2	DLD2	High	6	2	0.989	1.164	0.886	0.689
298	D-2-hydroxyglutarate--pyruvate transhydrogenase DLD3	DLD3	High	5	2	1.138	1.136	1.108	1.017
299	DNA replication ATP-dependent helicase/nuclease	DNA2	Medium	0	1	1.131	0.01	1.464	4.901
300	Phospholipid-transporting ATPase DNF1	DNF1	High	2	2	0.01	0.124	0.891	0.86
301	Dynamin-related protein DNM1	DNM1	High	8	5	1.653	1.153	0.923	0.538
302	Protein DOA1	DOA1	High	3	1	0.585	100	100	0.01
303	2-deoxyglucose-6-phosphate phosphatase 1	DOG1	High	9	2	0.552	1.138	1.414	0.52
304	protein DOM34	DOM34	High	3	1	1.039	1.194	1.248	1.267
305	Protein dopey	DOP1	High	1	1	1.134	0.931	0.89	0.564
306	Diphthine methyl ester synthase	DPH5	High	10	3	1.004	0.934	1.341	1.158
307	sphingosine-1-phosphate lyase	DPL1	High	13	6	1.497	1.212	1.299	0.973

308	dolichol-phosphate mannosyltransferase	DPM1	High	40	9	1.133	1.018	1.067	0.798
309	Aspartate--tRNA ligase, cytoplasmic	DPS1	High	56	30	1.032	1.076	1.055	1.076
310	Fe-S cluster assembly protein	DRE2	Medium	3	1	1.26	1.006	1.342	1.588
311	ATP-dependent RNA helicase DRS1	DRS1	High	12	8	0.897	0.918	0.981	1.223
312	endo-1,3(4)-beta-glucanase 1	DSE4	High	1	1	1.057	0.832	0.868	1.115
313	transcription elongation factor S-II	DST1	High	7	2	1.048	0.924	1.324	1.482
314	D-aminoacyl-tRNA deacylase	DTD1	High	7	1	0.873	0.951	0.939	1.379
315	Cys-Gly metallodipeptidase dug1	DUG1	High	23	8	1.075	0.956	1.121	0.976
316	DNA damage response protein	DUN1	High	4	1			0.01	0.01
317	DASH complex subunit DUO1	DUO1	Medium	5	1	0.01			0.111
318	tRNA-dihydrouridine(47) synthase [NAD(P)(+)]	DUS3	High	5	2	0.933	0.929	0.993	0.913

319	deoxyhypusine synthase	DYS1	High	32	10	1.016	1.28	1.161	1.218
320	rRNA-processing protein EBP2	EBP2	High	9	4	1.405	0.98	0.881	0.913
321	Protein EBS1	EBS1	Medium	2	1				
322	Heat shock protein SSC3,	ECM10	High	12	1	0.93	0.7	1.051	1.169
323	Putative metallocarboxypeptidase ECM14	ECM14	Low	3	1	0.01	1.848	0.487	0.01
324	Probable ATP-dependent RNA helicase	ECM16	High	4	3	0.94	1.433	0.766	0.817
325	Protein ECM25	ECM25	High	5	2	2.329	9.362	0.834	0.143
326	Proteasome component ECM29	ECM29	High	5	6	1.401	1.185	1.138	1.225
327	Cell wall protein Ecm33	ECM33	High	10	4	1.217	0.929	1.097	0.988
328	Glutathione S-transferase omega-like 2	ECM4	High	9	2	8.026	7.394	2.73	1.216
329	Enhancer of mRNA-decapping protein	EDC3	High	5	2	1.065	0.905	1.133	0.903

330	EH domain-containing and endocytosis	EDE1	High	1	1	0.96	0.937	1.01	0.917
331	Elongation factor 1-beta	EFB1	High	30	4	0.897	0.803	0.556	0.729
332	rRNA-processing protein EFG1	EFG1	High	6	1	0.657	0.971	0.942	1.564
333	Protein-lysine N-methyltransferase EFM1	EFM1	High	3	1	1.003	1.328	0.01	0.01
334	protein EFR3	EFR3	High	1	1	0.931	0.864	1.281	0.01
335	Elongation factor 2	EFT2; EFT1	High	64	52	1.059	0.922	1.072	1.051
336	Nascent polypeptide-associated complex subunit	EGD1	High	55	4	1.039	1.149	0.596	0.177
337	Nascent polypeptide-associated complex subunit	EGD2	High	34	5	1.156	0.837	0.972	1.094
338	Protein EGT2	EGT2	Low	3	1	0.803	7.617	0.886	1.059
339	Medium-chain fatty acid ethyl	EHT1	High	11	4	0.774	0.707	0.971	0.662
340	Elongation of fatty acids	ELO1	High	3	1	1.025	1.295	1.131	1.33

341	elongator complex protein 2	ELP2	High	7	4	1.001	1.015	1.125	1.304
342	elongator complex protein 3	ELP3	High	2	1	0.565	1.063	0.876	0.332
343	ER membrane protein complex	EMC1	High	5	2	1.248	1.046	1.13	0.659
344	ER membrane protein complex	EMC2	High	16	4	1.163	0.959	1.024	0.963
345	ER membrane protein complex	EMC4	High	5	1	1.021	0.865	1.011	0.891
346	ER membrane protein complex	EMC5	High	24	3	0.949	0.984	1.005	1.197
347	Ribosomal RNA small subunit	EMG1	High	31	6	1.137	1.233	0.763	0.966
348	Putative glucokinase-2	EMI2	High	19	8	0.94	1.248	1.012	0.938
349	Endosomal protein P24B	EMP24	High	14	2	1.322	1.048	0.968	0.493
350	Protein EMP47	EMP47	High	10	3	1.308	1.024	0.956	0.957
351	Transmembrane 9 superfamily member	EMP70	High	3	2	0.707	1.176	0.756	0.539

352	Essential for maintenance of	EMW1	High	5	3	1.059	0.917	1.09	1.148
353	Sodium transport ATPase 5	ENA5	High	4	4	0.948	0.764	1.007	0.771
354	Enolase 1	ENO1	High	56	11	0.838	0.801	0.833	0.768
355	Enolase 2	ENO2	High	63	17	0.86	0.812	1.047	0.659
356	Essential nuclear protein 1	ENP1	High	26	10	1.075	0.912	1.057	0.993
357	epsin-1	ENT1	High	4	1	0.945	1.098	1.05	0.723
358	epsin-2	ENT2	High	7	3	1.062	1.012	1.056	1.117
359	Epsin-3	ENT3	High	14	5	0.791	1.124	0.777	0.899
360	epsin-5	ENT5	High	3	1	1.082	0.928	1.072	1.213
361	ER-retained PMA1-suppressing protein 1	EPS1	Low	1	1	10.376	0.814	1.258	1.302
362	Ribosome biogenesis protein ERB1	ERB1	High	12	7	0.836	0.971	0.979	1.232

363	squalene monooxygenase	ERG1	High	4	2	0.367	0.629	0.258	0.162
364	acetyl-CoA acetyltransferase	ERG10	High	44	12	1.378	0.883	1.329	0.893
365	lanosterol 14-alpha demethylase	ERG11	High	16	6	0.775	0.937	0.783	0.378
366	mevalonate kinase	ERG12	High	6	2	1.432	1.517	0.947	1.012
367	Hydroxymethylglutaryl-CoA synthase	ERG13	High	37	12	0.909	1.118	1.063	1.021
368	C-8 sterol isomerase	ERG2	High	13	2	0.95	1.078	1.033	0.621
369	Farnesyl pyrophosphate synthase	ERG20	High	34	10	1.132	0.919	1.207	1.066
370	Methylsterol monooxygenase	ERG25	High	6	1		1	0.01	0.01
371	sterol-4-alpha-carboxylate 3-dehydrogenase, decarboxylating	ERG26	High	3	1				
372	3-keto-steroid reductase	ERG27	High	17	5	0.971	0.997	0.939	0.659
373	Ergosterol biosynthetic protein 28	ERG28	High	16	2	0.826	1.101	0.786	0.835

374	Delta(7)-sterol 5(6)-desaturase	ERG3	High	4	1	0.579	1.406	0.897	0.442
375	Delta(24(24(1)))-sterol reductase	ERG4	High	12	6	0.956	1.422	0.843	0.433
376	Cytochrome P450 61	ERG5	High	8	4	0.893	1.224	0.587	0.349
377	Sterol 24-C-methyltransferase	ERG6	High	47	16	1.035	0.944	1.157	0.637
378	lanosterol synthase	ERG7	High	2	1	0.709	1.225	0.856	0.01
379	squalene synthase	ERG9	High	19	8	1.107	1.012	1.104	1.153
380	Endoplasmic oxidoreductin-1	ERO1	High	10	5	0.958	0.872	1.148	1.322
381	Protein ERP1	ERP1	High	16	3	0.983	0.888	1.138	0.985
382	Protein ERP2	ERP2	High	5	1	1.067	1.316	1.082	0.869
383	Protein ERP3	ERP3	Low	3	1	2.589	1.09	0.01	2.665
384	Enolase-related protein 1	ERR2; ERR1	Low	2	1	0.797	1.009	1.182	1.359

385	ER-derived vesicles protein ERV14	ERV14	High	8	1	0.798	1.026	0.821	0.458
386	FAD-linked sulfhydryl oxidase ERV2	ERV2	High	7	1	0.862	0.84	0.904	0.104
387	Endoplasmic reticulum vesicle protein	ERV25	High	14	2	1.016	1.011	0.769	0.533
388	ER-derived vesicles protein ERV29	ERV29	High	20	4	0.863	1.14	1.099	1.089
389	ER-derived vesicles protein ERV41	ERV41	Low	3	1	1.351	0.918	1.688	0.945
390	ER-derived vesicles protein ERV46	ERV46	High	8	3	0.891	0.874	1.092	0.871
391	EST/SMG-like protein 2	ESL2; YKR096W	High	1	1	1	1	0.439	0.052
392	Peptidyl-prolyl cis-trans isomerase ESS1	ESS1	High	16	2	1.19	1.241	0.993	1.04
393	Enoyl-[acyl-carrier-protein] reductase, mitochondrial	ETR1	Medium	3	1	1.34	1.061	0.956	0.123
394	Enhancer of translation termination	ETT1	High	8	3	0.933	1.015	0.925	0.849
395	glucan 1,3-beta-glucosidase I/II	EXG1	High	25	8	0.865	0.936	0.702	0.842

396	Long-chain-fatty-acid--CoA ligase 1	FAA1	High	30	15	1.01	0.895	1.311	0.991
397	Long-chain-fatty-acid--CoA ligase 4	FAA4	High	9	5	0.998	1.192	1.059	0.618
398	Fatty acid synthase subunit	FAS1	High	45	75	1.021	0.957	1.083	0.922
399	Fatty acid synthase subunit	FAS2	High	53	85	0.965	1.013	1.08	1.142
400	Very long-chain fatty acid	FAT1	High	2	1	0.932	0.878	1.069	1.059
401	fructose-bisphosphate aldolase	FBA1	High	58	18	0.786	0.885	0.914	0.641
402	MICOS complex subunit Mic60	FCJ1; MIC60	High	27	10	1.117	0.929	1.18	0.566
403	Purine-cytosine permease FCY2	FCY2	Medium	2	1	0.568	0.753	0.01	0.241
404	Elongation of fatty acids	FEN1; ELO2	High	7	2	0.661	1.09	0.848	0.795
405	Hsp70 nucleotide exchange factor	FES1	High	3	1	1.135	1.004	1.285	0.603
406	Iron transport multicopper oxidase	FET3	High	12	4	0.671	0.881	0.743	0.368

407	Iron transport multicopper oxidase	FET5	High	5	2	0.876	0.857	0.672	0.75
408	mitochondrial fission 1 protein	FIS1	High	5	1	1.085	1.151	0.93	1.164
409	1,3-beta-glucan synthase component FKS1	FKS1	High	20	15	0.77	0.985	0.746	0.532
410	Flavin carrier protein 2	FLC2	High	2	2	0.749	0.893	0.724	0.847
411	fluconazole resistance protein 1	FLR1	High	6	3	35.224	100	1.416	
412	uncharacterized mitochondrial membrane protein	FMP10	High	7	1	1.023	0.784	1.25	1.052
413	uncharacterized mitochondrial hydrolase FMP41	FMP41	High	15	2	1.452	1.121	1.449	0.33
414	SUR7 family protein FMP45	FMP45	High	5	1	100	0.01		100
415	Protein FMP52, mitochondrial	FMP52	High	13	2	1.323	1.063	0.981	0.619
416	DNA replication fork-blocking protein	FOB1	High	2	1	0.147	1.443	0.01	0.01
417	Peroxisomal hydratase-dehydrogenase-epimerase	FOX2	High	3	2	100	1.465	100	100

418	FK506-binding protein 1	FPR1	High	49	4	0.609	0.865	0.672	0.614
419	FK506-binding nuclear protein	FPR3	High	25	8	0.816	1.055	1.019	1.272
420	FK506-binding protein 4	FPR4	High	19	5	0.807	0.932	1.027	1.211
421	Fumarate reductase 1	FRD1; YEL047C	High	22	9	1.204	1.12	1.022	1.139
422	Ferric/cupric reductase transmembrane component	FRE1	High	2	1	100	100	100	100
423	fatty acid repression mutant	FRM2	High	6	1	100	100	100	100
424	Phenylalanine--tRNA ligase beta subunit	FRS1	High	37	15	1.1	0.904	1.197	1.102
425	Phenylalanine--tRNA ligase alpha subunit	FRS2	High	24	9	1.264	0.832	1.023	1.01
426	Probable mitochondrial transport protein	FSF1	High	5	1	0.635	1.027	1.049	0.459
427	Family of serine hydrolases	FSH1	High	13	3	1.453	1.071	1.389	0.85
428	plasma membrane iron permease	FTR1	High	10	3	0.694	1.1	0.933	0.737

429	Uridine permease	FUI1	Medium	2	1	0.306	0.777	0.01	0.01
430	fumarate hydratase, mitochondrial	FUM1	High	18	7	1.143	0.873	1.186	1.377
431	Eukaryotic translation initiation factor	FUN12	High	20	16	0.964	0.968	1.131	1.361
432	uracil phosphoribosyltransferase	FUR1	High	37	8	0.976	0.983	1.158	1.032
433	GPI transamidase component GAA1	GAA1	High	3	1	1.472	0.829	1.889	0.933
434	glutamate decarboxylase	GAD1	High	6	3	0.924	0.956	1.073	1.928
435	H/ACA ribonucleoprotein complex subunit	GAR1	High	6	1	3.493	0.276	0.75	2.356
436	1,3-beta-glucanosyltransferase gas1	GAS1	High	20	12	1.021	1.016	1.051	0.77
437	Probable 1,3-beta-glucanosyltransferase GAS3	GAS3	High	13	5	1.002	1.074	0.931	0.626
438	1,3-beta-glucanosyltransferase GAS5	GAS5	High	10	3	0.757	1.315	0.918	0.864
439	Single-strand telomeric DNA-binding protein	GBP2	High	6	2	1.124	1.395	0.87	0.349

440	Translation initiation factor eIF-2B	GCD1	High	6	3	0.879	0.973	1.804	1.139
441	tRNA (adenine(58)-N(1))-methyltransferase non-catalytic subunit	GCD10	High	4	1	0.925	0.997	1.267	1.007
442	Eukaryotic translation initiation factor	GCD11	High	35	13	0.971	1.006	1.084	1.112
443	Translation initiation factor eIF-2B	GCD6	High	9	6	1.109	1.209	1.265	0.959
444	Translation initiation factor eIF-2B	GCD7	High	3	1	0.952	0.916	0.993	1.126
445	eIF-2-alpha kinase activator GCN1	GCN1	High	27	59	1.062	0.939	1.07	0.912
446	protein GCN20	GCN20	High	8	5	1.564	0.814	1.001	0.904
447	ADP-ribosylation factor GTPase-activating protein	GCS1	High	7	2	0.255	100	1.039	0.247
448	Aminomethyltransferase, mitochondrial	GCV1	High	10	3	0.798	0.8	0.429	0.445
449	Glycine dehydrogenase (Decarboxylating), mitochondrial	GCV2	High	11	7	1.045	1.038	0.443	0.44
450	Glycine cleavage system H	GCV3	High	22	2	0.766	1.222	0.586	0.403

451	Glycerol 2-dehydrogenase (NADP(+))	GCY1	High	22	3	0.846	0.902	0.996	0.971
452	guanosine-diphosphatase	GDA1	High	11	3	1.224	0.925	1.183	0.379
453	glycogen debranching enzyme	GDB1	Medium	1	1	1.548	1.092	0.886	1.475
454	Glycerophosphocholine phosphodiesterase Gde1	GDE1	High	3	3	0.914	0.992	0.898	0.619
455	NADP-specific glutamate dehydrogenase 1	GDH1	High	68	25	0.875	0.878	0.997	0.758
456	NAD-specific glutamate dehydrogenase	GDH2	High	20	19	1.919	1.06	1.064	1.266
457	Rab GDP-dissociation inhibitor	GDI1	High	23	8	1.088	0.997	1.063	1.152
458	ARF guanine-nucleotide exchange factor	GEA2	High	1	1	1.342	100	100	0.332
459	Golgi to ER traffic	GET1	High	11	2	0.983	0.869	0.882	0.813
460	Golgi to ER traffic	GET2	High	13	2	0.914	0.85	1.047	0.499
461	ATPase get3	GET3	High	17	6	1.088	1.208	1.274	1.066

462	Golgi to ER traffic	GET4	High	4	1	1.541	1.085	0.716	0.744
463	Glutamine--fructose-6-phosphate aminotransferase [isomerizing]	GFA1	High	29	15	1.043	0.859	1.184	1.214
464	ADP-ribosylation factor-binding protein GGA1	GGA1	High	4	2	1.15	1.453	1.307	0.968
465	ADP-ribosylation factor-binding protein GGA2	GGA2	High	10	5	1.149	0.909	1.065	0.914
466	Mitochondrial GTP/GDP carrier protein	GGC1	High	32	8	1.166	0.917	0.986	0.734
467	Zinc finger protein GIS2	GIS2	High	20	2	0.927	1.771	0.825	0.827
468	1,4-alpha-glucan-branching enzyme	GLC3	High	5	3	1.052	1.257	1.112	1.191
469	Serine/threonine-protein phosphatase PP1-2	GLC7	High	33	6	1.083	0.939	1.044	1.01
470	Glucokinase-1	GLK1	High	43	16	1.246	1.379	0.947	1.359
471	Glutamine synthetase	GLN1	High	24	8	0.975	0.855	0.66	0.714
472	glutamine--tRNA ligase	GLN4	High	35	25	0.956	0.957	1.139	1.12

473	lactoylglutathione lyase	GLO1	High	3	1	0.893	0.925	0.978	2.397
474	Hydroxyacyl glutathione hydrolase, cytoplasmic isozyme	GLO2	Medium	4	1	1.029	0.836	1.109	0.861
475	ADP-ribosylation factor GTPase-activating protein	GLO3	High	6	2	0.642	0.894	1.018	1.231
476	glutathione reductase	GLR1	High	26	10	1.484	1.428	1.238	1.272
477	Glutamate synthase [NADH]	GLT1	High	15	22	0.991	0.842	1.029	0.851
478	Low specificity L-threonine aldolase	GLY1	High	42	12	1.047	0.947	0.938	1.29
479	6-phosphogluconate dehydrogenase, decarboxylating 1	GND1	High	64	20	1.251	1.641	1.018	1.158
480	6-phosphogluconate dehydrogenase, decarboxylating 2	GND2	High	23	2	100	100	1.305	100
481	high-affinity glutamine permease	GNP1	High	3	1	1.283	3.992	0.204	0.058
482	Glyoxylate reductase 1	GOR1	High	7	2	9.202	1.152	100	2.18
483	Golgi SNAP receptor complex	GOS1	High	11	2	1.039	1.102	1.095	0.896

484	Guanine nucleotide-binding protein alpha-1	GPA1	High	10	3	0.977	0.946	1.177	0.866
485	Glycerol-3-phosphate dehydrogenase [NAD(+)] 1	GPD1	High	14	4	1.001	1.253	1.299	1.645
486	Glycerol-3-phosphate dehydrogenase [NAD(+)] 2,	GPD2	High	15	3	1.057	0.968	0.922	1.078
487	glycogen phosphorylase	GPH1	High	27	19	0.845	1.01	0.817	0.908
488	GPI transamidase component GPI17	GPI17	High	10	4	0.728	1.314	1.211	0.511
489	Phosphoglycerate mutase 1	GPM1	High	58	17	0.786	0.923	0.836	1.009
490	glycerol-3-phosphate O-acyltransferase 2	GPT2	High	9	6	1.658	1.95	1.581	1.517
491	Glutathione peroxidase-like peroxiredoxin 2	GPX2	High	31	3	8.566	100	2.093	3.186
492	NADPH-dependent methylglyoxal reductase GRE2	GRE2	High	16	4	5.617	7.648	4.123	10.065
493	NADPH-dependent aldose reductase GRE3	GRE3	High	37	10	1.13	1.396	1.341	2.039
494	Glycine--tRNA ligase 1, mitochondrial	GRS1	High	47	28	1.112	1.08	1.233	1.063

495	Glutaredoxin-2, mitochondrial	GRX2	High	26	3	2.127	3.218	1.624	1.962
496	Monothiol glutaredoxin-3	GRX3	High	14	3	1.391	1.014	0.763	0.654
497	monothiol glutaredoxin-4	GRX4	High	10	2	0.923	1.126	0.632	0.62
498	1,3-beta-glucan synthase component GSC2	GSC2	High	12	4	0.695	0.989	0.718	0.567
499	Glucose-signaling factor 2	GSF2	High	42	14	1.101	0.877	1.182	0.817
500	Glutamate--cysteine ligase	GSH1	High	3	2	1.439	1.666	1.487	1.402
501	glutathione synthetase	GSH2	High	11	4	1.304	1.117	1.401	1.185
502	GTP-binding nuclear protein GSP2/CNR2	GSP2	High	33	8	0.788	1.047	0.948	1.154
503	Glycogen [starch] synthase isoform	GSY1	High	4	1			0.01	0.01
504	Glycogen [starch] synthase isoform	GSY2	High	18	9	1.047	1.12	1.145	1.196
505	Protein GTS1	GTS1	High	3	1	1.11	1.009	1.174	1.588

506	Glutathione S-transferase 1	GTT1	High	14	3	1.205	0.982	1.128	2.206
507	Glutathione S-transferase 2	GTT2	Low	5	1	100	100	100	100
508	Glutathione transferase 3	GTT3	Low	3	1	1.404	0.68	1.568	1.226
509	GMP synthase [glutamine-hydrolyzing]	GUA1	High	46	20	0.95	0.976	1.206	1.07
510	guanylate kinase	GUK1	High	33	6	0.665	1.022	0.952	0.522
511	Glutamate--tRNA ligase, cytoplasmic	GUS1	High	47	31	1.028	1.008	1.066	1.189
512	Glycerol-3-phosphate dehydrogenase, mitochondrial	GUT2	High	16	10	1.632	0.959	1.227	0.866
513	Protein GVP36	GVP36	High	40	9	1.025	1.026	1.026	1.119
514	GPI-anchored wall transfer protein	GWT1	High	2	1		10.962	0.01	0.01
515	Inosine triphosphate pyrophosphatase	HAM1	High	12	2	1.082	1.662	1.129	0.644
516	ATP-dependent RNA helicase HAS1	HAS1	High	20	9	0.918	0.851	0.924	1.211

517	Putative nitroreductase HBN1	HBN1	High	30	5	14.815	12.07	3.268	3.94
518	elongation factor 1 alpha-like	HBS1	High	3	1	1.762	1.204	1.904	1.421
519	ATP-dependent RNA helicase HCA4	HCA4	High	1	1	0.787	0.89	0.918	0.597
520	Hsp90 co-chaperone HCH1	HCH1	High	21	2	0.637	1.442	1.321	1.148
521	Eukaryotic translation initiation factor	HCR1	High	7	2	1.083	0.61	1.15	1.458
522	Heterogeneous nuclear rnp K-like	HEK2	High	22	6	1.018	1.002	1.007	1.199
523	5-aminolevulinate synthase, mitochondrial	HEM1	High	3	1	1.425	1.222	1.171	0.486
524	Oxygen-dependent coproporphyrinogen-III oxidase	HEM13	High	4	1	0.843	1.035	0.85	1.193
525	protoporphyrinogen oxidase	HEM14	High	2	1				
526	Ferrochelatase, mitochondrial	HEM15	High	3	1	100	100	1	0.01
527	Delta-aminolevulinic acid dehydratase	HEM2	High	18	5	1.212	1.036	1.102	1.012

528	porphobilinogen deaminase	HEM3	High	7	2	1.141	0.983	1.357	1.208
529	uroporphyrinogen-III synthase	HEM4	High	4	1	1.001	1.275	0.937	0.421
530	HMG2-induced ER-remodeling protein 1	HER1	Low	1	1	0.756	1.025	1.242	1.191
531	Fatty aldehyde dehydrogenase HFD1	HFD1	High	5	2	1.273	0.77	0.272	1.089
532	Protein HGH1	HGH1	High	10	3	1.158	1.062	1.219	1.278
533	histone H4	HHF1; HHF2	High	55	10	0.882	0.835	0.75	0.764
534	Histone H1	HHO1	High	9	2	1.149	0.826	1.345	1.017
535	Histone H3	HHT2; HHT1	High	17	3	0.81	0.766	0.86	0.832
536	ATP phosphoribosyltransferase	HIS1	High	30	6	0.837	0.893	0.953	0.54
537	histidine biosynthesis trifunctional protein	HIS4	High	9	5	0.67	0.731	0.489	0.392
538	imidazole glycerol phosphate synthase	HIS7	High	20	9	1.136	1.256	0.878	0.65

539	Protein HLJ1	HLJ1	Medium	4	1	0.981	1.081	1.414	1.511
540	protein HMF1	HMF1	High	37	3	0.822	0.932	0.683	0.599
541	3-hydroxy-3-methylglutaryl-coenzyme A reductase 1	HMG1	High	1	1	0.876	0.88	1.136	0.907
542	High mobility group protein	HMO1	High	5	1	0.679	100	0.919	0.365
543	protein arginine N-methyltransferase 1	HMT1	High	11	3	1.108	1.026	0.735	0.99
544	Hit family protein 1	HNT1	High	41	4	1.034	1.427	0.848	0.463
545	mitogen-activated protein kinase hog1	HOG1	High	20	5	1.202	1.382	1.05	1.093
546	Aspartate-semialdehyde dehydrogenase	HOM2	High	42	12	1.197	0.885	1.089	0.994
547	Aspartokinase	HOM3	High	15	6	1.063	0.955	1.274	0.956
548	Homoserine dehydrogenase	HOM6	High	59	19	1.009	0.998	1.019	0.941
549	Glycerol-1-phosphate phosphohydrolase 2	HOR2; GPP2	High	29	2	0.795	0.845	1.108	1.52

550	Histone deacetylase HOS3	HOS3	Medium	1	1	0.712	0.846	1.168	1.082
551	Histone promoter control protein	HPC2	Low	2	1				
552	Hypoxanthine-guanine phosphoribosyltransferase	HPT1	High	43	7	0.731	0.818	0.467	0.384
553	Protein HRI1	HRI1	High	49	9	0.747	0.997	0.823	1.078
554	Nuclear polyadenylated RNA-binding protein	HRP1	High	10	3	1.098	0.801	1.209	1.319
555	casein kinase I homolog	HRR25	High	2	1	1.562	1.372	1.227	0.923
556	ATP-dependent molecular chaperone HSC82	HSC82	High	50	10	1.021	1.057	1.175	1.413
557	10 kDa heat shock	HSP10	High	28	2	8.381	1.433	0.102	0.887
558	heat shock protein 104	HSP104	High	46	37	1.291	1.313	1.9	3.761
559	heat shock protein 26	HSP26	High	54	8	2.937	1.274	1.69	9.802
560	30 kDa heat shock	HSP30	High	22	4	100		100	100

561	heat shock protein 42	HSP42	High	22	5	1.935	0.954	2.278	3.023
562	heat shock protein 60,	HSP60	High	54	31	1.29	0.961	1.455	1.301
563	Heat shock protein 78,	HSP78	High	13	8	1.143	1.359	1.433	2.011
564	ATP-dependent molecular chaperone HSP82	HSP82	High	49	8	1.052	1.234	1.266	2.281
565	Histone H2A.2	HTA2	High	35	4	1.179	0.734	0.345	0.489
566	Histone H2B.1	HTB1	High	40	6	0.83	0.804	0.846	0.848
567	Histidine--tRNA ligase, mitochondrial	HTS1	High	41	18	1.263	1.003	1.077	1.061
568	Histone H2A.Z	HTZ1	High	30	3	0.876	0.881	0.924	1.188
569	Hexokinase-1	HXK1	High	72	28	0.761	1.097	0.879	0.909
570	Hexokinase-2	HXK2	High	55	23	0.904	0.937	0.91	0.968
571	Hexose transporter HXT14	HXT14	Medium	1	1	0.91	0.901	1.181	1.482

572	High-affinity glucose transporter HXT2	HXT2	High	14	5	0.699	0.963	0.587	0.452
573	High-affinity hexose transporter HXT6	HXT6	High	31	1	0.726	1.138	0.704	0.383
574	High-affinity hexose transporter HXT7	HXT7	High	31	4	0.51	0.951	0.709	0.629
575	Eukaryotic translation initiation factor	HYP2	High	54	8	0.953	0.869	0.88	0.805
576	Glutathione peroxidase-like peroxiredoxin HYR1	HYR1	High	8	1	0.867	1.08	1.175	1.216
577	isocitrate lyase	ICL1	High	8	4	2.217	1.043	1.361	1.36
578	Intermediate cleaving peptidase 55	ICP55	Low	2	1				
579	Isocitrate dehydrogenase [NAD] subunit	IDH1	High	38	12	1.234	0.984	1.304	1.242
580	Isocitrate dehydrogenase [NAD] subunit	IDH2	High	35	9	1.26	1.009	1.351	1.485
581	isopentenyl-diphosphate delta-isomerase	IDI1	High	13	3	1.105	1.26	0.886	0.973
582	Isocitrate dehydrogenase [NADP], mitochondrial	IDP1	High	61	20	0.976	0.905	0.962	0.977

583	Isocitrate dehydrogenase [NADP] cytoplasmic	IDP2	High	12	1	100	0.341	0.75	100
584	Very-long-chain 3-oxoacyl-CoA reductase	IFA38	High	18	5	1.175	0.989	0.983	0.711
585	Elongator complex protein 1	IKI3	High	2	2	0.731	1.094	1.003	0.582
586	isoleucine--tRNA ligase, cytoplasmic	ILS1	High	37	36	0.9	1.009	1.053	1.076
587	Threonine dehydratase, mitochondrial	ILV1	High	30	10	1.266	1.438	1.068	0.56
588	Acetolactate synthase catalytic subunit,	ILV2	High	20	10	1.092	0.953	1.504	1.115
589	Dihydroxy-acid dehydratase, mitochondrial	ILV3	High	44	15	0.883	0.918	1.008	1.075
590	ketol-acid reductoisomerase, mitochondrial	ILV5	High	53	15	0.993	1.065	0.767	0.687
591	Acetolactate synthase small subunit,	ILV6	High	31	6	1.1	0.815	0.924	0.576
592	Inosine-5'-monophosphate dehydrogenase 3	IMD3	High	32	5	1.108	0.949	1.132	0.812
593	Inosine-5'-monophosphate dehydrogenase 4	IMD4	High	24	3	0.927	1.016	1.234	1.132

594	54S ribosomal protein IMG1,	IMG1	High	6	1	1.128	1.146	0.996	0.887
595	54S ribosomal protein IMG2,	IMG2	Medium	8	1	0.746	1.019	1.32	1.078
596	Golgin IMH1	IMH1	Medium	1	1	1.079	1.265	0.825	1.062
597	Mitochondrial outer membrane protein	IML2	High	2	1	0.812	1.067	0.892	0.325
598	U3 small nucleolar ribonucleoprotein	IMP3	High	14	2	0.666	1.101	0.891	0.924
599	inositol-3-phosphate synthase	INO1	High	39	16	1.632	0.829	0.744	1.115
600	Putative DNA helicase ino80	INO80	High	1	1	1.035	1.116	1.385	1.442
601	Phosphatidylinositol 4,5-bisphosphate 5-phosphatase INP51	INP51	Low	2	1	1		100	
602	Polyphosphatidylinositol phosphatase INP53	INP53	High	4	3	0.991	0.981	1.068	1.319
603	ISWI one complex protein	IOC3	High	1	1	0.685	100	0.684	0.281
604	pre-rRNA-processing protein IPI3	IPI3	High	4	2	0.935	0.879	0.962	1.278

605	Inorganic pyrophosphatase	IPP1	High	76	18	0.922	1.103	1.062	0.81
606	Inhibitory regulator protein IRA1	IRA1	High	0	1	0.734	1.017	0.994	0.312
607	Benzil reductase ((S)-benzoin forming)	IRC24	High	4	1	0.901	1.151	1.233	1.244
608	cohesin subunit SCC3	IRR1	High	1	1	0.708	1.189	1.003	0.586
609	IMP-specific 5'-nucleotidase 1	ISN1	High	2	1	1.134	0.794	1.489	1.316
610	Increased sodium tolerance protein	IST2	High	12	8	0.916	1.197	1.103	0.885
611	iron sulfur cluster assembly	ISU1	High	7	1	1.213	100	100	2.29
612	ISWI chromatin-remodeling complex ATPase	ISW1	High	8	5	0.902	1.211	1.07	1.074
613	iswi chromatin-remodeling complex atpase	ISW2	High	3	1				
614	myo-inositol transporter 1	ITR1	High	7	2	0.248	0.607	0.01	0.01
615	Protein IVY1	IVY1	High	2	1				

616	ADIPOR-like receptor IZH2	IZH2	High	3	1				
617	Importin subunit beta-2	KAP104	High	4	3	1.105	0.989	1.18	0.851
618	Importin beta-like protein KAP120	KAP120	High	1	1	0.913	1.202	1.025	0.561
619	Importin beta-like protein KAP122	KAP122	High	2	2	1.022	0.835	1.015	0.928
620	Importin subunit beta-4	KAP123	High	37	31	1.148	0.948	1.361	1.061
621	Importin subunit beta-1	KAP95	High	6	4	1.412	1.062	0.853	0.628
622	78 kDa glucose-regulated protein	KAR2	High	27	18	1.119	0.877	1.247	1.109
623	Inositol hexakisphosphate kinase 1	KCS1	High	1	1	1.005	1.037	0.798	0.535
624	Kelch repeat-containing protein 3	KEL3	High	2	1	0.844	0.928	1.252	1.245
625	Oxysterol-binding protein homolog 4	KES1	High	27	9	0.954	0.985	1.127	1.072
626	2-oxoglutarate dehydrogenase, mitochondrial	KGD1	High	28	20	1.136	1.026	1.019	1.046

627	Dihydrolipoyl lysine-residue succinyltransferase component of	KGD2	High	20	6	0.995	1.02	1.16	0.983
628	Glycolipid 2-alpha-mannosyltransferase	KRE2	High	19	6	0.794	0.959	0.846	0.531
629	RNA cytidine acetyltransferase	KRE33	High	11	9	0.824	0.881	0.992	0.795
630	Killer toxin-resistance protein 5	KRE5	High	1	1	1.393	10.613	0.835	0.01
631	beta-glucan synthesis-associated protein KRE6	KRE6	High	8	4	0.86	1.003	1.117	0.796
632	Protein Kri1	KRI1	High	4	2	0.721	1.012	0.866	1.05
633	KRR1 small subunit processome	KRR1	High	12	3	0.956	1.113	0.98	1.115
634	lysine--tRNA ligase, cytoplasmic	KRS1	High	44	24	1.068	0.995	1.176	1.314
635	Alpha-1,2 mannosyltransferase KTR1	KTR1	High	23	8	0.87	0.827	0.804	0.398
636	Probable mannosyltransferase KTR3	KTR3	High	9	3	1.03	1.014	1.031	0.857
637	Mannosyltransferase KTR6	KTR6	High	2	1	0.925	0.662	0.955	0.01

638	AP-1 accessory protein LAA1	LAA1	High	1	1	1	8.13	0.388	0.01
639	sphingosine N-acyltransferase lag1	LAG1	Low	6	1	0.01	1.504	8.113	1.137
640	Leukotriene A-4 hydrolase homolog	LAP2	High	8	4	1.126	1.185	1.201	1.078
641	Cysteine proteinase 1, mitochondrial	LAP3	High	25	9	1.024	1.622	0.761	1.429
642	Proline-rich protein LAS17	LAS17	High	2	1	0.954	0.846	1.132	1.406
643	Dihydrolipoyllysine-residue acetyltransferase component of	LAT1	High	15	7	1.053	1.2	1.231	0.99
644	serine palmitoyltransferase 1	LCB1	High	5	2	1.076	0.994	0.982	0.674
645	Serine palmitoyltransferase 2	LCB2	High	7	3	0.917	0.982	1.1	0.998
646	Protein LDB19	LDB19	Medium	1	1	0.974	0.963	0.77	1.205
647	alkylphosphocholine resistance protein LEM3	LEM3	High	5	2	0.798	1.089	1.119	0.794
648	3-isopropylmalate dehydratase	LEU1	High	27	14	0.912	1.166	1.012	1.013

649	2-isopropylmalate synthase	LEU4	High	23	7	1.249	1.104	1.211	1.123
650	2-isopropylmalate synthase 2, mitochondrial	LEU9	High	9	1	1.177	0.887	1.044	1.391
651	La protein homolog	LHP1	High	10	2	1.155	1.058	1.038	0.508
652	Deoxyhypusine hydroxylase	LIA1	High	31	8	0.81	0.75	0.881	0.762
653	Ceramide synthase subunit LIP1	LIP1	High	18	2	1.438	1.037	0.962	0.392
654	Dihydrolipoyl dehydrogenase, mitochondrial	LPD1	High	71	34	0.991	0.996	0.917	1.257
655	LAS seventeen-binding protein 3	LSB3	High	5	2	0.938	1.16	1.29	0.855
656	LAS seventeen-binding protein 5	LSB5	High	4	1		1.387	0.01	
657	Succinate--CoA ligase [ADP-forming] subunit	LSC1	High	46	11	1.016	0.884	1.22	0.948
658	Succinate--CoA ligase [ADP-forming] subunit	LSC2	High	41	12	1.057	1.067	0.953	0.875
659	Large subunit GTPase 1	LSG1	High	7	4	0.929	0.866	1.215	1.065

660	U6 snRNA-associated Sm-like protein	LSM2	High	36	3	1.075	0.898	0.67	0.402
661	U6 snRNA-associated Sm-like protein	LSM4	High	10	2	1.641	1.446	1.316	1.712
662	Sphingolipid long chain base-responsive	LSP1	High	39	10	1.088	1.071	1.158	1.287
663	Protein LTV1	LTV1	High	2	1	0.491	1.444	100	2.097
664	Saccharopine dehydrogenase [NAD(+), L-lysine-forming]	LYS1	High	15	4	1.452	1.474	0.907	1.393
665	Homoisocitrate dehydrogenase, mitochondrial	LYS12	High	14	4	1.387	0.962	1.161	1.07
666	L-2-aminoadipate reductase	LYS2	High	10	10	1.176	1.116	1.231	1.5
667	homocitrate synthase, cytosolic isozyme	LYS20	High	45	4	6.961	4.911	3.148	2.185
668	Homocitrate synthase, mitochondrial	LYS21	High	35	1	1.229	1.51	1.059	0.645
669	Homoaconitase, mitochondrial	LYS4	High	2	1	1.23	1.369	1.078	1.169
670	Saccharopine dehydrogenase [NADP(+), L-glutamate-forming]	LYS9	High	9	3	1.381	1.459	1.003	0.834

671	N-alpha-acetyltransferase, 35 NatC auxiliary	MAK10	Medium	1	1				
672	Protein MAK11	MAK11	High	18	7	0.835	0.999	0.975	1.287
673	Protein MAK16	MAK16	High	20	5	0.854	0.823	0.88	0.935
674	Ribosome biogenesis protein MAK21	MAK21	High	8	7	0.951	1.084	1.054	0.705
675	Protein MAM3	MAM3	High	2	1				
676	Mitochondrial acidic protein MAM33	MAM33	High	6	1	1.358	0.898	1.209	0.928
677	Methionine aminopeptidase 1	MAP1	High	10	4	0.919	0.976	1.089	1.178
678	methionine aminopeptidase 2	MAP2	High	5	2	1.328	1.206	0.986	1.223
679	mitochondrial-processing peptidase subunit beta	MAS1	High	6	3	1.031	0.967	1.135	1.345
680	Mitochondrial-processing peptidase subunit alpha	MAS2	High	4	1	1.044	0.958	3.223	0.753
681	multiprotein-bridging factor 1	MBF1	High	38	5	1.168	1.005	1.299	1.774

682	Metacaspase-1	MCA1	High	8	2	0.728	1	0.239	0.01
683	GPI ethanolamine phosphate transferase	MCD4	High	2	2	0.893	1.118	0.943	0.579
684	protein kinase MCK1	MCK1	High	29	9	0.89	0.998	0.912	0.963
685	DNA replication licensing factor	MCM2	High	4	3	0.873	0.943	1.049	1.326
686	DNA replication licensing factor	MCM3	High	1	1	0.893	0.927	0.974	0.945
687	NADH-cytochrome b5 reductase 2	MCR1	High	30	7	1.195	1.072	1.046	0.961
688	Malate dehydrogenase, mitochondrial	MDH1	High	69	17	1.168	0.926	1.371	1.016
689	Malate dehydrogenase, cytoplasmic	MDH2	High	3	1	0.879	1.085	1.742	1.135
690	Malate dehydrogenase, peroxisomal	MDH3	High	31	9	1.201	1.084	0.8	0.977
691	DnaJ homolog 1, mitochondrial	MDJ1	High	3	1				
692	ATP-dependent permease MDL2, mitochondrial	MDL2	High	2	1				

693	N-terminal acetyltransferase B complex	MDM20	High	1	1	1.049	0.902	1	0.956
694	Mitochondrial distribution and morphology	MDM38	High	26	11	1.128	1.134	1.272	0.956
695	Midasin	MDN1	High	3	13	0.947	1.034	0.852	0.42
696	Negative regulator of sporulation	MDS3	Low	1	1	0.01	1	0.01	0.976
697	Ubiquitin-like protein MDY2	MDY2	Medium	5	1	1.288	0.871	1.306	1.178
698	Methionine--tRNA ligase, cytoplasmic	MES1	High	28	18	1.001	0.977	1.186	1.121
699	methylenetetrahydrofolate reductase 1	MET12	High	4	2	1.348	0.349	0.86	1.732
700	DNA repair/transcription protein MET18/MMS19	MET18	High	2	2	0.93	1.054	1.097	1.315
701	5-methyltetrahydropteroyltriglutamate--homocysteine methyltransferase	MET6	High	61	38	0.712	0.779	0.755	0.788
702	folylpolyglutamate synthase	MET7	High	6	2	0.316	0.728	0.558	2.375
703	S-methyl-5'-thioadenosine phosphorylase	MEU1	High	3	1	0.773	1.049	0.915	0.763

704	mRNA export factor mex67	MEX67	High	2	1				
705	GrpE protein homolog, mitochondrial	MGE1	High	4	1	1.023	0.926	0.896	1.59
706	Mitochondrial genome maintenance protein	MGM101	High	10	2	1.131	0.779	0.963	0.651
707	Mitochondrial homologous recombination protein	MHR1	High	11	2	1.077	0.886	1.102	0.989
708	Mitochondrial intermembrane space import	MIA40	High	25	5	0.877	1.197	1.206	0.994
709	mitochondrial phosphate carrier protein	MIR1	High	50	15	1.167	0.955	1.059	0.688
710	C-1-tetrahydrofolate synthase, mitochondrial	MIS1	High	16	12	1.132	0.924	1.129	1.104
711	protein MLP1	MLP1	Medium	1	1	100	0.907	1.28	1.415
712	Malate synthase 1, glyoxysomal	MLS1	Medium	2	1	100	1.263	0.894	0.01
713	Protein mmf1, mitochondrial	MMF1	High	48	5	1.1	0.985	0.99	1.139
714	E3 ubiquitin-protein ligase linker	MMS1	Medium	1	1	8.768	1.659	1	0.217

715	Probable alpha-1,6-mannosyltransferase MNN10	MNN10	High	3	1	0.852	0.895	0.982	1.134
716	probable alpha-1,6-mannosyltransferase MNN11	MNN11	High	9	2	1.114	1.002	1.107	0.986
717	Alpha-1,2-mannosyltransferase MNN2	MNN2	High	12	5	0.841	0.805	1.051	0.84
718	Alpha-1,2-mannosyltransferase MNN5	MNN5	High	20	7	0.997	1.054	0.942	0.654
719	Mannan polymerase complexes subunit	MNN9	High	3	1	1.158	1.128	0.907	0.365
720	CBK1 kinase activator protein	MOB2	High	5	1	0.784	9.74	0.762	0.393
721	Protein MON2	MON2	High	1	1	0.793	1.219	1.097	1.22
722	MICOS complex subunit Mic10	MOS1; MIC10	High	34	3	1.064	0.949	1.045	0.892
723	TATA-binding protein-associated factor MOT1	MOT1	High	0	1	100	6.814	0.392	0.105
724	Mitochondrial peculiar membrane protein	MPM1	High	5	1	2.195	9.892	0.42	0.01
725	Multiple RNA-binding domain-containing protein	MRD1	High	6	4	0.795	0.895	0.662	0.949

726	Protein MRH1	MRH1	High	18	2	0.541	1.061	0.909	1.077
727	methylthioribose-1-phosphate isomerase	MRI1	High	23	6	1.035	1.27	0.903	0.893
728	37S ribosomal protein MRP1,	MRP1	High	9	2	1.106	1.038	1.26	1.364
729	37S ribosomal protein MRP13,	MRP13	High	10	2	1.258	0.996	0.964	1.031
730	54S ribosomal protein L2,	MRP7	High	4	1	0.981	0.831	0.979	1.026
731	Uncharacterized protein MRP8	MRP8	High	28	4	1.294	1.465	0.976	0.819
732	54S ribosomal protein L1,	MRPL1	High	14	2	1.727	1.087	1.069	0.228
733	54S ribosomal protein L11,	MRPL11	High	8	1	1.164	1.012	1.489	1.013
734	54S ribosomal protein L15,	MRPL15	Medium	4	1	0.817	0.969	1.134	0.703
735	54S ribosomal protein L17,	MRPL17	High	5	1	100	100	13.413	1.866
736	54S ribosomal protein L19,	MRPL19	Medium	13	1	1.213	1.169	1.034	0.32

737	54S ribosomal protein L24,	MRPL24	High	4	1	0.01	0.733	100	5.717
738	54S ribosomal protein L27,	MRPL27	High	9	1	1.233	1.106	0.86	1.056
739	54S ribosomal protein L38,	MRPL38	High	10	1	1.151	0.771	0.982	1.21
740	54S ribosomal protein L51,	MRPL51	High	7	1	0.01	1		0.109
741	37S ribosomal protein S17,	MRPS17	High	5	1	1.682	100	1.147	1.096
742	37S ribosomal protein S9,	MRPS9	High	8	2	1.019	0.883	1.14	1.394
743	Rab proteins geranylgeranyltransferase component	MRS6	High	3	2	0.884	0.824	1.081	1.124
744	Ribosome assembly factor mrt4	MRT4	High	16	3	0.954	0.807	0.891	0.837
745	Morphogenesis-related protein MSB1	MSB1	Medium	1	1	100	100	0.4	0.01
746	Meiotic sister chromatid recombination	MSC1	High	5	2	1.453	1.367	2.158	6.978
747	Meiotic sister-chromatid recombination protein	MSC6	High	4	2	1.537	4.808	0.782	0.174

748	Putative aldehyde dehydrogenase-like protein	MSC7	High	5	2	1.177	0.732	0.787	0.813
749	Protein msn5	MSN5	High	6	5	0.831	1.131	1.021	0.924
750	ATP-dependent RNA helicase MSS116,	MSS116	High	14	8	1.103	0.922	0.941	1.079
751	Protein MSS51, mitochondrial	MSS51	High	14	5	1.005	1.045	1.157	0.876
752	Maintenance of telomere capping	MTC1	High	21	8	1.162	0.912	1.267	1.245
753	Methylenetetrahydrofolate dehydrogenase [NAD(+)]	MTD1	High	23	5	0.75	0.631	0.342	0.348
754	ATP-dependent RNA helicase DOB1	MTR4	High	5	4	0.814	0.822	0.515	0.56
755	high-affinity methionine permease	MUP1	Medium	1	1	0.646	1.125	0.397	1.376
756	Diphosphomevalonate decarboxylase	MVD1	High	24	5	0.862	1.167	0.996	0.991
757	peptide methionine sulfoxide reductase	MXR1	Medium	4	1	0.543	1.494	0.976	0.715
758	myosin-2	MYO2	High	11	12	0.928	1.013	1.078	0.98

759	Myosin-3	MYO3	High	5	2	1.07	1.116	0.996	1.172
760	Myosin-4	MYO4	High	3	1	100	6.745	0.6	0.01
761	Myosin-5	MYO5	High	8	4	1.02	0.78	1.178	0.934
762	nuclear polyadenylated rna-binding protein	NAB2	High	7	2	1.01	0.811	0.982	1.011
763	Nuclear polyadenylated RNA-binding protein	NAB3	High	3	2	1.548	0.899	1.037	1.22
764	ATP-dependent helicase NAM7	NAM7	High	3	2	1.161	0.861	10.14	100
765	NET1-associated nuclear protein 1	NAN1	High	11	7	0.951	0.872	1.058	0.854
766	nucleosome assembly protein	NAP1	High	31	7	0.923	1.098	1.186	0.954
767	probable 26S proteasome regulatory	NAS6	High	15	3	1.037	1.083	0.967	1.225
768	N-terminal acetyltransferase A complex	NAT1	High	13	9	0.875	0.855	0.953	1.118
769	Putative N-terminal acetyltransferase 2	NAT2	High	5	1	0.96	1.098	1.127	0.849

770	Nuclear control of ATPase	NCA2	High	4	2	1.286	0.547	1.333	0.557
771	Non-classical export protein 2	NCE102	High	16	2	1.038	1.03	1.957	2.413
772	Carbonic anhydrase	NCE103	High	43	7	4.968	1.757	7.923	6.379
773	Multisite-specific tRNA:(cytosine-C(5))-methyltransferase	NCL1	High	20	10	0.899	1.048	0.997	0.879
774	NADPH--cytochrome P450 reductase	NCP1	High	22	11	1.15	0.947	1.146	0.829
775	External NADH-ubiquinone oxidoreductase 1,	NDE1	High	34	15	0.919	0.872	1.124	0.845
776	Rotenone-insensitive NADH-ubiquinone oxidoreductase, mitochondrial	NDI1	High	15	6	1.044	0.998	0.976	0.672
777	[NU+] prion formation protein	NEW1	High	21	17	0.919	0.888	1.129	1.15
778	Cysteine desulfurase, mitochondrial	NFS1	High	10	4	1.212	1.271	1.19	1.613
779	NifU-like protein, mitochondrial	NFU1	Medium	5	1	1.248	1.202	1.093	0.964
780	H/ACA ribonucleoprotein complex subunit	NHP2	High	24	3	0.829	0.866	0.791	0.987

781	Non-histone chromosomal protein 6B	NHP6B	High	13	1	1.058	0.819	0.929	1.233
782	nucleoporin NIC96	NIC96	High	5	4	1.194	1.152	1.235	0.98
783	NGG1-interacting factor 3	NIF3	High	40	8	0.919	0.978	1.065	1.13
784	Eukaryotic translation initiation factor	NIP1	High	27	18	1.009	0.926	1.038	1.017
785	60S ribosome subunit biogenesis	NIP7	High	5	1	1.06	0.81	0.836	1.151
786	Omega-amidase NIT3	NIT3	High	13	3	1.043	1.158	0.941	0.808
787	Pro-apoptotic serine protease NMA111	NMA111	High	2	2	0.923	0.834	1.07	1.305
788	60S ribosomal export protein	NMD3	High	21	9	0.937	1.014	0.858	0.95
789	nonsense-mediated mRNA decay protein	NMD5	High	2	2	1.266	0.885	1.373	0.809
790	20S-pre-rRNA D-site endonuclease NOB1	NOB1	High	6	2	0.843	0.938	0.84	1.113
791	nucleolar complex protein 2	NOC2	High	14	8	0.887	1.059	0.985	1.153

792	nucleolar complex-associated protein 3	NOC3	High	12	7	1.025	1.1	0.652	1.17
793	Nucleolar GTP-binding protein 1	NOG1	High	12	6	0.747	0.909	0.735	0.854
794	Nucleolar GTP-binding protein 2	NOG2	High	15	6	0.867	0.849	0.804	0.793
795	rRNA 2'-O-methyltransferase fibrillarin	NOP1	High	53	16	1.103	0.708	0.895	0.855
796	H/ACA ribonucleoprotein complex subunit	NOP10	Medium	16	1	0.774	0.636	0.971	0.987
797	Nucleolar protein 12	NOP12	High	14	6	0.892	0.929	0.98	1.134
798	Nucleolar protein 13	NOP13	High	2	1	1.055	0.785	0.968	1.284
799	nucleolar complex protein 14	NOP14	High	7	5	0.796	1.19	0.942	0.732
800	nucleolar protein 16	NOP16	High	10	2	0.903	0.808	0.991	1.197
801	25S rRNA (cytosine(2870)-C(5))-methyltransferase	NOP2	High	14	7	0.91	1.002	1.062	1.27
802	Nucleolar protein 4	NOP4	High	9	4	0.821	0.63	0.956	1.208

803	Nucleolar protein 56	NOP56	High	50	20	0.988	0.868	0.96	0.806
804	Nucleolar protein 58	NOP58	High	35	15	0.954	0.953	0.913	0.941
805	Nucleolar protein 6	NOP6	High	11	1	0.862	0.99	1.484	1.047
806	Pescadillo homolog	NOP7	High	17	7	0.935	1.161	0.846	1.025
807	Nucleolar protein 9	NOP9	High	3	2	0.787	0.858	1.077	1.17
808	General negative regulator of	NOT3	High	8	4	0.999	1.222	1.002	0.774
809	GPN-loop GTPase 1	NPA3	High	10	3	1.131	0.96	1.177	0.487
810	Phosphatidyl glycerol/pho sphatidylino sitol transfer protein	NPC2	High	6	1	1.063	0.844	0.96	1.322
811	Nucleolar protein 3	NPL3	High	9	3	1.117	0.879	1.136	1.235
812	Chromatin structure-remodeling complex subunit	NPL6	High	4	1	0.947	1.208	1.111	1.514
813	nicotinate phosphoribo syltransferas e	NPT1	High	15	6	1.005	0.927	0.935	0.913

814	Transaldolase NQM1	NQM1	High	10	2		10.677	100	100
815	Ribosome biogenesis protein NSA1	NSA1	High	8	3	1.24	1.003	1.064	1.287
816	Non-structural maintenance of chromosome	NSE4	Medium	2	1	0.748	0.856	1.301	1.059
817	Nuclear localization sequence-binding protein	NSR1	High	42	17	0.855	0.919	0.774	0.968
818	Protein N-terminal amidase	NTA1	High	2	1	0.575	1.22	1.134	0.815
819	nuclear transport factor 2	NTF2	High	19	2	1.153	1.432	0.642	0.98
820	neutral trehalase	NTH1	High	12	7	1.024	1.03	1.372	1.899
821	mitochondrial nuclease	NUC1	High	4	1	1.022	0.758	2	0.292
822	nuclear GTP-binding protein NUG1	NUG1	High	33	14	0.932	0.88	0.957	0.853
823	Nucleoporin nup120	NUP120	High	1	1	0.52	100	0.437	0.01
824	Nucleoporin NUP133	NUP133	High	5	5	1.547	0.956	1.237	0.942

825	Nucleoporin NUP145	NUP145	High	2	2	1.087	0.896	0.804	1.049
826	Nucleoporin NUP157	NUP157	High	1	1				
827	Nucleoporin NUP170	NUP170	High	1	1	1.541	0.748	1.552	1.133
828	Nucleoporin NUP188	NUP188	High	3	4	0.963	0.973	1.086	1.151
829	Nucleoporin NUP192	NUP192	High	2	3	100	0.765	100	0.01
830	nucleoporin NUP2	NUP2	High	9	5	1.09	0.798	1.093	1.51
831	Nucleoporin NUP57	NUP57	High	2	1	1.007	0.791	1.133	1.159
832	Nucleoporin NUP85	NUP85	High	2	1	1.005	0.967	1.159	1.24
833	Uncharacterized PH domain-containing protein	NVJ2	High	2	1	0.971	0.693	0.378	0.421
834	Mitochondrial oxaloacetate transport protein	OAC1	High	7	2	1.003	0.869	1.259	0.991
835	Putative tyrosine-protein phosphatase OCA1	OCA1	High	7	1	0.706	9.651	0.943	0.01

836	Mitochondrial 2-oxodicarboxylate carrier 1	ODC1	High	3	1	1.166	0.796	0.99	0.802
837	Mitochondrial 2-oxodicarboxylate carrier 2	ODC2	High	10	3	1.107	0.802	1.107	0.783
838	obg-like ATPase 1	OLA1	High	57	18	1.018	0.976	1.081	0.893
839	Acyl-CoA desaturase 1	OLE1	High	21	10	0.486	1.007	0.302	0.39
840	Mitochondrial outer membrane protein	OM14	High	25	2	1.284	1.034	1.107	0.93
841	Mitochondrial outer membrane protein	OM45	High	15	5	2.248	1.005	1.43	1.859
842	Transcriptional repressor OPI1	OPI1	High	3	1	0.89	0.902	0.988	0.876
843	phosphatidyl-N-methylethanolamine N-methyltransferase	OPI3	High	31	4	0.876	0.924	0.805	0.761
844	Protein ORM2	ORM2	High	18	2	1.277	1.153	1.056	0.531
845	Oxysterol-binding protein homolog 7	OSH7	High	4	2	0.86	1.003	1.073	0.737
846	Fumarate reductase 2	OSM1	High	3	1	1.345	1.402	1.257	0.347

847	Dolichyl-diphosphooligosaccharide--protein glycosyltransferase subunit 1	OST1	High	6	2	0.887	1.071	1.114	0.643
848	Dolichyl-diphosphooligosaccharide--protein glycosyltransferase subunit OST2	OST2	High	19	2	0.748	1.271	0.91	0.322
849	Dolichyl-diphosphooligosaccharide--protein glycosyltransferase subunit 3	OST3	High	6	2	1.073	0.792	1.086	0.313
850	Ubiquitin thioesterase OTU1	OTU1	High	7	1		10.91	1	
851	Nadph dehydrogenase 2	OYE2	High	44	16	2.187	1.421	2.029	1.705
852	NADPH dehydrogenase 3	OYE3	High	21	7	17.332	8.76	5.145	6.704
853	Polyamine N-acetyltransferase 1	PAA1	High	37	6	0.905	0.953	0.885	0.543
854	polyadenylate-binding protein, cytoplasmic and	PAB1	High	51	27	1.078	0.959	1.152	1.072
855	RNA polymerase II-associated protein	PAF1	High	6	1	0.732	1.323	1.005	1.496
856	Mitochondrial import inner membrane	PAM16	High	26	2	0.889	1.208	1.042	0.825

857	Presequence translocated-associated motor subunit	PAM17	High	16	2	0.873	0.871	0.956	0.66
858	mitochondrial import inner membrane	PAM18	High	9	1	0.803	0.854	0.79	0.379
859	Actin cytoskeleton-regulatory complex protein	PAN1	High	2	2	0.912	0.846	1.553	2.068
860	PAN2-PAN3 deadenylation complex subunit	PAN3	High	2	1	0.959	0.893	0.851	0.845
861	2-dehydropantoate 2-reductase	PAN5	High	13	4	1.017	0.869	1.19	0.842
862	pantoate--beta-alanine ligase	PAN6	High	3	1	0.967	0.962	1.077	0.9
863	poly(A) polymerase	PAP1	High	3	1	2.89	0.848	0.69	0.219
864	DNA topoisomerase 2-associated protein	PAT1	High	3	2	1.475	0.956	1.213	1.199
865	PAB1-binding protein 1	PBP1	High	2	1	1.032	0.724	1.309	1.281
866	Probable tubulin--tyrosine ligase PBY1	PBY1	High	1	1	0.975	1.164	1.246	1.152
867	phosphoacetylglucosamine mutase	PCM1	High	10	5	1.035	0.982	1.03	1.017

868	peroxisomal-coenzyme A synthetase	PCS60	High	8	4	1.289	0.924	0.917	1.499
869	Pyruvate dehydrogenase E1 component	PDA1	High	44	16	1.124	1.051	1.179	1.032
870	Pyruvate dehydrogenase E1 component	PDB1	High	34	9	1.12	1.008	1.243	0.999
871	pyruvate decarboxylase isozyme 1	PDC1	High	66	23	0.814	0.96	1.08	0.883
872	Pyruvate decarboxylase isozyme 2	PDC5	High	15	1	0.82	0.835	1.367	0.816
873	pyruvate decarboxylase isozyme 3	PDC6	High	17	1	0.739	1.27	1.246	2.35
874	Probable 2-methylcitrate dehydratase	PDH1	High	5	2	1.69	1.198	0.789	1.182
875	Protein disulfide-isomerase	PDI1	High	30	15	1.115	1.041	1.096	1.005
876	Phosphatidyl inositol transfer protein PDR16	PDR16	High	3	1	1.531	1.509	1.564	1.246
877	pleiotropic ABC efflux transporter	PDR5	High	2	4	0.743	1.033	1.143	1.071
878	pyridoxamine 5'-phosphate oxidase	PDX3	High	20	3	0.952	1.045	1.003	1.017

879	saccharopep sin	PEP4	High	30	13	0.923	1.278	0.782	0.815
880	ADP,ATP carrier protein 2	PET9	High	62	27	1.01	0.824	0.973	0.735
881	Peroxisomal membrane protein PMP27	PEX11	High	8	2	1.433	0.866	0.923	1.069
882	peroxisome assembly protein 12	PEX12	High	3	1	1	100	100	0.01
883	peroxisomal membrane protein PEX25	PEX25	High	11	3	0.664	1.045	0.692	0.384
884	Peroxisomal membrane protein PEX30	PEX30	High	7	2	1.364	1.129	1.277	1.299
885	ATP-dependent 6-phosphofruc tokinase subunit alpha	PFK1	High	47	37	0.933	1.024	1.115	1.175
886	ATP-dependent 6-phosphofruc tokinase subunit beta	PFK2	High	34	25	1.007	0.944	1.226	1.249
887	Prospore formation at selected	PFS1	Low	3	1	0.928	0.791	0.994	0.888
888	Profilin	PFY1	High	34	3	0.645	1.304	0.502	0.74
889	Plasma membrane-associated coenzyme Q6	PGA3	High	8	2	1.504	1.115	1.405	0.907

890	glucose-6-phosphate isomerase	PGI1	High	58	26	0.985	1.081	0.919	1.177
891	Phosphoglycerate kinase	PGK1	High	83	38	0.942	1.033	1.112	1.133
892	Phosphoglucomutase 1	PGM1	High	17	5	0.783	1.07	1.196	0.938
893	Phosphoglucomutase 2	PGM2	High	21	7	1.273	1.609	0.971	1.429
894	prohibitin-1	PHB1	High	17	4	1.493	0.875	1.779	0.941
895	Prohibitin-2	PHB2	High	16	4	1.145	1.069	1.125	0.665
896	Acid phosphatase PHO12	PHO12	High	7	1	1.235	1.102	0.479	0.29
897	4-nitrophenylphosphatase	PHO13	High	10	2	0.779	1.206	0.899	0.65
898	Repressible acid phosphatase	PHO5	High	11	3	0.542	0.607	0.71	0.794
899	repressible alkaline phosphatase	PHO8	High	3	1	0.67	0.749	0.714	0.758
900	Phosphate system positive regulatory	PHO81	High	7	6	1.233	0.964	1.102	0.622

901	Inorganic phosphate transporter PHO84	PHO84	High	30	12	0.499	0.915	0.262	0.551
902	Cyclin-dependent protein kinase PHO85	PHO85	High	11	2	1.209	1.033	1.065	1.151
903	inorganic phosphate transporter PHO86	PHO86	High	24	6	1.364	1.167	0.791	0.771
904	SRP-independent targeting protein 3	PHO88	High	55	10	1.074	0.944	1.055	0.792
905	Phosphate permease PHO89	PHO89	High	12	7	0.58	0.375	0.068	0.122
906	Low-affinity phosphate transporter PHO91	PHO91	High	3	2	1.222	0.26	0.678	2.327
907	Very-long-chain (3R)-3-hydroxyacyl-CoA dehydratase PHS1	PHS1	High	6	1	0.772	1.24	0.921	1.532
908	Mitochondrial phosphate carrier protein	PIC2	High	6	2	1.091	1.524	1.669	2.371
909	sphingolipid long chain base-responsive	PIL1	High	40	9	0.908	0.977	1.147	1.06
910	Lon protease homolog, mitochondrial	PIM1	High	9	9	1.286	1.04	1.161	1.406
911	CDP-diacylglycerol--inositol 3-phosphatidyltransferase	PIS1	High	19	3	0.704	1.453	0.913	0.62

912	V-type ATPase assembly factor	PKR1	High	25	2	1.211	0.971	0.969	1.094
913	plasma membrane ATPase 1	PMA1	High	40	40	0.973	1.093	1.24	1.095
914	mannose-6-phosphate isomerase	PMI40	High	23	8	0.895	0.976	1.077	0.913
915	Calcium-transporting atpase 1	PMR1	High	6	5	0.874	0.811	1.196	1.03
916	Dolichyl-phosphate-mannose--protein mannosyltransferase 1	PMT1	High	20	11	0.911	0.998	1.06	0.847
917	dolichyl-phosphate-mannose--protein mannosyltransferase 2	PMT2	High	14	7	0.861	1.062	1.133	0.827
918	Dolichyl-phosphate-mannose--protein mannosyltransferase 4	PMT4	High	6	3	0.732	1.164	0.844	0.5
919	Nicotinamidase	PNC1	High	29	4	1.071	1.589	1.032	1.049
920	pre-rRNA-processing protein PNO1	PNO1	High	22	5	0.842	0.879	0.959	0.535
921	FACT complex subunit pob3	POB3	High	15	6	0.869	0.998	1.162	1.23
922	proliferating cell nuclear antigen	POL30	High	31	7	0.889	0.874	0.919	0.753

923	DNA polymerase V	POL5	High	10	8	0.865	1.003	0.949	1.207
924	nucleoporin Pom152	POM152	High	1	1	0.774	1.144	1.043	0.535
925	Pore membrane protein of	POM33	High	5	1	0.954	1.161	1.29	1.735
926	Nucleoporin POM34	POM34	High	3	1	0.939	0.839	1.406	1.02
927	Mitochondrial outer membrane protein	POR1	High	67	18	1.144	0.876	1.28	0.81
928	leucine carboxyl methyltransferase 1	PPM1	Medium	4	1	1.056	0.848	1.268	1.413
929	Serine/threonine-protein phosphatase T	PPT1	High	6	2	0.88	1.31	0.678	0.656
930	Serine/threonine-protein phosphatase PP-Z1	PPZ1	High	4	1	0.461	12.626	0.01	0.01
931	cerevisin	PRB1	High	10	6	1.106	1.031	1.013	1.611
932	carboxypeptidase Y	PRC1	High	3	2	1.538	1.307	1.056	0.866
933	Saccharolysin	PRD1	High	3	2	0.78	1.264	1.053	0.98

934	Proteasome subunit beta type-4	PRE1	High	24	4	1.434	0.906	1.356	1.148
935	Probable proteasome subunit alpha	PRE10	High	13	3	1.073	0.952	1.09	1.286
936	proteasome subunit beta type-5	PRE2	High	17	4	1.253	0.996	1.171	1.717
937	proteasome subunit beta type-1	PRE3	High	15	3	1.044	1.217	1.209	0.798
938	Proteasome subunit alpha type-6	PRE5	High	47	7	1.308	0.99	1.107	1.41
939	Proteasome subunit alpha type-4	PRE6	High	21	3	1.064	1.181	0.76	0.472
940	Proteasome subunit beta type-6	PRE7	High	17	3	0.957	0.858	0.979	1.338
941	Proteasome subunit alpha type-2	PRE8	High	22	4	1.386	1.006	1.262	1.609
942	Proteasome subunit alpha type-3	PRE9	High	19	4	1.167	1.092	1.1	0.806
943	glutamate 5-kinase	PRO1	High	8	2	1.175	1.263	0.923	0.756
944	Gamma-glutamyl phosphate reductase	PRO2	High	26	8	1.076	1.076	1.208	1.112

945	Pyrroline-5-carboxylate reductase	PRO3	High	10	3	0.806	0.936	1.552	0.91
946	Pre-mRNA-processing factor 19	PRP19	High	5	2				
947	pre-mRNA-splicing factor ATP-dependent RNA	PRP22	Low	1	1	1	1.116	0.01	100
948	Pre-mRNA-splicing ATP-dependent RNA helicase	PRP28	High	2	1	0.516	9.271	0.68	0.17
949	pre-mRNA-splicing factor ATP-dependent RNA	PRP43	High	13	8	1.022	0.909	1.093	0.837
950	Pre-mRNA-processing ATP-dependent RNA helicase	PRP5	Medium	1	1	1.185	1.017	1.27	0.816
951	Pre-mRNA-splicing factor 8	PRP8	High	1	2	0.066	2.121	0.658	0.01
952	ribose-phosphate pyrophosphokinase 1	PRS1	High	9	3	1.021	1.139	1.038	0.924
953	Ribose-phosphate pyrophosphokinase 3	PRS3	High	20	6	1.023	0.928	0.965	1.249
954	ribose-phosphate pyrophosphokinase 4	PRS4	High	3	1	0.878	0.893	1.032	1.213
955	Ribose-phosphate pyrophosphokinase 5	PRS5	High	9	3	1.01	1.027	0.652	0.609

956	Eukaryotic translation initiation factor	PRT1	High	21	14	1.054	0.974	1.229	1.039
957	Peroxiredoxin PRX1, mitochondrial	PRX1	High	39	10	5	4.068	1.193	1.829
958	mannose-1-phosphate guanyltransferase	PSA1	High	47	13	0.854	0.979	1.008	0.786
959	Phosphatidylserine decarboxylase proenzyme 1,	PSD1	High	5	2	0.752	0.964	0.669	0.408
960	Importin subunit beta-3	PSE1	High	12	9	1.109	0.83	0.727	0.5
961	Serine/threonine-protein kinase psk1	PSK1	High	1	1	100	100	0.427	0.01
962	protein PSP2	PSP2	High	2	1	0.99	1	0.317	0.052
963	Protoplast secreted protein 2	PST2	High	29	6	0.469	1.494	0.86	0.957
964	Serine/threonine-protein phosphatase 4 regulatory	PSY2	High	2	2	0.792	1.133	1.04	0.427
965	pre-tRNA-processing protein PTA1	PTA1	Medium	2	1	1.036	1.081	1.181	1.392
966	Protein phosphatase 2C homolog	PTC2	High	11	2	0.929	0.926	1.221	1.879

967	Membrane protein PTM1	PTM1	High	2	1	0.809	0.993	1.05	1.052
968	Peptide transporter PTR2	PTR2	High	2	1	0.495	1.177	0.312	0.01
969	Nuclear and cytoplasmic polyadenylated	PUB1	High	4	2	0.976	0.909	1.208	0.984
970	Pumilio homology domain family	PUF4	High	3	2	0.815	0.865	1	0.648
971	Pumilio homology domain family	PUF6	High	12	8	0.921	0.937	0.855	1.333
972	Protein PUN1	PUN1	High	5	1	1.003	0.97	1.247	1.238
973	proteasome subunit beta type-2	PUP1	High	8	2	1.147	1.025	1.071	1.681
974	Proteasome subunit alpha type-5	PUP2	High	20	5	1.18	0.942	1.185	1.248
975	proteasome subunit beta type-3	PUP3	High	21	3	1.191	1.181	0.91	0.66
976	tRNA pseudouridine synthase 1	PUS1	High	15	7	1.054	1.064	0.962	1.348
977	Multisubstrate pseudouridine synthase 7	PUS7	Medium	2	1	1.098	0.894	0.74	0.916

978	Delta-1-pyrroline-5-carboxylate dehydrogenase, mitochondrial	PUT2	Low	1	1	1.354	0.936	1.273	1.643
979	Periodic tryptophan protein 1	PWP1	High	5	3	0.879	1.12	1.011	1.398
980	Periodic tryptophan protein 2	PWP2	High	4	4	0.915	0.879	1.037	0.868
981	pyruvate carboxylase 1	PYC1	High	34	10	1.762	1.209	1.696	1.914
982	pyruvate carboxylase 2	PYC2	High	31	8	0.783	0.704	0.966	1.036
983	cytochrome b-c1 complex subunit	QCR10	High	26	2	0.976	1.271	0.914	0.609
984	Cytochrome b-c1 complex subunit	QCR2	High	58	22	1.202	0.861	1.223	0.908
985	Cytochrome b-c1 complex subunit	QCR6	High	8	1	1.026	0.946	0.983	0.961
986	Cytochrome b-c1 complex subunit	QCR7	High	35	4	1.231	0.837	0.997	0.656
987	Cytochrome b-c1 complex subunit	QCR8	High	13	1	1.005	1.147	1.006	1.004
988	cytochrome b-c1 complex subunit	QCR9	High	17	1	0.775	0.907	0.835	0.542

989	quinidine resistance protein 2	QDR2	High	4	2	0.57	1.339	1.052	0.996
990	glutamine-dependent NAD(+) synthetase	QNS1	High	8	4	1.287	0.853	1.023	1.339
991	UDP-N-acetylglucosamine pyrophosphorylase	QRI1	High	11	5	0.782	1.05	1.141	0.837
992	UV excision repair protein	RAD23	High	15	4	1.048	1.101	0.936	1.051
993	DNA-binding protein rap1	RAP1	High	4	3	1.092	0.769	1.213	1.025
994	Ras-like protein 2	RAS2	High	18	4	1.143	0.958	1.303	1.208
995	ribosome-interacting GTPase 1	RBG1	High	12	3	0.963	0.954	1.181	0.858
996	Ribosome-interacting GTPase 2	RBG2	High	10	3	0.985	1.094	1.171	0.994
997	Respiratory supercomplex factor 2,	RCF2	High	13	3	0.777	0.852	1.134	1.541
998	Serine/threonine-protein kinase RCK2	RCK2	High	14	6	0.744	0.967	0.948	1.169
999	RNA 3'-terminal phosphate cyclase-like	RCL1	High	10	3	1.076	0.823	0.981	0.977

1000	Rho GDP-dissociation inhibitor	RDI1	High	22	4	1.214	1.022	0.905	1.198
1001	Thiosulfate sulfurtransferase RDL1, mitochondrial	RDL1	High	24	2	0.893	2.017	0.359	0.19
1002	DNA-binding protein REB1	REB1	High	5	3	1.04	1.015	1.109	1.313
1003	Regulation of enolase protein	REE1	High	18	2	1.188	14.588	0.949	0.399
1004	Cytoplasmic 60S subunit biogenesis	REH1	Low	3	1	1.123	0.993	1.102	1.676
1005	Protein RER1	RER1	High	10	1	100	100	0.01	0.01
1006	DNA-directed RNA polymerase III	RET1	High	2	2	0.882	0.926	1.02	0.678
1007	Coatomer subunit delta	RET2	High	7	4	0.934	0.996	1.206	1.161
1008	coatomer subunit zeta	RET3	High	7	1	0.986	0.972	0.967	0.962
1009	Replication factor A protein	RFA1	High	4	2	1.159	0.786	0.967	0.881
1010	Replication factor C subunit	RFC2	High	3	1	1.256	0.799	1.047	0.967

1011	replication factor C subunit	RFC3	High	4	1			0.01	
1012	Replication factor C subunit	RFC5	High	3	1				
1013	Protein RFS1	RFS1	High	20	3	0.597	1.131	0.994	1.075
1014	oligosaccharide translocation protein RFT1	RFT1	Medium	2	1	0.01		0.01	0.01
1015	Respiratory growth induced protein	RGI1	High	25	2	1.241	1.429	1.085	1.613
1016	GTP-binding protein RHO1	RHO1	High	27	7	0.892	0.931	0.986	0.955
1017	GTP-binding protein RHO3	RHO3	High	13	3	0.878	0.8	1.045	0.949
1018	Glycerol-1-phosphate phosphohydrolase 1	RHR2; GPP1	High	43	6	0.662	0.852	0.702	1.103
1019	Ribosome assembly protein 1	RIA1	High	1	1	1.123	0.738	0.996	1.713
1020	GTP cyclohydrolase-2	RIB1	High	5	1	1.176	1.341	1.531	1.286
1021	3,4-dihydroxy-2-butanone 4-phosphate synthase	RIB3	High	16	2	100	100	4.323	1

1022	6,7-dimethyl-8-ribityllumazine synthase	RIB4	High	34	4	0.737	0.818	1.081	0.871
1023	Single-stranded DNA-binding protein RIM1,	RIM1	High	28	3	0.865	0.81	0.873	1.044
1024	Serine/threonine-protein kinase rio2	RIO2	High	6	2	1.02	0.861	1.06	1.51
1025	cytochrome b-c1 complex subunit	RIP1	High	30	4	1.065	1.114	1.531	0.665
1026	Pre-rRNA-processing protein RIX1	RIX1	High	2	1	0.752	1.244	0.404	0.234
1027	ribose-5-phosphate isomerase	RKI1	High	22	5	1.216	0.956	0.952	1.162
1028	E3 ubiquitin-protein ligase listerin	RKR1	High	3	5	1.02	0.575	0.995	1.32
1029	translation initiation factor rli1	RLI1	High	29	15	0.94	1.041	1.04	1.055
1030	Ribosome biogenesis protein rlp24	RLP24	High	5	1	0.819	0.848	0.794	1.052
1031	Ribosome biogenesis protein RLP7	RLP7	High	21	5	0.844	0.984	0.813	0.714
1032	Sporulation protein RMD5	RMD5	Medium	2	1	0.896	0.575	1.21	1.522

1033	Protein RMD9, mitochondrial	RMD9	High	2	1	1.266	1.002	0.912	0.648
1034	54S ribosomal protein RML2,	RML2	High	3	1	100	7.225	0.872	1.034
1035	Protein arginine N-methyltransferase 2	RMT2	High	3	1	0.936	1.143	1.005	1.007
1036	Ran GTPase-activating protein 1	RNA1	High	44	13	0.891	1.049	0.851	0.606
1037	mRNA 3'-end-processing protein rna14	RNA14	High	2	1	0.982	0.979	0.806	0.559
1038	RNA exonuclease 1	RNH70	Medium	3	1	0.01	7.487	1.081	0.778
1039	ribonucleoside-diphosphate reductase large chain	RNR1	High	8	7	0.845	0.822	1.131	0.91
1040	Ribonucleoside-diphosphate reductase small chain	RNR2	High	38	13	1.429	1.265	0.991	1.246
1041	Ribonucleoside-diphosphate reductase small chain	RNR4	High	56	16	1.201	1.419	0.968	1.237
1042	DNA-directed RNA polymerase I	RPA12	High	12	1	0.863	0.843	0.914	1.085
1043	DNA-directed RNA polymerase I	RPA135	High	13	11	0.97	1	1.104	1.002

1044	DNA-directed RNA polymerase I	RPA190	High	22	26	0.998	0.907	1.038	1.214
1045	DNA-directed RNA polymerase I	RPA43	High	15	3	0.935	0.76	1.258	0.985
1046	DNA-directed RNA polymerase I	RPA49	High	20	7	1.178	0.859	1.027	1.045
1047	DNA-directed RNA polymerase II	RPB2	High	15	13	0.999	0.99	0.976	1.112
1048	DNA-directed RNA polymerases I,	RPB5	High	5	1	0.704	0.997	1.08	0.876
1049	DNA-directed RNA polymerase II	RPB7	High	15	2	1.062	0.939	1.064	1.179
1050	DNA-directed RNA polymerases I,	RPB8	High	8	1	0.813	0.851	1.013	0.955
1051	DNA-directed RNA polymerases I	RPC40	High	15	5	1.277	0.947	1.147	1.138
1052	DNA-directed RNA polymerase III	RPC82	High	6	3	1.069	1.019	0.973	1.228
1053	Ribosome production factor 1	RPF1	High	4	1	0.857	0.884	1.168	0.01
1054	Ribosome biogenesis protein RPF2	RPF2	High	5	2	1.081	0.905	0.814	0.646

1055	Eukaryotic translation initiation factor	RPG1	High	37	31	0.938	1.011	1.053	1.173
1056	60S ribosomal protein L10	RPL10	High	50	17	0.945	0.954	0.978	1.129
1057	60S ribosomal protein L11-B	RPL11B	High	53	10	0.894	0.908	0.927	1.163
1058	60S ribosomal protein L12-B	RPL12A; RPL12B	High	65	10	0.772	0.847	0.864	0.44
1059	60S ribosomal protein L13-A	RPL13A	High	52	1	0.468	1.748	0.767	0.285
1060	60S ribosomal protein L13-B	RPL13B	High	52	1	0.44	1.111	0.805	0.348
1061	60S ribosomal protein L14-A	RPL14A	High	46	1	0.917	0.932	0.879	1.171
1062	60S ribosomal protein L14-B	RPL14B	High	46	1	0.968	1.06	1.011	1.4
1063	60S ribosomal protein L15-A	RPL15A	High	37	8	0.902	0.958	0.937	0.896
1064	60S ribosomal protein L16-A	RPL16A	High	42	8	0.92	1.035	1.066	1.354
1065	60S ribosomal protein L16-B	RPL16B	High	43	8	0.886	1.003	0.945	1.211

1066	60S ribosomal protein L17-A	RPL17A	High	51	1	0.997	0.934	1.075	1.129
1067	60S ribosomal protein L17-B	RPL17B	High	51	1	0.948	0.932	0.969	1.202
1068	60S ribosomal protein L18-A	RPL18A; RPL18B	High	41	8	0.957	0.962	0.923	1.093
1069	60S ribosomal protein L19-A	RPL19B; RPL19A	High	42	12	0.856	1.055	0.923	1.126
1070	60S ribosomal protein L1-B	RPL1B; RPL1A	High	46	12	1.068	0.88	0.973	1.119
1071	60S ribosomal protein L20-A	RPL20B; RPL20A	High	46	11	1.037	0.978	1.02	1.157
1072	60S ribosomal protein L21-A	RPL21A	High	48	1	1.072	0.999	0.88	1.158
1073	60S ribosomal protein L21-B	RPL21B	High	48	1	0.996	1.137	0.926	1.115
1074	60S ribosomal protein L22-A	RPL22A	High	47	3	0.464	0.917	0.684	0.911
1075	60S ribosomal protein L23-B	RPL23A; RPL23B	High	46	8	1	0.718	1.039	0.757
1076	60S ribosomal protein L24-A	RPL24A	High	34	2	1.564	0.859	1.331	1.118

1077	60S ribosomal protein L24-B	RPL24B	High	34	1	1.13	0.899	1.38	1.42
1078	60S ribosomal protein L25	RPL25	High	51	10	0.902	0.859	1.113	1.227
1079	60S ribosomal protein L26-A	RPL26A	High	55	2	0.951	0.954	1.062	1.188
1080	60S ribosomal protein L26-B	RPL26B	High	55	3	0.987	1.006	0.938	1.263
1081	60S ribosomal protein L27-A	RPL27A	High	57	10	0.789	1	0.925	1.047
1082	60S ribosomal protein L28	RPL28	High	54	10	0.84	0.851	0.834	0.841
1083	60S ribosomal protein L29	RPL29	Medium	14	1	1.219	0.777	1.218	1.513
1084	60S ribosomal protein L2-B	RPL2A; RPL2B	High	61	15	0.952	0.856	0.977	1.164
1085	60S ribosomal protein L3	RPL3	High	55	28	1.023	0.908	1.117	1.271
1086	60S ribosomal protein L30	RPL30	High	69	8	0.837	1.061	0.917	0.947
1087	60S ribosomal protein L31-A	RPL31A	High	57	1	0.873	0.877	1.001	0.991

1088	60S ribosomal protein L31-B	RPL31B	High	57	1	0.696	0.878	1.206	1.922
1089	60S ribosomal protein L32	RPL32	High	36	6	0.894	0.946	1.016	1.093
1090	60S ribosomal protein L33-A	RPL33A	High	48	2	0.924	1.14	0.908	0.763
1091	60S ribosomal protein L33-B	RPL33B	High	48	2	0.956	1.319	0.93	0.701
1092	60S ribosomal protein L34-B	RPL34B	High	21	2	0.925	0.9	0.81	0.931
1093	60S ribosomal protein L35-A	RPL35B; RPL35A	High	42	9	0.987	1.048	0.947	1.459
1094	60S ribosomal protein L36-A	RPL36A	High	50	2	0.793	0.714	1.147	1.347
1095	60S ribosomal protein L36-B	RPL36B	High	50	2	0.892	0.81	0.888	1.171
1096	60S ribosomal protein L37-A	RPL37A	High	32	3	1.068	0.781	1.194	1.178
1097	60S ribosomal protein L37-B	RPL37B	High	23	2	1.588	1.255	1.314	1.18
1098	60s ribosomal protein l38	RPL38	High	53	6	1.169	0.822	0.957	1.044

1099	60S ribosomal protein L39	RPL39	High	22	2	1.278	0.992	0.843	0.959
1100	60S ribosomal protein L42-A	RPL42A; RPL42B	High	15	2	0.863	0.977	1.017	1.145
1101	60S ribosomal protein L43-B	RPL43A; RPL43B	High	54	9	0.831	1.044	0.894	1.023
1102	60S ribosomal protein L4-A	RPL4A	High	59	2	1.361	0.966	1.5	1.516
1103	60S ribosomal protein L4-B	RPL4B	High	59	2	1.483	0.964	1.318	1.436
1104	60S ribosomal protein L5	RPL5	High	41	10	1.192	0.845	0.916	1.168
1105	60S ribosomal protein L6-A	RPL6A	High	56	5	0.997	1.028	0.939	1.159
1106	60s ribosomal protein l6-b	RPL6B	High	55	4	0.884	1.019	0.976	1.165
1107	60S ribosomal protein L7-A	RPL7A	High	55	1	0.762	0.893	1.046	1.108
1108	60S ribosomal protein L7-B	RPL7B	High	55	1	0.944	0.948	1.062	1.128
1109	60S ribosomal protein L8-A	RPL8A	High	64	5	0.987	1.174	0.972	0.87

1110	60S ribosomal protein L8-B	RPL8B	High	65	6	1.183	0.865	0.974	0.913
1111	60S ribosomal protein L9-A	RPL9A	High	43	9	1.029	0.908	0.982	1.165
1112	Ribonuclease P protein component,	RPM2	High	1	1			0.915	
1113	26S proteasome regulatory subunit	RPN1	High	23	18	1.066	1.143	1.076	1.371
1114	26S proteasome regulatory subunit	RPN10	High	29	7	0.996	0.904	0.933	1.185
1115	Ubiquitin carboxyl-terminal hydrolase RPN11	RPN11	High	26	6	1.34	1.016	1.147	1.161
1116	26S proteasome regulatory subunit	RPN12	High	14	3	1.513	0.991	0.916	0.801
1117	26S proteasome regulatory subunit	RPN13	High	28	4	0.985	1.059	0.817	1.162
1118	26S proteasome regulatory subunit	RPN2	High	19	18	1.199	1.014	1.128	1.382
1119	26S proteasome regulatory subunit	RPN3	High	20	9	0.914	1.091	1.029	1.31
1120	26S proteasome regulatory subunit	RPN5	High	15	7	1.256	0.944	1.057	1.614

1121	26S proteasome regulatory subunit	RPN6	High	24	9	1.15	1.06	1.038	1.244
1122	26S proteasome regulatory subunit	RPN7	High	13	6	1.423	1.013	1.162	1.644
1123	26S proteasome regulatory subunit	RPN8	High	19	4	1.225	1.262	0.958	0.97
1124	26S proteasome regulatory subunit	RPN9	High	25	8	1.262	1.117	0.961	1.28
1125	DNA-directed RNA polymerase II	RPO21	High	8	12	1.149	0.964	1.2	0.97
1126	DNA-directed RNA polymerase III	RPO31	High	1	1		0.01	0.01	100
1127	60S acidic ribosomal protein	RPP0	High	37	13	0.98	0.955	1.054	1.066
1128	60s acidic ribosomal protein	RPP1A	High	8	1	0.956	0.758	0.96	1.041
1129	60S acidic ribosomal protein	RPP1B	High	15	1	0.748	0.875	0.819	0.438
1130	60S acidic ribosomal protein	RPP2B	High	34	3	1.487	0.875	1.075	0.94
1131	40S ribosomal protein S0-A	RPS0A	High	41	7	0.928	0.992	0.858	0.691

1132	40S ribosomal protein S10-B	RPS10B	High	47	5	1.877	0.681	0.793	0.794
1133	40S ribosomal protein S11-A	RPS11B; RPS11A	High	43	7	0.751	1.028	0.92	1.157
1134	40S ribosomal protein S12	RPS12	High	47	7	0.917	0.894	0.876	1.025
1135	40S ribosomal protein S13	RPS13	High	65	11	0.817	0.952	0.924	0.923
1136	40S ribosomal protein S14-B	RPS14B	High	67	11	0.929	0.924	1.012	0.997
1137	40S ribosomal protein S15	RPS15	High	39	4	0.879	0.781	1.021	0.992
1138	40S ribosomal protein S16-B	RPS16B; RPS16A	High	60	11	0.91	0.932	0.971	0.937
1139	40S ribosomal protein S17-B	RPS17B	High	64	11	0.943	1.052	0.902	0.93
1140	40S ribosomal protein S18-A	RPS18B; RPS18A	High	64	14	0.959	0.858	1.027	0.95
1141	40S ribosomal protein S19-A	RPS19A	High	60	10	0.838	1.006	0.949	0.827
1142	40S ribosomal protein S1-A	RPS1A	High	71	6	1.027	0.918	1.059	1.047

1143	40S ribosomal protein S1-B	RPS1B	High	68	5	1.008	0.932	1.049	1.06
1144	40S ribosomal protein S2	RPS2	High	50	11	0.891	0.898	1.041	0.92
1145	40S ribosomal protein S20	RPS20	High	49	9	0.884	1.027	1.006	1.093
1146	40S ribosomal protein S21-B	RPS21B	High	74	6	0.907	0.957	0.828	0.979
1147	40S ribosomal protein S22-A	RPS22A	High	68	8	0.969	0.84	0.854	0.939
1148	40S ribosomal protein S23-A	RPS23B; RPS23A	High	26	4	0.82	0.94	0.881	1.143
1149	40S ribosomal protein S24-A	RPS24A; RPS24B	High	53	10	0.961	0.928	0.932	0.961
1150	40S ribosomal protein S25-A	RPS25A	High	34	5	0.916	0.923	0.888	1.015
1151	40S ribosomal protein S26-B	RPS26B	High	30	3	0.863	1.009	0.888	0.873
1152	40S ribosomal protein S27-B	RPS27B	High	18	2	0.872	0.747	0.98	1.146
1153	40S ribosomal protein S28-A	RPS28A	High	42	4	0.691	0.988	0.908	0.743

1154	40S ribosomal protein S29-A	RPS29A	High	32	2	1.307	0.759	0.99	1.156
1155	40S ribosomal protein S29-B	RPS29B	High	32	2	1.095	0.918	1.051	1.163
1156	40S ribosomal protein S3	RPS3	High	70	20	1.09	0.921	1.07	0.97
1157	40S ribosomal protein S30-B	RPS30B; RPS30A	High	16	1	1.723	0.684	1.621	1.371
1158	Ubiquitin-40S ribosomal protein S31	RPS31	High	53	8	0.752	0.887	0.896	1.015
1159	40S ribosomal protein S4-A	RPS4B; RPS4A	High	62	20	1.08	0.906	1.007	1.128
1160	40S ribosomal protein S5	RPS5	High	39	12	0.922	0.877	1.012	1.032
1161	40S ribosomal protein S6-B	RPS6B; RPS6A	High	61	18	0.972	0.901	1.126	1.11
1162	40S ribosomal protein S7-A	RPS7A	High	52	7	1	0.969	0.847	0.451
1163	40S ribosomal protein S7-B	RPS7B	High	56	5	0.945	0.944	0.867	0.728
1164	40S ribosomal protein S8-A	RPS8B; RPS8A	High	47	9	0.838	0.943	1.027	0.981

1165	40S ribosomal protein S9-A	RPS9A	High	53	1	0.968	1.07	0.945	1.217
1166	40S ribosomal protein S9-B	RPS9B	High	52	1	0.931	1.005	1.001	1.218
1167	26S proteasome regulatory subunit	RPT1	High	26	9	1.224	1.003	1.194	1.51
1168	26S proteasome regulatory subunit	RPT2	High	15	5	1.426	1.023	1.463	1.535
1169	26S proteasome regulatory subunit	RPT3	High	14	5	0.931	1.001	0.916	1.217
1170	26S proteasome subunit RPT4	RPT4	High	19	6	1.259	1.144	1.069	0.88
1171	26S proteasome regulatory subunit	RPT5	High	28	8	1.517	0.996	1.076	0.989
1172	26S proteasome regulatory subunit	RPT6	High	30	8	1.331	0.992	1.149	1.479
1173	Ribosome assembly protein RRB1	RRB1	High	9	3	1.13	1.071	1.232	0.754
1174	Ribosomal RNA-processing protein 1	RRP1	High	21	4	0.976	0.938	0.928	1.225
1175	Ribosomal RNA-processing protein 12	RRP12	High	11	10	1.144	0.965	0.86	0.906

1176	Ribosomal RNA-processing protein 14	RRP14	High	6	2	0.868	0.881	1.005	1.608
1177	ATP-dependent rRNA helicase RRP3	RRP3	High	5	2	1.153	0.948	1.159	0.629
1178	Exosome complex component Rrp4	RRP4	Medium	3	1	0.76	0.929	0.912	1.414
1179	exosome complex component RRP40	RRP40	High	16	2	0.896	1.287	1.093	0.806
1180	Exosome complex component RRP42	RRP42	High	6	1				
1181	rRNA biogenesis protein RRP5	RRP5	High	27	37	0.812	0.924	0.924	0.912
1182	Exosome complex exonuclease rrp6	RRP6	High	2	1	1.206	0.887	0.955	1.561
1183	25S rRNA (adenine(645)-N(1))-methyltransferase	RRP8	High	4	1	4.247	100	0.684	0.139
1184	Chromatin structure-remodeling complex subunit	RSC2	High	2	2		100	100	
1185	Chromatin structure-remodeling complex protein	RSC6	High	7	2	0.852	1.155	1.009	0.827
1186	Chromatin structure-remodeling complex protein	RSC8	High	7	3	1.249	1.009	0.927	0.489

1187	Chromatin structure-remodeling complex subunit	RSC9	Medium	2	1	1.092	1.104	0.842	0.326
1188	37S ribosomal protein S10,	RSM10	High	9	1	1.08	1.328	0.927	0.764
1189	37S ribosomal protein S23,	RSM23	High	6	2	0.828	0.91	1.075	0.981
1190	Uncharacterized protein RSN1	RSN1	High	5	3	1.018	1.071	0.921	0.73
1191	E3 ubiquitin-protein ligase RSP5	RSP5	High	10	5	1.062	1.077	1.034	1.159
1192	Ras-related protein RSR1	RSR1	High	7	2	0.984	0.833	0.889	1.081
1193	Restriction of telomere capping	RTC3	High	10	1				100
1194	RNA polymerase-associated protein RTF1	RTF1	High	6	3	0.801	1.291	0.967	0.746
1195	Retrograde regulation protein 2	RTG2	High	8	3	1.016	1.431	1.109	0.85
1196	Reticulon-like protein 1	RTN1	High	61	14	0.873	1.035	0.927	0.813
1197	Reticulon-like protein 2	RTN2	High	10	2		100	100	100

1198	Serine/threonine-protein phosphatase 2A 56	RTS1	High	1	1	0.928	0.861	1.256	0.647
1199	Regulator of Ty1 transposition	RTT103	Low	2	1	2.592	4.388	1.818	2.872
1200	RuvB-like protein 1	RVB1	High	24	8	0.996	0.925	1.196	1.028
1201	RuvB-like protein 2	RVB2	High	10	4	1.193	0.893	1.129	1.214
1202	Reduced viability upon starvation	RVS161	High	21	4	1.014	0.882	0.795	0.676
1203	Reduced viability upon starvation	RVS167	High	14	5	1.065	0.969	1.349	0.963
1204	Phosphoinositide phosphatase SAC1	SAC1	High	39	17	1.177	0.949	1.121	0.743
1205	fimbrin	SAC6	High	40	20	1.036	1.01	1.097	1.158
1206	Adenosylhomocysteinase	SAH1	High	45	24	0.701	0.841	0.89	1.128
1207	S-adenosylmethionine synthase 1	SAM1	High	56	6	0.831	0.742	0.921	0.899
1208	S-adenosylmethionine synthase 2	SAM2	High	66	11	0.85	0.891	1.05	0.906

1209	S-adenosylmethionine permease SAM3	SAM3	High	2	1	0.665	0.923	0.671	0.01
1210	Homocysteine S-methyltransferase 2	SAM4	High	10	3	0.963	1.022	0.894	1.252
1211	SIT4-associating protein SAP190	SAP190	High	2	2	0.939	0.968	1.394	1.208
1212	transcriptional regulatory protein SAP30	SAP30	Low	7	1	1.022	1.018	0.907	1.405
1213	Small COPII coat GTPase	SAR1	High	52	7	1.233	0.922	1.127	0.726
1214	Something about silencing protein	SAS10	High	4	2	1.085	0.86	1.076	1.486
1215	Co-chaperone protein SBA1	SBA1	High	20	3	1.023	1.207	0.813	1.042
1216	Protein transport protein SBH2	SBH2	High	15	1	0.774	0.836	0.731	0.647
1217	Single-stranded nucleic acid-binding protein	SBP1	High	33	9	1.16	1.017	0.943	1.128
1218	protein SCD6	SCD6	High	4	1	0.776	0.525	1.409	1.502
1219	dnaJ-related protein SCJ1	SCJ1	High	6	2	0.59	0.971	0.614	0.653

1220	Proteasome subunit alpha type-1	SCL1	High	27	6	1.128	1.184	1.159	1.554
1221	Protein SCP160	SCP160	High	32	33	1.021	0.911	1.345	1.191
1222	Vesicle-associated membrane protein-associated protein	SCS2	High	40	10	0.953	0.976	1.14	1.013
1223	Ceramide very long chain	SCS7	High	4	1	0.255	0.678	0.51	0.087
1224	Glycerol-3-phosphate O-acyltransferase 1	SCT1	Medium	1	1				
1225	probable family 17 glucosidase	SCW4	High	13	4	1.22	1.105	1.072	0.892
1226	protein sda1	SDA1	High	4	2	1.002	1.179	0.827	0.771
1227	Succinate dehydrogenase [ubiquinone] flavoprotein	SDH1	High	23	10	1.123	0.867	1.292	0.904
1228	Succinate dehydrogenase [ubiquinone] iron-sulfur	SDH2	High	26	6	1.28	0.946	1.14	0.823
1229	Succinate dehydrogenase [ubiquinone] cytochrome	SDH3	High	10	2	1.058	1.046	0.938	0.76
1230	Succinate dehydrogenase [ubiquinone] cytochrome	SDH4	High	24	4	1.061	0.946	1.009	0.849

1231	Protein SDS23	SDS23	High	6	2	100	0.486	0.302	0.01
1232	Protein transport protein sec1	SEC1	Medium	2	1	1.043	0.777	0.984	1.147
1233	Signal peptidase complex catalytic	SEC11	High	5	1	2.427	1.148	0.66	0.186
1234	Guanine nucleotide-exchange factor SEC12	SEC12	High	5	2	0.853	0.899	1.369	0.974
1235	Protein transport protein SEC13	SEC13	High	25	6	0.999	0.909	1.011	0.879
1236	SEC14 cytosolic factor	SEC14	High	48	10	1.145	1.013	1.144	1.049
1237	Exocyst complex component Sec15	SEC15	Low	1	1	0.966		1	
1238	alpha-soluble nsf attachment protein	SEC17	High	10	2	1.312	1.035	1.377	1.267
1239	vesicular-fusion protein SEC18	SEC18	High	9	5	0.968	1.114	1.132	1.219
1240	Coatomer subunit gamma	SEC21	High	26	17	1	1.008	1.115	0.956
1241	Protein transport protein SEC23	SEC23	High	21	13	0.927	0.92	1.087	1.176

1242	Protein transport protein sec24	SEC24	High	15	10	0.936	0.902	1.063	1.055
1243	Coatomer subunit beta	SEC26	High	12	9	0.952	0.993	1.05	1.24
1244	Coatomer subunit beta'	SEC27	High	24	17	1.034	1.003	1.106	1.269
1245	coatomer subunit epsilon	SEC28	Low	5	1	1.159	1.04	1.221	1.164
1246	Protein transport protein sec31	SEC31	High	16	15	0.753	1.033	1.054	1.129
1247	Ras-related protein SEC4	SEC4	High	47	7	1.084	0.967	1.303	0.818
1248	Exocyst complex component SEC5	SEC5	High	4	3	0.872	0.806	1.007	0.345
1249	phosphoma nnomutase	SEC53	High	55	13	0.815	0.933	0.846	0.898
1250	Protein transport protein SEC61	SEC61	High	8	4	0.963	0.914	0.969	0.944
1251	translocation protein sec62	SEC62	High	3	1	1.338	1.036	0.897	0.496
1252	protein translocation protein SEC63	SEC63	High	13	8	1.012	0.961	1.069	0.791

1253	signal recognition particle subunit	SEC65	High	8	2	1.27	0.946	0.858	0.57
1254	translocation protein sec66	SEC66	High	16	3	0.994	0.979	1.079	0.983
1255	protein transport protein SEC7	SEC7	High	10	15	0.932	0.886	0.973	0.717
1256	Eisosome protein SEG1	SEG1	High	1	1	100	1.084	1.426	1.32
1257	nucleoporin Seh1	SEH1	High	9	3	0.988	0.862	1.25	1.069
1258	phosphoserine aminotransferase	SER1	High	22	8	0.954	0.855	0.828	0.737
1259	D-3-phosphoglycerate dehydrogenase 1	SER3	High	21	8	0.515	0.552	0.426	0.581
1260	Serine--tRNA ligase, cytoplasmic	SES1	High	54	21	1.098	0.979	1.178	1.15
1261	protein sey1	SEY1	High	2	2	1.087	0.955	1.173	0.81
1262	S-(hydroxymethyl)glutathione dehydrogenase	SFA1	High	5	2	1.9	1.374	1.511	1.299
1263	SED5-binding protein 3	SFB3	High	6	5	0.905	1.007	0.931	1.16

1264	Succinate/fumarate mitochondrial transporter	SFC1	High	9	2	3.727	1.725	1.267	1.365
1265	Phosphatidylinositol transfer protein sfh5	SFH5	High	3	1	1.07	1.036	1.043	1.43
1266	Protein arginine N-methyltransferase SFM1	SFM1; YOR021C	High	22	3	1.082	0.736	0.821	1.05
1267	Protein transport protein sft2	SFT2	High	11	2	0.792	1.083	0.879	0.739
1268	Small glutamine-rich tetratricopeptide repeat-containing	SGT2	High	11	3	1.054	0.96	0.853	1.203
1269	serine/threonine-protein kinase bur1	SGV1	Medium	2	1	0.829	0.958	1.184	1.22
1270	sedoheptulose 1,7-bisphosphatase	SHB17	High	26	5	0.92	1.101	0.983	1.082
1271	Outer spore wall assembly	SHE10	High	14	7	1.074	1.089	1.112	0.934
1272	Serine hydroxymethyltransferase, mitochondrial	SHM1	High	44	15	0.947	0.99	1.14	1.447
1273	Serine hydroxymethyltransferase, cytosolic	SHM2	High	59	26	0.887	0.667	0.321	0.268
1274	UBX domain-containing protein 1	SHP1	High	9	2	1.048	0.961	1.189	1.259

1275	secretory component protein shr3	SHR3	High	5	1	0.95	0.982	0.911	0.971
1276	Seventh homolog of septin	SHS1	High	2	1	1.111	0.433	1.504	1.197
1277	Probable secreted beta-glucosidase SIM1	SIM1	High	3	1	0.934	1	1.103	0.974
1278	transcriptional regulatory protein SIN3	SIN3	High	2	2	0.833	1.061	1.011	0.907
1279	Protein SIP5	SIP5	High	3	1	1.212	100	1.474	1.896
1280	Regulatory protein SIR3	SIR3	High	1	1	0.696	0.889	0.919	0.772
1281	Protein SIS1	SIS1	High	34	9	0.962	0.847	1.433	1.639
1282	antiviral helicase SKI2	SKI2	High	1	1				
1283	Superkiller protein 3	SKI3	High	3	3	0.829	1.092	1.146	1.019
1284	Antiviral protein SKI8	SKI8	Low	2	1	0.601	0.753	0.878	1.117
1285	Suppressor of kinetochore protein	SKP1	High	13	2	0.937	1.046	0.905	1.158

1286	Actin cytoskeleton -regulatory complex protein	SLA1	High	6	4	0.839	1.035	0.992	0.84
1287	Protein SLA2	SLA2	High	14	9	0.928	0.999	1.405	0.97
1288	Probable 1-acyl-sn-glycerol-3-phosphate acyltransferase	SLC1	High	12	3	0.835	0.989	1.081	0.513
1289	Protein SLF1	SLF1	Medium	3	1				
1290	Phosphatidylinositol 4,5-bisphosphate-binding protein SLM1	SLM1	High	2	1	1.288	0.871	1.429	1.608
1291	Mitogen-activated protein kinase SLT2/MPK1	SLT2	High	5	1	100	0.905	1.051	0.354
1292	Protein sly1	SLY1	High	4	2	1.411	1.085	1.228	0.414
1293	small nuclear ribonucleoprotein-associated protein	SMB1	Medium	4	1	1.334	0.913	1.241	1.504
1294	structural maintenance of chromosomes	SMC1	Low	1	1				
1295	Structural maintenance of chromosomes	SMC3	High	4	3		0.01	0.01	0.01
1296	iron transporter SMF3	SMF3	High	3	1				

1297	Cell wall assembly regulator	SMI1	High	16	5	0.894	1	1.075	0.93
1298	ubiquitin-like protein SMT3	SMT3	High	40	3	0.709	1.071	0.881	1.077
1299	Carbon catabolite-derepressing protein kinase	SNF1	High	4	2	1.169	1.047	1.056	1.042
1300	5'-AMP-activated protein kinase subunit	SNF4	High	16	4	0.921	1.07	0.668	0.516
1301	vacuolar-sorting protein snf7	SNF7	High	5	1	1.084	0.983	0.976	1.394
1302	Protein SNQ2	SNQ2	High	1	1	2.248	1.721	1.62	1.605
1303	Pre-mRNA-splicing factor SNU114	SNU114	High	1	1	1.118	0.881	1.11	1.579
1304	13 kDa ribonucleoprotein-associated protein	SNU13	High	31	3	0.789	0.725	0.841	0.817
1305	Sorting nexin-41	SNX41	Low	2	1	1.254	1.103	1.083	0.89
1306	Superoxide dismutase [Cu-Zn]	SOD1	High	60	6	1.074	2.106	0.995	1.245
1307	Superoxide dismutase [Mn], mitochondrial	SOD2	High	32	5	2.306	1.927	1.232	0.945

1308	6-phosphogluconolactonase-like protein 2	SOL2	High	12	3	1.007	1	1.187	1.493
1309	6-phosphogluconolactonase 3	SOL3	High	10	2	0.619	1.402	0.892	0.512
1310	27S pre-rRNA (guanosine(2922)-2'-O)-methyltransferase	SPB1	High	4	2	0.628	0.904	0.571	1.18
1311	Signal peptidase complex subunit	SPC2	High	7	1	1.014	1.036	0.994	0.438
1312	Signal peptidase complex subunit	SPC3	High	13	2	1.075	0.869	1.062	0.795
1313	ornithine decarboxylase	SPE1	High	2	1	0.01	1.905	3.038	2.59
1314	S-adenosylmethionine decarboxylase proenzyme	SPE2	High	6	2	0.92	0.917	0.941	1.185
1315	spermidine synthase	SPE3	High	45	11	0.913	0.992	0.946	0.946
1316	Manganese-transporting ATPase 1	SPF1	High	27	23	1.022	1.115	1.132	0.858
1317	Transcription factor SPN1	SPN1	High	27	8	0.928	0.964	0.851	0.7
1318	sporulation-specific protein 71	SPO71	High	1	1	1.192	0.721	0.151	0.207

1319	TATA-box-binding protein	SPT15	High	9	2	1.211	0.912	1.112	1.118
1320	FACT complex subunit SPT16	SPT16	High	19	18	1.078	0.993	1.13	1.169
1321	Transcription elongation factor Spt5	SPT5	High	19	16	0.872	0.933	1.05	1.103
1322	transcription elongation factor spt6	SPT6	High	8	9	0.857	1.008	0.994	1.074
1323	Transcription factor SPT8	SPT8	High	3	1				
1324	Ribosome assembly protein SQT1	SQT1	High	6	1		100	0.01	0.01
1325	mediator of RNA polymerase	SRB4	High	3	1				
1326	Guanine nucleotide exchange factor	SRM1	High	5	2	1.129	1.163	1.116	0.867
1327	RNA-binding protein SRO9	SRO9	High	27	6	1.111	1.219	1.231	0.688
1328	Importin subunit alpha	SRP1	High	15	5	1.345	0.901	1.306	0.914
1329	signal recognition particle subunit	SRP14	High	8	1	100	100	0.01	0.01

1330	signal recognition particle subunit	SRP21	High	24	2			0.01	
1331	Suppressor protein SRP40	SRP40	High	14	3	0.871	0.984	0.706	0.727
1332	signal recognition particle subunit	SRP54	High	7	4	0.947	1.091	1.136	1.054
1333	Signal recognition particle subunit	SRP68	High	15	6	1.05	0.941	1.131	1.236
1334	Signal recognition particle subunit	SRP72	High	10	5	0.951	1.193	0.944	0.757
1335	Adenylyl cyclase-associated protein	SRV2	High	16	6	1.291	1.105	1.134	1.034
1336	Sulfiredoxin	SRX1	High	55	4	8.486	4.448	1.256	41.062
1337	heat shock protein SSA1	SSA1	High	65	9	1.448	1.384	1.52	1.936
1338	Heat shock protein SSA2	SSA2	High	56	7	1.429	0.956	1.826	1.862
1339	Heat shock protein SSA4	SSA4	High	16	3	1.384	0.682	1.49	3.697
1340	Ribosome-associated molecular chaperone SSB1	SSB1	High	64	2	1.045	0.889	1.17	0.728

1341	Ribosome-associated molecular chaperone SSB2	SSB2	High	64	2	1.126	0.881	1.138	1.036
1342	Heat shock protein SSC1,	SSC1	High	46	19	1.148	1.07	1.342	1.189
1343	protein SSD1	SSD1	High	4	4	1.372	1.216	1.097	1.302
1344	Heat shock protein homolog	SSE1	High	50	29	1.249	1.129	1.316	0.917
1345	Heat shock protein homolog	SSE2	High	8	1	1.357	1.387	100	3.579
1346	Ribosome biogenesis protein SSF1	SSF1	High	8	3	0.804	0.897	0.813	1.46
1347	sec sixty-one protein homolog	SSH1	High	17	6	0.782	1.037	1.01	0.931
1348	ERAD-associated E3 ubiquitin-protein ligase	SSM4	High	2	2	0.829	1.959	0.863	0.631
1349	Protein SSO1	SSO1	High	3	1	0.961	0.945	1.154	1.048
1350	protein SSP120	SSP120	High	10	2	1.078	1.085	1.128	1.221
1351	protein transport protein SSS1	SSS1	High	23	2	0.866	0.899	1.013	0.88

1352	Protein SST2	SST2	High	3	2	0.722	0.948	0.969	0.439
1353	Ribosome-associated complex subunit SSZ1	SSZ1	High	36	13	1.163	0.961	1.4	1.165
1354	Pheromone alpha factor receptor	STE2	High	3	1	0.447	0.882	0.676	0.512
1355	Serine/threonine-protein kinase ste20	STE20	High	1	1	1.107	0.937	1.271	1.253
1356	A-factor-processing enzyme	STE23	Medium	1	1	1.067	0.866	1.258	1.074
1357	CAAX prenyl protease 1	STE24	High	24	8	1.037	1.141	1.072	0.836
1358	Nuclear protein STH1/NPS1	STH1	High	3	3	0.989	0.926	0.895	1.023
1359	Heat shock protein STI1	STI1	High	33	15	1.188	0.989	1.556	1.661
1360	Suppressor protein STM1	STM1	High	56	17	1.011	0.992	1.147	1.059
1361	Nuclear cap-binding protein complex	STO1	High	4	3	1.644	0.871	0.68	0.514
1362	Dolichyl-diphosphooligosaccharide--protein glycosyltransferase subunit STT3	STT3	High	7	5	0.889	1.04	1.027	0.816

1363	phosphatidyl inositol 4-kinase STT4	STT4	High	1	1	100	100	0.469	0.01
1364	Protein stu1	STU1	Low	0	1				
1365	Transcriptio n initiation factor IIB	SUA7	High	3	1	1.133	0.768	1.296	0.806
1366	RNA polymerase II transcription al	SUB1	High	4	1	0.853	1.071	1.135	1.543
1367	ATP-dependent RNA helicase SUB2	SUB2	High	58	19	1.005	0.897	1.076	0.787
1368	Invertase 2	SUC2	High	10	5	1.22	1.163	1.047	1.2
1369	eukaryotic translation initiation factor	SUI1	High	47	3	0.788	1.116	0.753	0.685
1370	eukaryotic translation initiation factor	SUI2	High	28	8	0.96	0.976	1.167	0.899
1371	Eukaryotic translation initiation factor	SUI3	High	29	7	0.973	0.895	0.979	1.043
1372	Eukaryotic peptide chain release	SUP35	High	27	14	0.952	0.979	1.031	1.028
1373	Eukaryotic peptide chain release	SUP45	High	20	9	1.026	0.943	1.195	1.018

1374	Sphingolipid C4-hydroxylase SUR2	SUR2	Medium	3	1	0.782	0.284	1.135	0.01
1375	elongation of fatty acids	SUR4; ELO3	High	17	4	0.812	1.146	0.708	0.767
1376	Protein SUR7	SUR7	High	10	3	1.28	0.923	0.899	1.124
1377	Survival factor 1	SVF1	High	19	7	0.836	1.539	0.798	0.727
1378	Styryl dye vacuolar localization	SVL3	High	2	1	1.822	1.603	0.979	0.398
1379	Auxilin-like clathrin uncoating factor	SWA2	High	2	1	0.693	0.96	0.979	0.536
1380	Oxysterol-binding protein homolog 1	SWH1	High	3	2	1.008	1.358	1.126	1.174
1381	SWI/SNF chromatin-remodeling complex subunit	SWI1	High	1	1	0.975	0.788	1.178	1.247
1382	Dolichyl-diphosphooligosaccharide--protein glycosyltransferase subunit swp1	SWP1	High	5	1	1.596	0.794	1.044	0.729
1383	Importin beta SMX1	SXM1	High	8	6	1.043	0.923	0.797	0.739
1384	Synchronized import protein 1	SYO1; YDL063C	Medium	2	1	1.083	1.071	0.896	0.999

1385	Suppressor of Yeast Profilin	SYP1	High	2	2	1.026	0.885	1.506	1.203
1386	Ribosome quality control complex	TAE2; RQC2	High	7	6	0.997	1.168	0.976	0.807
1387	transcription initiation factor TFIID	TAF1	Low	1	1				
1388	Transcription initiation factor TFIID	TAF14	High	14	2	1.364	1.108	1.017	1.128
1389	Transcription initiation factor TFIID	TAF6	High	2	1		11.344	0.325	0.01
1390	Transaldolase	TAL1	High	69	26	1.289	1.259	0.981	1.391
1391	tRNA acetyltransferase TAN1	TAN1	High	16	3	1.027	0.787	0.757	1.271
1392	Cell morphogenesis protein PAG1	TAO3	Medium	0	1	100	1	1	0.01
1393	Valine/tyrosine/tryptophan amino-acid permease 1	TAT1	High	2	1	0.456	1.128	0.31	0.235
1394	tricalbin-1	TCB1	High	8	7	1.243	0.949	1.345	0.982
1395	Tricalbin-2	TCB2	High	2	2	1.443	0.869	1.326	1.061

1396	Tricalbin-3	TCB3	High	8	9	1.11	1.06	1.256	0.735
1397	tRNA threonylcarbamoyladenosine dehydratase 1	TCD1; YHR003C	Medium	3	1	1.256	0.97	0.981	0.871
1398	tRNA threonylcarbamoyladenosine dehydratase 2	TCD2; YKL027W	High	6	2	0.982	0.871	0.989	0.406
1399	T-complex protein 1 subunit	TCP1	High	20	9	1.216	0.911	1.225	1.044
1400	Putative oxidoreductase TDA3	TDA3	High	2	1	0.884	1.041	100	0.447
1401	Probable transcription factor TDA9	TDA9	Low	1	1	8.192	8.744	0.01	0.041
1402	glyceraldehyde-3-phosphate dehydrogenase 1	TDH1	High	29	6	1.876	2.754	1.279	1.517
1403	glyceraldehyde-3-phosphate dehydrogenase 2	TDH2	High	9	3	0.934	0.942	0.95	1.405
1404	Glyceraldehyde-3-phosphate dehydrogenase 3	TDH3	High	18	5	0.883	1.008	0.551	1.011
1405	Protein TED1	TED1	High	2	1	1.352	1.353	1.484	0.01
1406	elongation factor 1-alpha	TEF2; TEF1	High	64	30	1.005	1.008	0.955	1.029

1407	Elongation factor 1-gamma 2	TEF4	High	42	16	0.838	0.958	0.986	1.298
1408	Peroxisomal acyl-coenzyme A thioester	TES1	High	4	1	0.674	1.387	1.026	0.399
1409	Transcription initiation factor IIF	TFG1	High	2	1	1.114	1.178	1.614	1.586
1410	thiamine pyrophosphokinase	THI80	High	5	1	1.18	1.247	0.928	0.447
1411	Protein THO1	THO1	High	11	2	0.999	0.904	0.958	1.441
1412	THO complex subunit 2	THO2	High	1	1	0.868	0.938	0.988	0.588
1413	homoserine kinase	THR1	High	18	5	0.972	0.995	1.147	1.193
1414	threonine synthase	THR4	High	30	15	1.002	0.943	1.107	1.105
1415	Threonine--tRNA ligase, cytoplasmic	THS1	High	37	25	0.961	0.979	1.097	0.965
1416	eukaryotic translation initiation factor	TIF11	High	31	5	0.921	0.965	0.874	1.196
1417	ATP-dependent RNA helicase eIF4A	TIF2; TIF1	High	64	27	1.084	0.954	1.01	0.89

1418	eukaryotic translation initiation factor	TIF3	High	51	15	0.958	0.876	1.169	1.078
1419	Eukaryotic translation initiation factor	TIF34	High	40	11	1.009	0.795	1.153	0.807
1420	Eukaryotic translation initiation factor	TIF35	High	35	7	0.957	0.827	1.122	1.133
1421	Eukaryotic initiation factor 4F	TIF4631	High	24	16	0.749	1.043	0.877	1.096
1422	eukaryotic initiation factor 4F	TIF4632	High	6	2	0.92	0.957	1.004	0.743
1423	Eukaryotic translation initiation factor	TIF5	High	33	11	0.928	0.875	1.091	1.134
1424	eukaryotic translation initiation factor	TIF6	High	18	3	1.254	1.018	1.093	0.802
1425	ATP synthase subunit e,	TIM11	High	34	3	0.97	0.909	0.958	0.837
1426	Mitochondrial import inner membrane	TIM21	High	5	1				
1427	Mitochondrial import inner membrane	TIM23	High	14	2	1.56	1.215	1.409	0.524
1428	Mitochondrial import inner membrane	TIM44	High	17	6	1.087	0.992	1.031	0.657

1429	Mitochondrial import inner membrane	TIM50	High	25	9	1.114	0.985	1.129	0.847
1430	transketolase 1	TKL1	High	38	26	1.032	1.084	1.246	1.189
1431	transketolase 2	TKL2	High	7	3	1.375	0.845	1.068	1.085
1432	protein TMA108	TMA108	High	2	2	1.38	1.403	0.912	0.255
1433	translation machinery-associated protein 16	TMA16	High	7	1	0.848	0.865	0.752	1.292
1434	Translationally-controlled tumor protein homolog	TMA19	High	45	10	0.746	0.926	0.812	1.019
1435	Translation machinery-associated protein 20	TMA20	High	20	4	1.093	1.082	0.996	1.299
1436	Translation machinery-associated protein 22	TMA22	High	15	2	1.007	1.149	1.144	1.023
1437	Translation machinery-associated protein 46	TMA46	High	4	1	0.847	1.219	0.935	0.01
1438	High-affinity nicotinic acid transporter	TNA1	High	2	1	0.51	1.189	0.674	0.537
1439	E3 ubiquitin-protein ligase TOM1	TOM1	High	2	7	0.904	0.901	0.851	0.97

1440	mitochondrial import receptor subunit	TOM20	High	36	4	1.101	0.908	1.285	0.655
1441	Mitochondrial import receptor subunit	TOM22	High	5	1	2.205	0.641	1.241	0.904
1442	Mitochondrial import receptor subunit	TOM40	High	21	5	1.047	0.851	1.354	0.612
1443	Mitochondrial import receptor subunit	TOM70	High	25	11	1.235	0.864	1.418	0.966
1444	DNA topoisomerase 1	TOP1	High	2	1	1.049	1.047	1.155	1.756
1445	DNA topoisomerase 2	TOP2	High	1	1				
1446	Protein TOS1	TOS1	High	11	3	1.022	0.869	1.014	0.679
1447	Prolyl 3,4-dihydroxylase TPA1	TPA1	High	8	4	1.153	1.242	0.975	0.707
1448	protein phosphatase PP2A regulatory	TPD3	High	15	7	1.04	1.092	0.763	1.4
1449	Triosephosphate isomerase	TPI1	High	56	15	0.966	0.969	0.841	1.051
1450	polyamine transporter tpo5	TPO5	Medium	2	1	0.662	1.331	1.016	0.58

1451	Alpha,alpha-trehalose-phosphate synthase [UDP-forming] 56	TPS1	High	31	10	1.266	1.278	1.257	1.809
1452	trehalose-phosphatase	TPS2	High	14	10	1.161	1.171	1.461	2.013
1453	Trehalose synthase complex regulatory	TPS3	High	8	5	0.934	0.964	1.217	1.375
1454	transcription-associated protein 1	TRA1	High	1	4	0.895	1.474	1.228	0.909
1455	high-affinity potassium transport protein	TRK1	Medium	1	1	1.094	0.847	1.139	1.347
1456	tRNA ligase	TRL1	High	5	3	1.941	100	0.498	0.259
1457	tRNA (guanine(26)-N(2))-dimethyltransferase, mitochondrial	TRM1	High	12	5	1.165	0.771	1.23	0.883
1458	tRNA (Guanosine(18)-2'-O)-methyltransferase	TRM3	High	4	5	0.901	0.898	1.005	1.198
1459	tRNA (guanine(37)-N1)-methyltransferase	TRM5	High	3	1	1.091	2.06	0.946	0.326
1460	tRNA (cytidine(32)-2'-O)-methyltransferase non-catalytic subunit	TRM732; YMR259C	High	1	1	0.583	1.065	0.917	0.722
1461	tRNA (guanine-N(7)-)-methyltransferase	TRM8	High	9	2	0.692	0.804	0.636	1.068

1462	tRNA (guanine-N(7)-)-methyltransferase non-catalytic subunit	TRM82	High	13	5	0.881	1.094	0.946	1.206
1463	anthranilate synthase component 1	TRP2	High	35	14	1.212	1.167	1.182	1.476
1464	Multifunctional tryptophan biosynthesis protein	TRP3	High	5	2	0.733	1.155	0.749	0.855
1465	Tryptophan synthase	TRP5	High	35	17	1.038	1.134	1.179	0.871
1466	thioredoxin reductase 1	TRR1	High	60	14	3.961	5.319	1.501	1.506
1467	thioredoxin reductase 2, mitochondrial	TRR2	High	12	1	3.565	1.797	1.718	3.222
1468	thioredoxin-1	TRX1	High	30	1	1.067	1.333	0.715	0.484
1469	thioredoxin-2	TRX2	High	66	5	3.48	6.586	1.506	2.742
1470	Peroxiredoxin TSA1	TSA1	High	63	14	1.572	2.393	1.105	0.938
1471	Peroxiredoxin TSA2	TSA2	High	48	9	38.346	54.441	12.997	23.283
1472	3-ketodihydrosphingosine reductase TSC10	TSC10	Low	4	1	0.768	0.773	0.91	0.565

1473	Very-long-chain enoyl-CoA reductase	TSC13	High	11	3	0.975	1.266	0.78	0.913
1474	Trehalose synthase complex regulatory	TSL1	High	20	15	1.238	1.889	1.441	2.629
1475	Ribosome biogenesis protein TSR1	TSR1	Low	1	1	0.901	0.94	1.065	0.01
1476	tubulin alpha-1 chain	TUB1	High	29	6	1.163	1.351	1.046	0.541
1477	tubulin beta chain	TUB2	High	24	10	1.017	1.039	1.042	0.826
1478	Tubulin alpha-3 chain	TUB3	High	14	1	4.851	0.98	0.973	0.169
1479	elongation factor Tu, mitochondrial	TUF1	High	51	16	1.047	1.013	1.034	0.961
1480	Thiosulfate sulfurtransferase TUM1	TUM1	High	16	3	0.857	1.311	0.835	0.566
1481	General transcriptional corepressor TUP1	TUP1	High	14	6	1.014	0.888	1.329	1.143
1482	Golgi apparatus membrane protein	TVP18	Medium	8	1	1.007	1.37	1.007	1.181
1483	Tyrosine--tRNA ligase, cytoplasmic	TYS1	High	26	10	1.052	0.91	1.136	1.398

1484	S-adenosyl-L-methionine-dependent tRNA 4-demethylwyosine synthase	TYW1	High	2	1	0.817	0.833	1.069	0.73
1485	ubiquitin-activating enzyme E1 1	UBA1	High	33	29	0.977	1.174	1.111	1.385
1486	Ubiquitin-activating enzyme E1-like	UBA2	High	4	2	0.918	0.96	1.212	0.819
1487	ubiquitin-conjugating enzyme E2 1	UBC1	High	26	5	1.045	0.96	1.003	0.898
1488	Ubiquitin-conjugating enzyme E2 13	UBC13	High	17	2	0.958	1.279	0.984	1.224
1489	ubiquitin-conjugating enzyme E2 4	UBC4	High	7	1	0.855	1.053	0.877	1.05
1490	ubiquitin-conjugating enzyme E2 6	UBC6	High	8	1	0.01	1.022	1.261	2.573
1491	Ubiquitin carboxyl-terminal hydrolase 1	UBP1	High	6	3	1.131	1.414	1.125	1.311
1492	Ubiquitin carboxyl-terminal hydrolase 12	UBP12	High	1	1	1	1.041	0.01	0.442
1493	ubiquitin carboxyl-terminal hydrolase 15	UBP15	Medium	1	1	1.106	1.064	1.057	1.232
1494	Ubiquitin carboxyl-terminal hydrolase 2	UBP2	High	1	1	0.01	100	1.374	1.975

1495	Ubiquitin carboxyl-terminal hydrolase 3	UBP3	High	6	4	0.979	1.13	1.007	0.747
1496	Ubiquitin carboxyl-terminal hydrolase 6	UBP6	High	7	3	1.356	1.226	0.816	1.229
1497	UBX domain-containing protein 2	UBX2	Medium	2	1	1.068	1.044	1.186	1.883
1498	UBX domain-containing protein 4	UBX4	Low	3	1				
1499	E4 ubiquitin-protein ligase UFD2	UFD2	Low	1	1	1.379	1.105	1.362	1.513
1500	4-aminobutyrate aminotransferase	UGA1	High	5	1		1	0.043	0.01
1501	Succinate-semialdehyde dehydrogenase [NADP(+)]	UGA2	High	3	1	2.297	1.845	2.098	100
1502	UTP--glucose-1-phosphate uridylyltransferase	UGP1	High	35	13	1.01	1.116	1.279	1.579
1503	Dihydroorotate dehydrogenase (Fumarate)	URA1	High	28	6	0.712	0.907	0.757	0.729
1504	Protein URA2	URA2	High	37	67	1.064	0.964	1.149	0.967
1505	dihydroorotase	URA4	High	13	3	0.734	0.781	0.902	0.651

1506	Orotate phosphoribosyltransferase 1	URA5	High	37	7	0.966	0.969	0.936	0.778
1507	uridylate kinase	URA6	High	27	5	0.763	0.998	0.743	0.552
1508	CTP synthase 1	URA7	High	15	7	0.996	0.859	1.12	0.895
1509	nucleolar pre-ribosomal-associated protein 1	URB1	High	5	6	1.012	0.888	0.633	1.087
1510	Nucleolar pre-ribosomal-associated protein 2	URB2	High	2	2	1.047	0.679	1.009	1.381
1511	Transcriptional regulator URE2	URE2	High	5	1	100	1	0.48	0.053
1512	Intracellular protein transport protein	USO1	High	1	1	0.01	100	11.29	0.01
1513	U3 small nucleolar RNA-associated	UTP10	High	12	19	0.96	0.906	0.853	0.922
1514	U3 small nucleolar RNA-associated	UTP13	High	1	1	1.17	1.542	1.343	2.012
1515	U3 small nucleolar RNA-associated	UTP14	Medium	1	1	1.091	0.847	1.296	1.221
1516	U3 small nucleolar RNA-associated	UTP15	High	2	1	0.894	0.955	0.874	0.624

1517	U3 small nucleolar RNA-associated	UTP20	High	5	10	0.963	0.949	0.739	0.761
1518	U3 small nucleolar RNA-associated	UTP21	High	5	4	1.23	0.901	0.816	0.445
1519	U3 small nucleolar RNA-associated	UTP22	High	13	10	0.961	0.847	0.935	0.974
1520	rRNA-processing protein utp23	UTP23	Medium	6	1	0.836	0.781	1.131	1.319
1521	U3 small nucleolar RNA-associated	UTP25	High	5	3	0.583	1.081	1.07	0.847
1522	U3 small nucleolar RNA-associated	UTP4	High	6	4	1.25	0.999	0.78	0.658
1523	U3 small nucleolar RNA-associated	UTP5	High	3	2	1.081	1.022	0.826	0.914
1524	U3 small nucleolar RNA-associated	UTP6	High	6	3	0.977	0.928	0.8	0.919
1525	U3 small nucleolar RNA-associated	UTP7	High	2	1	0.853	0.851	1.094	1.177
1526	U3 small nucleolar RNA-associated	UTP8	High	9	4	0.971	0.927	0.957	1.063
1527	U3 small nucleolar RNA-associated	UTP9	High	10	5	0.897	1.032	0.84	0.494

1528	Probable glycosidase CRH2	UTR2	High	2	1	0.871	0.716	0.8	0.688
1529	Enolase-phosphatase E1	UTR4	High	10	2	0.832	1.288	0.924	0.861
1530	Vacuolar protein 8	VAC8	High	7	3	0.899	0.991	0.709	0.977
1531	Vacuolar morphogenesis protein 10	VAM10	Low	9	1	0.574	9.049	0.933	0.01
1532	Mannan polymerase I complex	VAN1	Medium	2	1	0.712	1.117	1.18	1.021
1533	Valine--tRNA ligase, mitochondrial	VAS1	High	42	36	0.993	1.03	1.13	1.154
1534	Vacuolar calcium ion transporter	VCX1	High	3	1	0.749	1.248	0.01	0.845
1535	vitamin H transporter	VHT1	High	11	5	0.58	1.058	0.388	0.212
1536	Vacuolar import and degradation	VID22	High	1	1	0.847	1.432	0.923	1.106
1537	Vacuolar import and degradation	VID27	Medium	1	1	1.268	1.085	1.302	1.568
1538	Vacuolar import and degradation	VID30	High	1	1	100	0.01	0.989	100

1539	Inositol hexakisphosphate and diphosphoinositol-pentakisphosphate	VIP1	High	8	8	0.956	0.907	1.064	1.045
1540	V-type proton ATPase catalytic	VMA1	High	42	40	1.005	0.938	1.099	1.118
1541	V-type proton ATPase subunit	VMA11	High	11	1	1.246	1.184	0.869	0.591
1542	V-type proton ATPase subunit	VMA13	High	38	15	1.213	1.063	1.222	0.833
1543	V-type proton ATPase subunit	VMA16	High	6	1	0.494	0.606	0.705	1.07
1544	V-type proton ATPase subunit	VMA2	High	61	27	1.017	0.961	1.235	1.185
1545	V-type proton ATPase subunit	VMA3	High	11	1	1.848	7.519	0.206	0.172
1546	V-type proton ATPase subunit	VMA4	High	49	10	0.938	0.936	1.041	1.102
1547	V-type proton ATPase subunit	VMA5	High	32	10	0.947	1.079	0.953	0.674
1548	V-type proton ATPase subunit	VMA6	High	7	2	1.013	0.967	0.874	0.319
1549	V-type proton ATPase subunit	VMA8	High	9	3	1.079	1.021	1.028	0.993

1550	V-type proton ATPase subunit	VMA9	Low	12	1	0.783	8.093	0.844	0.757
1551	Protein VMS1	VMS1	High	1	1				
1552	Low affinity vacuolar monovalent	VNX1	High	2	1	1.145	1.172	1.292	1.228
1553	V-type proton ATPase subunit	VPH1	High	19	16	1.043	1.008	1.186	0.728
1554	vacuolar protein sorting-associated protein	VPS1	High	37	20	1.145	0.975	1.22	1.067
1555	Vacuolar protein sorting-associated protein	VPS13	Low	0	1				
1556	Vacuolar protein sorting-associated protein	VPS17	High	2	1	100	1.197		0.01
1557	Vacuolar protein sorting-associated protein	VPS21	High	30	4	1.169	1.035	0.904	0.552
1558	Vacuolar protein sorting-associated protein	VPS29	High	4	1				
1559	Vacuolar protein sorting-associated protein	VPS30	High	1	1	1.004	0.962	0.959	1.012
1560	Vacuolar protein sorting-associated protein	VPS4	Medium	4	1	1.149	0.753	100	0.719

1561	Vacuolar protein sorting-associated protein	VPS54	High	1	1	1.243	0.901	0.871	0.472
1562	Vacuolar protein sorting-associated protein	VPS72	Medium	1	1	0.58	0.786	1.023	1.128
1563	Vacuolar protein sorting-associated protein	VPS74	High	7	2	0.917	0.92	1.176	1.23
1564	vacuolar protein sorting-associated protein	VPS9	High	2	1	0.86	0.948	0.99	0.831
1565	vacuolar protein sorting-associated protein	VTA1	High	8	2	0.991	0.947	1.205	1.148
1566	Vacuolar transporter chaperone 1	VTC1	Low	6	1	100	9.412	0.759	1
1567	Vacuolar transporter chaperone 2	VTC2	High	28	19	0.918	0.978	1.055	0.834
1568	Vacuolar transporter chaperone 3	VTC3	High	36	25	0.89	0.898	1.126	0.827
1569	Vacuolar transporter chaperone 4	VTC4	High	33	26	1.024	0.904	1.121	0.932
1570	Dolichyl-diphosphooligosaccharide--protein glycosyltransferase subunit WBP1	WBP1	High	16	6	1.066	1.006	1.119	0.537
1571	Growth regulation protein	WHI2	High	5	2	1.291	7.731	12.016	100

1572	protein WHI3	WHI3	High	4	2	1.115	0.815	1.191	0.678
1573	Tryptophan--tRNA ligase, cytoplasmic	WRS1	High	18	7	1.115	0.983	1.063	1.151
1574	Transcriptional modulator WTM1	WTM1	High	30	10	1.245	0.894	1.323	1.336
1575	xylulose kinase	XKS1	High	2	1				
1576	xanthine phosphoribosyltransferase 1	XPT1	High	5	1	0.978	0.648	0.541	0.489
1577	5'-3' exoribonuclease 1	XRN1	High	14	18	0.929	0.943	1.012	1.111
1578	Pyridoxal phosphate homeostasis protein	YBL036C	High	6	1	1.061	1.281	0.921	0.731
1579	deoxyribonuclease Tat-D	YBL055C	High	3	1	1.155	0.89	1.001	1.306
1580	Uncharacterized protein YBR053C	YBR053C	High	3	1	0.998	1.294	1.182	1.569
1581	uncharacterized glycosyl hydrolase YBR056W	YBR056W	High	6	3	1.048	1.313	1.248	1.355
1582	Uncharacterized protein YBR096W	YBR096W	High	5	1	0.096	0.098	0.947	0.815

1583	Uncharacterized protein YBR255C-A	YBR255C-A; RCF3	Low	11	1	1.258	0.78	0.868	0.686
1584	uncharacterized transporter YBR287W	YBR287W	High	2	1	0.787	0.943	1.009	0.997
1585	ATP-dependent bile acid permease	YBT1	High	1	2	0.781	0.917	1.087	0.837
1586	metal resistance protein YCF1	YCF1	High	6	7	1.23	1.541	1.038	0.972
1587	Condensin complex subunit 3	YCG1	Low	1	1	3.169	0.539	0.623	2
1588	Casein kinase I homolog	YCK2	High	10	4	0.948	0.87	0.933	1.024
1589	Flavoprotein-like protein YCP4	YCP4	High	53	8	0.533	0.869	0.888	1.162
1590	Uncharacterized protein YCR016W	YCR016W	High	2	1	1.426	1.154	0.791	0.712
1591	UPF0587 protein YCR090C	YCR090C	High	5	1	0.929	1.105	0.95	0.97
1592	Alkaline ceramidase YDC1	YDC1	Medium	3	1	3.876	9.293	0.615	0.247
1593	Mitochondrial protein import protein	YDJ1	High	43	14	1.189	0.971	1.267	1.144

1594	MIOREX complex component 9	YDL027C; MRX9	High	3	1	0.829	1.069	1.057	1.03
1595	Putative carboxymethylenebutenolidase	YDL086W	High	17	3	1.109	0.945	1.057	0.905
1596	NADPH-dependent alpha-keto amide reductase	YDL124W	High	31	6	1.672	2.095	1.011	1.084
1597	Uncharacterized membrane protein YDL218W	YDL218W	High	19	4		100	100	100
1598	arginine--tRNA ligase, cytoplasmic	YDR341C	High	51	27	1.133	1.033	1.02	1.098
1599	elongation factor 3A	YEF3	High	57	59	0.95	0.934	1.081	1.244
1600	Uncharacterized protein YEL025C	YEL025C	High	1	1	0.062	1.078	0.72	0.114
1601	Putative magnesium-dependent phosphatase YER134C	YER134C	Medium	7	1	0.561	1.469	0.812	0.01
1602	UPF0160 protein YER156C	YER156C	High	13	4	0.877	0.881	0.788	0.915
1603	Endoplasmic reticulum transmembrane protein	YET1	High	32	5	1.143	1.276	1.118	1.033
1604	Endoplasmic reticulum transmembrane protein	YET3	High	11	2	1.319	1.182	1.294	0.904

1605	Uncharacterized protein YFR016C	YFR016C	Medium	1	1	0.875	1.109		1
1606	putative uncharacterized oxidoreductase YGL039W	YGL039W	High	4	1	1.169	1.726	1.25	1.386
1607	Protein-lysine N-methyltransferase EFM5	YGR001C; AML1; EFM5	High	9	2	0.655	1.001	0.843	0.952
1608	putative cysteine synthase	YGR012W; MCY1	High	5	2	1.054	0.583	1.133	1.357
1609	Uncharacterized protein YGR017W	YGR017W	High	3	1	0.847	1.058	1.003	1.171
1610	Eukaryotic translation initiation factor	YGR054W	High	12	6	1.023	1.041	0.979	1.075
1611	Uncharacterized protein YGR111W	YGR111W	High	3	1	1.015	0.98	1.073	100
1612	uncharacterized vacuolar membrane protein	YGR125W	High	2	1	0.808	0.13	0.01	0.114
1613	Uncharacterized protein YGR130C	YGR130C	High	2	2	0.989	1.015	1.262	0.885
1614	Uncharacterized GTP-binding protein YGR210C	YGR210C	High	7	2	0.864	0.611	0.784	0.851
1615	Uncharacterized protein YGR237C	YGR237C	Medium	1	1				

1616	Flavohemoprotein	YHB1	High	58	15	1.079	1.098	0.917	0.62
1617	Citrate/oxoglutarate carrier protein	YHM2	High	18	4	0.968	0.89	1.071	0.718
1618	Putative proline--tRNA ligase YHR020W	YHR020W	High	51	26	0.956	1.097	1.219	0.889
1619	Protein transport protein YIF1	YIF1	High	8	2	0.928	0.971	1.144	0.781
1620	putative zinc metalloproteinase YIL108W	YIL108W	High	2	1	2.259	1.297	1.238	1.626
1621	Protein YIM1	YIM1	High	3	1	0.916	1.09	1.015	0.649
1622	Prenylated rab acceptor 1	YIP3	High	32	6	0.988	0.977	0.907	0.61
1623	protein YIP5	YIP5	High	3	1	0.955	0.698	1.125	1.109
1624	LOG family protein YJL055W	YJL055W	High	20	3	1.038	1.017	1.061	1.147
1625	S-formylglutathione hydrolase	YJL068C	High	17	3	0.724	1.527	0.901	0.472
1626	Cell wall protein YJL171C	YJL171C; TOH1	High	6	2	1.012	1.209	1.131	1.154

1627	MIOREX complex component 12	YJR003C; MRX12	Low	2	1	0.85	0.709	1.162	1.237
1628	Cop9 signalosome complex subunit	YJR084W	High	3	1		1	0.047	0.01
1629	Uncharacterized oxidoreductase YJR096W	YJR096W	High	4	1	0.8	1.793	1.33	1.211
1630	Uncharacterized protein YJR154W	YJR154W	High	5	1	100	0.626	0.01	0.131
1631	Uncharacterized oxidoreductase YKL071W	YKL071W	High	18	3	100	100	100	100
1632	uncharacterized protein YKL077W	YKL077W	High	5	2	1.06	1.105	1.083	0.766
1633	Probable intramembrane protease YKL100C	YKL100C; YPF1	High	5	3	0.949	0.956	1.085	1.011
1634	ATP-dependent (S)-NAD(P)H-hydrate dehydratase	YKL151C; NNR2	High	6	2	1.453	1.257	1.167	1.961
1635	Mitochondrial outer membrane protein	YKR018C	High	5	3	1.204	1.118	1.225	1.371
1636	Synaptobrevin homolog YKT6	YKT6	High	50	7	1.247	1.24	1.092	0.696
1637	LETM1 domain-containing protein YLH47,	YLH47	High	11	3	1.225	0.955	0.979	0.991

1638	Membrane-anchored lipid-binding protein LAM6	YLR072W; LAM6	Low	2	1	7.954	0.01	0.01	0.66
1639	Uncharacterized protein YLR179C	YLR179C	High	9	2	0.749	0.996	0.857	0.579
1640	Uncharacterized protein YLR257W	YLR257W	Low	3	1	1.409	0.896	1.259	1.323
1641	Mitochondrial inner membrane i-AAA	YME1	High	5	3	1.383	0.934	1.255	0.915
1642	Uncharacterized membrane protein YML131W	YML131W	High	13	4	8.614	10.049	3.424	6.274
1643	54S ribosomal protein yml6,	YML6	High	7	2	0.994	0.872	1.29	1.325
1644	Uncharacterized membrane protein YMR010W	YMR010W; ANY1	High	8	2	0.45	1.065	0.689	0.87
1645	protein-glutamate O-methyltransferase	YMR027W	High	8	3	0.879	1.188	0.868	0.893
1646	Transposon Ty1-MR1 Gag-Pol polyprotein	YMR045C	High	16	1	10.915	100	0.989	1.834
1647	UPF0659 protein YMR090W	YMR090W	Medium	3	1	100	100	100	100
1648	glucose-6-phosphate 1-epimerase	YMR099C	High	45	11	0.863	1.139	1.07	0.973

1649	uncharacterized protein YMR196W	YMR196W	High	1	1	1	7.997	0.872	0.716
1650	NADP-dependent 3-hydroxy acid dehydrogenase	YMR226C	High	53	10	1.183	1.09	0.989	1.264
1651	37S ribosomal protein YMR-31,	YMR31	High	10	1	0.809	1.043	0.912	0.522
1652	Uncharacterized protein YMR315W	YMR315W	High	30	7	1.856	1.833	1.203	1.452
1653	Nucleoside diphosphate kinase	YNK1	High	77	11	1.068	1.077	0.915	1.22
1654	Uncharacterized phosphatase YNL010W	YNL010W	High	30	5	0.941	0.811	0.921	0.725
1655	Transposon Ty1-NL2 Gag-Pol polyprotein	YNL054W-B	High	19	1	0.234	0.96	1.738	0.486
1656	Uncharacterized vacuolar membrane protein	YNL115C	High	5	2	1.025	1.316	1.356	1.737
1657	Uncharacterized protein YNL134C	YNL134C	High	20	5	6.518	10.775	4.063	6.326
1658	NAD(P)H-hydrate epimerase	YNL200C; NNR1	Medium	5	1			0.01	0.058
1659	Uncharacterized protein YNL208W	YNL208W	High	17	2	1.481	0.904	0.434	0.252

1660	Cysteine--tRNA ligase	YNL247W	High	12	7	0.987	0.992	1.068	1.023
1661	Uncharacterized membrane protein YNL320W	YNL320W	High	4	1	1.038	100	0.741	0.01
1662	UPF0674 endoplasmic reticulum membrane	YNR021W	High	24	6	1.013	0.979	1.057	0.717
1663	Uncharacterized membrane protein YOL019W	YOL019W	High	3	1	0.055	0.101	0.01	0.01
1664	Probable dipeptidyl peptidase 3	YOL057W	High	5	3	0.898	1.273	1.015	0.822
1665	Uncharacterized ABC transporter ATP-binding	YOL075C	Low	1	1	0.967	1.006	1.026	1.25
1666	Probable vacuolar amino acid	YOL092W; YPQ1	High	13	3	0.932	1.071	0.965	0.926
1667	Uncharacterized protein YOL098C	YOL098C; SDD3	High	6	5	1.008	1.272	0.968	1.049
1668	Protein YOP1	YOP1	High	4	1	0.9	0.865	1.047	1.005
1669	Oligomycin resistance ATP-dependent permease	YOR1	High	1	1	0.683	0.703	1.077	1.583
1670	Putative uncharacterized hydrolase YOR131C	YOR131C	High	7	1	9.969	7.296	0.01	0.048

1671	Autophagy-related protein 40	YOR152C; ATG40	High	5	1	2.122	1.191	0.558	0.309
1672	Broad-specificity phosphatase YOR283W	YOR283W	High	6	1	0.985	0.988	0.886	1.086
1673	Serine/threonine-protein kinase YPK1	YPK1	High	12	6	1.15	1.02	0.93	0.404
1674	Protein PBDC1 homolog	YPL225W	High	21	4	1.283	1.706	0.809	0.949
1675	UPF0662 protein YPL260W	YPL260W; CUB1	High	8	3	1.163	1.328	0.97	0.377
1676	Cargo-transport protein YPP1	YPP1	High	2	2	1.01	1.014	1.006	0.551
1677	UPF0495 protein YPR010C-A	YPR010C-A	High	26	2	1.094	1.075	0.723	0.669
1678	Uncharacterized protein YPR063C	YPR063C	High	9	1	1.059	0.978	1.002	0.96
1679	PX domain-containing protein YPR097W	YPR097W	High	1	1	100	100	0.656	0.01
1680	Uncharacterized mitochondrial outer membrane	YPR098C	Medium	6	1	0.936	0.925	0.865	0.905
1681	putative reductase 1	YPR1	High	29	5	1.395	1.672	1.211	1.052

1682	Uncharacterized TLC domain-containing protein	YPR114W	High	3	1	0.694	1.269	1.108	0.804
1683	Putative pyridoxal reductase	YPR127W	High	9	3	1.004	1.427	1.507	2.213
1684	uncharacterized protein YPR148C	YPR148C	High	3	1	1.069	1.067	1.143	1.128
1685	GTP-binding protein ypt1	YPT1	High	33	5	1.093	1.152	1.084	0.989
1686	GTP-binding protein YPT31/YPT8	YPT31	High	21	4	1.027	0.854	0.987	0.84
1687	GTP-binding protein YPT52	YPT52	High	19	3	1.187	1.17	1.031	1.232
1688	GTP-binding protein YPT6	YPT6	High	10	1	1.116	0.947	1.168	1.121
1689	GTP-binding protein ypt7	YPT7	High	38	6	0.895	1.095	0.89	0.585
1690	RNA annealing protein YRA1	YRA1	High	36	7	0.944	0.849	0.963	1.437
1691	Ran-specific GTPase-activating protein 1	YRB1	High	36	4	0.955	1.056	0.964	1.186
1692	Ran-specific GTPase-activating protein 2	YRB2	High	5	1	0.878	1.125	1.315	1.385

1693	Ran-specific GTPase-activating protein 30	YRB30	High	5	2	0.818	0.784	1.208	1.297
1694	protein YRO2	YRO2	High	13	1	1.256	4.827	5.53	100
1695	ADP-ribose pyrophosphatase	YSA1	High	12	2	0.762	1.183	1.088	0.719
1696	protein YSC84	YSC84	High	3	1	0.892	1.052	1.43	1.519
1697	endoribonuclease ysh1	YSH1	High	1	1	0.785	1.214	1.162	0.607
1698	Ribosome biogenesis protein YTM1	YTM1	High	5	2	1.083	0.965	1.162	1.092
1699	probable mannosyltransferase YUR1	YUR1	Low	3	1		100	100	0.01
1700	Calcium channel YVC1	YVC1	High	2	1	1.202	1.061	1.146	0.925
1701	Protein ZDS1	ZDS1	Medium	1	1				
1702	protein ZEO1	ZEO1	High	10	1	1.121	0.763	1.625	1.205
1703	Zinc finger protein ZPR1	ZPR1	High	12	5	1.06	0.939	1.188	1.113

1704	Zinc/cadmium resistance protein	ZRC1	High	23	5	0.82	1.244	0.905	0.728
1705	Zinc-regulated transporter 1	ZRT1	High	13	3	0.01	100	0.01	0.01
1706	Zinc-regulated transporter 3	ZRT3	High	2	1	0.886	0.819	0.806	0.737
1707	zuotin	ZUO1	High	37	16	1.095	0.981	1.114	1.062
1708	Glucose-6-phosphate 1-dehydrogenase	ZWF1	High	38	14	1.893	1.818	1.131	1.291

Appendix II: First page to published manuscripts

Chapter 2: Quantifying heme-protein maturation from ratiometric fluorescence lifetime measurements on the single fluorophore in its GFP fusion

THE JOURNAL OF PHYSICAL CHEMISTRY A

pubs.acs.org/JPCA Article

Quantifying Heme–Protein Maturation from Ratiometric Fluorescence Lifetime Measurements on the Single Fluorophore in Its GFP Fusion

Samaneh Dastpeyman, Robert Godin, Gonzalo Cosa,* and Ann M. English*

Cite This: *J. Phys. Chem. A* 2020, 124, 746–754 Read Online

ABSTRACT: Protein maturation by heme insertion is a common post-translation modification of key biological importance. Nonetheless, where and when this maturation occurs in eukaryotic cells remain unknown for most heme proteins. Here, we demonstrate for the first time that the maturation of a chromosomally expressed, endogenous heme protein fused to a green fluorescent protein (GFP) can be tracked in live cells. Selecting yeast cytochrome c peroxidase (Ccp1) as our model heme-binding protein, we first characterized the emission in vitro of recombinant Ccp1–GFP with GFP fused C-terminally to Ccp1 by the linker GRRIPGLIN. Time-correlated single-photon counting reveals a single fluorescence lifetime for heme-free apoCcp1–GFP, $\tau_0 = 2.84 \pm 0.01$ ns. Heme bound to Ccp1 only partially quenches GFP fluorescence since holoCcp1–GFP exhibits two lifetimes, $\tau_1 = 0.95 \pm 0.02$ and $\tau_2 = 2.46 \pm 0.03$ ns with fractional amplitudes $a_1 = 38 \pm 1.5\%$ and $a_2 = 62 \pm 1.5\%$. Also, τ and a are independent of Ccp1–GFP concentration and solution pH between 5.5 and 8.0, and a standard plot of a_1 vs % holoCcp1–GFP in mixtures with apoCcp1–GFP is linear, establishing that the fraction of Ccp1–GFP with heme bound can be determined from a_1. Fluorescence lifetime imaging microscopy (FLIM) of live yeast cells chromosomally expressing the same Ccp1–GFP fusion revealed 30% holoCcp1–GFP (i.e., mature Ccp1) and 70% apoCcp1–GFP in agreement with biochemical